



19th International Workshop on Osteoarthritis Imaging

Cambridge, United Kingdom July 9-12, 2025



Welcome!

Dear Colleagues, Collaborators and Friends,

We are delighted to extend a warm summer welcome to all of you joining us in Cambridge, UK, for the 2025 International Workshop of Osteoarthritis Imaging (IWOAI).

Not only is the University of Cambridge steeped in tradition across the sciences, arts and humanities, but the city and surrounding countryside also display the signs of a rich global history that includes Ely Cathedral at the heart of the Fenlands, the Cambridge American Cemetery and Memorial in Madingley and the pre-Roman settlements north of the city (to name but a few).

Cambridge has attracted people from across the globe to study, live and change the world, and now stands as one of the foremost and cosmopolitan biomedical and technological research centres in the world. We felt this was the perfect setting for the IWOAI mission that likewise has such important ambitions.

It is against this backdrop that we invite you to the award-winning conference facilities at Cripps Court in Magdalene College, Cambridge. Running along the riverbank astride its namesake bridge, Magdalene College is one of the truly beautiful settings of the city that we hope will inspire your visit.

We are honoured to be able to share it and the city with you during the conference, at the evening events, and through the Saturday social day as we punt ourselves along the iconic Backs of the River Cam.

As the organisers, we want nothing more than to make sure you end your visit with new ideas, new friends, and a lasting memory of Cambridge and IWOAI as somewhere to return to again and again.

Thank you for joining us and bringing yourselves with your tremendous research to share with the rest of our IWOAI community.

Warmest regards,

Prof. Tom Turmezei Prof. Cecilia Brasset

Co-organisers of IWOAI 2025, Magdalene College, Cambridge, UK.

19th International Workshop in Osteoarthritis Imaging ANATOMY: the Basis of Shape, Structure & Function

Chairs

Prof. Tom Turmezei, Norfolk and Norwich University Hospital, Norwich, UK Prof. Cecilia Brassett, University of Cambridge, UK

Scientific Committee

Jamie Collins
Mylene Jansen
Mohamed Jarraya
James Johnston
Vidyani Suryadevara
Janus Uhd Nybing

Conference Organizer

Tristan Whitmarsh

The 2025 conference theme is "ANATOMY: the basis of shape, structure & function"

All scientific sessions and lunches will take place at Cripps Court Conference Centre, Magdalene College, Cambridge,1-3 Chesterton Rd, Cambridge CB4 3AD. Conference attendees will have access to all college grounds during the conference.

All speakers are confirmed but may be subject to change. Talk titles are representative for the session topic.

DAY 1 - Wednesday 9th July 2025

10:00-12:00	PRE-CONFERENCE WORKSHOP Human Anatomy Centre, Anatomy Building, Downing Site, Cambridge, CB2
	3DY
	*This is a costed ticketed event with limited numbers
11:30	REGISTRATION OPENS
	At conference venue
12:30-13:30	LUNCH
	At conference venue
13:30-14:00	CONFERENCE OPENING
	Welcome from ISOAI President, Prof. Ali Guermazi
	Welcome from IWOAI 2025 hosts, Prof. Tom Turmezei & Prof. Cecilia Brassett
14:00-15:30	SESSION 1 - QUANTITATIVE MRI - Latest in structure & function
14:00-14:20	K1.1 Keynote speaker 1 - Rupsa Bhattacharjee - Quantitative MRI
14:20-14:40	K1.2 Keynote speaker 2 - <u>Feliks Kogan</u> - PET-MRI
14:40-14:50	Questions and discussion
14:50-15:03	\$1.1 Ananya Goyal, USA THE AGING JOINT: QUANTITATIVE [18F]NAF PET-MR IMAGING OF
	CELLULAR & MOLECULAR CHANGES IN BONE, CARTILAGE AND MUSCLE ACROSS THE LIFESPAN
15:03-15:16	S1.2 Vidyani Suryadevara, USA
	CLINICAL TRANSLATION PIPELINE FOR DETECTING SENESCENCE IN OSTEOARTHRITIS USING THE BGALACTOSIDASE RESPONSIVE GD-
45.40.45.00	CHELATE
15:16-15:30	\$1.3 Krithika Balaji, UK COMPARATIVE STUDY: QDESS VERSUS RAFO-4 PERFORMANCE IN 5-
	MINUTE, SIMULTANEOUS, RELIABLE 3D T2 MAPPING AND
	MORPHOLOGICAL MR IMAGING
15:30-16:30	BREAK WITH REFRESHMENTS inc. GUIDED POSTER TOURS
16:30-18:00	SESSION 2 - MICRO-CT IN OSTEOARTHRITIS - Scaling up with CT
16:30-16:50	K2.1 Keynote speaker 1 - <u>Kathryn Stok</u> - The spectrum of micro-CT in osteoarthritis

16:50-17:10	K2.2 Keynote speaker 2 - <u>Andrew Pitsillides</u> - Imaging animal models of osteoarthritis
17:10-17:20	Questions and discussion
17:20-17:33	S2.1 Andy Kin On Wong, Canada COMPROMISED TRABECULAR BONE OF THE KNEE IS A DOSE-DEPENDENT CORRELATE OF MORE SEVERE OSTEOPHYTES AND ADVANCED KLG
17:33-17:46	S2.2 Neil Segal, USA EVALUATION OF DIFFERENT METHODS OF AUTOMATED 3-D JOINT SPACE MAPPING FROM WEIGHT BEARING CT SUGGESTS A TIBIAL MESH-TO-MESH APPROACH IS MOST SENSITIVE
17:46-18:00	S2.3 Ali Guermazi, USA PHASE II RANDOMISED CLINICAL TRIAL OF LEVI-04, A NOVEL NEUROTROPHIN-3 INHIBITOR, IN PEOPLE WITH KNEE OSTEOARTHRITIS: IMAGING EXCLUSIONS DURING SCREENING
18:00-18:15	Osteoarthritis Imaging
	Prof. Frank Roemer - Editor-in-Chief
19:30-23:30	DINNER EVENT The Maharajah Restaurant, 9-13 Castle St., Cambridge, CB3 0AH *This is a ticketed event with limited numbers

DAY 2 - Thursday 10th July 2025

09:00-11:00	SESSION 3 - COHORTS vs CLINICAL TRIALS - Strength in numbers?
09:00-09:20	K3.1 Keynote speaker 1 - <u>Neil Segal</u> - The past, present and future WBCT in MOST
09:20-09:40	K3.2 Keynote speaker 2 - <u>Jamie MacKay</u> - Experimental trial options in osteoarthritis
09:40-09:50	Questions and discussion
09:50-11:00	P1 Clinical Trials Panel - led by David Hunter
	Panel members TBC - Update on osteoarthritis clinical trials from the last 12 months
11:00-11:30	BREAK WITH REFRESHMENTS
11:30-12:30	SESSION 4 - JOINT BIOLOGY & IMAGING - From tissue to pixel
11:30-11:50	K4.1 Keynote speaker 1 - <u>Tonia Vincent</u> - Joint biology and radiographic osteoarthritis
11:50-12:10	K4.2 Keynote speaker 2 - <u>Andrew McCaskie</u> - Bone and cartilage regeneration
12:10-12:20	Questions and discussion
12:20-12:35	S4.1 Simon Westbrook, UK LEVI-04 REDUCES BONE MARROW LESION AREA AND PRESENCE IN KNEE OSTEOARTHRITIS: RESULTS FROM A PHASE II RCT
12:30-14:00	LUNCH
	Optional Samuel Pepys Tour
	*This is a free ticketed event with limited numbers
14:00-15:30	SESSION 5 - SHAPE IN OSTEOARTHRITIS - "Built to fail?"

14:00-14:20	K5.1 Keynote speaker 1 - <u>Jenny Gregory</u> - Shape, osteoarthritis risks and outcomes
14:20-14:40	K5.2 Keynote speaker 2 - <u>Anthony Gatti</u> - MRI, shape and other parameters
	Questions and discussion
14:40-14:50	
14:50-15:03	S5.1 Fleur Boel, The Netherlands BEYOND ACETABULAR DYSPLASIA AND PINCER MORPHOLOGY: REFINING HIP OSTEOARTHRITIS RISK ASSESSMENT THROUGH STATISTICAL SHAPE MODELING
15:03-15:16	S5.2 Anoosha Pai, USA
	NEURAL SHAPE MODEL QUANTIFIES EARLY AND PROGRESSIVE
45 40 45 00	BONE SHAPE CHANGES AFTER ACLR
15:16-15:30	S5.3 Myrthe van den Berg, The Netherlands
	ADVANCING HIP OSTEOARTHRITIS PREDICTION: INSIGHTS FROM MULTI-MODAL PREDICTIVE MODELING WITH INDIVIDUAL
	PARTICIPANT DATA OF THE WORLD COACH CONSORTIUM
	PARTICIPANT DATA OF THE WORLD COACH CONSORTIUM
15:30-16:30	BREAK WITH REFRESHMENTS inc. GUIDED POSTER TOURS
16:30-18:00	SESSION 6 - LATEST IN COMPUTED TOMOGRAPHY - A CT world
16:30-16:50	K6.1 Keynote speaker 1 - Edwin Oei - Photon counting CT for osteoarthritis
16:50-17:10	K6.2 Keynote speaker 2 - Graham Treece - CT, bone, and data visualisation
17:10-17:20	Questions and discussion
17:20-17:33	S6.1 Mohamed Jarraya, USA
	PHOTON-COUNTING CT-BASED TRABECULAR BONE ANALYSIS IN THE KNEE: A COMPARATIVE STUDY OF ADVANCED OSTEOARTHRITIS AND HEALTHY CONTROLS
17:33-17:46	S6.2 Susan Li, USA
	BASELINE C-SCORE ON WEIGHT-BEARING CT PREDICTS 2-YEAR WORSENING OF KNEE PAIN IN WOMEN
17:46-18:00	S6.3 Tom Turmezei, UK
	REPEATABILITY OF CT OSTEOARTHRITIS KNEE SCORE (COAKS) AND
	A PROTOTYPE CT-GENERATED KELLGREN AND LAWRENCE GRÂDE
18:00-18:15	Day close
19:30-23:30	DINNER EVENT
	The Graduate by Hilton Hotel Cambridge

Including pre-dinner drinks and entertainment

*This is a costed ticketed event with limited numbers

DAY 3 - Friday 11th July 2025

09:00-10:30	SESSION 7 - LATEST AI IN OSTEOARTHRITIS IMAGING - "Hype of the
	machines"
09:00-09:20	K7.1 Keynote speaker 1 - Akshay Chaudhari - Al segmentation techniques
09:20-09:40	K7.2 Keynote speaker 2 - Aleksei Tiulpin - Multimodal AI in adaptive clinical
	trials
09:40-09:50	Questions and discussion

09:50-10:03	\$7.1 Anthony Gatti, USA AUTOMATIC MENISCUS ANALYSIS DEMONSTRATES REPAIR IS NOT SUPERIOR TO MENISCECTOMY IN IMPROVING MENISCAL UTE-T2* PROPERTIES 2-YEARS POST ACLR
10:03-10:16	S7.2 Rayan Harari, USA PREDICTING KNEE OSTEOARTHRITIS PROGRESSION USING EXPLAINABLE MACHINE LEARNING AND CLINICAL IMAGING DATA
10:16-10:30	S7.3 Wolfgang Wirth, Austria A FULLY-AUTOMATED TECHNIQUE FOR KNEE CARTILAGE AND DENUDED BONE AREA MORPHOMETRY IN SEVERE RADIOGRAPHIC KNEE OA – METHOD DEVELOPMENT AND VALIDATION
10:30-11:00	BREAK WITH REFRESHMENTS
11:00-12:30	SESSION 8 - ANATOMY & OSTEOARTHRITIS - "A blueprint for motion"
11:00-11:20	K8.1 Keynote Speaker 1 - Felix Eckstein - Sex differences in osteoarthritis
	anatomy
11:20-11:40	K8.2 Keynote Speaker 2 - Piers Mitchell - Archaeology, anthropology and OA
11:40-11:50	Questions and discussion
11:50-12:03	\$8.1 Noël Spoedler, The Netherlands
	TOPOGRAPHY OF SEX-RELATED FEMOROTIBIAL CARTILAGE
	THICKNESS DIFFERENCES: A MATCHED MALE-FEMALE PAIR ANALYSIS CONTROLLING FOR AGE, BMI, AND HEIGHT
12:03-12:16	S8.2 Jamie Collins, USA
	DATA-DRIVEN DISCOVERY OF KNEE OSTEOARTHRITIS SUBGROUPS
40.40.40.00	VIA CLUSTER ANALYSIS OF MRI BIOMARKERS
12:16-12:30	\$8.3 Philip Conaghan, UK LEVI-04, A NOVEL NEUROTROPHIN-3 INHIBITOR, DEMONSTRATED
	SIGNIFICANT IMPROVEMENTS IN PAIN AND FUNCTION AND WAS NOT
	ASSOCIATED WITH DELETERIOUS EFFECTS ON JOINT STRUCTURE IN
	PEOPLE WITH KNEE OA IN A PHASE II RCT
12:30-14:00	LUNCH
	Optional Samuel Pepys Tour
	*This is a free ticketed event with limited numbers
14:00-15:30	SESSION 9 - BIOMECHANICS & IMAGING - "A moving target"
14:00-14:20	K9.1 Keynote speaker 1 - <u>Erin Macri</u> - Gait, imaging and OA
14:20-14:40	K9.2 Keynote speaker 2 - <u>Jari Salo</u> - Weight bearing CT in orthopaedic
14:40-14:50	practice Questions and discussion
14:50-15:03	S9.1 Jordan Broberg, Canada
14.00 10.00	EFFECT OF LATERAL MENISCUS POSTERIOR ROOT TEARS ON
	CARTILAGE AND MENISCAL MECHANICS
15:03-15:16	S9.2 Rosemarijn van Paassen, The Netherlands
	PATELLAR AND FEMORAL BONE MORPHOLOGY AND ITS ASSOCIATION WITH LOADING IN YOUNG ADOLESCENT BOYS AND
	GIRLS
15:16-15:30	S9.3 Zhe Wang, USA
	DEEP LEARNING MODELS FOR AUTOMATIC JOINT SPACE WIDTH
	MEASUREMENT
15:30-16:30	BREAK WITH REFRESHMENTS inc. GUIDED POSTER TOURS
16:30-17:30	SESSION 10 - INTERACTIVE DEBATE - "Is it worth the weight?"
	P2 - Panel discussion - panel members TBC

17:30-17:45 AWARD CEREMONY

Young Investigator Awards

Top abstract Awards
Top poster Awards

17:45-18:00 WELCOME TO IWOAI 2026, MUNICH, GERMANY

Prof. Frank Roemer & Dr. Wolfgang Wirth

18:00 CONFERENCE CLOSE

19:30-22:00 GALA DINNER

The Hall, Magdalene College, Cambridge

Including pre-dinner drinks reception and entertainment

*This is a costed ticketed event with limited numbers

SOCIAL DAY - Saturday 12th July 2025

10:00-12:00 WALKING TOUR OF CAMBRIDGE

See a different side of Cambridge with <u>Terrible Tours of Cambridge</u>
*This is a part of the day's costed ticketed package with limited numbers

12:00-14:00 LUNCH

The Hall, Christ's College, Cambridge

Ticket holders will have access to all college grounds around the event *This is a part of the day's costed ticketed package with limited numbers

14:00-14:30 Walking from Christ's College to the Mill Pond for punting

14:30-16:30 PUNTING ON THE CAM

Punt yourself along the beautiful Backs of Cambridge from <u>Scudamore's</u> *This is a part of the day's costed ticketed package with limited numbers

18:00 to late CAMBRIDGE BY NIGHT

Relive student days on a tour of the finest establishments Cambridge has to

offer

*This is a non-ticketed post-conference tour open to one-and-all





19th INTERNATIONAL WORKSHOP OF OSTEOARTHRITIS IMAGING MAGDALENE COLLEGE, CAMBRIDGE, UK Conference Days 9th-11th July 2025 | Social Day 12th July 2025



POSTERS

ALZAHER: INCREASED BMI IS A MODIFIABLE RISK FACTOR OF SUBCHONDRAL INSUFFICENCY FRACTURE OF THE KNEE

BALAJI: SIMULTANEOUS 3D CARTILAGE T_2 MAPPING AND MORPHOLOGICAL IMAGING WITH RAFO-4 MRI, A MACHINE LEARNING ALGORITHM

BODDU: 3-D LANDMARKING REPEATABILITY EMPHASIZES CHALLENGES IN SCAN POSITIONING DURING WEIGHT BEARING CT OF THE KNEE

BOEL: SEX-SPECIFIC CONTINUOUS JOINT SPACE WIDTH: AN ALTERNATIVE TO RHOA GRADING

BREJNEBOL: THE EFFECT OF WEIGHT LOSS AND GLUCAGON-LIKE PEPTIDE-1 RECEPTOR AGONIST ON STRUCTURAL CHANGES IN KNEE OSTEOARTHRITIS: SECONDARY ANALYSIS OF THE RANDOMISED, PLACEBO-CONTROLLED LOSEIT TRIAL

BURSON-THOMAS: QUANTIFYING JOINT GEOMETRY IN HUMAN HANDS FROM IMAGING DATA

COLLINS: WHAT IS THE DISTRIBUTION OF MRI-ASSESSED CARTILAGE DAMAGE AND OSTEOPHYTES WITHIN RADIOGRAPHIC KL GRADE?

DAM: STUDY POPULATION SELECTION USING MACHINE LEARNING FROM THE FNIH BIOMARKERS CONSORTIUM PROGRESS OA COHORT

DRIBAN: REVEALING THE HIDDEN CULPRIT: CONTRALATERAL KNEE'S ROLE IN OSTEOARTHRITIS DISEASE ACTIVITY: DATA FROM THE OSTEOARTHRITIS INITIATIVE

DURYEA: NEW JSW MEASUREMENTS INCREASE RESPONSIVENSS TO CHANGE

ECKSTEIN: POTENTIAL IMPACT OF DIABETES MELLITUS ON CARTILAGE THICKNESS AND COMPOSITION IN SUBJECTS WITH AND WITHOUT OSTEOARTHRITIS – A MATCHED CASE-CONTROL STUDY

GHEISARI: EXPLORING THE RELATIONSHIP BETWEEN LIGAMENT MICROSTRUCTURE AND MECHANICS IN OA-AFFECTED HUMAN KNEES

GOYAL: AUTOMATING IMAGING BIOMARKER ANALYSIS FOR KNEE OSTEOARTHRITIS USING AN OPEN-SOURCE MRI-BASED DEEP LEARNING PIPELINE

HARANDI: PAIN PHENOTYPE AS AN EFFECT MODIFIER: EXPLORING THE ROLE OF PAIN-DETECT IN THE ASSOCIATION BETWEEN WOMAC SCORES AND MRI-DETECTED STRUCTURAL DAMAGE

HARVEY: FROM MENISCAL DEGENERATION TO OSTEOARTHRITIS: TRACKING EARLY DISEASE PROGRESSION WITH MRI-BASED COMPOSITE SCORES: DATA FROM THE OSTEOARTHRITIS INITIATIVE

HEALD: A FIRST-IN-HUMAN PHASE 1/2A CLINICAL STUDY OF ICM-203 AAV GENE THERAPY: PROMISING SIGNALS AS A DMOAD CANDIDATE

HENDRIKS: PREVALENCE OF ACETABULAR DYSPLASIA IN 6-YEAR-OLDS IN A GENERAL POPULATION

HOU: GENETIC SULFATE WASTING, A MONOGENIC CAUSE OF SEVERE INTERVERTEBRAL DISC HEIGHT LOSS

JOHNSTON: REGIONAL DEPTH-SPECIFIC SUBCHONDRAL BONE DENSITY IN OA AND NORMAL DISTAL FEMORA: PRECISION AND PRELIMINARY COMPARISONS

KAMPHUIS: EXPLORING SEX-BASED HIP MORPHOLOGY DIFFERENCES IN YOUNG ADULTS USING AN AUTOMATED 3D METHOD

KARJALAINEN: EX VIVO IMAGING OF DIFFERENT CALCIFICATION TYPES IN POSTERIOR HORN OF HUMAN MENISCUS USING MICRO-COMPUTED TOMOGRAPHY

KNIGHT: STRUCTURAL EFFICACY OF INTRA-ARTICULAR SPRIFERMIN TREATMENT ON KNEE OSTEO-ARTHRITIS AS A FUNCTION OF SYMPTOMATIC AND RADIOGRAPHIC DISEASE SEVERITY - A POST-HOC ANALYSIS FROM THE FORWARD PHASE 2 RANDOMIZED CONTROLLED TRIAL

KOGAN: FEASIBILITY OF NON-CONTRAST MRI TO DETECT CHANGES IN SYNOVITIS AFTER ACL RECONSTRUCTION SURGERY

KUCZYNSKI: REGIONAL VARIATION IN TRAPEZIOMETACARPAL BONE MICROARCHITECTURE IN FEMALES WITH OSTEOARTHRITIS USING HR-PQCT

LIU: IN VIVO MICRO COMPUTED TOMOGRAPHY IMAGING ALLOWS LONGITUDINAL ASSESSMENT OF MULTI-SCALE CHANGES TO WHOLE JOINT WITH PROGRESSION OF OA

LIU: REVEALING EARLY SUBCHONDRAL BONE STRUCTURAL CHANGES IN OSTEOARTHRITIS PROGRESSION IN A COLLAGENASE-INDUCED MOUSE MODEL USING MICRO COMPUTED TOMOGRAPHY

MAHALLEH: STATIN USE AND LONGITUDINAL CHANGES IN KNEE MRI-DERIVED THREE-DIMENSIONAL BONE SHAPE: DATA FROM THE OSTEOARTHRITIS INITIATIVE

NEVANRANTA: CHARACTERIZING MENISCAL CALCIFICATIONS WITH PHOTON COUNTING-BASED DUAL-ENERGY COMPUTED TOMOGRAPHY

NIELSEN: AGREEMENT BETWEEN IN VIVO AND EX VIVO PHOTON-COUNTING CT MEASURES OF SUBCHONDRAL BONE FEATURES IN PATIENTS WITH KNEE OSTEOARTHRITIS

OZEKI: PROJECTED CARTILAGE AREA RATIO, EVALUATED USING THREE-DIMENSIONAL MRI ANALYSIS SOFTWARE, IS A USEFUL INDEX FOR ASSESSING CARTILAGE IN THE MEDIAL COMPARTMENT OF THE KNEE JOINT, COMPARABLE TO CARTILAGE THICKNESS MEASUREMENTS

PATARINI: EARLY DETECTION OF KNEE OA – THE ROLE OF A COMPOSITE DISEASE ACTIVITY SCORE: DATA FROM THE OSTEOARTHRITIS INITIATIVE

PEITSO: HIGH-RESOLUTION 3D IMAGING OF BOVINE TAIL INTERVERTEBRAL DISC DEGENERATION USING IODINE-ENHANCED X-RAY MICROSCOPY

PRADEEP: A NEW LENS ON SYNOVITIS: LABEL-FREE IMAGING OF WHOLE-MOUNT HUMAN PATHOLOGICAL SYNOVIAL MEMBRANE WITH MULTIPHOTON MICROSCOPY

QUAYYUM: THE EFFECT OF RECONSTRUCTION KERNEL AND MONOCHROMATIC ENERGY PAIRS USED IN DUAL ENERGY CT IMAGING OF THE PROXIMAL HUMERUS

RAZA: PREDICTING KNEE OSTEOARTHRITIS PROGRESSION USING STRUCTURAL BIOMARKERS FROM MULTIPLE JOINTS: DATA FROM THE OSTEOARTHRITIS INITIATIVE

ROEMER: DO RATES OF FEMOROTIBIAL CARTILAGE LOSS IN KELLGREN-LAWRENCE 2 AND 3 KNEES DIFFER BETWEEN THOSE WITH MILD-MODERATE VS. SEVERE PATELLOFEMORAL STRUCTURAL DAMAGE?

ROEMER: TRANSLATION OF X-RAY TO MRI: DIAGNOSTIC PERFORMANCE OF MRI-DEFINED SIMULATED KELLGREN-LAWRENCE GRADING

SALZLECHNER: SPONTANEOUS CARTILAGE THICKENING IN OSTEOARTHRITIS KNEES: DATA FROM IMI-APPROACH AND THE OAI

SAUNDERS: COORDINATED VARIATIONS IN HIP SHAPE WITH SEX, AGE AND OA IN UK BIOBANK

SAUNDERS: OSTEOARTHRITIS AND CHRONIC BACK PAIN ARE ASSOCIATED WITH LATERAL SPINE SHAPE: A STUDY USING THE UK BIOBANK

SCHADOW: UNCOVERING STRUCTURAL DISEASE PATTERNS OF EARLY POST-TRAUMATIC OSTEOARTHRITIS IN A DMM MOUSE MODEL USING CONTRAST-ENHANCED MICRO-COMPUTED TOMOGRAPHY

SEGAL: ASSESSING TEST-RETEST RELIABILITY OF JSW MEASUREMENTS FOR THE MOST4 KNEE RADIOGRAPH POSITIONING PROTOCOL

SHERMAN: CAN COMBINED NEUROPHYSIOLOGICAL AND MRI EVALUATION HELP GAIN NEW INSIGHTS IN ARTHROGENIC MUSCLE INHIBITION AMONG PATIENTS WITH KNEE PAIN? PROOF OF CONCEPT

SHIHUA: OPTIMIZED DEEP LEARNING METHOD FOR AUTOMATED SEGMENTATION OF BONE MARROW LESIONS

SIMONIS: THE INFLUENCE OF WEIGHT-BEARING AND FLEXION ON 3D JOINT SPACE WIDTH IN KNEE OSTEOARTHRITIS

STILES: VALIDATING INTERNAL DENSITY CALIBRATION IN THE PROXIMAL HUMERUS TO ESTIMATE BONE STIFFNESS FOR STEMLESS SHOULDER ARTHROPLASTY

STIRLING: FINITE ELEMENT MODELING OF IN VIVO HUMAN KNEE BONES USING HR-PQCT: EFFECTS OF BOUNDARY CONDITIONS AND MODEL CONFIGURATION ON PREDICTED STRAIN ENERGY DENSITY

STIRLING: LONGITUDINAL PROGRESSION OF TRAUMATIC BONE MARROW LESIONS FOLLOWING ANTERIOR CRUCIATE LIGAMENT INJURY: ASSOCIATIONS WITH KNEE PAIN AND CONCOMITANT INJURIES

TRENTADUE: STATISTICAL SHAPE MODELING OF COMPUTED TOMOGRAPHY-DERIVED CARPAL BONES REFLECTS SCAPHOLUNATE INTEROSSEOUS LIGAMENT INJURY

TURMEZEI: REPEATABILITY OF CT OSTEOARTHRITIS KNEE SCORE (COAKS) MULTICOMPONENT MEASURES

VAN DEN BERG: OSTEOARTHRITIS IS A MULTI-JOINT DISEASE. OR IS IT?

VAN PAASSEN: AUTOMATIC EXTRACTION OF KNEE ALIGNMENT AND MORPHOLOGY MEASURES FROM 3D MODELS IN A YOUNG-ADOLESCENT OPEN-POPULATIONS COHORT STUDY

VUONONVIRTA: CHANGES IN JOINT SPACE WIDTH ONE YEAR AFTER WEIGHT LOSS SURGERY

WATERTON: IMPROVED DCE-MRI OF OA SYNOVITIS IN THE PRESENCE OF EFFUSION

WHITE: TOWARD OPENLY AVAILABLE KNEE MRI SEGMENTATIONS FOR THE OAI: MULTI-MODEL EVALUATION AND CONSENSUS GENERATION ON 9,360 SCANS

WIRTH: CAN REGISTRATION-BASED LOCATION-INDEPENDENT MEASUREMENT INCREASE THE SENSITIVITY TO BETWEEN-GROUP DIFFERENCES IN LONGITUDINAL CHANGE OF LAMINAR CARTILAGE T2?

ZHONG: A SYSTEMATIC POST-PROCESSING APPROACH FOR T_{1P} IMAGING OF KNEE ARTICULAR CARTILAGE

ZHOU: AUTOMATED QUANTIFICATION OF MENISCUS EXTRUSION IN MRI VIA AI FOUNDATION MODEL: PROOF OF CONCEPT USING A TRAINING-FREE FEW-SHOT SEGMENTATION APPROACH

THIS MEETING IS SUPPORTED BY

GOLD SUPPORT

Levicept

SILVER SUPPORT



sanofi



BRONZE SUPPORT

Formation Bio ©ICM







Planmed bioxydyn

ELSEVIER

Contents lists available at ScienceDirect

Osteoarthritis Imaging

journal homepage: www.elsevier.com/locate/ostima



19th International Workshop on Osteoarthritis Imaging: Oral presentation

THE AGING JOINT: QUANTITATIVE [18 F] NAF PET-MR IMAGING OF CELLULAR & MOLECULAR CHANGES IN BONE, CARTILAGE AND MUSCLE ACROSS THE LIFESPAN

A. Goyal, Y. Vainberg, F. Belibi, A.A. Gatti, M.S. White, R. Shalit, F. Kogan Department of Radiology, Stanford University, Stanford, CA, USA

INTRODUCTION: Osteoarthritis (OA) is increasingly recognized as a whole-joint disease, affecting cartilage, subchondral bone and periarticular muscles. While structural changes throughout the lifespan have been investigated in prior work, few studies have explored early cellular and molecular changes, such as bone metabolism, cartilage matrix composition, and muscle quality. In this study, we simultaneously assessed bone metabolic activity, cartilage microstructure, and muscle morphometry and composition in vivo, and examined their associations with key OA risk factors including age, body mass index (BMI), and sex.

OBJECTIVE: To characterize cellular and molecular features of bone, cartilage, and muscle in asymptomatic adults, and determine how these metrics vary with key OA risk factors of age, BMI, and sex.

METHODS: Forty-five asymptomatic subjects (23-79 years old, 22 female) with no history of knee injury or symptomatic arthritis underwent bilateral knee imaging on a 3T GE PET-MRI scanner (Figure 1). Quantitative DESS MR images (TEs 6 and 30.4 ms) were used to compute mean cartilage T2 relaxation time and thickness in femoral, tibial and patellar subregions, which were segmented using a previously validated automated pipeline. Dynamic [18F]NaF PET scans were acquired before and after a stair-climbing exercise (2.5mCi dose/injection) and were used to quantify Standardized Uptake Value measures (SUVmean, SUVmax) and their exercise-induced change: Δ SUVmean, Δ SUVmax. Iterative Decomposition of water and fat with Echo Assymetry and Least squares estimation (IDEAL) scans of the bilateral thighs were also acquired. The quadriceps, hamstrings, and hip adductors were segmented using an automated pipeline (MuscleMap) and muscle volume (normalized to BMI), fat fraction, and lean muscle mass were calculated for each muscle. Statistical analysis included a linear mixed effects model for each tissue outcome (cartilage, bone, and muscle metrics), where sex (male vs. female), age (years) and BMI (kg/m²) were included as fixedeffect predictors, and random intercepts for subject and for side nested within subject (to account for the paired left/right measures) captured

within-individual correlation. Significance threshold was set at p < 0.05 for this analysis.

RESULTS: Table 1 shows results from the linear mixed effects model.

- 1) Higher BMI was associated with markedly greater baseline (SU-Vmean and SUVmax) and post-exercise bone tracer uptake (Δ SUVmean and Δ SUVmax), indicating increased bone turnover in individuals with higher body mass. Age was linked specifically to higher maximum uptake measures (SUVmax and Δ SUVmax), suggesting that focal sites of remodeling intensify with aging even if the overall mean uptake remains relatively stable.
- 2) In cartilage, T2 relaxation times rose progressively across whole, deep, and superficial layers as participants grew older, while cartilage thickness was consistently lower in female subjects. Deep T2 also showed a positive association with BMI.
- 3) Muscle composition also shifted with age and adiposity: intramuscular fat fraction increased in individuals who are older and had higher BMI; overall muscle volume declined with advancing age; and lean muscle mass was significantly lower in women and continued to decrease over the lifespan.

CONCLUSION: This comprehensive in vivo assessment suggests that age and BMI are associated with increased subchondral bone activity, cartilage matrix degeneration, and muscle deterioration, with sexspecific differences in cartilage thickness and muscle mass. These coordinated changes under established OA risk factors highlight the need for integrated, whole-joint analyses to develop composite biomarkers and multi-targeted treatments. Future work will incorporate longitudinal imaging, larger cohorts, additional knee tissues (e.g., menisci), and exploration of cross-tissue interactions.

SPONSOR: Wu Tsai Human Performance Alliance, Stanford DARE Fellowship, NIH R01AR079431.

DICLOSURE STATEMENT: AAG is a shareholder of NeuralSeg, NodeAI, and GeminiOV

ACKNOWLEDGMENT: Dawn Holley and Drew Dreisbach for their assistance with PET.

CORRESPONDENCE ADDRESS: agoyal5@stanford.edu

Figures can be found on next page.

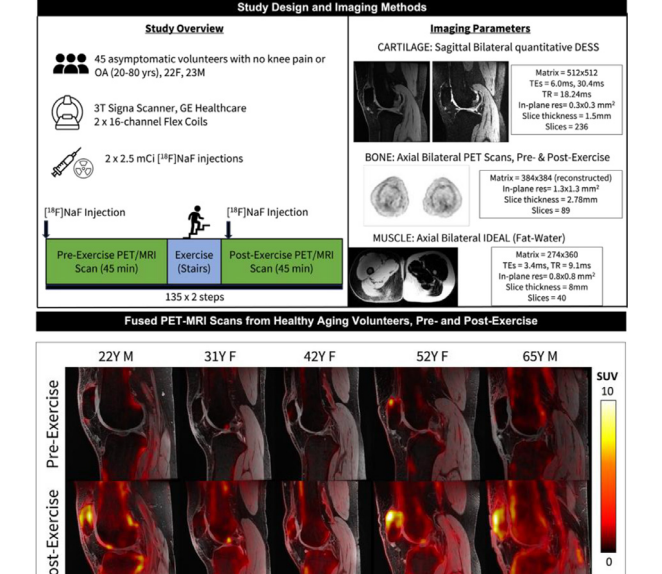


Figure 1. Top panel shows the overview of the study, involving imaging of bone, muscle and cartilage in an asymptomatic cohort. Sample PET-MRIs from pre- and post-exercise are included in the bottom panel and highlight increased SUV, with notable increases in the patella and tibial tuberosity.

Table 1. Linear mixed effects model results for each tissue metric, using a 20-year-old male with BMI 17 kg/m² as baseline. Significant results are bolded and color-coded. BMI was positively associated with all bone PET metrics, while age was associated with higher SUVmax and Δ SUVmax. Age was correlated with increased T2 values, and females exhibited thinner cartilage. Age and BMI were correlated with increased muscle fat fraction and decreased lean muscle mass, while females had lower muscle volume and lean muscle mass.

Tissue	Metric	Predictor	Estimate	p_value	CI	Tissue	Metric	Predictor	Estimate		
		Intercept	0.12	0.61	(-0.35, 0.6)			Intercept	30.31	<0.001	(28, 33)
	SUVmean	Sex[T.Female]	0.22	0.15	(-0.078, 0.52)			Sex[T.Female]	1.50	0.05	(-0.00028, 3)
		Age	0.01	0.21	(-0.003, 0.014)		Whole T2	Age	0.08	<0.001	(0.04, 0.13)
-		BMI	0.06	<0.001	(0.027, 0.099)			ВМІ	0.10	0.29	(-0.084, 0.28)
		Group Var	1.52	< 0.001	(0.94, 2.1)			Group Var	0.45	<0.001	(0.26, 0.64)
		Intercept		0.78	(-1.1, 1.5)		Intercept	24.37	<0.001	(23, 26)	
		Sex[T.Female]	0.57	0.17	(-0.25, 1.4)			Sex[T.Female]	0.89	0.11	(-0.21, 2)
	SUVmax	Age	0.03	0.01	(0.0062, 0.053)		Deep T2	Age	0.05	< 0.001	(0.019, 0.082)
		BMI	0.15	<0.001	(0.056, 0.25)			BMI	0.16	0.02	(0.025, 0.29)
		Group Var	0.46	< 0.001	(0.27, 0.66)			Group Var	0.21	<0.001	(0.11, 0.31)
Bone		Intercept	0.63	0.06	(-0.026, 1.3)	Cartilage		Intercept	35.92	<0.001	(33, 39)
		Sex[T.Female]	0.37	0.08	(-0.039, 0.77)			Sex[T.Female]	2.01	0.06	(-0.053, 4.1)
	ΔSUVmean	Age	0.01		Superficial	Age	0.12		(0.059, 0.18)		
		BMI	0.08	< 0.001	(0.035, 0.13)		T2	BMI	0.06	0.63	(-0.19, 0.31)
\vdash		Group Var	0.67	< 0.001	(0.4, 0.94)			Group Var	0.60	<0.001	(0.35, 0.84)
	ΔSUVmax	Intercept	1.41	0.03	(0.13, 2.7)			Intercept	2.04		(1.9, 2.2)
		Sex[T.Female]	0.56	0.17	(-0.24, 1.4)			Sex[T.Female]	-0.21		(-0.31, -0.098)
		Age	0.03	0.01	(0.0087, 0.054)		Thickness	Age	0.00		(-0.0029, 0.00
		BMI	0.17	<0.001	(0.072, 0.26)			BMI	0.01	0.31	(-0.0062, 0.02
		Group Var	0.25	< 0.001	(0.14, 0.37)			Group Var	0.20	< 0.001	(0.1, 0.3)
		Intercept	4.51	<0.001	(2.8, 6.2)						
		Sex[T.Female]	-0.40	0.43	(-1.4, 0.59)						
	Fat Fraction	Age	0.07	< 0.001	(0.038, 0.097)						
		BMI	0.16	0.02	(0.031, 0.29)						
		Group Var	0.35	<0.001	(0.19, 0.51)						
		Intercept	11.46	< 0.001	(9.9, 13)						
	Volume (per	ex[T.Female]	-2.00	<0.001	(-2.9, -1.1)						
Muscle	BMI)	Age	-0.03	0.04							
		Group Var	0.00	1.00	(-0.027, 0.027)						
- 1		Intercept		<0.001	(18, 26)						
		ex[T.Female]	-4.66	<0.001	(-6.92.4)						
	Lean Muscle	Age	-0.08	0.02	(-0.15, -0.011)						
	Mass	BMI	0,60	<0.001	(0.3, 0.89)						
		Group Var	0.00	1.00	(-0.025, 0.025)						

CLINICAL TRANSLATION PIPELINE FOR DETECTING SENESCENCE IN OSTEOARTHRITIS USING THE B-GALACTOSIDASE RESPONSIVE GD-CHELATE

V. Suryadevara ¹, R. von Kruechten ¹, J.H. Tang ², A.M. Dreisbach ¹, Z. Shokri Varniab ¹, S.B. Singh ¹, A. Lubke ³, T. Liang ¹, J. Wong ¹, J. Wang ¹, R. Duwa ¹, J. Wang ¹, M. Barbieri ¹, F. Kogan ¹, S.B. Goodman ⁴, L. Chou ⁴, D. Oji ⁴, J. Chan ⁴, T.J. Meade ², H.E. Daldrup-Link ¹

INTRODUCTION: Cellular senescence is one of the key mechanisms implicated in the development and progression of OA. The identification of senescence-mediated molecular mechanisms in OA needs novel imaging tools to detect senescence and monitor the efficacy of new senolytic therapies. Progress in molecular imaging techniques has led to the creation of a novel β -gal responsive Gd-chelate for identifying senescence using MRI, the widely used imaging modality for OA.

OBJECTIVE: The hypothesis is that β -gal responsive Gd-chelate can detect senescence *in vitro*, *in vivo* and in human OA specimens.

METHODS: Senescence was induced in mesenchymal stem cells (MSCs) using 400nM doxorubicin over 5 days. Control and senescent cell suspensions incubated with 0.25 mM β-gal responsive Gd-chelate underwent MRI on a 3T MRI scanner (Bruker BioSpec, Billerica, MA). Further cartilage defects created in pig knees were implanted with control and senescent cells, followed by MRI after intraarticular injection of 2.5 mM β -gal responsive Gd-chelate. As a first step of clinical translation, human OA specimens were obtained from 30 patients undergoing hip/knee/ankle replacement. The fresh specimens were incubated with 2.5 mM of β -gal responsive Gd-chelate for an hour, before and after which MRI was performed using the following parameters: fatsaturated PD-weighted fast spin-echo sequence (TR=1500ms, matrix size=512×512pixels, slice thickness(=1mm, FOV=15cm, and NEX=2); SMART1 MAP sequence (TR = 40, 75, 150, 300, 500, 700, and 2,000 ms, matrix size=160×160 pixels SL=6mm, FOV=15 cm, and NEX=1) and T_1 weighted fast SE sequence (TR=500ms, matrix size=512×512 pixels, SL=1mm, FOV=15cm, and NEX=2). T1 maps were generated to calculate the T1 relaxation times.

RESULTS: Senescence was first confirmed with immunohistochemistry for senescence markers including p16, p21 and β -gal. *In vitro* studies indicated that senescent MSCs demonstrated a notable increase in MRI signal after being incubated with the β -gal responsive Gd-chelate probe,

compared to control cells (Fig. 1A). *In vivo*, the probe was injected intraarticularly into pig knee joints, and a marked decrease in T1 relaxation times indicated the retention of the probe and it's activation by senescent cells in cartilage defects (Fig. 1B). The Wilcoxon ranksum test was used to determine the significance between control and senescence group. In human OA specimens, areas with severe cartilage damage as graded by a radiologist using Outerbridge score demonstrated higher number of senescent cells seen on immunohistochemistry. MRI indicated that there is pronounced hyperintense signal in the T1-SE images upon incubation with the β -gal responsive Gd-chelate probe, compared to MRI of the specimens before incubation. This was further quantified on T1 maps and indicated a significant reduction in T1 relaxation times, which also correlated with the Outerbridge score (Fig. 1C). The ordinal logistic regression indicated a significant negative correlation between T1 relaxation times and Outerbridge score (p<0.0001).

CONCLUSIONS: This study demonstrates the clinical translation of the β -gal responsive Gd-chelate for detecting senescent cells *in vitro*, *in vivo* and in human OA specimens.

SPONSOR: NIH (UG3CA268112), NINDS 5R01NS115571) and NIBIB 5R01EB005866-08.

DISCLOSURE STATEMENT: V.S. provides consulting services for IGC Pharma.

ACKNOWLEDGEMENT: We thank Maggie Fung from GE Healthcare for helping us optimize the MR sequences on the clinical scanner. CORRESPONDENCE ADDRESS: vidyani@stanford.edu

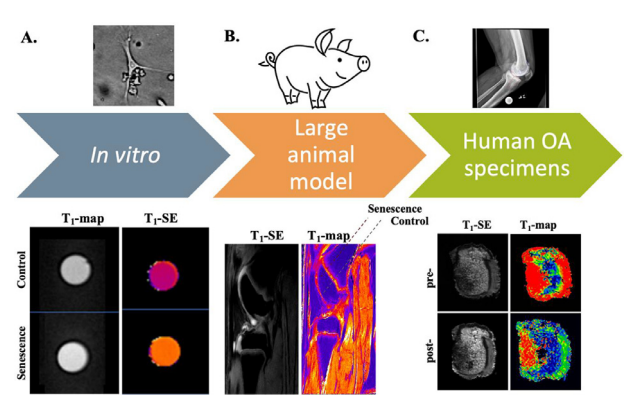


Figure. 1: MRI with β -gal responsive Gd-chelate can detect senescence in pig mesenchymal stem cells, cartilage defects of pig knees and human osteoarthritic joint specimens.

¹ Department of Radiology, Molecular Imaging Program at Stanford (MIPS), Stanford University School of Medicine, Stanford, CA, USA

² Department of Chemistry, Molecular Biosciences, Neurobiology and Radiology, Northwestern University, Evanston, IL, USA

³ Institute of Pathology, University Medical Center Hamburg-Eppendorf, Hamburg, Germany

⁴Department of Orthopedic Surgery, Stanford University, Stanford, CA, USA

COMPARATIVE STUDY: QDESS VERSUS RAFO-4 PERFORMANCE IN 5-MINUTE, SIMULTANEOUS, RELIABLE 3D $\rm T_2$ MAPPING AND MORPHOLOGICAL MR IMAGING

K. Balaji 1 , P.M. Vicente 1 , S. Kukran 1,2 , M. Mendoza 1 , A.A. Bharath 1 , P.J. Lally 1 , N.K. Bangerter 1,3

INTRODUCTION: Cartilage T_2 is a non-invasive MRI biomarker for KOA as it is sensitive to the underlying collagen hydration/organization. Cartilage microstructural changes seen in early KOA result in elevated T_2 . Cartilage T_2 maps could be used in DMOAD clinical trials.

Quantitative DESS (qDESS) simultaneously acquires 3D, morphological whole knee images and quantitative T_2 maps in \sim 5 minutes. Recently, we developed RaFo-4 balanced Steady State Free Precession (RaFo-4 bSSFP) that also has the potential to simultaneously acquire 3D, morphological whole knee images with high SNR efficiency and quantitative cartilage T_2 maps in \sim 5 minutes. RaFo-4 uses machine learning (Random Forest) to estimate voxel-level cartilage T_2 from bSSFP images. In this preliminary study, we compared qDESS and RaFo-4 bSSFP in morphological imaging and cartilage T_2 mapping.

OBJECTIVE: 1) Which technique (qDESS or RaFo-4 bSSFP) has better test-retest repeatability of cartilage T_2 maps? 2) Which technique gives higher quality morphological images, as quantified using SNR of femoral, patellar, and tibial cartilage and CNR of cartilage-muscle, cartilage-synovial fluid, and synovial fluid-muscle?

METHODS: 10 healthy volunteers (HVs: 7F, 3M, 20-40 age range) were scanned on a 3T Siemens Verio (Erlangen, Germany) using an 8-channel knee coil with ethics approval. Test-retest 3D (80 slices) sagittal knee images were acquired using qDESS (water excitation, 20° flip angle, 21.77 ms TR, 6 ms TE, 364 Hz/Px receiver bandwidth, 0 dummy scans per volume) and bSSFP (water excitation, 22° flip angle, 8.6 ms TR, 4.3 ms TE, 364 Hz/Px receiver bandwidth, 0 dummy scans per volume) for both knees of each HV with knee repositioning, qDESS and bSSFP were resolution- $(0.4 \times 0.4 \times 1.5 \text{ mm}^3 \text{ voxel volume}, 150 \times 150 \times 120 \text{ mm}^3$ field of view) and scan time-matched (5:05 min. for qDESS and 5:04 min for bSSFP). 4 separate phase-cycled bSSFP images were acquired with phase cycling increments [0°, 90°, 180°, 270°]. Parallel imaging was used (GRAPPA R=2 for bSSFP and qDESS with 24 reference lines; 6/8th phase/slice partial Fourier for bSSFP). Cartilage in qDESS images was segmented using DOSMA and those segmentation masks were used on the bSSFP images. Test-retest repeatability was calculated using the ICC and coefficient of variation (CoV) after removing outlier T2 estimates (T_2 < 20 ms, T_2 > 90 ms). The percentage of outlier estimates was also calculated. For quantitatively evaluating morphological image quality, SNR and CNR were calculated from the Root Sum of Squares (RSOS) of the two qDESS echos and four phase-cycled bSSFP images.

RESULTS: 1) In Fig1, RaFo-4 preserves cartilage T_2 spatial variations seen in qDESS T_2 maps (red and pink arrows indicate regions of low

and high T $_2$ values, respectively) and it produces visually smoother maps. While 10-20% of qDESS estimates are outliers, RaFo-4 estimates no outliers, a unique feature of the algorithm. RaFo-4 bSSFP shows good to excellent test-retest repeatability without estimating any outliers (ICC = 0.74-0.91, CoV = 2.01-3.58%) whereas qDESS shows excellent test-retest repeatability after removing outliers (ICC = 0.87-0.97, CoV = 1.48-1.61%). 2) RaFo-4 bSSFP has consistently higher SNRs and higher/comparable CNRs compared to qDESS (Tab1).

CONCLUSION: RaFo-4 bSSFP is a promising 5-minute alternative to qDESS as it provides more reliable cartilage T_2 maps and better morphological image quality. Future work includes testing both techniques on a larger cohort of HVs and early KOA patients and comparing performance.

SPONSOR: NIH (RO1EB002524), NIHR Imperial Biomedical Research Center

DICLOSURE STATEMENT: I have no disclosures.

ACKNOWLEDGMENT: I thank the participants for volunteering for this study.

CORRESPONDENCE ADDRESS: kb4317@ic.ac.uk

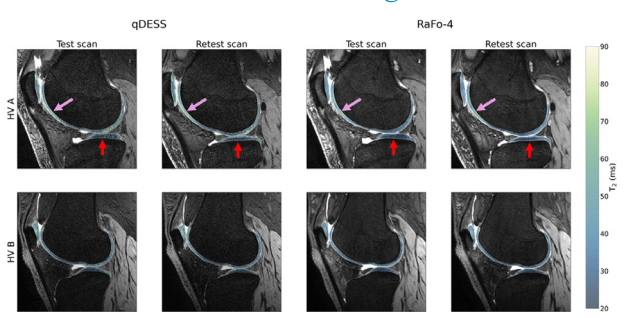


Fig. 1: qDESS and Rafo-4 test-retest cartilage T_2 maps. RaFo-4 has visually less noisier maps while preserving spatial variations in T_2 seen in qDESS maps (the red arrows show regions of low T_2 while the pink arrows show regions of high T_2).

Table 1: Comparison of SNR (a) and CNR (b) between qDESS and bSSFP RSOS images. bSSFP has better morphological image quality than qDESS as seen by how it has consistently higher SNRs than qDESS across the different cartilage regions and comparable or higher CNRs than qDESS across the different tissues.

SNR (a.	u.)		CNR (a.u.)				
Cartilage Regions	qDESS	bSSFP	Tissue Pairs	qDESS	bSSFP		
Femoral Cartilage (FC)	35	58	Cartilage-Muscle (C-M)	6	10		
Patellar Cartilage (PC)	38	64	Cartilage-Synovial Fluid (C-SF)	28	103		
Tibial Cartilage (TC)	26	43	Synovial Fluid-Muscle (SF-M)	26	101		
a.			b.				

¹ Imperial College London, London, UK

² Case Western Reserve University, Cleveland, OA, USA

³ Boise State University, Boise, ID, USA

COMPROMISED TRABECULAR BONE OF THE KNEE IS A DOSE-DEPENDENT CORRELATE OF MORE SEVERE OSTEOPHYTES AND ADVANCED KLG

A.K.O. Wong 1,2,3 , S. Costa 1,2 , D. Jain 1,2 , M.E. Hernandez 1,2 , A. Cagnoni 1,2 , S. Liu 1 , V. Anwari 1 , A. Naraghi 1 , R. Mohankumar 1 , J.D. Johnston 4 , L. Giangregorio 5

INTRODUCTION: Previous studies have shown that bone turnover is elevated, and fracture risk is higher among knee osteoarthritis (KOA) patients, especially in later stages of disease. While there have been mixed findings with respect to areal bone mineral density (BMD)'s association with KOA severity, it remains unclear how volumetric bone morphometry at the knee is related to the development of radiographic disease features such as osteophytosis and attrition.

OBJECTIVE: It was hypothesized that having definite osteophytosis and attrition are each associated with compromised subchondral bone, including lower volumetric(v) BMD, apparent v.Tissue Mineral Density (vTMD) and a wider Tb.Sp.

METHODS: In this cross-sectional study, women 50-85 years old were recruited by convenience sample if they experienced knee pain ≥ 3 days a week, each lasting >3 hours, and if self-reported body mass index (BMI) was <30 kg/m². On the knee with worse symptoms, they completed a peripheral quantitative CT (pQCT) knee scan, one slice (2.3±0.5mm, 200µm in-plane) prescribed per tibiofemoral compartment; and an anteroposterior knee X-ray for KLG, including breakdown semi-quantitative evaluation of osteophytosis, attrition, JSN, and sclerosis. pQCT knee images were analyzed using a previously reported iterative threshold-seeking algorithm (Tam et al. Skeletal Muscle 27(14) 2024) to separate trabecular bone from marrow. Apparent structural parameters were derived from bone volume, bone surface, and total volume according to equations by Parfitt's model of parallel plates. General linear models examined how KLG and osteophyte score, and each of established (score > 2) KOA (KL), osteophytosis, and attrition were related to knee vBMD, vTMD, app: Tb.Sp, Tb.Th, Tb.N, and BV/TV. Models adjusted for age, BMI, use of pain medications, antiresorptives, glucocorticoids or intra-articular steroid injections.

RESULTS: Among 105 women (mean(SD) age: 62.6(9.0)yrs, BMI: 24.2(3.5)kg/m², median KLG: 1(1,2), 41(39.1%) with established KOA), a higher KLG or established KOA were each associated with lower vBMD and vTMD (with effects larger for vTMD), and a larger app.Tb.Sp; though, only in advanced stage (KLG3/4) individuals (Table1). Attrition was only associated with larger Tb.Sp in the lateral femur. Having more advanced osteophytosis was dose-dependently linked to lower vBMD and larger app.Tb.Sp (Figure 1). These effects were only present at the femur and not the tibia, with magnitudes appearing larger in the

medial compartment among moderate grade (score 2) knees, but dose-dependently only in the lateral compartment.

CONCLUSION: Among peri- to post-menopausal women without obesity, compromised bone characterized by lower apparent bone density and less intact trabecular structure, may be key correlates of having more advanced radiographic KOA largely driven by osteophytosis. Structural differences may not be adequately apparent in the subchondral tibia using pQCT, perhaps due to damage that may simulate higher bone volume fraction. More sensitive techniques or metrics are needed to distinguish damaged bone from intact but diminished structures.

SPONSOR: CIHR 156274,166012 Arthritis Society 21-0035 *CORRESPONDENCE: andy.wong@uhn.ca

Table 1. Regression coefficients for general linear models examining each radiographic parameter's association with trabecular bone parameters at the knee.

Parameter	Site	BMD_Estimate	TMD_Estimate	TbSp_Estimate
KOA (established)	LatFem	-13.02(-25.30,-0.73)	-15.36(-31.24,0.52)	0.006(-0.002,0.014)
KLG 2 vs 0/1	LatFem	-14.03(-27.73,-0.32)	-19.05(-36.7,-1.40)	0.003(-0.006,0.012)
KLG 3/4 vs 0/1	LatFem	-10.63(-29.37,8.11)	-6.65(-30.78,17.47)	0.014(0.002,0.026)
Osteophyte (per +1)	LatFem	-8.33(-14.77,-1.89)	-7.84(-16.23,0.55)	0.006(0.001,0.010)
Osteophyte 2 vs 0/1	LatFem	-23.32(-40.85,-5.80)	-25.28(-48.09,-2.47)	0.008(-0.003,0.020)
Osteophyte 3 vs 0/1	LatFem	-24.09(-45.37,-2.81)	-18.53(-46.23,9.16)	0.021(0.007,0.035)
Sclerosis (established) Attrition	LatFem	1.45(-16.45,19.35)	10.71(-12.13,33.56)	0.012(0.001,0.024)
(established)	LatFem	-3.14(-26.71,20.42)	5.05(-25.16,35.26)	0.016(0.001,0.031)
KOA (established)	MedFem	-27.88(-49.31,-6.45)	-21.30(-56.30,13.70)	-0.004(-0.042,0.035)
KLG 2 vs 0/1	MedFem	-33.00(-56.82,-9.19)	-31.31(-70.12,7.50)	-0.007(-0.050,0.036)
Osteophyte 2 vs 0/1	MedFem	-31.52(-58.42,-4.63)	-2.17(-49.82,45.48)	0.014(-0.042,0.070)

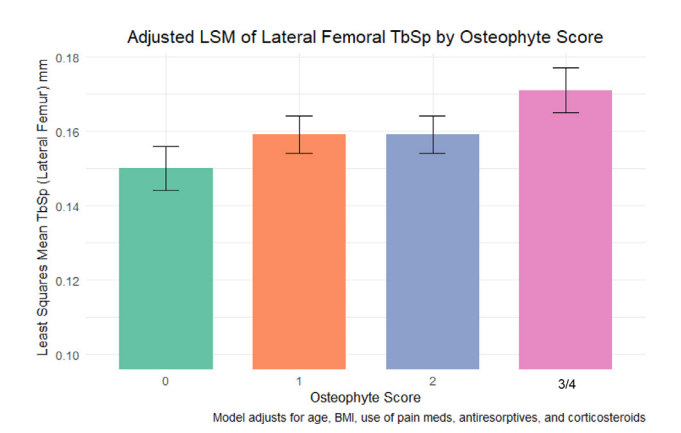


Figure 1. Comparison of Tb.Sp (least square means (LSM) adjusted for covariates) across osteophyte severity scores (0 to 3/4) as part of KL grading.

¹ Joint Department of Medical Imaging, University Health Network, Toronto, ON, Canada

² Schroeder Arthritis Institute, University Health Network, Toronto, ON, Canada

³ Dalla Lana School of Public Health, University of Toronto, Toronto, ON, Canada

⁴ Biomedical Engineering, University of Saskatchewan, Saskatoon, SK, Canada

 $^{^{\}rm 5}$ Department of Kinesiology, University of Waterloo, Waterloo, ON, Canada

EVALUATION OF DIFFERENT METHODS OF AUTOMATED 3-D JOINT SPACE MAPPING FROM WEIGHT BEARING CT SUGGESTS A TIBIAL MESH-TO-MESH APPROACH IS MOST SENSITIVE

N.A. Segal ¹, T. Whitmarsh ², N.H. Degala ¹, J.A. Lynch ³, T.D. Turmezei ⁴

- ¹ University of Kansas Medical Center, Kansas City, KS, USA
- ² University of Cambridge, Cambridge, UK
- ³ University of California San Francisco, San Francisco, CA, USA
- ⁴ Norfolk and Norwich University Hospital, Norwich, UK

INTRODUCTION: Weight bearing CT (WBCT) has the distinct advantage over radiography of being able to provide 3-D imaging of the knee joint while standing. It is also more practicable and better at depicting mineralized joint structures than MRI. Several different approaches to 3-D JSW measurement have been developed, but their repeatability has not been directly compared.

OBJECTIVE: To compare the test-retest repeatability of three different methods of 3-D joint space mapping (JSM) of the tibiofemoral compartment from WBCT imaging data.

METHODS: 14 individuals recruited and consented at the University of Kansas Medical Center had baseline and follow-up WBCT imaging suitable for analysis. Participant demographics were: mean \pm SD age 61.3 ± 8.4 years, BMI 30.7 ± 4.3 kg/m² and male:female ratio 8:6. All scanning was performed on the same XFI WBCT scanner (Planmed Oy, Helsinki, Finland) with the mean \pm SD interval between baseline and follow-up attendances 14.9 \pm 8.1 days. A Synaflexer TM device was used to standardize knee positioning during scanning. Imaging acquisition parameters were 96 kV tube voltage, 51.4 mA tube current, 3.5 s exposure time. A standard bone algorithm was applied for reconstruction with 0.3 mm isotropic voxels and a 21 cm vertical scan range. Both knees were included in all analyses with SD adjustments made for multiple observations from the same individual. Participant ID and scan sequence were anonymized prior to analyses. An algorithm based on U-net was implemented in C++ using LibTorch and integrated into ScanXM software for automatic segmentation of the femur and tibia from all knees. Three different JSM techniques were applied: (1) femur-to-tibia deconvolution in which the femur was the base (performed in Stradview); (2) tibia-to-femur deconvolution in which the same was done but from the tibia; and (3) tibia-to-femur mesh-to-mesh distance using a custom MAT-LAB script. Results from each technique were registered using wxReg-Surf and displayed on their average halfway joint space mesh (i.e. the middle plane of the joint space) using custom MATLAB scripts. Bland Altman descriptive statistics were calculated as 3-D bias (follow-up minus baseline) and limit of agreement (LOA) maps for all knees. Summary statistics also included root mean square coefficient of variation (RM-SCV) and LOA as a % of the mean.

RESULTS: 3-D bias and LOA maps for all knees are displayed on the halfway joint space patches as if viewing the right knee from the inferior aspect (Figure 1). Both deconvolution techniques showed similar noise patterns of bias around a zero value, while the mesh-to-mesh technique suggested systematically wider anterior and narrower posterior JSW at follow-up, but this was of sub-millimeter magnitude. Both deconvolution techniques also showed a pattern of worsening LOA towards the joint space patch margins, recognized as where errant or null values can

be exaggerated by data smoothing. Mesh-to-mesh LOA was more robust across the whole joint space. When comparing repeatability measures for KLG < 2 and KLG = 2 groups (Table 1), LOAs from the whole joint space were similar for all techniques, ranging from 1.29 to 1.46 mm across groups, while the best LOA value of 0.13 mm was seen in the mesh-to-mesh KLG = 2 group at the inner aspect of both compartments.

CONCLUSION: Although differences between the three approaches to JSM were subtle, a tibial-based mesh-to-mesh technique may be more robust, in particular at the margins of the joint space. This approach also appeared to have a greater potential sensitivity for detecting smaller changes in JSW from having the lowest LOA (thus smallest detectable difference) in individuals with KLG=2, an important stratification in OA clinical trials before structural disease is too severe. However, the caveat for a mesh-to-mesh approach to JSM derived from segmentation is that it relies on the accuracy of the segmentation technique that may vary between approaches, whereas a deconvolution approach has been proven to be accurate and is only marginally less repeatable.

SPONSOR: None.

DISCLOSURE STATEMENT: NS is a consultant for Trice Medical, Arthrex, and Pacira Biosciences. TT is the director of KNEE3D Ltd. TW is director of Minogame Ltd.

ACKNOWLEDGEMENT: None.

CORRESPONDENCE ADDRESS: nsegal@kumc.edu

Figure 1

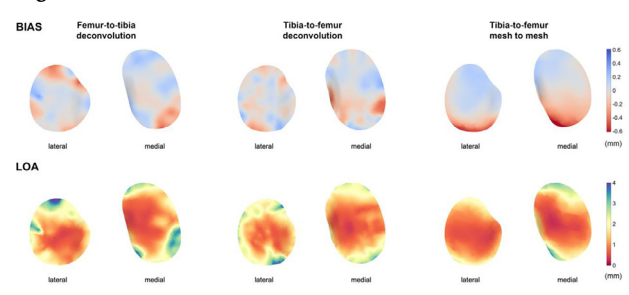


Table 1

	Femur-to-tibia deconvolution algorithm		Tibia-to-femo deconvolutio		Tibia-to-femur mesh-to-mesh distance	
	KLG < 2	KLG = 2	KLG < 2	KLG = 2	KLG < 2	KLG = 2
N of knees (pairs)	10 (3)	6 (1)	10 (3)	6 (1)	10 (3)	6 (1)
Mean ± SD (mm)	6.09 ±	5.56 ±	$6.21 \pm$	5.55 ±	$6.72 \pm$	5.82 ±
	1.72	1.89	1.73	1.86	2.40	2.16
Bias (mm)	-0.03	-0.05	0.01	0.08	-0.04	0.04
LOA (mm)	1.42	1.29	1.41	1.46	1.40	1.44
LOA lower	-1.45	-1.24	-1.40	-1.38	-1.44	-1.40
(range)	(-1.48,-	(-1.27,-	(-1.42,-	(-1.42,-	(-1.47,-	(-1.44,-
	1.42)	1.20)	1.37)	1.35)	1.41)	1.37)
LOA upper (range)	1.40	1.33	1.42	1.54	1.35	1.48
	(1.37, 1.42)	(1.30, 1.37)	(1.40, 1.45)	(1.50, 1.57)	(1.31, 1.37)	(1.45, 1.52)
LOA min. (mm)	0.35	0.21	0.21	0.19	0.23	0.13
LOA (% of mean)	19.9	26.4	21.0	24.6	20.2	20.8
RMSCV (%)	8.2	8.4	7.8	10.7	6.7	7.6

PHASE II RCT OF LEVI-04, A NOVEL NEUROTROPHIN-3 INHIBITOR, IN PEOPLE WITH KNEE OSTEOARTHRITIS: IMAGING EXCLUSIONS DURING SCREENING

A. Guermazi 1 , P.G. Conaghan 2 , C.M. Perkins 3 , C. Herholdt 3 , I. Bombelka 3 , S.L. Westbrook 3

Introduction: LEVI-04 is a first-in-class fusion protein (p75NTR-Fc) that supplements the endogenous p75NTR binding protein, providing analgesia via inhibition of NT-3 activity. Like p75NTR, LEVI-04 binds all the neurotrophins (NTs) with differing affinities, with highest to NT-3 and lowest affinity and reversibly to NGF, distinguishing the LEVI-04 mechanism of action from that of anti-NGF antibodies. As serious joint adverse events were seen in the anti-NGF trials, rigorous surveillance of joint safety was performed in this study. In order to properly categorise the risk of adverse joint events with LEVI-04, participants with potentially confounding findings at screening were excluded. LEVI-04 was well tolerated, with no increased incidence of joint pathologies compared to placebo. ¹

Methods: This was a phase II multicentre (Europe and Hong Kong) RCT in adults with knee OA. Participants were randomized to 4-weekly IV placebo or 0.3, 1, or 2 mg/kg LEVI-04 through week 16, with the final visit at week 20 and a telephone safety follow-up at week 30. Participants who met initial clinical inclusion criteria underwent X-rays of bilateral shoulders, hips and knees, and then MRI of both knees (in some cases, MRI was performed in parallel with X-rays). All images were read centrally and assessed for eligibility. At week 20, all X-rays were repeated, and MRI of the target knee was performed.

Results: 1598 people with painful knees were screened and 518 participants enrolled. 1080 people (86%) did not proceed past screening. 345 people exited the study before X-rays were performed (151 due to not meeting initial minimum pain in at least one knee, others due to other entry criteria, or sponsor, investigator or participant decision), such that a total of 1253 participants had X-rays of the large joints (Table 1). 514 (41%) people had knee exclusion criteria on X-ray, however this included 207 (left) and 188 (right) knees of KL grade<2. Only one knee was required to have KL grade >2, resulting in 108 (8.6%) people failing on KL grade. Excessive malalignment and atrophic OA were the next highest criteria, with 43 (3.4%) and 42 (3.3%) failures respectively. 766 people proceeded to MRI of both knees. 234 (30.5%) of these failed, 168 (22.9%) due to meniscal root tear, and 42 (5.4%) due to subchondral insufficiency fracture. There were 7 (0.9%) cases of findings suggestive of primary or metastatic tumor detected on MRI and 1 (0.1%) on knee X-ray. 30 (2.4%) people were excluded on hip and 4 (0.3%) on shoulder X-rays. 5 hip and 24 knee joints had arthroplasty, but these were not exclusionary. Several people exhibited more than one pathology, so reasons for exclusion slightly exceed the total number of people excluded.

Conclusion: A significant proportion of people with OA show radiologic findings at screening. Excluding these patients is important to distinguish existing pathologies from treatment-emergent events in early tri-

als. Rigorous radiologic surveillance supported determination of LEVI-04 joint safety; LEVI-04 was not associated with an increase in adverse joint events compared to placebo in this study¹. Phase 3 trials are in planning.

SPONSOR: Levicept Ltd

DISCLOSURE STATEMENT: AG, PC consult for; SLW, PCM, CH, IB are employees of; Levicept Ltd.

ACKNOWLEDGMENTS: Igor Avdejev, IAG Ltd, for technical support CORRESPONDENCE ADDRESS: simon@levicept.com

Table 1. Imaging Exclusions

	X-Ray			MRI
	Knees	Hips		Knees
			Shoulders	
Number of Participants with Imaging	1253	1253	1253	766
Performed, n				
Number of Participants Excluded, n (%)	514^{1}	30 (2.4)	4 (0.3)	234
	(41.0)			(30.5)
Reasons for exclusion ² , n (%)				
Posterior Meniscal Root Tear	0	N/A	N/A	168
				(22.9)
KL<2 in the target knee	108 (8.6)	N/A	N/A	N/A
Excessive Malalignment	43 (3.4)	N/A	N/A	0
Atrophic OA	42 (3.3)	7 (0.6)	0	0
Subchondral Insufficiency Fracture	19 (1.5)	0	2 (0.3)	42 (5.4)
Congenital Hip Dysplasia with	N/A	12 (1.6)	N/A	N/A
Degenerative Joint Disease				
Articular Bone Fragmentation	6 (0.5)	2 (0.3)	0	3 (0.4)
Inflammatory Joint Disease	0	0	0	10 (1.3)
Primary/Metastatic Tumor ³	1 (0.1)	0	0	7 (0.9)
Severe Pseudogout	7 (0.6)	1 (0.1)	0	0
Extensive Subchondral Cysts	6 (0.5)	4 ()	0	3 (0.4)
Stress Fracture/Reaction	0	0	0	6 (0.8)
Osteochondritis Dissecans	1 (0.1)	0	0	3 (0.4)
Osteonecrosis	0	4 (0.3)	0	4 (0.5)
Recent Fracture	0	1 (0.1)	1 (0.1)	5 (0.7)
Paget's Disease	0	1 (0.1)	0	0
Significant Articular Bone Loss	1 (0.1)	0	0	0
Synovial chondromatosis	1 (0.1)	0	0	4 (0.5
Severe bone marrow reconversion	0	0	0	2 (0.3)
Enchondroma (large)	1 0.1)	0	0	1 (0.1)
Hereditary Multiple	$2(0.3)^4$	$1(0.1)^4$	$1(0.1)^4$	0
Osteochondromatosis (HMO) ⁴				
Heterotopic Ossification	1 (0.1)	0	0	0
Lipoma (large)	0	0	0	1 (0.1)
Medial Meniscal Cyst (large, complex)	0	0	0	1 (0.1)
Chronic Osteomyelitis	0	0	0	1 (0.1)

 $^{^1}$. Includes 207 (left knee) and 188 (right knee) exclusions for KL<2; for inclusion only one knee was required to meet KL \geq 2, therefore the final number excluded due to KL <2 was 108.

¹ Boston University School of Medicine, Boston, MA, USA

² University of Leeds, Leeds, UK

³Levicept Ltd, Sandwich, Kent, UK

² Some patients presented more than one finding, potentially in more than one joint in the same patient, so the number of exclusions exceeds the number of people excluded.

³ Findings suggestive of the following tumors were detected on X-ray: large benign bone tumor of the femur (unicameral bone cyst) with risk of pathological fracture (1); and on MRI: tenosynovial giant cell tumor of the Hoffa-fat pad (4), tenosynovial giant cell tumor of the patellar tendon (1), tenosynovial giant cell tumor around the knee (1) and large benign enchondroma of the femur (with possibility of low grade chondrosarcoma).

 $^{^{\}rm 4}$ $\,$ HMO was reported for knees (bilateral), hip, and shoulder X-rays for one patient.

LEVI-04 REDUCES BONE MARROW LESION AREA AND PRESENCE IN KNEE OSTEOARTHRITIS: RESULTS FROM A PHASE II RCT

S.L. Westbrook 1, A. Guermazi 2, P.G. Conaghan 3

- ¹ Levicept Ltd, Sandwich, Kent, UK
- ² Boston University School of Medicine, Boston, MA, USA
- ³ University of Leeds, Leeds, UK

INTRODUCTION: Bone marrow lesions (BMLs), detectable on MRI as areas of ill-defined high signal intensity on fluid-sensitive sequences, are a common feature of osteoarthritis (OA), representing areas of increased bone turnover, oedema, and fibrosis. BMLs are prevalent in ~80% of symptomatic knee OA patients, correlate with radiographic severity (Kellgren-Lawrence [KL] grade) and knee pain. Changes in BMLs are associated with fluctuations in knee pain. Excess neurotrophins (NTs) are implicated in OA pain. LEVI-04, a first-in-class p75NTR-Fc fusion protein that supplements endogenous p75NTR, provides analgesia primarily via inhibition of neurotrophin-3 (NT-3) activity. In this Phase II RCT. LEVI-04 demonstrated statistically significant and clinically meaningful improvements versus placebo for the primary endpoint (WOMAC pain) and secondary endpoints including WOMAC physical function and stiffness, patient global assessment (PGA) and pain on movement (StEPP) across all doses. LEVI-04 was generally well tolerated, with no increased incidence of SAEs, TEAEs, or AESIs concerning joint pathologies compared to placebo.1

OBJECTIVE: This analysis investigated LEVI-04's effects on BMLs in people with painful knee OA.

METHODS: 518 participants with symptomatic knee OA (WOMAC pain $\geq 4/10$, KL grade ≥ 2) were enrolled in a Phase II multicentre randomized double-blinded placebo-controlled trial. Participants received placebo or LEVI-04 (0.3, 1, or 2 mg/kg) every 4 weeks through week 16. BML area (mm²) was measured in a blinded fashion from coronal proton density-weighted fat-suppressed (PD-FS) sequences (slice thickness 3 mm, TE/TR 35/3000 ms) of the target knee at baseline and week 20. For each participant, the BML area was determined as the largest area within the MRI sequence of ill-defined high signal intensity of the subchondral bone marrow, and without presence of a fracture line. The perimeter of each BML was highlighted and the area measured electronically using IAG Dynamika SoftwareTM. For BML presence, participants were categorized as BML positive if one or more lesions were identified in the target knee. The presence of BML and change in BML area were assessed in response to LEVI-04.

RESULTS: BML area was greater in knees with higher KL grade (figure 1). The presence of BMLs at baseline was similar across treatment and placebo groups (74-79%). At week 20, there was a significant and dose-dependent reduction in the proportion of patients with BMLs in the LEVI-04 groups (figure 2). Furthermore, a statistically-significant, dose-dependent reduction in mean BML area from baseline to week 20 was observed in LEVI-04 groups compared to placebo (figure 3).

CONCLUSION: In this Phase II trial, a statistically significant and dose-dependent reduction in both the presence of BMLs and BML area was seen for all LEV-04 treatment groups compared with placebo following 20 weeks of treatment. These findings suggest LEVI-04 may have structure-modifying potential in addition to providing analgesia. LEVI-04 holds promise as potentially the first therapy to demonstrate modification of structure (BMLs) and symptoms of OA.

SPONSOR: Levicept Ltd

DISCLOSURE STATEMENT: SLW is an employee of Levicept Ltd. AG and PC provide consulting services to Levicept Ltd.

ACKNOWLEDGMENTS: IAG Ltd for imaging and Kerry af Forselles for medical writing support

CORRESPONDENCE ADDRESS: simon@levicept.com

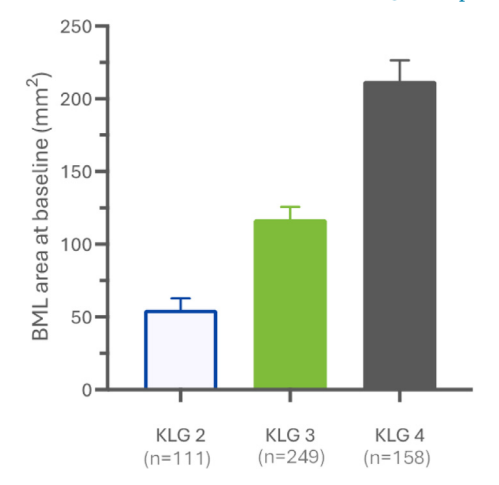


Figure 1. BML area (mm²) at baseline versus KL-grade for target knee.

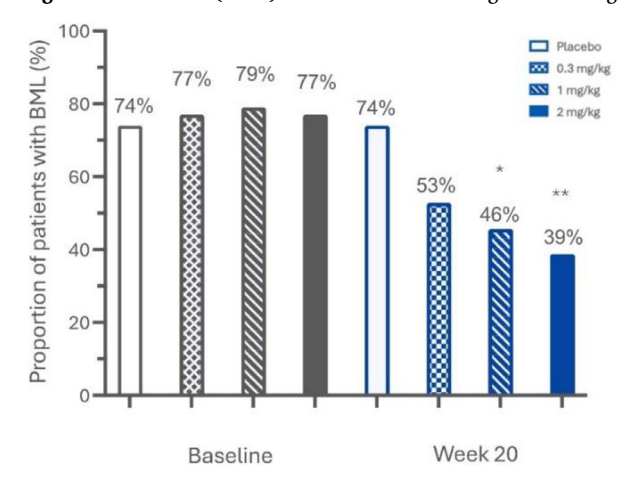


Figure 2. Proportion of participants with bone marrow lesions at baseline and week 20. *P<0.05; **P<0.01 vs placebo.

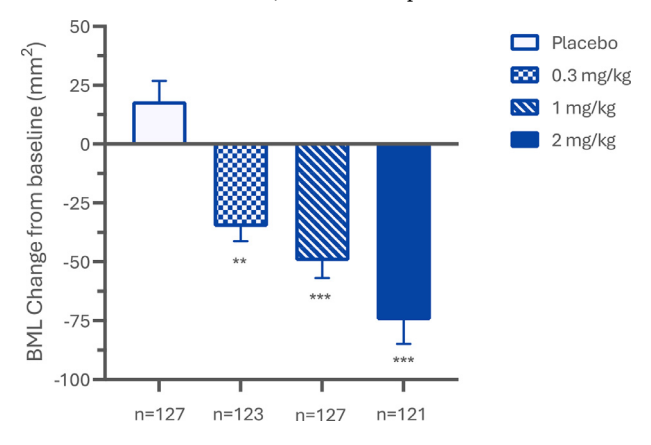


Figure 3. Change from baseline in bone marrow lesion area (mm^2) in placebo or LEVI-04 0.3, 1 or 2 mg/kg groups at week 20. **P<0.01; ***P<0.001 vs placebo.

BEYOND ACETABULAR DYSPLASIA AND PINCER MORPHOLOGY: REFINING HIP OSTEOARTHRITIS RISK ASSESSMENT THROUGH STATISTICAL SHAPE MODELING

F. Boel ¹, M.A. van den Berg ¹, N.S. Riedstra ¹, M.M.A. van Buuren ¹, J. Tang ¹, H. Ahedi ², N. Arden ³, S.M.A. Bierma-Zeinstra ¹, C.G. Boer ¹, F.M. Cicuttini ⁴, T.F. Cootes ⁵, K.M. Crossley ⁶, D.T. Felson ⁷, W.P. Gielis ⁸, J.J. Heerey ⁶, G. Jones ², S. Kluzek ³, N.E. Lane ⁹, C. Lindner ⁵, J.A. Lynch ¹⁰, J.B.J. van Meurs ¹, A. Mosler ⁶, A.E. Nelson ¹¹, M.C. Nevitt ¹⁰, E.H. Oei ¹, H. Weinans ⁸, J. Runhaar ¹, R. Agricola ¹

- ¹ Erasmus Medical Center, Rotterdam, The Netherlands
- $^{2}\ University$ of Tasmania Menzies, Hobart, Tasmania, Australia
- ³ University of Oxford Nuffield, Oxford, Oxfordshire, UK
- ⁴ Monash University, Melbourne, Victoria, Australia
- ⁵ The University of Manchester, Manchester, UK
- ⁶La Trobe Sport and Exercise Medicine Research Centre, La Trobe University School of Allied Health Human Services and Sport, Melbourne, Victoria, Australia
- ⁷ Boston University School of Medicine, Boston, MA, USA
- ⁸ UMC Utrecht, Utrecht, Netherlands
- ⁹ University of California Davis School of Medicine, Sacramento, CA, USA
- 10 University of California San Francisco, San Francisco, CA, USA
- ¹¹ The University of North Carolina at Chapel Hill, Chapel Hill, NC, USA

INTRODUCTION: Hip morphology has been recognized as an important risk factor for the development of hip OA. In previous studies within the Worldwide Collaboration on OsteoArthritis prediction for the Hip consortium (World COACH), both acetabular dysplasia (AD) and pincer morphology—characterized by acetabular under- and overcoverage of the femoral head—were associated with the development of radiographic hip OA (RHOA) within 4-8 years, with an odds ratio (OR) of 1.80 (95% confidence interval (CI) 1.40-2.34) and 1.50 (95% CI 1.05-2.15), respectively. However, we know that not everyone with AD or pincer morphology will develop RHOA. Specific baseline characteristics or variations in hip shape among individuals with AD and pincer morphology may influence their risk of developing RHOA. Statistical shape models (SSM), describing the mean hip shape of a population and a range of independent shape variations, can be utilized to study these variations in hip shape.

OBJECTIVE: To evaluate whether specific hip shape variations or baseline characteristics within individuals with either AD or pincer morphology are associated with the development of RHOA within 4-8 years.

METHODS: We pooled individual participant data from seven prospective cohort studies within the World COACH consortium. Standardized anteroposterior (AP) pelvic radiographs were obtained at baseline and within 4-8 years follow-up. RHOA was scored by KLG or (modified) Croft grade. We harmonized the RHOA scores into "No OA" (KLG/Croft = 0), "doubtful OA" (KLG/Croft = 1), or "definite OA" (KLG/Croft \geq 2 or total hip replacement). The Wiberg center edge angle (WCEA), measuring the weight-bearing femoral head coverage, and the lateral center edge angle (LCEA), measuring the bony femoral head coverage, were automatically determined using a validated method. Hips were included if they had baseline and follow-up RHOA scores, no RHOA at baseline, and either AD defined by a WCEA ≤ 25° or pincer morphology defined by a LCEA ≥45°. For both populations, an SSM was created of the acetabular roof, posterior wall, femoral head and neck, and teardrop (Fig 1). We analyzed the first 13 shape modes that explained around 90% of total shape variation in the population. The association between each shape mode, sex, baseline age, BMI, diabetes and smoking habits, and the development of RHOA was estimated using univariate generalized linear mixed-effects models. The mixed effects were added to account for the potential clustering within cohorts and participants. The results were expressed as ORs with 95% CIs.

RESULTS: The AD population consisted of 4,737 hips, of which 2.6% developed incident RHOA (Table 1). Four of the 13 shape modes (Fig 1) were associated with the development of RHOA. Additionally, in hips with AD, females had higher odds of incident RHOA than males (OR

2.85, 95% CI 1.46-5.58), and each year increase in baseline age was associated with higher odds of incident RHOA (OR 1.05, 95% CI 1.02-1.09). Neither baseline BMI, diabetes, nor smoking habits were associated with RHOA within people with AD. The pincer morphology population comprised 1,118 hips, of which 2.8% developed incident RHOA. Only one of the shape modes was associated with incident RHOA (Fig 1). Sex, baseline age, BMI, diabetes, and smoking habits were not associated with RHOA within people with pincer morphology.

CONCLUSION: Variations in shape among individuals with AD and pincer morphology contribute to the odds of developing RHOA. In individuals with AD, both sex and baseline age were also associated with RHOA development. However, this was not observed in those with pincer morphology. These findings may inform the development of personalized risk assessment tools and preventative strategies for hip OA.

SPONSOR: The Dutch Arthritis Society (grant no. 18-2-203 and 21-1-205), the Dutch Research Council (NWO Veni grant scheme no. 09150161910071) and the Erasmus MC, University Medical Center, Rotterdam (Erasmus MC Fellowship), Wellcome Trust and Royal Society (223267/Z/21/Z).

DICLOSURE STATEMENT: We have nothing to disclose.

ACKNOWLEDGMENT: We would like to thank all participants and researchers of the cohort studies for their contribution.

CORRESPONDENCE ADDRESS: f.boel@erasmusmc.nl

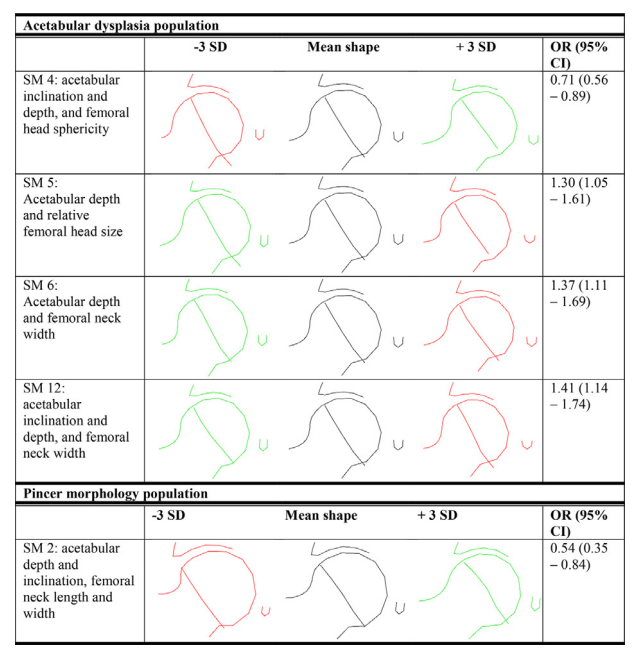


Figure 1: Shape modes (SM) visualization and interpretation of the shape modes associated with RHOA development within 4-8 years for hips with acetabular dysplasia or pincer morphology at baseline. The odds ratios (OR) are per 1 standard deviation (SD) increase in shape mode value.

Table 1: Baseline characteristics.

Population	Participants,	Hips, n	Female,	Age	BMI	Diabetes,	Smoking	g, n (%)
	n		n (%)	[years], mean (SD)	[kg/m ²], mean (SD)	n (%)	Current	Former
Acetabular	3512	4691	3343	60.8 (8.2)	27.6 (4.4)	180 (4)	653	1550
dysplasia			(71)				(14)	(33)
Pincer mor-	930	1108	801	64.5 (8.5)	27.2 (4.4)	56 (5)	145	371
phology			(72)				(13)	(34)

Numbers and percentages for baseline characteristics are presented at a hip level. SD: standard deviation. BMI: body mass index.

NEURAL SHAPE MODEL QUANTIFIES EARLY AND PROGRESSIVE BONE SHAPE CHANGES AFTER ACLR

S.A. Pai, M. Black, K. Young, S. Sherman, C. Chu, A. Williams, G. Gold, F. Kogan, B. Hargreaves, A. Chaudhari, A. Gatti

Stanford University, Stanford, CA, USA

INTRODUCTION: Femoral bone shape scores (B-Score) derived from shape models quantify 3D structural features associated with OA^{1,2}. A higher B-Score is indicative of more OA-like bone shape. B-Scores have high sensitivity to quantify OA progression and stratify patients for interventions¹. Neural Shape Models (NSM) capture non-linear bone shape features and outperform traditional Statistical Shape Models (SSMs) in encoding OA-related shapes³. Prior work that used a SSM-based B-Score showed that anterior cruciate ligament reconstructed (ACLR) knees exhibit higher B-Scores than their contralateral knees 2 years post-surgery, reflecting OA-like bone shape features⁴. However, little is known about how femoral bone shape changes immediately following ACLR and how it progresses during the early post-surgical period—a critical window when post-traumatic osteoarthritis (PTOA) may still be most responsive to intervention.

OBJECTIVE: To use a Neural Shape Model-based B-Score to quantify femoral shape differences between ACLR and contralateral knees immediately post-surgery (3-weeks) and to detect early PTOA bone shape changes over 30 months.

METHODS: ACLR and contralateral knees of 17 subjects (11M/6F, age=38±10 yrs, BMI=24±2 kg/m²) were scanned at 3 weeks (baseline), 3, 9, 18, and 30 months post-ACLR in a 3T MRI scanner (GE Healthcare, USA) using a qDESS sequence (TE/TR=6/22 ms. flip angle=25°, $FOV=160 \times 160$ mm, bandwidth=31.25 kHz, pixel spacing=0.42 \times 0.50 mm, slice thickness=1.5 mm). The femur was automatically segmented, and the B-Score was computed for each subject at all visits using a NSM that was trained on 9,376 femoral segmentations from the baseline DESS images in the OAI dataset1. To assess bone shape differences immediately after surgery, we compared B-Scores between the ACLR and contralateral knees at the baseline visit using a linear mixed effects model. To capture longitudinal bone shape changes after surgery, we calculated change in B-Score at each follow-up visit with respect to the baseline visit. We used a linear mixed effects model to assess the effect of kneetype and time post-surgery on B-Scores. Effect sizes $[\eta_p^2]$ is small (0.01), medium (0.06), or large (0.14)] were computed for significant effects

RESULTS AND DISCUSSION: At baseline, the ACLR knee B-Score was significantly lower than the contralateral knee (η_p^2 =0.40, p=0.005; Fig. 1A). Longitudinally, ACLR knees showed a significantly greater increase in B-Score than contralateral knees (η_p^2 =0.19, p<0.001; Fig 2A). The lower B-Scores in ACLR knees at baseline indicate that the surgical knee had a healthier, less OA-like bone shape than the contralateral knee. Visualization revealed that ACLR knees had a wider intercondylar notch compared to their contralateral knee resulting from notchplasty that were confirmed on surgical notes (Fig. 1B). Since idiopathic OA-like features typically include notch narrowing², the surgically altered geometry, particularly the widened intercondylar notch yields a shape less characteristic of OA, resulting in a lower B-Score. Longitudinally, however, we observe early osteophyte lipping, particularly in the trochlea, intercondylar notch, and medial-posterior condyle-bone shape changes that align with idiopathic OA and likely explain the steep increase in B-Score for ACLR knees over time (Fig. 2B and C).

CONCLUSION: Neural shape modeling characterizes femoral shape changes due to ACLR surgery. Accounting for surgically induced shape changes enables detection of OA-like features as early as 3 months post-ACLR and enhances sensitivity to track these changes longitudinally, potentially serving as a sensitive biomarker for early detection and monitoring of PTOA.

SPONSOR: NIH, CIHR, Stanford Graduate Fellowship, Wu Tsai Human Performance Alliance.

DICLOSURE STATEMENT: A.C. has provided consulting services to Patient Square Capital, Chondrometrics GmbH, and Elucid Bioimaging; is co-founder of Cognita; has equity interest in Cognita, Subtle Medical, LVIS Corp, Brain Key. A.G is a shareholder of NeuralSeg, GeminiOV, and NodeAI.

CORRESPONDENCE ADDRESS: anoopai@stanford.edu

REFERENCES:

- [1] Bowes, M.A. et al. Ann Rheum Dis 80, 502-508 (2021).
- [2] Gatti, A.A. et al. IEEE Transac on Medical Imaging 1-1 (2024).
- [3] Gatti, A.A., et al. Osteoarthritis Imaging 3, 100101 (2023).
- [4] Williams, A.A. et al. Am J Sports Med 51, 3677-3686 (2023).

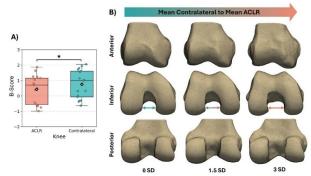


Figure 1: Neural Shape Model based analysis of the femur bone of ACLR and contralateral knees 3-weeks following surgery. A) The B-Score in ACLR knees was significantly lower compared to the contralateral knees $(\eta_p^2=0.40,\ p=0.005)$. B) Neural shape model visualizations illustrate the transition from the mean contralateral femur (0 SD) to the mean ACLR femur shape (3 SD). The most prominent shape difference is a widening of the intercondylar notch (indicated by double-sided allow) in the ACLR knees—consistent with surgical alterations such as notchplasty. Since idiopathic OA-like bone shape features typically include notch narrowing, the surgically altered geometry leads to an initially healthier looking bone shape and thus lower B-Score. ACLR=Anterior cruciate ligament reconstruction. OA=Osteoarthritis. SD=Standard deviation. * indicate statistically significant difference (p<0.05).

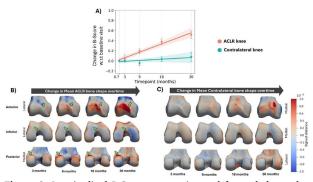


Figure 2: Longitudinal B-Score progression and femoral shape changes in ACLR and contralateral knees with respect to baseline (3-weeks post-ACLR). A) ACLR knees exhibit a significant (η_p^2 =0.19, p<0.001) increase in B-Score compared to contralateral knees from 3 to 30 months after surgery. B and C) Neural shape model-based visualizations of the mean bone shape at each follow-up timepoint. The colormap is the signed distance of the bone surface at a given visit relative to baseline. Red indicates outward protrusion from baseline (i.e., osteophyte growth), blue indicates surface contraction. B) The visualization reveals that bone shape changes in ACLR knees begin as early as 3 months post-surgery and show continual OA-like progression, particularly in the trochlear region, intercondylar notch, and medial posterior condyle (green arrows) over 30 months. C) The contralateral knees show minimal, random, and spatially diffused shape changes over the same period, that are not consistent and progressive as in the ACLR knees.

ADVANCING HIP OSTEOARTHRITIS PREDICTION: INSIGHTS FROM MULTI-MODAL PREDICTIVE MODELING WITH INDIVIDUAL PARTICIPANT DATA OF THE WORLD COACH CONSORTIUM

M.A. van den Berg 1 , F. Boel 1 , M.M.A. van Buuren 1 , N.S. Riedstra 1 , J. Tang 1 , H. Ahedi 2 , N. Arden 3 , S.M.A. Bierma-Zeinstra 1 , C.G. Boer 1 , F.M. Cicuttini 4 , T.F. Cootes 5 , K.M. Crossley 6 , D.T. Felson 7 , W.P. Gielis 8 , J.J. Heerey 6 , G. Jones 2 , S. Kluzek 3 , N.E. Lane 9 , C. Lindner 5 , J.A. Lynch 10 , J.B.J. van Meurs 1 , A. Mosler 6 , A.E. Nelson 11 , M.C. Nevitt 10 , E.H. Oei 1 , J. Runhaar 1 , H. Weinans 8 , J.H. Krijthe 12 , R. Agricola 1

INTRODUCTION: Radiographic hip osteoarthritis (RHOA) is a multifactorial disease, making early detection of individuals at risk challenging yet essential for timely intervention and evaluation of preventive strategies. Integrating information on multiple different data modalities using individual participant data from diverse cohorts may enhance predictive modeling in the early stages of RHOA. A focus on model interpretability may further enable the identification of clinically relevant patient subgroups and potential intervention targets.

OBJECTIVE: Creating a multi-modal prediction model for improving the performance of RHOA incidence prediction models compared to clinical features alone, and investigating the estimated predictor effects and the generalizability of the models to similar populations.

METHODS: We pooled individual participant data from nine prospective cohort studies within the Worldwide Collaboration on OsteoArthritis prediCtion for the Hip (World COACH consortium). All studies included standardized anteroposterior pelvic, long-limb, and/or hip radiographs, assessed for RHOA at baseline and after 4-8 years of follow-up. Incident RHOA was defined as the development of RHOA (grade \geq 2) in hips without definite RHOA at baseline (grade <2). The original cohort values of clinical predictors including age, birth-assigned sex, body mass index (BMI), smoking status, diabetes, and hip pain were harmonized into one consistent dataset. X-ray-derived predictors describing the hip morphology, the alpha angle and the lateral center edge angle, were automatically and uniformly determined using automated landmark points placed with Bonefinder®. Additionally, the values of 13 shape modes explaining 85% of the variation from a landmark-based statistical shape model were included. This SSM was built on all baseline RHOA grade <2 hips within World COACH. Risk prediction models were built with generalized linear mixed effects models (GLMM) and Random Forest (RF) models while adjusting for correlations within cohorts and individuals. The discriminative performance (AUC) of different model configurations and the linear versus non-linear approaches were compared through stratified 5-fold cross-validation. For each model configuration, predictions were made with and without cohort labels to assess heterogeneity between cohorts.

RESULTS: In total, 29,110 hips without definite RHOA at baseline were included of which 5.0% developed RHOA within 4-8 years (mean age 63.7 (8.6) years, 75.5% female, mean BMI 27.5 (4.7) kg/m²). When comparing our uni-modal prediction model using only the clinical predictors (Model 1) to those with X-ray information added (Table 1), we observed a higher discriminative performance for the multi-modal models. Overall, including cohort information significantly improved model

performance (p < 0.05), and the RF models have a slightly but not significantly better performance than the GLMMs. Comparing the average effects of the significant predictors of the models including all predictors on incident RHOA (Figure 1), showed most differences between the GLMM and RF estimated effects at the maximum and minimum predictor values.

CONCLUSION: By leveraging multi-modal data, we could improve our predictions of incident RHOA compared to clinical features alone. Our findings indicate that there would be a benefit for considering non-linear modeling approaches for this task in future work.

SPONSOR: The Dutch Arthritis Society (grant no. 18-2-203 and 21-1-205), the Dutch Research Council (NWO Veni grant scheme no. 09150161910071) and the Erasmus MC, University Medical Center, Rotterdam (Erasmus MC Fellowship), Wellcome Trust and Royal Society (223267/Z/21/Z).

DISCLOSURE STATEMENT: We have nothing to disclose.

ACKNOWLEDGMENT: We would like to thank all staff, team members, and participants of the cohorts studies for their contribution.

CORRESPONDENCE ADDRESS: m.a.vandenberg@erasmusmc.nl

Table 1. Model performance through stratified 5-fold cross-validation for the generalized linear mixed model and random forest models.

Predictions made using	AUC mean (SD)					
	GLMM		RF			
	cohort-specific intercept	Marginal intercept	cohort labels	no cohort labels		
Model						
Baseline age, sex, BMI, smoking status, diabetes, hip pain	0.72 (0.02)	0.50 (0.01)	0.73 (0.05)	0.54 (0.03)		
2) Model 1 + RHOA grade + AA + LCEA*	0.79 (0.01)	0.69 (0.02)	0.82 (0.03)	0.73 (0.03)		
3) Model 1 + RHOA grade + 13 SSM shape modes	0.80 (0.01)	0.69 (0.02)	0.82 (0.05)	0.74 (0.05)		
4) Model 2+13 SSM shape modes	0.80 (0.01)	0.69 (0.01)	0.82 (0.05)	0.75 (0.05)		

AUC: Area under the ROC curve, GLMM: generalized linear mixed effects model, RF: random forest model, BMI: Body Mass Index, AA: alpha angle, LCEA: lateral center edge angle.

* variable with natural cubic spline (df=2) transformation in GLMM.

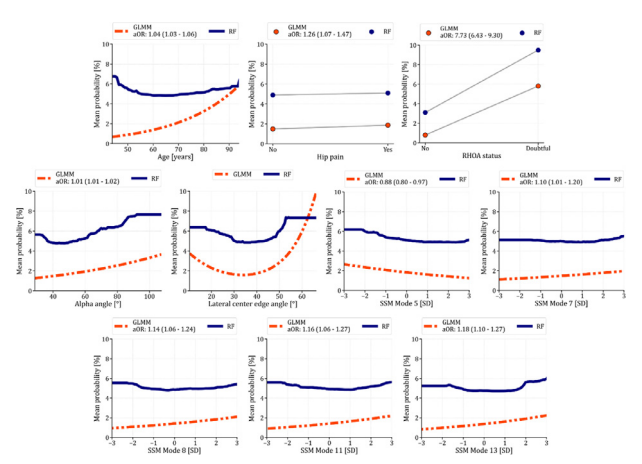


Figure 1. Partial dependence plots for significant predictors in model identified by the generalized linear mixed model (GLMM). Dashed orange lines indicate predictions from the GLMM, solid blue lines represent those from the random forest (RF). Each point on the x-axis shows the average predicted incident RHOA probability across all included hips, with the other 21 predictors held constant. If applicable, adjusted odds ratios (aORs) and their 95% confidence interval estimated by the GLMM are shown in the legend and correspond to the same units as the x-axis in the subsequent plot.

¹ Erasmus Medical Center, Rotterdam, The Netherlands

 $^{^2}$ University of Tasmania Menzies, Hobart, Tasmania, Australia

³ University of Oxford Nuffield, Oxford, Oxfordshire, UK

⁴ Monash University, Melbourne, Victoria, Australia

⁵ The University of Manchester, Manchester, UK

⁶La Trobe Sport and Exercise Medicine Research Centre, La Trobe University School of Allied Health Human Services and Sport, Melbourne, Victoria, Australia

⁷ Boston University School of Medicine, Boston, MA, USA

⁸ UMC Utrecht, Utrecht, Netherlands

⁹ University of California Davis School of Medicine, Sacramento, CA, USA

¹⁰ University of California San Francisco, San Francisco, CA, USA

¹¹ The University of North Carolina at Chapel Hill, Chapel Hill, NC, USA

¹² Delft University of Technology, Delft, The Netherlands

PHOTON-COUNTING CT-BASED TRABECULAR BONE ANALYSIS IN THE KNEE: A COMPARATIVE STUDY OF ADVANCED OSTEOARTHRITIS AND HEALTHY CONTROLS

M. Jarraya ¹, W. Issa ¹, C. Chane ¹, A. Zheng ¹, D. Guermazi ², K. Sariahmed ³, M. Mohammadian ¹, M. Kim ¹, K.A. Flynn ¹, T.L. Redel ¹, F. Liu ¹, M. Loggia ¹

INTRODUCTION: The advent of photon counting CT is a major advance in the development of CT technology. Its enhanced spatial resolution, compared to conventional CT, and its much-reduced radiation dose make it a promising tool for in vivo assessment of bone microarchitecture in clinical settings. For example, prior studies relying on HR-pQCT and Micro CT have shown greater volumetric bone mineral density (vBMD) and trabecular (Tb) thickness (Th) were significantly higher in the medial compartment and associated with increased disease severity. There is no data on trabecular bone structure using photon counting CT in patients with osteoarthritis (OA).

OBJECTIVE: To compare High-Resolution PCCT-defined trabecular bone microstructure between patients with advanced OA versus healthy controls.

METHODS: We used data from the ongoing DIAMOND knee study which investigates the role of neuroinflammation in chronic postoperative pain after TKR. To date, 9 healthy controls and 36 patients with advanced knee OA scheduled for total knee replacements have been recruited, including 7 patients who underwent unilateral PCCT. All other patients and healthy controls had bilateral knee scans. We used a Naeotom 144 Alpha PCCT scanner manufactured by Siemens Healthineers (Erlangen, Germany). Scans were performed with a tube voltage of (120 keV) and, to provide maximum scan performance and minimum noise deterioration, slice increments of 0.2 were used. We also utilized a slice thickness of 0.2 mm, rotation time 0.5 seconds, and pitch 0.85 Images were reconstructed with sharp bone kernel Br89 and matrix 1024 × 1024.. The field of view varied depending on the patient's size, thus resulting in a variable voxel in plane dimension (0.2-0.4 mm). Regions of interests were defined for the proximal tibia and distal femur in a stack height defined by slices equivalent to $1/6^{\text{th}}$ to $1/4^{\text{th}}$ of the measured joint width, prescribed distally or proximally from the joint line, respectively. Images were analyzed using a previously reported iterative threshold-seeking algorithm with 3D connectivity check to separate trabecular bone from marrow. Apparent structural parameters were derived from bone volume (BV), bone surface (BS), and total volume (TV) according to equations by Parfitt's model of parallel plates (Tb.Th, Tb.Separation, BV/TV). These trabecular bone measures were compared between OA and healthy knees using independent sample t-test or nonparametric Wilcoxon tests, depending on normality assumptions. All of the analyses were performed compartment-wise in all four ROIs. These images analyses steps were derived from methods previously published by Wong et al. (DOI: https://doi.org/10.1016/j.jocd.2018.04.001).

RESULTS: We analyzed data from 12 knees of 12 patients with advanced knee OA (mean age 66.0 ± 9.4 years, 67% female) and 17 knees from 9 healthy controls (mean age 60.8 ± 10.7 years, 56% female). Total

Tb volume was consistently greater in OA knees compared to controls in both the medial (OA: $M = 267.15 \text{ mm}^3$, SD = 31.53; HC: $M = 245.26 \text{ mm}^3$, SD = 26.51) and lateral (OA: $M = 278.45 \text{ mm}^3$, SD = 43.83; HC: $M = 252.99 \text{ mm}^3$, SD = 30.54) tibial compartments. Although differences in other bone parameters were not consistent across the four compartments, OA knees tended to show slightly higher trabecular thickness and lower BV/TV. Variability between compartments was observed, particularly in the femur, where group differences were less apparent, though none of these measures reached statistical significance.

CONCLUSION: In this preliminary study using high-resolution PCCT, knees with advanced OA consistently exhibited larger trabecular regions in the tibia compared to healthy controls. Subtle differences in bone structure were also observed, which may reflect early subchondral bone remodeling in response to altered joint loading and mechanical stress. However, interpretation of these microstructural changes is limited by the small sample size and variability in voxel size across scans, both of which could affect the precision of morphometric estimates.

SPONSOR: The study was funded by the David Borsook Project (Cathedral Fund), and the International Skeletal Society (ISS) Seed Grant. **DICLOSURE STATEMENT**: None.

CORRESPONDANCE: mjarraya@mgh.harvard.edu

Table 1. Patients' characteristics patients with osteoarthritis and healthy control group.

Variable	OA group (n = 12)	Healthy controls (n=9)	P-value
Age, mean ± SD	66.00 ± 9.44	60.78 ± 10.71	0.26
Female sex, n (%)	8 (66.7)	5 (55.6)	0.67*
Height cm, mean ± SD	170 ± 6.3	166 ± 5.2	0.18
Weight kg, mean ± SD	85.43 ± 18.41	74.15 ± 16.02	0.21

^{*} These P-values were measured by non-parametric tests.

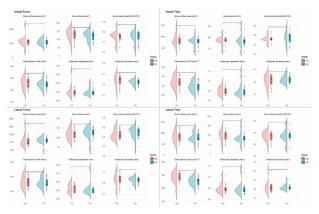


Figure 1. Raincloud plots showing trabecular bone measures across four knee compartments comparing OA (red) and healthy controls (blue). Each plot includes a half-violin (distribution), boxplot (central tendency and spread), and individual data points. Asterisks indicate group differences: $p < 0.2^*$, $p < 0.1^{**}$, $p < 0.05^{***}$.

¹ Mass General Brigham, Harvard Medical School, Boston, MA, USA

² The Warren Alpert Medical School of Brown University, Providence, RI, USA

 $^{^3}$ Boston Medical Center, Chobanian and Avedisian School of Medicine, Boston University, Boston, MA, USA

BASELINE C-SCORE ON WEIGHT-BEARING CT PREDICTS 2-YEAR WORSENING OF KNEE PAIN IN WOMEN

S. Li 1, N.A. Segal 2, I. Tolstykh 3, M.C. Nevitt 3, T.D. Turmezei 4

INTRODUCTION: The B-score is a statistical score derived from non-weight-bearing MRI to assess femoral bone shape and its relationship with knee OA. However, CT scans may offer a more reliable and robust evaluations of bone shape, as they not only provide clearer differentiation between bone and soft tissue but also eliminate distortion artefact that can occur with MRI.

OBJECTIVE: To investigate a new "C-score" for femoral bone shape derived from CT as a predictive imaging biomarker for worsening knee pain in men and women with or at risk for knee osteoarthritis.

METHODS: This study included 649 knees from 389 participants (219 women) with a mean±SD age of 63.8±9.6 years and BMI of 28.5±5.0 kg/m². C-scores were calculated from baseline weight-bearing CT (WBCT) imaging of the knee joint: 0.37 mm voxels, FOV 30×20 cm, 120 kVp, 5.0 mA on a LineUp scanner, Curvebeam LLC, Warrington, PA. All distal femurs were segmented using Stradview to produce a surface mesh. A canonical distal femur mesh was registered using wxRegSurf to each individual femur to build the study population shape model. Each knee's C-score was derived from the distance along the vector for femur shape between the average KLO/1 and KL2/3/4 shapes from the study population using a custom script in MATLAB. A single unit of the C-score was standardized as 1SD along this vector for the KL0/1 population (Figure 1). Generalized estimating equations adjusted for age, sex, BMI and presence of up to 2 knees per participant were used to assess associations between baseline C-score and 2-year minimally clinically important worsening (MCIW) of the Western Ontario McMaster's University Osteoarthritis Scale (WOMAC) pain subscore (2 points). MCIW is defined as the smallest difference on a pain scale that either patients perceive as worsening or requires change in treatment.

RESULTS: 186 knees demonstrated pain worsening (32.71% women and 23.2% men). 98 knees had MCIW of pain (19.0% women and 9.8% men). C-scores ranged from -2.64 to +3.34 in women and -3.96 to +2.83 in men, with mean \pm SD values of 0.16 ± 1.06 and -0.52 ± 1.01 respectively (p-value for difference between sexes p=0.0003). Women without

MCIW pain had a mean C-score of +0.31, while those with worsening pain had a mean C-score of +0.72. Men had mean C-scores of -0.03 and -0.01, respectively. In fully adjusted models, baseline C-score predicted 2-year MCIW pain (OR: 1.27, 95% CI: 1.00-1.62, p=0.047). In sex-stratified models, the odds ratios for 2-year MCIW pain in women and men were 1.49 (95% CI: 1.10-2.01, p=0.0159) and 1.01 (95% CI: 0.70-1.47, p=0.95), respectively.

CONCLUSION: Higher C-scores in women were significantly associated with worsening knee pain over 2 years, suggesting the C-score as a potential predictive biomarker for knee pain progression.

SPONSOR: NIH grants R01AR071648; U01AG18832; U01AG19069; and U01AG18820

DICLOSURE STATEMENT: TT is director of KNEE3D Ltd.; NS is a consultant for Trice Medical, Arthrex, and Pacira Biosciences.

ACKNOWLEDGMENT: N/A

CORRESPONDENCE ADDRESS: nsegal@kumc.edu



Figure 1. C-score range -2 to +4 from the study cohort as seen from the inferior view of a right knee. Score 0 is the average shape for all KL 0/1 knees with each unit of the C-score being 1SD of the KL0/1 population along the vector to the average KLG2/3/4 shape. Note the characteristic topographic changes from -2 to +4 that are similar to those derived from the B-score: (a) narrowing of the intercondylar notch, (b) widening of the medial weight bearing femoral articular surface, and (c) osteophyte "pie crust" formation.

Table 1. Statistical Comparison Between Women and Men with 2-Year MCIW Pain.

Outcome	Women (n=373 knees)	Men (n=276 knees)
2-year MCIW pain (2+ points)	N events=71 (19%)	N events=27 (9.78%)
Mean C-Score	+0.72	-0.01
Odds Ratio (95%CI)	1.49 (1.10 - 2.01)	1.01 (0.7 - 1.47)
P-value	0.016	0.95

¹ University of Kansas Medical Center, Kansas City, KS, USA

 $^{^2}$ University of Kansas Medical Center, Kansas City, KS, USA & The University of Iowa, Iowa City, IA, USA

³ University of California-San Francisco, San Francisco, CA, USA

⁴ Norfolk and Norwich University Hospital NHS Foundation Trust, Colney Lane, Norwich, UK & University of East Anglia, Norwich Research Park, Norwich, UK

REPEATABILITY OF THE CT OSTEOARTHRITIS KNEE SCORE (COAKS) AND A PROTOTYPE CT-GENERATED KELLGREN AND LAWRENCE GRADE

T.D. Turmezei $^{1,2},$ A. Boddu 1, Z. Akkaya 3, N.H. Degala 4, J.A. Lynch 5, N.A. Segal 4

- ¹ Norfolk and Norwich University Hospital, Norwich, UK
- ² University of East Anglia, Norwich, UK
- ³ Ankara University Faculty of Medicine Department of Radiology, Ankara, Turkey
- ⁴ University of Kansas Medical Center, Kansas City, KS, USA
- ⁵ University of California San Francisco, San Francisco, CA, USA

INTRODUCTION: The CT Osteoarthritis Knee Score (COAKS) is a semi-quantitative system for grading structural disease features of knee OA from weight bearing CT (WBCT). Previous work has demonstrated substantial to near-perfect inter- and intra-observer reliability of COAKS with the aid of a feature scoring atlas, but test-retest repeatability has not yet been evaluated. Given that x-ray and CT rely on the same fundamental physical properties, COAKS could also be harnessed to provide a CT-generated KLG and avoid the need for radiographic imaging.

OBJECTIVE: (1) To evaluate test-retest repeatability of COAKS; (2) to develop a CT-generated KLG (ctKLG) and evaluate its test-retest repeatability; and (3) to compare this prototype ctKLG against radiographic KLG (rKLG).

METHODS: 14 individuals recruited and consented at the University of Kansas Medical Center had baseline and follow-up WBCT imaging suitable for analysis. Participant demographics were: mean \pm SD age 61.3 ± 8.4 years, BMI 30.7 ± 4.3 kg/m² and male:female ratio 8:6. All scanning was performed on the same XFI WBCT scanner (Planmed Oy, Helsinki, Finland) with the mean ± SD interval between baseline and follow-up attendances 14.9 \pm 8.1 days. A SynaflexerTM device was used to standardize knee positioning during scanning. Imaging acquisition parameters were 96 kV tube voltage, 51.4 mA tube current, 3.5 s exposure time. A standard bone algorithm was applied for reconstruction with 0.3 mm isotropic voxels and a 21 cm vertical scan range. All scans were anonymized prior to analysis both according to the individual and imaging attendance. All knees were reviewed for their COAKS by an experienced musculoskeletal radiologist (T.D.T.). Scores were recorded in a cloud-based file on Google Sheets (alongside the feature atlas in Google Docs) and read by a custom MATLAB script to generate structural heat maps. Test-retest repeatability weighted Kappa (Kw) scores were calculated for each feature (J = JSW; O = osteophytes; C = subchondral cysts; S = subchondral sclerosis) at each compartment (MTF = medial tibiofemoral; LTF = lateral tibiofemoral; PF = patellofemoral; PTF = proximal tibiofibular). A custom MATLAB script applied a decision tree based on recognized KLG verbal definitions to generate ctKLGs for each knee, including a combined score for the MTF and LTF compartments to mimic single-view AP radiographic conditions. A second experienced musculoskeletal radiologist (Z.A.) read study inclusion radiographs for rKLG likewise blinded. Kw was also calculated for ctKLG and rKLG.

RESULTS: Structural heatmaps are shown in Figure 1 for participants with ctKLGs of 1 (study ID 117, right knee) and 4 (study ID 101, right knee) alongside difference maps (follow-up minus baseline). These maps give examples of minimal difference in baseline and follow-up grading at the extremes of structural disease. Best repeatability by feature and compartment was for JSW at the MTF compartment with a Kw (95% CI) of 0.94 (0.93-0.96) and for osteophytes at the PF compartment with a Kw of 0.91 (0.90-0.93). Repeatability for each feature across all compartments was near-perfect (0.82 and above), except being substantial for subchondral sclerosis (0.72, 0.69-0.74). Repeatability for ctKLG was substantial for all individual compartments and near-perfect for the combined tibiofemoral score (0.83,0.80-0.86). Kw was likewise near perfect for rKLG (0.90, 0.88-0.93). Full repeatability Kw (95% CI) results for COAKS, prototype ctKLG and rKLG are given in Tables 1 & 2.

It was noted that ctKLG scores were sensitive to small changes in the decision tree based on verbal rKLG interpretation.

CONCLUSION: COAKS repeatability results were similar to those previously demonstrated for intra-observer rating, suggesting that scan factors are consistent enough to have little effect on reader performance. A ctKLG derived from COAKS was similarly repeatable to rKLG with nearperfect performance. A ctKLG model offers a means to stratify structural disease from WBCT without the need for radiographs, however further development is needed to establish a robust decision tree in deriving this from COAKS.

SPONSOR: None.

DISCLOSURE STATEMENT: NS is a consultant for Trice Medical, Pacira Biosciences, and Arthrex. TT is the director of KNEE3D Ltd. TW is the director of Minogame Ltd.

ACKNOWLEDGEMENT: None.

CORRESPONDENCE ADDRESS: tom@turmezei.com

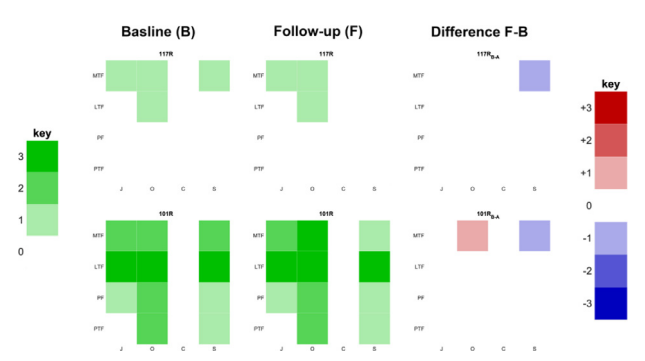


Figure 1.

Table 1.

COAKS	Feature	Kw	95% CI	Verbal
Medial tibiofemoral	Joint space	0.94	0.93-0.96	Near perfect
	Osteophytes	0.80	0.76-0.84	Substantial
	Cysts	0.80	0.73-0.87	Substantial
	Sclerosis	0.75	0.72-0.78	Substantial
Lateral tibiofemoral	Joint space	0.74	0.72-0.76	Substantial
	Osteophytes	0.88	0.86-0.91	Near perfect
	Cysts	0.49	0.42-0.57	Moderate
	Sclerosis	0.80	0.78-0.83	Substantial
Patellofemoral	Joint space	0.85	0.83-0.87	Near perfect
	Osteophytes	0.91	0.90-0.93	Near perfect
	Cysts	0.78	0.67-0.89	Substantial
	Sclerosis	0.59	0.53-0.65	Moderate
Proximal tibiofibular	Joint space	0.43	0.41-0.45	Moderate
	Osteophytes	0.50	0.46-0.54	Moderate
	Cysts	0.84	0.83-0.86	Near perfect
	Sclerosis	0.21	0.16-0.27	Fair
Across all compartments	Joint space	0.87	0.86-0.88	Near perfect
	Osteophytes	0.82	0.81-0.84	Near perfect
	Cysts	0.82	0.78-0.86	Near perfect
	Sclerosis	0.72	0.69-0.74	Substantial

Table 2

ctKLG by compartment	Kw	95% CI	Verbal
Tibiofemoral combined	0.83	0.80-0.86	Near perfect
Medial tibiofemoral	0.80	0.77-0.83	Substantial
Lateral tibiofemoral	0.78	0.74-0.81	Substantial
Patellofemoral	0.66	0.59-0.73	Substantial
Proximal tibiofibular	0.59	0.56-0.61	Moderate
rKLG	0.90	0.88-0.93	Near perfect

AUTOMATIC MENISCUS ANALYSIS DEMONSTRATES REPAIR IS NOT SUPERIOR TO MENISCECTOMY IN IMPROVING MENISCAL UTE-T2 $^{\circ}$ PROPERTIES 2-YEARS POST ACLR

A.A. Gatti 1, A.A. Williams 2, C.R. Chu 2

INTRODUCTION: Concomitant meniscus tear is common with ACL injury and amplifies OA risk. MRI ultrashort echo-time T2* (UTE-T2*) is sensitive to the compositional integrity of the meniscus and is histologically verified to associate with collagen fibril alignment. We implemented an automated pipeline to determine whether meniscal T2* composition 2-years after ACL reconstruction (ACLR) differs between patients with and without a meniscal tear at the time of surgery.

OBJECTIVE: To test whether menisci found to be torn at the time of ACLR exhibit, at 2-year follow-up, higher mean UTE-T2* reflecting greater compositional degeneration than intact menisci and whether meniscal repair demonstrates lower UTE-T2* than meniscectomy at 2-year follow-up.

METHODS: 111 ACLR patients (53/111(48%) female; mean[SD] age: 32[10]yrs; BMI: 25[3]kg/m2) underwent 3T MRI 2 years after ACLR (2.0[0.9]years). UTE-T2* maps were generated by fitting a monoexponential decay curve to sagittal T2*-weighted images using a Levenberg-Marquardt algorithm. Images were acquired at 8 TEs ($32\mu s$ -16ms, non-uniform spacing) using a radial-out 3D Cones acquisition, TR = 22ms, in-plane resolution = 0.313 to 0.364 mm, and 3mm slice thickness. Menisci were automatically segmented using a U-Net pretrained on >300 DESS volumes and fine-tuned to segment root-sumof-squares images combining Cones echoes 2-6. Training labels were generated by registering DESS images to Cones and propagating the segmentation. Automated segmentation was evaluated in a validation cohort using the dice similarity coefficient (DSC) and average symmetric surface distance (ASSD). The menisci were subdivided into anterior, middle, and posterior thirds using an automated polar coordinate-based system (Fig 1). Meniscal tear and treatment at the time of ACLR was assessed from operative reports. UTE-T2* differences between torn and intact menisci, and between repair versus meniscectomy were assessed with t-tests (or Mann-Whitney U tests). Statistical analyses were performed with SPSS (IBM) and Excel (Microsoft).

RESULTS: Automated segmentation in the validation cohort (n=16) had median DSC = 0.71 and ASSD = 0.52 mm for the medial, and DSC = 0.68 and ASSD = 0.51 mm for the lateral meniscus. At the time of ACLR, meniscal tears were observed in 56/111(50%) patients: 24/111(22%) of medial and 45/111(41%) of lateral menisci. More tears were resected: 11/24(45%) medial, 25/45(56%) lateral than repaired: 10/24(42%) medial, 15/45(33%) lateral. Patients with any medial meniscal tear had higher mean UTE-T2* in the middle (14%, p<0.001) and posterior (20%, p=0.002) regions compared to those with intact menisci, (Fig 2). Patients with any lateral meniscal tear had 20% higher mean UTE-T2* in the middle region of the lateral menisci compared to those with intact menisci (p=0.001). Two years post-ACLR, no mean UTE-T2* differences were detected between repaired and resected menisci (p>0.181).

CONCLUSION: Menisci torn at the time of ACLR showed elevated UTE-T2* at 2-year follow-up, regardless of treatment. These data suggest that repair does not fully restore compositional properties. While meniscal repair is often favored over meniscectomy to preserve function and potentially reduce OA risk, repair is more costly and requires longer rehabilitation. Further research should identify whether specific tear patterns or patient factors influence compositional recovery, and whether UTE-T2* at 2-year follow-up predicts OA development and progression. This study demonstrates that automatic segmentation and analysis of sub-regional meniscal UTE-T2* is feasible and can provide standardized

assessments across large data sets, including in knees with surgical hardware.

DICLOSURE STATEMENT: AAG is a shareholder of NeuralSeg, NodeAI, and GeminiOV.

 ${\bf SPONSOR}:$ DOD W81XWH-18-1-0590 (PI-CR Chu), RO1 AR051784 (PI-CR Chu), Wu Tsai Human Performance (AAG)

CORRESPONDENCE ADDRESS: chucr@stanford.edu

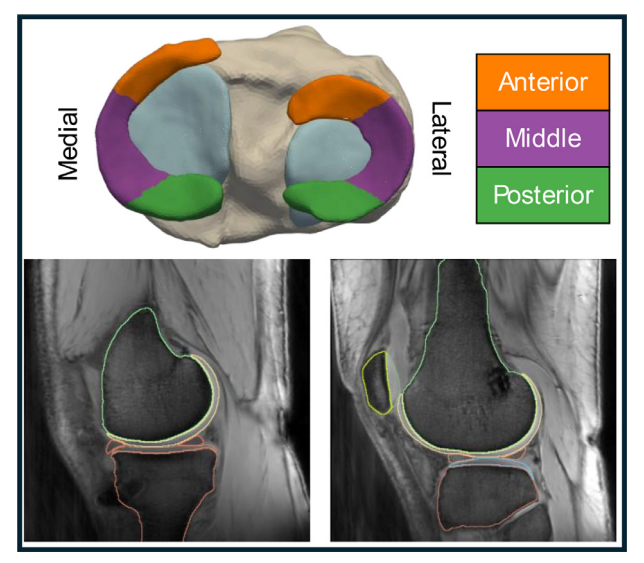


Figure 1. Top: Subregional division of the medial and lateral menisci into anterior, middle, and posterior thirds used for data analysis. Bottom: Example root-sum-of-squares (RSS) composite image from the Cones acquisition echoes 2-6 with automated segmentations overlaid.

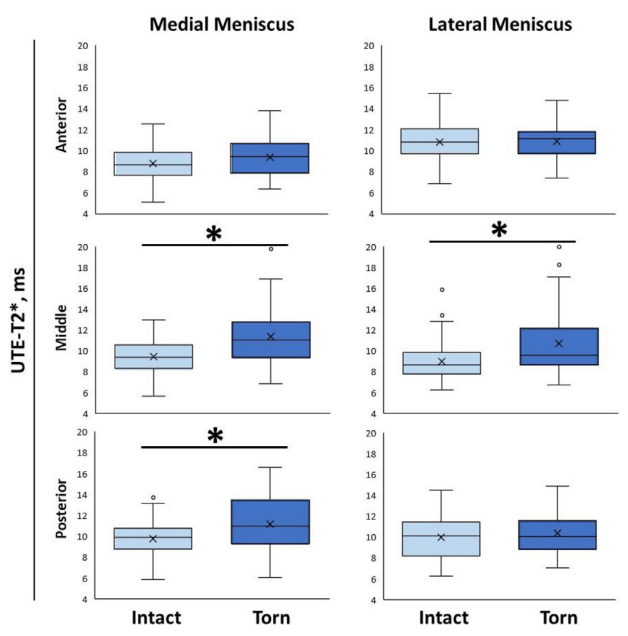


Figure 2. MRI collected at 2 years post-ACLR show elevated UTE-T2*, indicative of compositional degeneration, in menisci torn at the time of ACLR. Mean UTE-T2* across the middle portions of the medial and lateral menisci were higher in torn than intact menisci (mean[95%CI] UTE-T2* differences: medial 1.91ms (1.01, 2.81), p<0.001; lateral 1.75ms (0.72, 2.78), p=0.001). Likewise, mean UTE-T2* in the posterior portion of the medial meniscus was higher in torn than intact menisci (1.39ms (0.53,2.24), p=0.002). Solid central line indicates the sample median; X indicates the sample mean.

¹ Department of Radiology, Stanford University, Stanford, CA, USA

² Department of Orthopaedic Surgery, Stanford University, Stanford, CA, USA

PREDICTING KNEE OSTEOARTHRITIS PROGRESSION USING EXPLAINABLE MACHINE LEARNING AND CLINICAL IMAGING DATA

R.E. Harari 1, J. Collins 2, S.E. Smith 1, S. Wells 1, J. Duryea 1

INTRODUCTION: Accurate prediction of knee osteoarthritis (KOA) progression remains a clinical challenge due to its heterogeneous nature and discordance between structural and symptomatic outcomes. Integrated imaging and machine learning (ML) approaches may enhance prognostic modeling but often suffer from limited interpretability or reliance on static features.

OBJECTIVE: We aim to develop explainable ML models for predicting KOA progression using baseline and longitudinal imaging and clinical features. This study also aims to identify key imaging biomarkers associated with structural and symptomatic progression.

METHODS: Data and 3T MRI measurements from 600 participants in the FNIH OA Biomarkers Consortium were analyzed. Participants were grouped into four progression categories based on 48-month joint space narrowing and WOMAC pain: (1) radiographic + pain progressors, (2) radiographic-only, (3) pain-only, and (4) non-progressors. Two binary classification frameworks were defined: (1) radiographic + pain vs. all others (primary), and (2) all radiographic progressors vs. painonly + non-progressors (secondary). ML models included Random Forest, XGBoost, logistic regression, decision tree, and multilayer perceptron (MLP). The model used demographic information and imaging features from semi-automated segmentation software. We measured the volume of medial compartment femur cartilage (Cart), bone marrow lesion (BML) in the MF, LF, MT, LT, patella, and trochlea, osteophytes (Ost) in the MF, LF, MT, and LT, Hoffa's synovitis (HS), and effusion/synovitis (ES). Longitudinal delta values were computed over 24 months. Performance was assessed via 10-fold stratified cross-validation (AUC, F1-score). Explainability tools included SHAP, Gini importance, coefficients, and permutation importance.

RESULTS: In the cross-sectional setting, the Random Forest classifier achieved the highest discrimination performance, with AUC values of 0.672 for the primary task (radiographic+pain progressors vs. others) and 0.791 for the secondary task (all radiographic progressors vs. others). The MLP model showed similar results in the secondary task (AUC=0.743). AUC performance metrics for all models are shown in Table 1. Model performance improved notably when incorporating 24-month changes in imaging features. In the longitudinal analysis, Random Forest again performed best in the secondary task (AUC=0.873), followed by XGBoost and MLP. The strongest predictors in these models were changes in medial femoral cartilage thickness, medial tibial bone marrow lesions, and osteophyte scores. To better understand the basis of model predictions, we applied four feature ranking methods. Among them, the SHAP method produced the most consistent and clinically in-

terpretable results. As an example, shown in Figure 1 which show top 15 important features, SHAP highlighted 24-month reductions in cartilage thickness and increases in bone marrow lesion scores as the most influential variables, especially in the medial compartment.

CONCLUSION: Explainable ML models can identify individuals at risk of KOA progression using multimodal data. Longitudinal imaging features enhanced predictive power, and transparent interpretation techniques revealed important markers of joint deterioration.

SPONSOR: DISCLOSURE STATEMENT: The authors report no conflicts of interest.

ACKNOWLEDGMENT: We thank the OAI and FNIH teams for data access and curation.

CORRESPONDENCE ADDRESS: rharari@bwh.harvard.edu

Table 1. Summary of model performance (ROC AUC) across four predictive tasks—two cross-sectional and two longitudinal binary classification—using 10-fold stratified cross-validation.

Model	Cross AUC - Primary	Cross AUC - Secondary	Long AUC - Primary	Long AUC -Secondary
Random Forest	0.672	0.791	0.701	0.873
XGBoost	0.661	0.696	0.701	0.796
Logistic Regression	0.631	0.555	0.702	0.754
Decision Tree	0.523	0.701	0.462	0.764
MLP	0.611	0.743	0.739	0.801

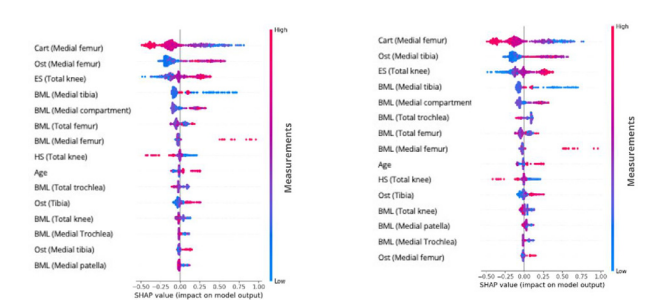


Figure 1. SHAP summary plots for the XGBoost classifier trained on longitudinal imaging features change. Feature contributions are visualized for the primary (left) and secondary (right) KOA progression classification tasks. Each dot represents a patient: color reflects the feature measurement value (red = high, blue = low), and position on the x-axis indicates the measurement's effect on model output (right = higher predicted risk, left = lower predicted risk). The spread shows how much the feature's impact varies across individuals. For example, in the primary classification, Cart (Medial femur) is the top predictor: patients with greater cartilage loss (red dots) are strongly shifted to the right, indicating a higher model-predicted risk of progression. In contrast, less cartilage loss (blue dots) is associated with a lower predicted risk.

¹ Department of Radiology, Mass General Brigham, Harvard Medical School, Boston, MA, USA

² Department of Orthopaedic Surgery, Mass General Brigham, Harvard Medical School, Boston, MA, USA

A FULLY-AUTOMATED TECHNIQUE FOR KNEE CARTILAGE AND DENUDED BONE AREA MORPHOMETRY IN SEVERE RADIOGRAPHIC KNEE OA – METHOD DEVELOPMENT AND VALIDATION

W. Wirth 1,2, F. Eckstein 1,2

INTRODUCTION: Automated cartilage segmentation using convolutional neural networks (CNN) has been shown to provide moderate to high accuracy in comparison with gold-standard manual approaches. It also displays similar sensitivity to longitudinal change and to between-group differences in change as has been reported for manual analysis [1-3]. Denuded areas of subchondral bone (dAB) provide challenges and impair the accuracy of automated cartilage segmentation in knees with severe radiographic OA (KLG 4). The reason is that CNNs are trained to detect cartilage, but encounter "difficulties" to properly segment areas where cartilage is lost entirely. CNNs therefore often segment cartilage cover in some areas of actual full thickness loss or ignore dABs entirely. This was observed to result in an overestimation of cartilage thickness and an underestimation of dABs in knees with severe OA [4].

OBJECTIVE: To improve CNN-based automated segmentation in severely osteoarthritic knee cartilage by using an automated post-processing algorithm that relies on a multi-atlas registration for reconstructing the total area of subchondral bone (tAB). We evaluate the agreement, accuracy and longitudinal sensitivity to cartilage change of this new methodology.

METHODS: Sagittal DESS and coronal FLASH MRIs were acquired by the Osteoarthritis Initiative (OAI). 2D U-Net models were trained for both MRI protocols using manual cartilage segmentations of knees with radiographic OA (KLG2-4, n training / validation set: 86/18 knees, baseline scans only) or severe radiographic OA (KLG4, n training/ validation set: 29/6 knees. These were trained either from baseline scans only [KLG4_{BL}] or from baseline and follow-up scans [KLG4_{BL+FU}]. The trained models were then applied to the test set comprising 10 KLG4 knees with manual cartilage segmentations from both DESS and FLASH MRI available and to n=125/14 knees with manual cartilage segmentations from either DESS or FLASH MRI available. Automated, registration-based post-processing was applied to reconstruct missing parts of the tAB and to refine the segmentations (Fig. 1), particularly in areas of denuded bone. The agreement and accuracy of automated cartilage analysis were evaluated in the test set for individual cartilages using Dice Similarity coefficients (DSC), correlation analysis, and by determining systematic offsets between manual and automated analysis. The sensitivity to one-year change was assessed using the standardized response mean (SRM) across the entire femorotibial joint in 104/24 (DESS/FLASH) knees with manual baseline and follow-up segmentations.

RESULTS: The strongest agreement (DSC 0.80 ± 0.07 to 0.89 ± 0.05) and lowest systematic offsets for cartilage thickness (1.2% to 8.5%) were observed for CNNs trained on KLG2-4 rather than KLG4 knees. Similar observations were made for dABs (-40.6% to 3.5%) and total subchondral bone area (-0.4% to 4.3%). Fig. 2 displays the offsets for

cartilage thickness together with the offsets previously observed without the registration-based post-processing. Cartilage thickness obtained from the KLG2-4 model was strongly correlated with that from manual segmentations (r=0.82 to r=0.97) whereas a moderate to strong correlation was observed for dABs (r=0.52 to r=0.92). The sensitivity to change across the entire femorotibial joint was greatest for manual segmentation of DESS (SRM -0.69; vs. automated: -0.28 to -0.56) but on the other hand for the automated segmentation of FLASH (-0.47 to -0.67; vs. manual = -0.44, Fig. 3) MRI.

CONCLUSION: CNN-based segmentation combined with registration-based post-processing for accurate delineation of tABs/dABs substantially improves fully-automated analysis of cartilage and subchondral bone morphology in knees with severe radiographic OA when compared to a previously used fully-automated approach without such post-processing [4]. This finding is consistent for two different MRI contrasts (DESS and FLASH) and orientations (sagittal and coronal). Our results additionally show that the more general (KLG2-4) model is well suited for automated segmentation of KLG4 knees, eliminating the need for a KLG4-specific model.

SPONSOR: Ludwig-Boltzmann Institute of Arthritis and Rehabilitation (LBIAR)

DICLOSURE STATEMENT: FE, WW: Chondrometrics GmbH

REFERENCES:

- [1] Eckstein et al. Arthritis Care Res. 2022;74:929-936.
- [2] Panfilov et al. J Orthop Res. 2022;40:1113-1124.
- [3] Dam et al. Osteoarthr Imaging. 2023;3(1).
- [4] Wisser et al. Osteoarthr Cartil. 2021;29:S319-S320.

CORRESPONDENCE ADDRESS: wolfgang.wirth@pmu.ac.at

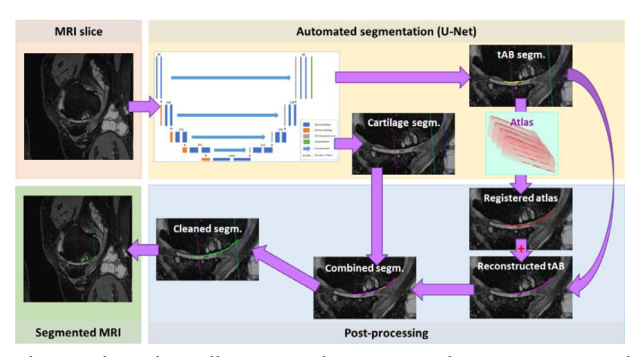


Fig. 1: Flow chart illustrating the automated segmentation and post-processing. The selected example shows the automated segmentation of the central medial femoral condyle. The automated segmentation relies on 2D U-Nets for separately segmenting the cartilage and the total area of subchondral bone (tAB) from MRI. The post-processing uses an atlas of manually segmented tABs that is registered to the automatically segmented tAB and the best-matching reference tAB is chosen for the reconstruction of the tAB. After the reconstruction of the tAB, the tAB is combined with the cartilage segmentation, before the combined segmentation is checked for segmentation errors and automatically cleaned.

Figures continued on next page.

¹ Chondrometrics GmbH, Freilassing, Germany

 $^{^2{\}it Center}$ for Anatomy and Cell Biology & LBIAR, Paracelsus Medical University, Salzburg, Austria

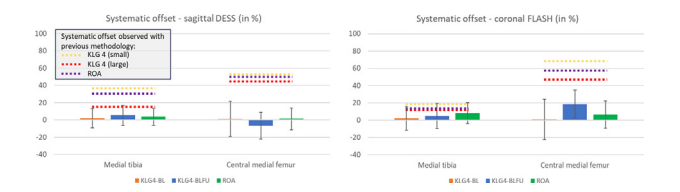


Fig. 2: Bar graphs showing the systematic offset of automated cartilage thickness measures in the more severely affected medial compartment from the three models (KLG4only(BL), KLG4only(BL+FU), KLG2-4(BL)) for both DESS (top) and FLASH MRI (bottom). The dotted lines indicate the systematic offsets observed with the previous automated segmentation technique (Wisser et al. [4]) that did not include the registration-based post-processing for reconstructing the total area of subchondral bone (tAB).

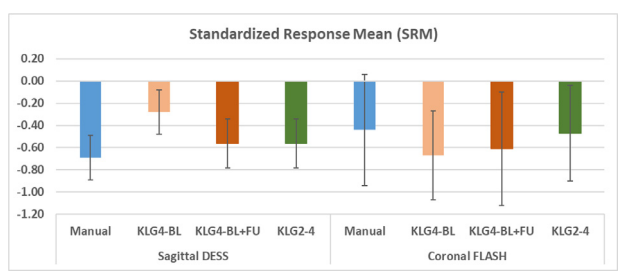


Fig. 3: Bar graphs showing the standardized response mean for one-year change in total femorotibial cartilage thickness measured using manual cartilage segmentations and using CNN-based cartilage segmentations trained from baseline scans of KLG 4 knees (KLG4-BL), from baseline and follow-up scans of KLG 4 knees (KLG4-BL+FU), and from knees with radiographic OA (KLG 2-4). The SRM was computed for 104 knees with sagittal DESS MRI and for 24 knees with coronal FLASH MRI. The 95% confidence intervals were computed using bootstrapping.

TOPOGRAPHY OF SEX-RELATED FEMOROTIBIAL CARTILAGE THICKNESS DIFFERENCES: A MATCHED MALE-FEMALE PAIR ANALYSIS CONTROLLING FOR AGE, BMI, AND HEIGHT

N. Spoelder ^{1,2}, W. Wirth ^{3,4}, T.D. Turmezei ^{5,6}, F. Eckstein ^{3,4}, D.A. Kessler ⁷, J.W. Mackay ^{6,7}, M. Karperien ², S.C. Mastbergen ¹, M.P. Jansen ¹

INTRODUCTION: Knee OA is both more common and progresses faster in women than in men. While it is well known that men exhibit thicker cartilage, it remains unclear whether this difference is inherently sexbased or attributable to confounding factors such as age, BMI, and/or height

OBJECTIVE: The aim of this study was to evaluate regional differences in knee cartilage thickness between men and women without radiographic OA, who were matched for age, BMI, and height.

METHODS: Participants without radiographic signs of knee OA were selected from the Osteoarthritis Initiative (OAI). Men and women were matched based on height (± 1 cm), age (± 5 years), and BMI (± 2 kg/m²), yielding 63 male-female pairs (n = 126; mean age 57 \pm 8 years, BMI 26 \pm 4 kg/m², height 170 \pm 5 cm). Right knee 3T MRI scans were processed using a deep learning model to generate preliminary automatic segmentations of the outer femoral and tibial contours and the inner cartilage boundaries. These segmentations were manually refined in Stradview and converted into 3D surface models. Cartilage thickness was computed at each vertex as the distance from the cartilage surface to the underlying bone, measured along the normal vector using model-based deconvolution. The femoral, medial tibial, and lateral tibial surfaces and their associated thickness maps were spatially aligned to canonical templates using wxRegSurf. Statistical analyses were performed in MAT-LAB using the SurfStat package, applying statistical parametric mapping (SPM) with linear mixed models to evaluate paired male-female differences. Significance was set at p < 0.05.

RESULTS: Figure 1 shows the average cartilage thickness in men and women, as well as the differences between sexes. The difference map is predominantly blue, indicating thicker cartilage in men. In both sexes, cartilage was thicker on the lateral side than on the medial side. The trochlea had the greatest thickness overall, with a maximum of 3.98 mm in men and 3.30 mm in women. Statistically significant differences in cartilage thickness between men and women were observed in specific regions of the femur, medial tibia, and lateral tibia (Figure 2). In those regions in the femur, cartilage was thicker in men, with a mean thickness of 2.77 mm compared to 2.42 mm in women, a difference of 0.36 mm (15%). In both the statistically significant different regions of the medial and lateral tibia, cartilage thickness was 0.09 mm (4%) greater in men than in women, with means of 2.26 mm versus 2.17 mm and 2.19 mm versus 2.10 mm, respectively.

CONCLUSION: Despite similar height, age, and BMI, men exhibited thicker femorotibial cartilage than women. Statistically significant differences were found across all three joint surfaces, with the largest difference observed in the trochlea. These findings underscore the need for further research into sex-related differences in femorotibial cartilage thickness as a potential contributor to the greater prevalence and severity of knee OA in women.

SPONSOR: None

DICLOSURE STATEMENT: T.D. Turmezei is director of KNEE3D Ltd.

ACKNOWLEDGMENT: None

CORRESPONDENCE ADDRESS: n.spoelder-2@umcutrecht.nl

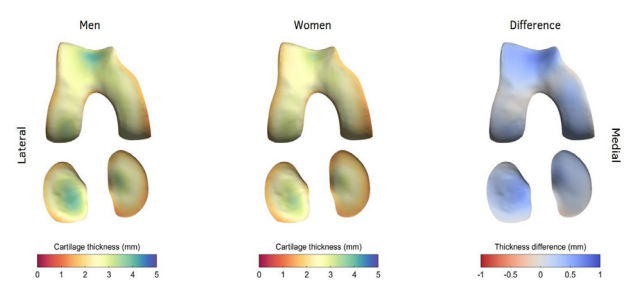
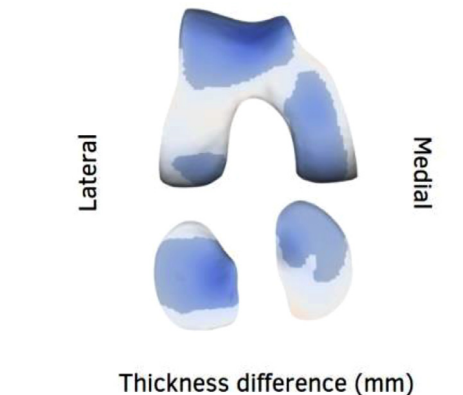


Figure 1: Mean cartilage thickness across the femorotibial joint in men (left) and women (middle), with the corresponding difference map (male minus female) shown on the right. Blue indicates thicker cartilage in men; red indicates thicker cartilage in women.



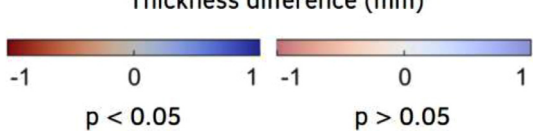


Figure 2: Whole-joint cartilage thickness differences between paired men and women. Two color scales are used: regions with statistically significant differences (p < 0.05) are shown in full color (left colorbar), while non-significant regions (p > 0.05) are shown in faded colors (right colorbar). Blue indicates thicker cartilage in men; red indicates thicker cartilage in women.

¹ University Medical Center Utrecht, Utrecht, Netherlands

² University of Twente, Enschede, Netherlands

³ Chondrometrics GmbH, Freilassing, Germany

⁴ Paracelsus Medical University, Salzburg, Austria

⁵ Norfolk & Norwich University Hospital, Norwich, UK

⁶ University of East Anglia, Norwich, UK

⁷ University of Cambridge, Cambridge, UK

DATA-DRIVEN DISCOVERY OF KNEE OSTEOARTHRITIS SUBGROUPS VIA CLUSTER ANALYSIS OF MRI BIOMARKERS

J.E. Collins ¹, L.A. Deveza ², D.J. Hunter ², V.B.K. Kraus ³, A. Guermazi ⁴, F.W. Roemer ⁵, J.N. Katz ¹, T. Neogi ⁶, E. Losina ¹

INTRODUCTION: Identifying structural morphotypes in knee OA, subgroups defined by anatomical and morphological attributes, may facilitate personalized treatment by aligning specific patterns of joint damage with treatment mechanism of action. Cluster analysis is a type of unsupervised machine learning used to uncover subgroups and may provide insight into structural morphotypes in knee OA.

OBJECTIVE: To use cluster analysis to investigate possible subgroups defined by imaging features in a cohort of persons with knee OA.

METHODS: We used data from the PROGRESS OA study, the second phase of the FNIH OA Biomarkers Consortium project, which includes data from the placebo arms of several completed RCTs testing various therapeutic interventions for symptomatic knee OA. MRIs were obtained at baseline and read according to the MRI OA Knee Score (MOAKS) by an experienced radiologist. We included MOAKS assessments of BML size, osteophytes, cartilage, Hoffa-synovitis, effusion-synovitis, and meniscus in the clustering algorithms. Raw ordinal MOAKS scores were used in this analysis. We used Partitioning Around Medoids (PAM) for clustering. PAM is similar to K-means, but instead of defining cluster center as the centroid (mean), the medoid is used, making the method more robust to outliers and appropriate for non-Gaussian data. We undertook several approaches to clustering to perform dimension reduction and incorporate correlations between MOAKS scores A: PAM on Gower's distance; B: PAM on the dissimilarity matrix from Spearman correlation; C: PAM after non-metric multidimensional scaling (NMDS) using Gower distance for dimension reduction. These approaches aimed to uncover patterns orthogonal to disease severity. The number of clusters was selected based on silhouette width and the gap statistic. Silhouette scores 0.25 to 0.5 indicate weak to reasonable fit.

RESULTS: 356 participants from four RCTs were included, 138 (39%) with KLG 2 radiographs and 218 (61%) with KLG 3. The cohort was 57% female with average age 62 (SD 8). The number of clusters ranged from 2 to 3 depending on method. There was modest to high overlap between clustering solutions from different methods, suggesting some stability of clustering solutions. Average silhouette scores were 0.19, 0.13, 0.40 for methods A, B, and C, suggesting poor to modest fit. This could suggest weak structure, overlapping clusters, or need for additional dimension reduction. Methods A and C had one cluster dominated (>95% KLG 3) by KLG 3 knees (Figure 1). Investigation of MOAKS assessments by cluster for each of three clustering solutions is shown in Table 1. For example, method C suggested 3 clusters. Clusters 1 and 2 are both approximately 55-60% KLG 2. Cluster 1 has more lateral cartilage damage, and higher BML and osteophyte scores, while cluster 2 has more medial cartilage damage and medial meniscal damage. Cluster 3 is 96% KLG 3

and has extensive medial cartilage damage, with 84% with widespread full-thickness damage in the MFTJ.

CONCLUSION: While knees can be separated into clusters based on tissue damage assessed by the MOAKS system, both level of disease severity and compartment involvement (medial vs. lateral) play important roles. Silhouette scores suggest the potential for overlapping clusters or the need for additional data reduction. The advanced disease stage common in DMOAD trial populations may limit the ability to identify meaningful structural morphotypes.

SPONSOR: NIH NIAMS K01AR075879. Support for the PROGRESS OA study is made possible through grants and direct and in-kind contributions provided by the following: Arthritis Foundation; Biosplice Therapeutics Inc.; Merck KGaA, Darmstadt, Germany; Novartis; Pfizer.

DICLOSURE STATEMENT: J.E.C. is a consultant for Boston Imaging Core Labs, LLC. A.G. has received consultancies fees from Novartis, ICM, Levicept, Scarcell, Peptinov, Pacira, Coval, 4Moving, Formation Bio, Paradigm, Medipost and TissueGene and is shareholder of Boston Imaging Core Lab. LLC.

ACKNOWLEDGMENT: We would like to thank the Foundation for the National Institutes of Health.

CORRESPONDENCE ADDRESS: JCollins13@bwh.harvard.edu

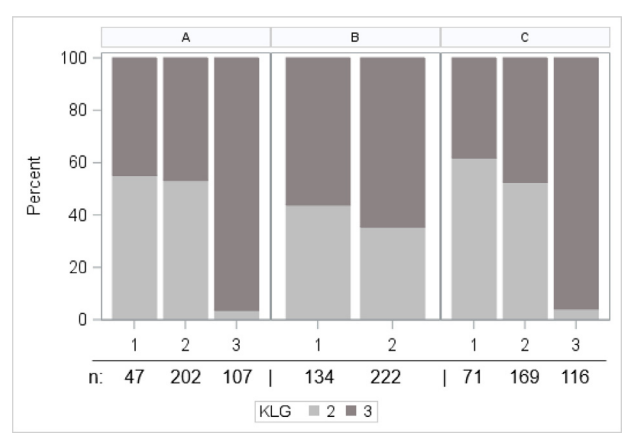


Figure 1. Distribution of KLG across clusters for three clustering solutions. A: PAM on Gower distance; B: PAM on Spearman dissimilarity matrix; C: PAM on Gower Distance after NMDS.

Table 1. Frequencies of select MOAKS parameters by cluster for three clustering solutions.

A	Cluster	Wide-spro full-thick damage	ead ness cartilage	Hoffa or effusion- synovitis	Maximum BML score =3	Maximum osteo- phyte	Medial meniscal maceration
		MFTJ	LFTJ	=3		score =3	or root tear
Overall Col	hort	41%	9%	6%	18%	12%	66%
В	1	9%	13%	6%	36%	30%	43%
	2	23%	6%	5%	11%	1%	63%
	3	89%	11%	8%	24%	23%	80%
Overall Coho A B	1	38%	12%	6%	23%	23%	53%
	2	42%	7%	6%	15%	5%	73%
A B C	1	6%	30%	7%	28%	17%	39%
	2	25%	1%	4%	8%	0%	65%
	3	84%	8%	9%	27%	26%	84%

 $^{^{\}mathrm{1}}$ Brigham and Women's Hospital, Harvard Medical School, Boston, MA, USA

 $^{^2}$ Sydney Musculoskeletal Health, Kolling Institute, University of Sydney, Sydney, NSW, Australia

³ Duke Molecular Physiology Institute, Department of Medicine, Duke University School of Medicine, Durham, NC, USA

⁴ VA Boston Healthcare & Boston University School of Medicine, Boston, MA, USA

⁵ Friedrich-Alexander-Universität Erlangen-Nürnberg, Erlangen, Germany & Boston University School of Medicine, Boston, MA, USA

⁶ Boston University School of Medicine, Boston, MA, USA

LEVI-04, A NOVEL NEUROTROPHIN-3 INHIBITOR, DEMONSTRATED SIGNIFICANT IMPROVEMENTS IN PAIN AND FUNCTION AND WAS NOT ASSOCIATED WITH DELETERIOUS EFFECTS ON JOINT STRUCTURE IN PEOPLE WITH KNEE OA IN A PHASE II RCT

P.G. Conaghan 1 , A. Guermazi 2 , N. Katz 3 , A.R. Bihlet 4 , D. Rom 5 , C.M. Perkins 6 , B. Hughes 6 , C. Herholdt 6 , I. Bombelka 6 , S.L. Westbrook 6

INTRODUCTION: Improvement in the symptoms of osteoarthritis (OA) remains a serious unmet medical need and new pharmacological treatments are urgently needed. Excess neurotrophins (NT) are implicated in OA and other painful conditions. Previous analgesic therapies selectively targeting NGF inhibition provided improvements in pain and function, but were dose-dependently associated with significant joint pathologies, including rapidly progressive OA (RPOA). LEVI-04 is a first-in-class fusion protein (p75NTR-Fc) that supplements the endogenous p75NTR binding protein, providing analgesia via inhibition of NT-3 activity. Here we present efficacy and safety data from the phase II RCT of LEVI-04 in people with knee OA.

METHODS: This was a PhII multicentre (Europe and Hong Kong) RCT in people with painful (≥4/10 WOMAC), radiographic (KL≥2) knee OA. Participants were randomised to baseline then 4-weekly IV placebo or 0.3, 1, or 2mg/kg LEVI-04 through week16. The primary efficacy endpoint was assessed at week 17, safety assessments were assessed to week 20, with a telephone safety follow-up at week 30. The primary endpoint was change in WOMAC pain to week 17, with additional outcomes including function, Patient Global Assessment (PGA), 50 and 70% pain responders, a novel pain on movement assessment (the Staircase-evoked Pain Procedure, StEPP) and daily NRS pain scores. Safety and tolerability, including Adverse Events of Special Interest (AESI) concerning joint pathologies, were key secondary endpoints. X-rays of 6 large joints and MRI of knees were utilised for inclusion/exclusion criteria at baseline, and safety evaluation at week 20. All safety events involving joints were escalated to an independent Adjudication Committee.

RESULTS: 518 people with knee OA were enrolled (mean age 63.1–65.4 years, mean BMI 29.3–30.3, female participants 51.5–61.5%). LEVI-04 demonstrated significant differences to placebo for the primary endpoint for all doses (Figure 1). WOMAC function and stiffness, PGA, daily pain scores, and StEPP were all statistically different to placebo. LEVI-04 was well tolerated, with no increased incidence of SAEs, TEAEs (Table 1) or joint pathologies, including RPOA (Table 2), compared to placebo.

CONCLUSION: LEVI-04 demonstrated significant and clinically meaningful improvement in pain, function and other efficacy outcomes. LEVI-04 was well tolerated at all doses studied, supporting the concept of supplementing endogenous p75NTR as a treatment for OA and other pain conditions. Phase III trials are in planning.

SPONSOR: Levicept Ltd

ACKNOWLEDGMENTS: Marc Hochberg, MD, MPH, John Carrino, MD, MPH & Edwin Oei, MD, PhD (Joint Safety Committee), Imaging services were provided by IAG Ltd

DISCLOSURE STATEMENT: SLW, MCP, BH, CH and IB are employees of Levicept Ltd. AG, PC and NK provide consulting services to Levicept Ltd.

CORRESPONDENCE ADDRESS: simon@levicept.com

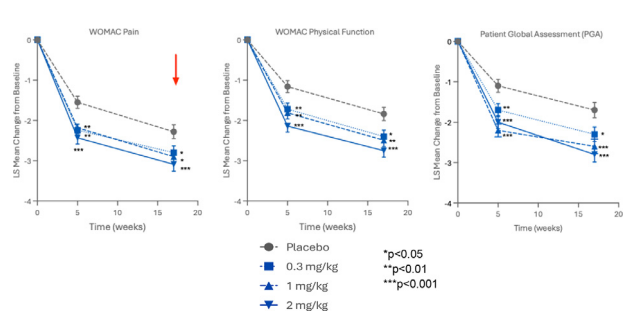


Figure 1: Efficacy Outcomes (Red arrow indicates Primary Endpoint).

Table 1: Treatment Emergent Adverse Events.

Adverse Events (AE), n (%)	0.3 mg/kg (N=129)	1.0 mg/kg (N=130)	2.0 mg/kg (N=129)	Placebo (N=129)									
Any Serious AE	0	1 (0.8)	3 (2.3)	3 (2.3)									
Any Treatment-	75 (58.1)	86 (66.2)	83 (64.3)	87 (67.4)									
Emergent AE													
(TEAE)													
(TEAE) TEAEs with more than 5% incidence, n (%) Arthralgia 11 (8.5) 15 (11.5) 15 (11.6) 20 (15.5)													
Arthralgia	11 (8.5)	15 (11.5)	15 (11.6)	20 (15.5)									
Nasopharyngitis	6 (4.7)	8 (6.2)	13 (10.1)	13 (10.1)									
Back pain	3 (2.3)	5 (3.8)	8 (6.2)	3 (2.3)									
Headache	4 (3.1)	3 (2.3)	8 (6.2)	6 (4.7)									
COVID-19	5 (3.9)	2 (1.5)	4 (3.1)	8 (6.2)									
Upper respiratory tract infection	4 (3.1)	4 (3.1)	5 (3.9)	7 (5.4)									
Pain in extremity	3 (2.3)	7 (5.4)	5 (3.9)	5 (3.9)									

Table continued on next page.

¹ University of Leeds, Leeds, UK

² Boston University School of Medicine, Boston, MA, USA

³ Ein Sof Innovation, Ltd, Wellesley, MA, USA

⁴ NBCD A/S, Soeborg, Denmark

⁵ Prosoft Clinical, Chesterbrook, PA, USA

⁶ Levicept Ltd, Sandwich, Kent, UK

Table 2: Incidence of Rapidly Progressive OA Type 1 & 2 (R1, R2), Subchondral Insufficiency Fracture (SIF), Osteonecrosis (ON), and Total Joint Replacements (TJR), n (%).

0.3 mg/kg 1 mg/kg				2 mg/kg				Placebo												
	R1	R2	SIF	ON	TJR	R1	R2	SIF	ON	TJR	R1	R2	SIF	ON	TJR	R1	R2	SIF	ON	TJR
Knees	0	0	0	0	1* (0.8)	2 [†] (1.5)	0	0	0	1* (0.8)	1 [†] (0.8)	0	0	0	1 (0.8)	1 [†] (0.8)	0	1 (0.8)	0	0
Hips	0	0	0	0	0	0	0	0	0	0	0	0	0	0	0	0	0	0	0	0
Shoulders	0	0	0	0	0	0	0	1* (0.8)	0	0	0	0	0	0	0	0	0	0	0	0

All joint events Kellgren-Lawrence grade 2–4 on entry, all TJRs Kellgren-Lawrence grade 4 on entry.

^{*}Elective surgery; †Moderate to severe meniscal extrusion reported; ‡OA of the shoulder present at baseline.

EFFECT OF LATERAL MENISCUS POSTERIOR ROOT TEARS ON CARTILAGE AND MENISCAL MECHANICS

J.S. Broberg, E. Hoptioncann, A. Kimbowa, A. Yung, K. Bale, I. Hacihaliloglu, P. Lodhia, D.R. Wilson

The University of British Columbia, Vancouver, BC, Canada

INTRODUCTION: Measuring cartilage and meniscal mechanics in loaded knees is essential to understanding the effects of lateral meniscus posterior root tears (LMPRTs) and the effectiveness of meniscal repair procedures that seek to protect the joint from degeneration. Studies have assessed mechanics with thin-film pressure sensors or finite element models, but their conclusions are limited by the invasiveness or inherent assumptions of the techniques employed. Ultra-high field MRI provides sufficient resolution to measure cartilage and meniscal mechanics during loading in a compatible loading device, without requiring disruption or simulation of the articulating joint surfaces. However, no studies have evaluated the impact of LMPRTs on the cartilage and meniscal mechanics in a human cadaveric knee using such a method.

OBJECTIVE: Test the hypothesis that LMPRTs increase femoral and tibial cartilage strain and meniscal extrusion.

METHODS: Six human knee lateral compartments (mean age 70 yrs) were tested. Anatomical alignment in full extension was maintained during preparation. The lateral meniscus and its roots, meniscotibial ligament, and attachment to the popliteus, as well as the ACL, were preserved. Specimens were placed in a novel pneumatic compression apparatus customized for use a 9.4T MRI scanner. Morphologic scans with a resolution of $0.06 \times 0.12 \times 0.4$ mm were acquired before loading and after 2 hours of loading (Figure 1). The load applied was constant and equivalent to 48% body weight to simulate two-legged standing. An artificial LMPRT was then created, and specimens were left unloaded until testing the next day with the same protocol. Joint tissues were manually segmented for both intact and LMPRT conditions, in both loaded and unloaded states. Flattened cartilage profiles were generated to calculate cartilage strain in the axial direction, with negative strain indicating compression. The mean and maximum strains in the tibiofemoral contact area were determined in both the femoral and tibial cartilage. Meniscal extrusion was measured as the perpendicular distance between the external edge of the meniscus and the line bisecting the external edge of the tibial plateau and femoral condyle in the most anterior slice of the popliteus' insertion. All measures were compared between conditions with paired Student's t-tests with significance set to 0.05.

RESULTS: Maximum compressive strain in the tibiofemoral contact region of the femoral (p=0.013) and tibial (p=0.010) cartilage increased significantly after the LMPRT (Figure 2). The increase in mean compressive strain in the tibiofemoral contact region after the LMPRT was not significantly different for the femoral (p=0.103) or tibial (p=0.065) cartilage. Likewise, the increase in meniscal extrusion after the LMPRT was not significantly different (p=0.143). Specimens with a greater increase in meniscal extrusion after the LMPRT tended to have a greater increase in maximum cartilage strain after the LMPRT.

CONCLUSION: Increases in maximum cartilage strain after LMPRT reflect higher cartilage stress, which is associated with cartilage degeneration. Our finding of more meniscal extrusion in specimens with greater increases in cartilage strain highlights a potential relationship between cartilage and meniscal mechanics, as well as the importance of restoring normal meniscal mechanics through a LMPRT repair. A key advantage of this approach to studying knee mechanics is the ability to simultaneously assess meniscal and cartilage mechanics with minimal disruption to the alignment and critical soft tissue. The approach has potential for assessment of the effectiveness of meniscal repair techniques.

SPONSOR: The Arthritis Society (Canada)

DICLOSURE STATEMENT: P. Lodhia is a speaker for Arthrex and has received support from Ossur.

ACKNOWLEDGMENT: We thank Emily Sullivan and Jessica Küpper for developing the pneumatic loading device.

CORRESPONDENCE ADDRESS: jordan.broberg@ubc.ca

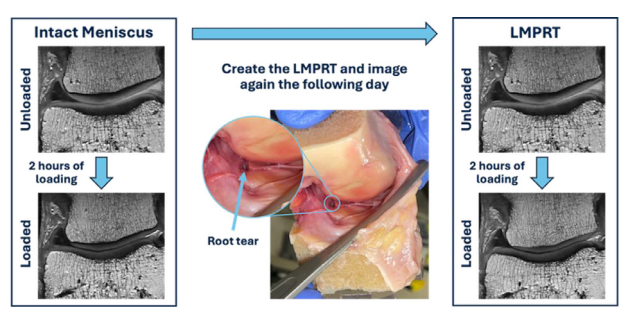


Figure 1: Schematic of the study protocol.

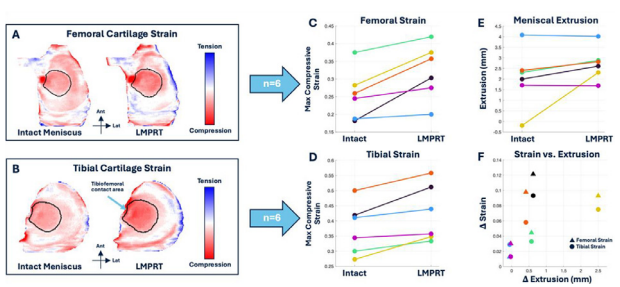


Figure 2: A) Axial strain map of femoral cartilage for one representative specimen for intact and LMPRT conditions, with red depicting compressive strain; B) Axial strain map of tibial cartilage for one representative specimen for intact and LMPRT conditions, with red depicting compressive strain; C) Maximum compressive strain of femoral cartilage within contact area for intact and LMPRT conditions for all six tested specimens. D) Maximum compressive strain of tibial cartilage within contact area for intact and LMPRT conditions for all six tested specimens. E) Meniscal extrusion for intact and LMPRT conditions for all six tested specimens. F) Change in femoral and tibial compressive strain between LMPRT and intact condition versus change in meniscal extrusion between LMPRT and intact condition.

PATELLAR AND FEMORAL BONE MORPHOLOGY AND ITS ASSOCIATION WITH LOADING IN YOUNG ADOLESCENT BOYS AND GIRLS

R. van Paassen 1 , N. Tumer 2 , J. Hirvasniemi 1,2 , T.M. Piscaer 1 , A.A. Zadpoor 2 , S. Klein 1 , S.M.A. Bierma-Zeinstra 1 , E.H.G. Oei 1 , M. van Middelkoop 1

INTRODUCTION: High levels of physical activity or high body mass index (BMI) during growth may negatively influence bone and cartilage, but little is known about how loading relates to the shape of the patella and femur. It is well established that bone shape is primarily determined during growth, and specific variations in bone shape are associated with a higher risk of osteoarthritis (OA). Therefore, we aim to identify the association between the 3D shape of the patella and femur bones and loading factors (i.e., body mass index (BMI) and sports participation) in young adolescents.

OBJECTIVE: Our objective is twofold: 1) to determine the differences in bone shape between boys and girls, and 2) to determine which bone shape variations are associated with loading parameters (i.e., BMI and sports participation).

METHODS: Data from 1912 participants, aged 14.1 (SD: 0.67), standardized BMI for age and sex (BMI-SDS) of 0.42 (1.20), were retrieved from the Generation R study. The Generation R study is a large population cohort study that follows children from fetal life until adulthood. A subset of participants who underwent knee MRI (3.0T, Discovery MR750w, GE Healthcare, Milwaukee, WI, USA) at the 13-year follow-up time point were included in the current study. Imaging was performed with two knees in full extension using a water excitation Gradient Recalled Acquisition in Steady State sequence. Patellae and distal femora were automatically segmented using a method that combines multi-atlas and appearance models. Two statistical shape models (SSM) were built based on the automatically segmented left and right patellae and femora. Shape modes explaining at least 1% of the total population variation were included in the analyses. Differences between boys and girls were determined using a 2-sample T-test. Generalized estimating equation models, separate for boys and girls, were used to analyze the association between BMI-SDS, sports participation (yes or no), and shape variation. Bonferroni correction was used to correct for multiple testing.

RESULTS: A total of 3638 patellae and 3355 femora were included in the shape models. Eleven patellar and fourteen femoral shape modes explained at least 1% of the total variation and were retained for analysis. Eight out of the eleven (modes 1-4, 6, 8, 10, and 11) patellar and twelve out of the fourteen (modes 1-10, 12, and 14) femoral shape modes showed significant differences between boys and girls. Four patella and two femur modes were significantly associated with BMI in both boys

and girls, while four patella and seven femur modes were significantly associated in either boys or girls only (Table 1). Patella shape mode 1 was significantly associated with sports participation in both boys and girls, as well as BMI in boys only. Femur shape mode 1 was associated with sports participation in girls and BMI in both boys and girls (Table 1; Figure 1). Femur mode 3, explaining variation in medial anterior condyle and epicondylar width, was only associated with BMI in boys. A higher BMI was associated with a slightly thicker medial anterior condyle and a narrower epicondylar width. Furthermore, patella mode 4, explaining variation in thickness of the dorsal side of the medial apex, was only associated with BMI in girls, with higher BMI being associated with a thicker dorsal side of the medial apex.

CONCLUSION: Multiple differences in shape variations between boys and girls were identified. Sports participation was associated only with the shape mode, explaining size, whereas BMI demonstrated more associations, indicating that BMI is a more important factor. However, sex-specific differences exist. For instance, a higher BMI was associated with a thicker dorsal medial apex in girls, but not in boys. In contrast, a slightly thicker medial anterior condyle was associated with BMI in boys, but not in girls. These varying relationships between BMI and shape in boys and girls highlight the necessity of conducting shape analyses separately during growth.

SPONSOR: Dutch Arthritis Association (21-1-204).

DISCLOSURE STATEMENT: None

CORRESPONDENCE ADDRESS: r.vanpaassen@erasmusmc.nl

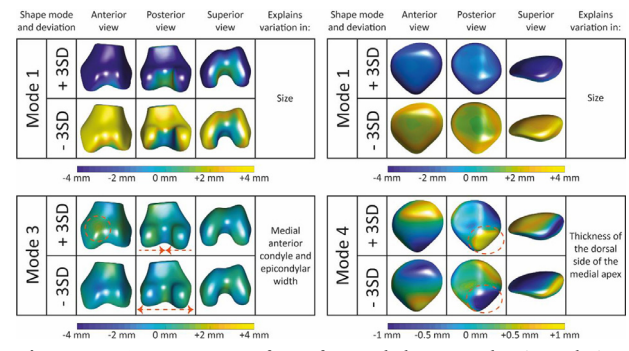


Figure 1: Distance maps of two femoral shape modes (1 and 3) and two patella shape modes (1 and 4) showing the distance (in millimeters) from the mean in the $\pm 3SD$ direction projected on the mean shape. The distance of femur mode 1, 3, and patella mode 1 ranges from -4 to +4 mm, and on the right ranges from -1 to +1 mm.

Table continued on next page.

¹ Erasmus University Medical Center, Rotterdam, The Netherlands

² Delft University of Technology, Delft, The Netherlands

Table 1: Association between BMI and patellar and femoral shape modes in boys and girls separately (Betas with 95% confidence interval).

	Patella			Femur					
	BMI		Sport		ВМІ		BMI Sport		
	Boys	Girls	Boys	Girls	Boys	Girls	Boys	Girls	
1	-0.22, -0.27;-0.17*	-0.04, -0.08;0	-0.29, -0.47;-0.11*	-0.31, -0.46;-0.16*	-0.35, -0.39;-0.3*	-0.16, -0.2;-0.12*	-0.24, -0.43;-0.06	-0.29, -0.42;-0.16*	
2	0.19, 0.14;0.24*	0.15, 0.11;0.20*	0.00, -0.19;0.19	-0.02, -0.16;0.13	-0.04, -0.08;0.01	-0.06, -0.1;-0.02	-0.08, -0.24;0.09	-0.09, -0.21;0.03	
3	0.36, 0.31;0.41*	0.38, 0.34;0.43*	0.12, -0.08;0.32	-0.11, -0.28;0.06	0.08, 0.03;0.13*	0.03, -0.01;0.08	-0.01, -0.2;0.18	-0.08, -0.21;0.05	
4	0.04, -0.01;0.08	0.10, 0.06;0.14*	0.04, -0.13;0.22	0.07, -0.08;0.22	-0.02, -0.07;0.02	-0.01, -0.05;0.03	0.01, -0.17;0.19	-0.1, -0.23;0.02	
5	-0.14, -0.19;-0.09*	-0.10, -0.15;-0.05*	0.03, -0.15;0.21	0.03, -0.13;0.19	-0.07, -0.12;-0.03*	-0.01, -0.06;0.03	0.18, -0.02;0.37	0.17, 0.02;0.32	
6	0.16, 0.11;0.21*	0.11, 0.06;0.16*	-0.11, -0.32;0.09	-0.09, -0.24;0.05	0.02, -0.02;0.07	0.11, 0.07;0.15*	-0.16, -0.33;0	-0.19, -0.32;-0.05	
7	0.07, 0.02;0.12	0.15, 0.10;0.20*	-0.09, -0.27;0.1	0, -0.15;0.16	0.08, 0.04;0.13*	0.05, 0;0.09	-0.05, -0.23;0.12	-0.08, -0.2;0.05	
8	0.07, 0.02;0.11	0.01, -0.03;0.05	-0.14, -0.34;0.05	-0.06, -0.19;0.07	-0.12, -0.16;-0.07*	-0.11, -0.16;-0.06*	-0.01, -0.19;0.17	-0.05, -0.19;0.09	
9	0.02, -0.03;0.06	-0.02, -0.06;0.02	0.03, -0.14;0.2	0.17, 0.03;0.31	-0.03, -0.07;0.01	-0.09, -0.13;-0.05*	-0.01, -0.17;0.16	-0.02, -0.16;0.11	
10	-0.04, -0.09;0.01	-0.09, -0.14;-0.05*	0.00 -0.21;0.22	0.04, -0.09;0.18	0.07, 0.02;0.12	0.05, 0;0.09	-0.14, -0.36;0.09	-0.09, -0.24;0.06	
11	-0.07, -0.12;-0.02*	-0.12, -0.16;-0.07*	-0.06, -0.26;0.14	0.15, 0;0.3	-0.06, -0.11;-0.01	-0.03, -0.07;0.02	0.06, -0.12;0.25	0.07, -0.07;0.2	
12					-0.02, -0.07;0.02	-0.07, -0.11;-0.02*	0.09, -0.07;0.25	0.06, -0.07;0.2	
13					0.04, -0.01;0.08	0.01, -0.03;0.06	-0.08, -0.25;0.09	-0.02, -0.16;0.12	
14					-0.04, -0.09;0.01	-0.09, -0.13;-0.04*	-0.13, -0.32;0.06	-0.02, -0.19;0.14	

All analyses were corrected for age. * Significant after Bonferroni correction. Level of significance of the patella P-value < 0.05/11=0.0045. Level of significance of the femur P-value < 0.05/14=0.0036. Statistically significant associations are shown in bold.

DEEP LEARNING MODELS FOR AUTOMATIC JOINT SPACE WIDTH MEASUREMENT

Z. Wang 1, J. Crawmer 1, A. Guermazi 2, J. Duryea 1,*, M. Jarraya 1,*

- ¹ Mass General Brigham, Harvard Medical School, Boston, MA, USA
- $^2\,\mbox{VA}$ Boston Healthcare System & Boston University School of Medicine, Boston, MA, USA
- *Shared last authorship

INTRODUCTION: Accurate and automated measurement of femorotibial JSW (fJSW) is crucial for assessing and monitoring OA. Current semi-automated (SA) fJSW measurement methods can be time-consuming and prone to inter-observer variability. This work describes the evaluation of a deep learning (DL) approach to substantially automate fJSW measurement from knee radiographs.

OBJECTIVE: To evaluate the performance of a DL method for automatic fJSW measurement by comparing it to a standard SA method.

METHODS: We randomly selected a single knee radiograph from 295 OAI participants (49 knees for each KL grade 0-4) that were not used for DL training. We measured the BL and 48mo. medial fixed-location fJSW at x=0.25 using both the SA and DL methods. fJSW(x=0.25) have been shown to be the most responsive location compared to other fJSW locations and minimum JSW. The SA fJSW measurement consists of a first step to delineate the femur for setting up the necessary coordinate system, followed by a second step to delineate the femur and tibia for measuring fJSW. We trained separate DL algorithms for each step. The models employed an Attention U-Net architecture for segmenting joint spaces. This network enhances the standard U-Net encoder-decoder structure with attention mechanisms. The U-Net's encoder path progressively captures contextual information through a series of convolutional and pooling layers. The decoder path then gradually reconstructs the segmentation map by up-sampling features and combining them with high-resolution features from the encoder via skip connection. To assess performance, we calculated failure rates (assessed visually) for each step, the fJSW_{DL} to fJSW_{SA} correlation (Pearson's R), and the responsiveness (standardized response mean: SRM). For DL coordinate system failures, the reader made manual corrections so all knees could be passed to the DL fJSW algorithm.

RESULTS: There were 58 coordinate systems failures (11.7%) with a KL distribution as follows: KL0:2, KL1:7, KL2:4, KL3:9, KL4:36, and 31

fJSW (6.2%) failures distributed as follows: KL0:4, KL1:1, KL2:4, KL3:7, KL4:15. We excluded the JSW failures leaving knees from 215 participants for the correlation and responsiveness analyses. The Pearson's correlation was R=0.97 and the SRM values were -0.64 (SA) and -0.67 (DL). Figure 1 is a Bland-Altman plot comparing the SA and DL fJSW, showing a minor bias and few outliers.

CONCLUSION: The results demonstrate that a DL algorithm can measure fJSW accurately with equivalent or better responsiveness compared to the SA method, dramatically reducing the reader time while maintaining performance. The majority of the failures were for KL4 knees, which are less utilized for KOA studies. The DL software has the potential to be used in very large studies and clinical trials of KOA.

SPONSOR: This project is supported by a *Ralph Schlaeger Research Fellowship* (MGH Radiology Departmental Award), NIH R01AR078187, and NIAMS grant K23-AR084603.

DICLOSURE STATEMENT: AG has received consultancies fees from Novartis, ICM, Levicept, Scarcell, Peptinov, Pacira, Coval, 4Moving, Formation Bio, Paradigm, Medipost and TissueGene and is shareholder of Boston Imaging Core Lab (BICL), LLC a company providing image assessment services. MJ has received consultancy fees from BICL, LLC.

ACKNOWLEDGMENT: None

CORRESPONDENCE ADDRESS: mjarraya@mgh.harvard.edu

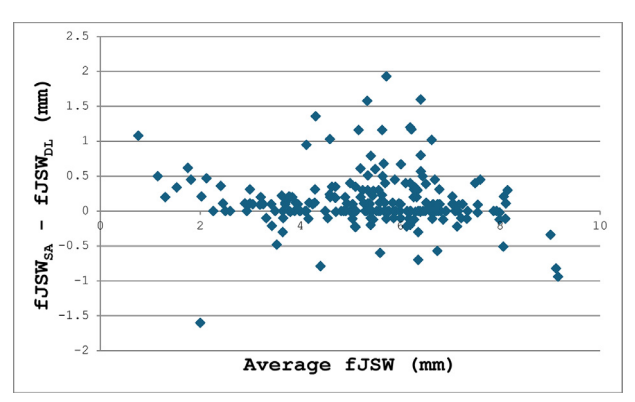


Figure 1: Bland-Altman plot comparing SA and DL fixed joint space width (fJSW).

ELSEVIER

Contents lists available at ScienceDirect

Osteoarthritis Imaging

journal homepage: www.elsevier.com/locate/ostima



19th International Workshop on Osteoarthritis Imaging: Posters

INCREASED BMI IS A MODIFIABLE RISK FACTOR OF SUBCHONDRAL INSUFFICENCY FRACTURE OF THE KNEE

M.Z. Alzaher¹, W. Issa², J. Husseini², A. Huang², A. Guermazi³, M. Jarraya²

INTRODUCTION: Subchondral insufficiency fractures of the knee (SIFK) are increasingly recognized as an important, but often underdiagnosed, cause of acute knee pain and functional decline, particularly in middle-aged and older adults. Existing studies on SIFK are often limited in number and lack a sufficient number of controls. Because of its rare occurrence in the general population and in major epidemiological studies, our understanding of the risk factors of SIFK remains limited. It has been hypothesized that excessive joint loading leads to focal stress concentrations within the subchondral bone plate, overwhelming its capacity for repair and ultimately predisposing to a microfracture. However, it remains unclear whether BMI is modifiable risk factor of SIFK.

OBJECTIVE: Our aim is to investigate the association between BMI and the occurrence of MRI-detected SIFK in a clinical setting.

METHODS: We conducted a case-control study at a tertiary academic hospital network from November 2022 to October 2024. Cases were identified using an institutional repository, based on MRI reports containing the diagnosis "subchondral insufficiency fracture". The diagnosis of SIFK was confirmed by a MSK radiologist who reviewed all images. Matched controls were defined as patients within 5 years of age who underwent knee MRI for knee pain over the same period (±10 days) and who did not have subchondral insufficiency fracture on MRI (both in the MR report and after review of images). Electronic medical records were manually checked for the primary independent variable, BMI, and other variables such as age, sex, dyslipidemia, statin use, diabetes mellitus, and hypertension. Univariable and multivariable logistic regression estimated odds ratios (ORs) and 95% confidence intervals (CIs) were estimated using SIFK as the primary dependent variable. Missing data on variables in the logistic regression model will be handled by listwise deletion.

RESULTS: The mean age (\pm SD) in years was 63.2 (\pm 10.2) for the cases and 64.3 (\pm 10.4) for the controls. Females made up 64% of the cases and 67% of the controls. Median (Q1–Q3) BMI was 29.5 kg/m² (26.0–34.4) for the cases and 27.1 kg/m² (23.7–31.4) for the controls. A two-sample t-test showed that BMI was significantly higher in the cases than in con-

trols (p-value = 0.015). Univariable logistic regression with SIFK as the dependent variable and BMI as the independent variable estimated an OR of 1.06 (95% CI: 1.01–1.10). This statistically significant result remained after adjusting potential confounders such as sex, dyslipidemia, and statin use with an estimated OR of 1.05 (95% CI: 1.01–1.10) (figure 1 and table 1). Figure 2 shows an example of SIFK.

CONCLUSION: Our preliminary results indicate that elevated BMI may be linked to greater odds of having SIFK. As we continue to enroll additional participants, we anticipate refining our effect estimates and strengthening the evidence for this association.

SPONSOR: This project was funded by the National Institute of Arthritis and Musculoskeletal and Skin Diseases (NIAMS) under grant K23-AR084603, and the Osteoarthritis Research Fund (MGH).

DICLOSURE STATEMENT: AG has received consultancies fees from Novartis, ICM, Levicept, Scarcell, Peptinov, Pacira, Coval, 4Moving, Formation Bio, Paradigm, Medipost and TissueGene and is shareholder of Boston Imaging Core Lab (BICL), LLC a company providing image assessment services. JC and MJ have received consultancy fees from BICL, LLC

ACKNOWLEDGMENT: We thank Drs. Edie Weller and Daniel I. Rosenthal for their statistical advice and expert opinion on the topic. CORRESPONDENCE ADDRESS: mjarraya@mgh.harvard.edu

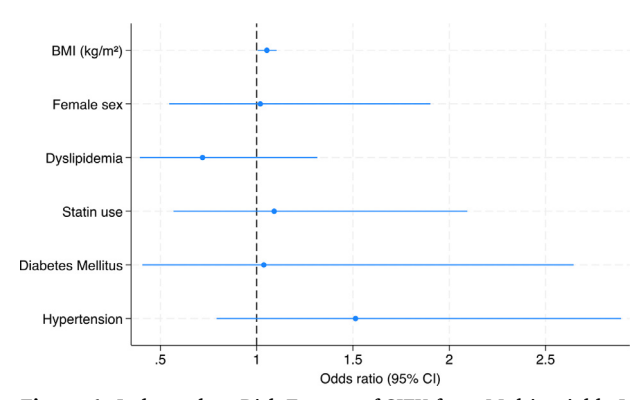


Figure 1. Independent Risk Factors of SIFK from Multivariable Logistic Regression Analysis.

¹ Harvard Medical School, Boston, MA, USA

² Mass General Brigham, Harvard Medical School, Boston, MA, USA

³ VA Boston Healthcare & Boston University School of Medicine, Boston, MA, USA

 Table 1. Results of Multivariable Logistic Regression Analysis.

Variable	SIFK+(n=97)	SIFK - (n=97)	Odds Ratio (95% CI)
BMI in kg/m ² – Median (Q1-Q3)	29.5 (26.0-34.4)	27.1 (23.7-31.4)	1.05 (1.01-1.10)
Female sex (n, % of outcome)	62 (63.9%)	65 (67.0%)	1.02 (0.55-1.90)
Dyslipidemia (n, % of outcome)	51 (52.6%)	57 (58.8%)	0.72 (0.39-1.31)
Statin use (n, % of outcome)	46 (47.4%)	39 (40.2%)	1.09 (0.57-2.09)
Diabetes Mellitus (n, % of outcome)	14 (14.4%)	10 (10.3%)	1.04 (0.41-2.65)
Hypertension (n, % of outcome)	49 (50.5%)	36 (37.1%)	1.51 (0.79-2.89)



Figure 2: Coronal fat-suppressed proton-density MR image showing a subchondral insufficiency fracture of the medial femoral condyle in a 73-year-old-female. Note the m assive subchondral edema of the medial femoral condyle, which is out or proportion for the degree of

SIMULTANEOUS 3D CARTILAGE T_2 MAPPING AND MORPHOLOGICAL IMAGING WITH RAFO-4 MRI, A MACHINE LEARNING ALGORITHM

K. Balaji ¹, M. Mendoza ¹, P.M. Vicente ¹, C. Galazis ¹, S. Kukran ^{1,2}, A.A. Bharath ¹, P.J. Lally ¹, N.K. Bangerter ^{1,3}

INTRODUCTION: Cartilage T_2 is a non-invasive, microstructural MRI biomarker for KOA, with elevated T_2 indicating early KOA onset. Cartilage T_2 maps could be used in clinical trials to test a drug candidate's effect on microstructure. Quantitative DESS (qDESS) is widely used for cartilage imaging as it simultaneously acquires 3D, morphological whole knee images and quantitative T_2 maps in \sim 5 minutes. Researchers are also developing T_2 mapping techniques using phase-cycled balanced Steady State Free Precession (pc-bSSFP). It is rapid and has higher SNR efficiency than qDESS, which could lead to better 3D morphological image quality and more reliable T_2 maps. PLANET is a technique that uses a minimum of six different pc-bSSFP acquisitions to analytically calculate T_2 . This is too time-consuming to be clinically feasible. In this study, we trained Random Forest (RaFo) machine learning models to estimate T_2 from fewer pc-bSSFP acquisitions to reduce scan time while still estimating reliable voxel-level T_2 values.

OBJECTIVE: 1) Train and test RaFo models on simulated 4 and 6 pcbSSFP data and benchmark performance with PLANET. 2) Test RaFo models on in vivo knee data and benchmark performance with the reference T₂ mapping technique (spin echo), PLANET, and qDESS.

METHODS: 70,000-sample training and 30,000-sample testing datasets were simulated. Each sample corresponded to 12 different pc-bSSFP measurements of the same voxel location in the tissue. The physicsinformed simulated datasets were pre-processed, which included subsampling from 12 pc-bSSFP measurements to 4 or 6. RaFo models were then trained to estimate T2 and tested on these pre-processed datasets. Finally, to evaluate performance on noisier in vivo data, fully sampled knee images of two healthy volunteers (HVs, 2F:24-25) were acquired on a 3T Siemens Verio (Erlangen, Germany) with an 8-channel knee coil using 12 measurements of bSSFP (water excitation, 8.6/4.3 ms TR/TE; 22° flip angle; $1 \times 1 \times 5$ mm³ voxel volume; $128 \times 128 \times 130$ mm³), qDESS (water excitation; 20° flip angle; 21.77 ms TR; 6 ms TE; 364 Hz/Px receiver bandwidth; 0 dummy scans per volume), and a gold-standard spin-echo T₂ mapping approach (2500 ms TR; 15, 45, 75 ms TE, 90° and 180° flip angle) with appropriate ethics approval. All images had $1 \times 1 \times 5$ mm³ voxel volume and 128×128 mm² field of view. PLANET was tested on 6 pc-bSSFP measurements (labelled PLANET-6). RaFo models were tested on 4 and 6 bSSFP measurements (labelled RaFo-4 and RaFo-6, respectively).

RESULTS: Fig1 shows results from simulated data tests, with similar performance across the RaFo models and PLANET. Fig2 shows the in vivo T_2

maps, with the RaFo models visually aligning best with the reference $\rm T_2$ maps while qDESS is biased towards lower values in HV1 and PLANET estimates large-valued outliers in HV2 (not visualized). The RaFo models had lower 95% confidence intervals of the difference between the reference and estimated $\rm T_2$ (~36ms) compared to qDESS (~49ms) and PLANET (~275ms).

CONCLUSION: The RaFo models best aligned with the reference T_2 maps, even when estimating T_2 using only 4 pc-bSSFP acquisitions. They also only estimated biologically feasible values as it can only estimate T_2 values it was trained on, a unique feature of the RaFo algorithm. Hence, RaFo-4 is a promising alternative to qDESS for cartilage morphological and quantitative imaging as it has the potential to have comparable scan times to qDESS, provide better morphological images and estimate more reliable T_2 maps. Future work includes testing RaFo-4 and qDESS on a larger cohort of early KOA patients and HVs.

SPONSOR: NIH (RO1EB002524), NIHR Imperial Biomedical Research Center

DICLOSURE STATEMENT: I have no disclosures.

ACKNOWLEDGMENT: I thank the participants for volunteering for this study.

CORRESPONDENCE ADDRESS: kb4317@ic.ac.uk

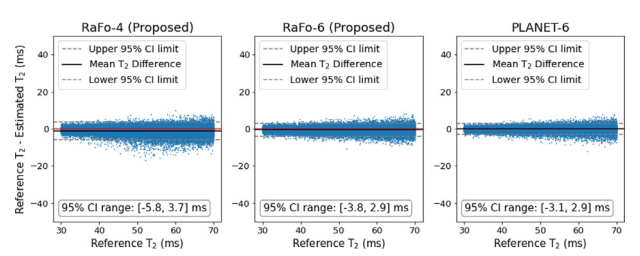


Fig. 1: Bland-Altman plot showing the difference between reference and estimated T₂. Similar results across PLANET and the RaFo models.

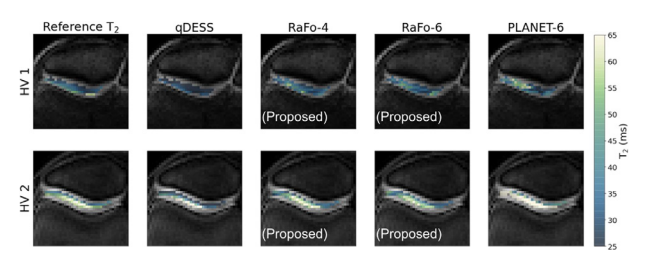


Fig. 2: The reference spin echo, qDESS, RaFo-4, RaFo-6, and PLANET-6 T_2 maps for 2 HVs. The RaFo models consistently preserve the spatial variations seen in the reference T_2 maps.

¹ Imperial College London, London, UK

² Case Western Reserve University, Cleveland, OH, USA

³ Boise State University, Boise, ID, USA

3-D LANDMARKING REPEATABILITY EMPHASIZES CHALLENGES IN SCAN POSITIONING DURING WEIGHT BEARING CT OF THE KNEE

A. Boddu 1 , T. Whitmarsh 2 , N.A. Segal 3 , N.H. Degala 3 , J.A. Lynch 4 , T.D. Turmezei 1,5

- ¹ Norfolk and Norwich University Hospital, Norwich, UK
- ² University of Cambridge, Cambridge, UK
- ³ University of Kansas Medical Center, Kansas City, KS, USA
- ⁴ University of California San Francisco, San Francisco, CA, USA
- ⁵ University of East Anglia, Norwich, UK

INTRODUCTION: Weight bearing CT (WBCT) has shown promise in the evaluation of the knee joint instead of radiography. However, bringing weight bearing to 3-D imaging poses technical challenges that have to be overcome if repeatability is to be optimised. From prior study and experience, maintaining knee flexion angle (KFA) and centering in the vertical scan range with consistency can be difficult. One means to evaluate these distance and angle measurements from WBCT is to use a bone surface landmarking system.

OBJECTIVE: (1) To evaluate the repeatability of a manual WBCT land-marking system of the femur and tibia at the knee; and (2) from this develop a technique for evaluating repeatability of KFA and vertical scan range centering.

METHODS: 14 individuals recruited and consented at the University of Kansas Medical Center had baseline and follow-up WBCT imaging suitable for analysis. Participant demographics were: mean ± SD age 61.3 ± 8.4 years, BMI 30.7 ± 4.3 kg/m² and male:female ratio 8:6. All scanning was performed on the same XFI WBCT scanner (Planmed Oy, Helsinki, Finland) with the mean \pm SD interval between baseline and follow-up attendances 14.9 \pm 8.1 days. A SynaflexerTM device was used to standardise knee positioning during scanning. Imaging acquisition parameters were 96 kV tube voltage, 51.4 mA tube current, 3.5 s exposure time. A standard bone algorithm was applied for reconstruction with 0.3 mm isotropic voxels and a 21 cm vertical scan range. Both knees were included in all analyses with SD adjustments made for multiple observations from the same individual. Participant identification and scan sequence were anonymised prior to analyses. A first observer (A.B.) placed 10 femoral and 12 tibial landmarks using Stradview. These landmarks were reviewed by a second observer (T.D.T.), who placed additional landmarks at the extremes of the vertical scan within the centre of the bone medullary cavities. Bone segmentations from ScanXM were used to register landmarks from follow-up to baseline in wxRegSurf; the follow-up-to-baseline femur registration was applied to the followup tibial co-ordinates to assess joint positioning. Landmark repeatability was taken as the mean \pm SD distance (mm) between baseline and followup for each landmark. A method to extract KFA and valgus alignment was developed as the angle between the lines of the extreme scan range landmarks (F00 and T00) and the centre of gravity (CoG) of the rest of the landmarks in the same bone. Valgus alignment was taken from the anterior view (<180° laterally = valgus) and KFA from lateral.

RESULTS: Landmark placement with their codes is shown in Figure 1a (in a left knee), with code definitions given in Table 1. An example of baseline and follow-up landmarking is shown on the same knee in Figure 1b with error results from all landmarks given in Table 1. Outside of the F00/T00 markers, the most notable mean error was seen at the central anterior and central posterior tibial plateau margins (T01 and T09) with mean \pm SD values of 6.0 ± 4.7 mm and 5.2 ± 3.8 mm respectively, and at the medial femoral trochlear superior articular margin (F03) at 5.4 ± 3.6 mm. Error metrics were expectedly similar for F00 and T00 with mean (max.) values of 23.2 (47.0) mm and 22.8 (45.7) mm respectively, serving as a surrogate marker for variation in central placement of the knee within the vertical (z-axis) scan range. Valgus angle was consistent, showing a mean \pm SD (range) difference of $0.2 \pm 1.1^{\circ}$ (-2.0 to 1.8°), whereas KFA values were less consistent at -2.5 \pm 5.9° (-15.5 to 9.8°) (Table 1).

CONCLUSION: Less well anatomically defined landmarks such as the tibial plateau margins are less repeatable, with worst mean repeatability error around 5 mm. Vertical knee centring varied substantially up to a max. value of 47 mm, while KFA varied widely from -15 to 10°. Positioning of the knee consistently during WBCT remains challenging. This *post hoc* evaluation derived from landmarking is valuable for verification, but work needs to be done on optimising positioning protocols that can be applied prospectively to ensure positioning remains consistent for evaluation of other parameters such as meniscal extrusion and 3-D JSW.

SPONSOR: None.

DISCLOSURE STATEMENT: NS is a consultant for Trice Medical, Arthrex, and Pacira Biosciences. TT is Director of KNEE3D Ltd. TW is Director of Minogame Ltd.

ACKNOWLEDGEMENT: None.

CORRESPONDENCE ADDRESS: abhinav.boddu@gmail.com



Figure 1

Table 1

Code	Landmark description	Error mean (mm)	Error SD (mm)	Error min. (mm)	Error max. (mm)
F00	central medullary cavity of femur in uppermost $\operatorname{frame}^{\mathbf{F}}$	23.2	15.7	4.1	47.0
F01	medial femoral epicondyle	2.8	3.0	0.8	9.9
F02	lateral femoral epicondyle	1.3	1.7	0.2	3.4
F03	medial femoral trochlear superior articular margin	5.4	3.6	0.3	10.7
F04	lateral femoral trochlear superior articular margin	2.6	2.6	0.8	5.7
F05	central anterior femoral condyle at base of trochlear groove	3.8	2.8	0.8	6.9
F06	central weight bearing medial femoral condyle at articular surface	2.9	2.1	0.6	9.3
F07	central weight bearing lateral femoral condyle at articular surface	4.0	1.8	1.5	6.3
F08	central femoral intercondylar notch	1.8	1.2	0.7	3.9
F09	posterior medial femoral condyle articular surface	2.6	2.0	0.6	10.3
F10	posterior lateral femoral condyle articular surface	2.4	1.7	0.5	4.8
-	centre of gravity of femoral landmarks (excluding F00) ^F	1.2	0.6	0.3	3.2
T00	central medullary cavity of tibia in lowermost $\operatorname{frame}^{\mathbf{T}}$	22.8	15.9	6.4	45.7
T01	central anterior margin tibial plateau	6.0	4.7	0.6	20.6
T02	medial margin medial tibial plateau	1.9	1.5	0.3	3.4
T03	central medial tibial condyle articular surface	1.9	1.8	0.6	3.0
T04	tip of medial tibial spine	2.0	2.1	0.4	8.9
T05	tip of lateral tibial spine	1.1	1.6	0.5	4.8
T06	central lateral tibial condyle articular surface	4.3	3.5	0.6	11.9
T07	lateral margin lateral tibial plateau	2.5	2.8	0.5	5.2
T08	posterior margin medial tibial plateau	3.8	2.5	1.0	9.8
T09	central posterior margin tibial plateau	5.2	3.8	0.9	9.4
T10	posterior margin lateral tibial plateau	3.9	2.3	0.4	9.3
T11	central aspect tibial facet for fibula	1.5	0.9	0.7	4.0
T12	tibial tuberosity	3.8	4.7	0.8	9.1
-	centre of gravity of tibial landmarks (excluding $\text{T00})^{\text{T}}$	1.3	0.6	0.4	2.6

F/T = used at the line markers for calculating

Table 2

	KFA baseline (B)	KFA follow-up (F)	F-B	Valgus baseline (B)	Valgus follow-up (F)	F-B
MEAN	174.6°	172.1°	-2.5°	179.5°	179.7°	0.2°
SD	6.0°	6.0°	5.9°	5.1°	5.4°	1.1°
MIN.	162.3°	160.3°	-15.5°	173.5°	174.0°	-2.1°
MAX.	184.9°	182.5°	9.8°	188.6°	187.4°	1.8°

SEX-SPECIFIC CONTINUOUS JOINT SPACE WIDTH: AN ALTERNATIVE TO RHOA GRADING

F. Boel ¹, M.A. van den Berg ¹, N.S. Riedstra ¹, M.M.A. van Buuren ¹, J. Tang ¹, H. Ahedi ², N. Arden ³, S.M.A. Bierma-Zeinstra ¹, C.G. Boer ¹, F.M. Cicuttini ⁴, T.F. Cootes ⁵, K.M. Crossley ⁶, D.T. Felson ⁷, W.P. Gielis ⁸, J.J. Heerey ⁶, G. Jones ², S. Kluzek ³, N.E. Lane ⁹, C. Lindner ⁵, J.A. Lynch ¹⁰, J.B.J. van Meurs ¹, A. Mosler ⁶, A.E. Nelson ¹¹, M.C. Nevitt ¹⁰, E.H. Oei ¹, H. Weinans ⁸, J. Runhaar ¹, R. Agricola ¹

- ¹ Erasmus Medical Center, Rotterdam, The Netherlands
- ² University of Tasmania Menzies, Hobart, Tasmania, Australia
- ³ University of Oxford Nuffield, Oxford, Oxfordshire, UK
- ⁴ Monash University, Melbourne, Victoria, Australia
- ⁵ The University of Manchester, Manchester, UK
- ⁶ La Trobe Sport and Exercise Medicine Research Centre, La Trobe University School of Allied Health Human Services and Sport, Melbourne, Victoria, Australia
- ⁷ Boston University School of Medicine, Boston, MA, USA
- ⁸ UMC Utrecht, Utrecht, Netherlands
- ⁹ University of California Davis School of Medicine, Sacramento, CA, USA
- ¹⁰ University of California San Francisco, San Francisco, CA, USA
- ¹¹ The University of North Carolina at Chapel Hill, Chapel Hill, NC, USA

INTRODUCTION: The reported prevalence of radiographic hip OA (RHOA) varies widely in literature and depends on the specific study population. The KLG and (modified) Croft grade are commonly used to quantify RHOA. Both these scoring systems are inherently subjective, and the reproducibility is largely dependent on the expertise of the reader. Furthermore, both of these RHOA grading system emphasize different features of RHOA, making them difficult to compare. Using automated RHOA grade would reduce subjectivity and allow for fast, reproducible, and reliable assessment of radiographs. Since JSW currently demonstrates the highest reliability as a ROA describing feature, utilizing continuous JSW measurements could be a promising step towards achieving an automated RHOA grade.

OBJECTIVE: To investigate the association between baseline demographics, RHOA, and automated, continuous JSW.

METHODS: We pooled individual participant data from two prospective cohort studies within the Worldwide Collaboration on OsteoArthritis prediction for the Hip (World COACH consortium). Both cohorts have standardized weight-bearing anteroposterior (AP) pelvic radiographs available at baseline, 4-5 years, and 8 years follow-up. JSW measurements were automatically determined on the AP radiographs based on landmarks on the acetabular sourcil and the femoral head contour. Four different JSW measurements were determined for each hip, namely at the most medial point, in the center and at the most lateral point of the sourcil, and the minimal JSW (Fig 1). RHOA was scored by KLG or modified Croft grade. Based on the baseline and follow-up RHOA grades, the RHOA pattern of the hip was defined as "no definite RHOA" (KLG/Croft < 2 at all timepoints), "baseline RHOA" (KLG/Croft ≥ 2 at baseline), or "incident RHOA" (KLG/Croft ≥ 2 at follow-up). Hips were included for analysis if they had JSW measurements available at all three time points, and RHOA grades available at baseline and follow-up. The association between baseline age, body mass index (BMI), and the RHOA pattern, and each definition of JSW over time was estimated using linear mixed-effects models (LMMs). The analyses were stratified by sex due to known differences in JSW and OA risk in males and females. The random effects included follow-up time, cohort, and participant, accounting for the repeated measurements and cohort clustering. No RHOA was defined as the reference category for RHOA pattern. The resulting model coefficients with 95% confidence intervals (CI) were presented.

RESULTS: A total of 2,895 participants were included in the current study. 3,368 hips of 1,698 females were included, with a mean baseline age of 60 \pm 8 years, a mean baseline BMI of 27.8 \pm 5.0 kg/m², 4.3% had baseline RHOA, and 3.9% had incident RHOA at follow-up. The JSW narrowed on average in all four locations, and the highest prevalence of narrowing of >1 mm of 9.8% was observed for the lateral JSW

(4.5% medial; 4.6% central; 3.2% minimal JSW). 2,379 hips of 1,197 males were included, with a mean baseline age of 60 ± 9 years, a mean baseline BMI of 28.4 ± 3.8 kg/m², 7.4% had baseline RHOA, and 2.0% had incident RHOA at follow-up. The JSW narrowed on average in all four locations, and again the highest prevalence was observed in the lateral JSW (5.3% medial; 5.0% central; 10.7% lateral; and 2.7% minimal JSW). The results of the four LLMs in males and females are presented in Figure 2. Older baseline age in females and lower baseline BMI in males were associated with narrower JSW over time at all locations. Baseline and incident RHOA were associated with narrower JSW over time compared to no definite RHOA for all locations except for the medial JSW.

CONCLUSION: The lateral JSW was the most susceptible to narrowing over time and showed consistent associations with baseline and incident RHOA in both males and females. These results suggest that automated, continuous JSW measurements might be a good alternative for RHOA grades. However, seeing the marked sex differences in JSW measurements of the hip, a different interpretation of JSW measurements in males and females is warranted.

SPONSOR: The Dutch Arthritis Society (grant no. 18-2-203 and 21-1-205), the Dutch Research Council (NWO Veni grant scheme no. 09150161910071) and the Erasmus MC, University Medical Center, Rotterdam (Erasmus MC Fellowship), Wellcome Trust and Royal Society (223267/Z/21/Z).

DICLOSURE STATEMENT: We have nothing to disclose.

ACKNOWLEDGMENT: We would like to thank all participants and researchers of the cohort studies for their contribution.

CORRESPONDENCE ADDRESS: f.boel@erasmusmc.nl

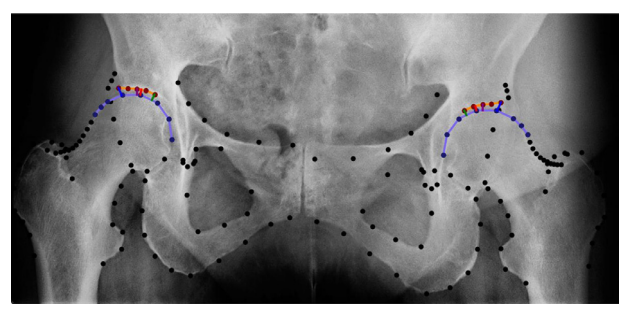


Figure 1: Example of the JSW measurements. The acetabular contour is depicted in orange, and the femoral head contour in periwinkle. The medial JSW is depicted in green, the central JSW in purple, the lateral JSW in blue, and the minimal JSW in red.

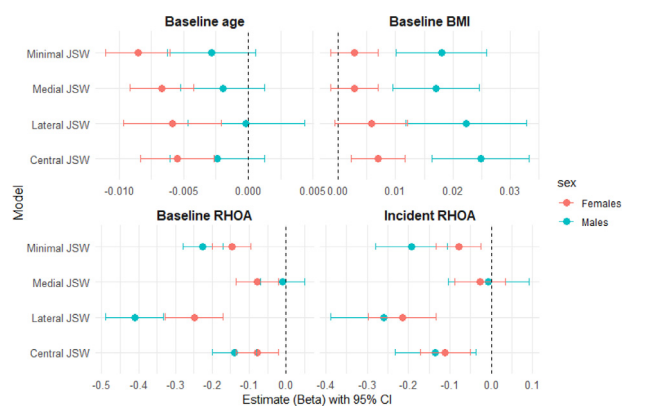


Figure 2: The linear mixed-effect model results for the sex-stratified analysis of the four different types of JSW over time. Estimated coefficients with 95% confidence intervals (CI) are presented for each unit increase in baseline age or body mass index (BMI), and no radiographic hip OA (RHOA) is used as the reference for baseline and incident RHOA.

THE EFFECT OF WEIGHT LOSS AND GLUCAGON-LIKE PEPTIDE-1 RECEPTOR AGONIST ON STRUCTURAL CHANGES IN KNEE OSTEOARTHRITIS: SECONDARY ANALYSIS OF THE RANDOMISED, PLACEBO-CONTROLLED LOSEIT TRIAL

M.W. Brejnebøl 1,2 , T. Haugegaard 1 , R. Christensen 1,3 , H. Gudbergsen 1 , H. Bliddal 1 , P. Hansen 2 , L.E. Kristensen 1 , C.T. Nielsen 1,2 , C.L. Daugaard 2 , J.U. Nybing 2 , M. Henriksen 1 , M. Boesen 1,2

OBJECTIVE: To compare the effect of weight loss and glucagon-like peptide-1 receptor agonist (GLP-1RA) (liraglutide), relative to weight loss and placebo, on structural knee osteoarthritis.

METHODS: This secondary analysis followed a superiority framework of data from the LOSEIT trial, a randomised, parallel-group, placebo-controlled trial. Participants aged 18 to 74 years with overweight (BMI ≥27 kg/m²), symptomatic and early-to-moderate radiographic knee OA were recruited. They underwent 8-week intensive diet intervention followed by randomisation to receive a GLP-1RA (liraglutide 3 mg/d) or placebo for 52 weeks. The primary outcome was the change in radiographic medial minimal joint space width (mmJSW). Analyses were conducted on the intention-to-treat population.

RESULTS: From November 14, 2016, through September 12, 2017, 156 participants were randomly assigned to GLP-1RA (n=80) or to placebo (n=76). As reported in the primary analysis of the data, the GLP-1RA group lost more weight than the placebo group (mean difference, - 3.21 kg, 95%CI: - 6.39 to - 0.03; P=0.050). The GLP-1RA group demonstrated an increase in mean mmJSW of 0.22 mm (95%CI: 0.06 to 0.38) while the placebo group did not change (0.07 mm, 95%CI: - 0.11 to 0.25). No evidence of a difference in mean mmJSW was observed between groups (0.15 mm, 95%CI: -0.06 to 0.36; P=0.17).

CONCLUSION: While the results indicate a potentially favourable effect on mmJSW within the GLP-1RA group, the observed difference in structural knee OA changes on radiographs compared to placebo did not reach statistical significance.

SPONSOR: The Oak Foundation and Novo Nordisk Inc.

DICLOSURE STATEMENT: Marius Henriksen reports a relationship with Thausne, Contura International, and Osteoarthritis and Cartilage Journal. Henning Bliddal reports a relationship with Inc and Contura International. Lars Erik Kristensen reports a relationship with AbbVie, Amgen, Biogen, Bristol Myers Squibb, Celgene, Eli Lilly, Janssen Biotech, Merck & Co, Novartis Pharmaceuticals, Novo Nordisk Inc, Sanofi, and LICB Inc.

CORRESPONDENCE ADDRESS: mikael.boesen@gmail.com

 $^{^{\}rm 1}$ The Parker Institute, Bispebjerg and Frederiksberg Hospital, Copenhagen, Denmark $^{\rm 2}$ Department of Radiology, Bispebjerg and Frederiksberg Hospital, Copenhagen, Denjerg and Denjerg an

³ Research Unit of Rheumatology, Department of Clinical Research, University of Southern Denmark, Odense University Hospital, Odense, Denmark

QUANTIFYING JOINT GEOMETRY IN HUMAN HANDS FROM IMAGING DATA

C.B. Burson-Thomas

University of Southampton, Southampton, UK

INTRODUCTION: The geometry of the same joint varies substantially between people. Typical variation in merely how conforming the two subchondral bone surfaces are can increase the peak compressive stress on the articular cartilage by as much as the additional loading from becoming obese will. The mechanical environment of joint tissues is considered to play a central role in OA development. Quantifying joint geometry using repeatable, reliable, and accessible metrics supports better understanding of the relative importance (or unimportance) of this source of variability between people on their individual OA risk and this factor's role at a population level.

OBJECTIVE: Previous methods of quantifying joint congruence (a measure of how conforming two surfaces are) have required detailed mathematical descriptions of the articulating surfaces and their relative position. We have developed a new method of measuring joint congruence that works directly from the 3D segmented point clouds. This has been applied to a joint in the thumb.

METHODS: The first step of the new methodology involves performing a Finite Element (FE) simulation of an elastic layer compressed between each set of segmented bones (Figure 1). The results of this are then interpreted using the elastic foundation model (Figure 2), enabling an equivalent, but far simpler, contact geometry to be identified. This far simpler equivalent geometry takes the form of a sphere contacting a flat surface. The identified congruence metric is the radius of this sphere, the 'equivalent radius', which produces an equivalent contact to that identified in each FE simulation. The minimal JSW (in this joint position) can also be estimated from the FE simulations. The new method has been applied to a small sample (n = 10) of healthy instances (5M:5F, mean age 31yrs) of the thumb metacarpophalangeal (MCP) joint (IRAS Ethics Ref: 14/LO/1059). Each participant's right hand was CT scanned with near-isotropic voxel size (0.293 × 0.293 × 0.312 mm) and the bones segmented using a greyscale threshold.

RESULTS: To enable an appropriate reduction of the complex geometry represented in the 3D points clouds to one number (the radius of an equivalent 'ball on flat'), this single parameter must continue to capture the joint's geometry as the contact area increases. For all thumb MCP geometries tested, the force-displacement response of the elastic layer could be well-described by an identified equivalent radius, unique to that particular joint (Figure 3). The thumb MCPs had a mean equivalent radius of 17.9 mm (SD = 10.6 mm) and mean minimal JSW of 0.86 mm (SD = 0.24 mm). No relationship between congruence and joint space width was observed (Figure 4).

CONCLUSION: The new method can perform an efficient quantification of congruence, reducing two 3D point clouds to a single parameter. However, further application of the method has been postponed until questions around the role of CT/MRI scan resolution and the spatially varying geometry of articular cartilage have been explored in more detail. Initial results examining these questions using a μ CT dataset of hands can be shared (Figures 5 and 6).

SPONSOR: Part of this research was conducted as part of the APRICOT project, which has received funding from the European Union's Horizon 2020 research and innovation program under grant agreement No. 863183.

DICLOSURE STATEMENT: None.

ACKNOWLEDGMENT: K. Garamanli and C. Simpson for the work shown in Figures 5 and 6.

 $CORRESPONDENCE\ ADDRESS:\ c.b. burson-thomas@soton.ac.uk$

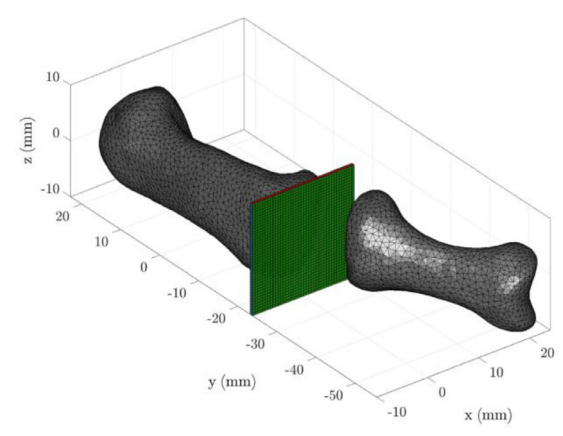


Figure 1: Finite Element (FE) simulation of elastic layer being compressed between two segmented bones. (The first proximal phalanx has been initially translated 6 mm distally to create space for the elastic layer between the surfaces of the bones.)

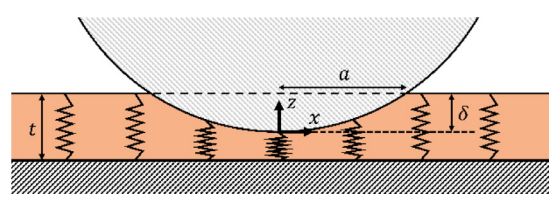


Figure 2: In the elastic foundation model, an elastic layer between two rigid surfaces is modelled as a set of independent springs. A two-dimensional plane is shown. However, the model is three-dimensional, with one surface being a plane and the other described by an elliptic paraboloid (a good approximation to a sphere). The maximum deformation of elastic layer by the rigid paraboloid, δ , occurs at the origin of the coordinate system. An elliptical contact area is generated. The thickness of the elastic layer is t.

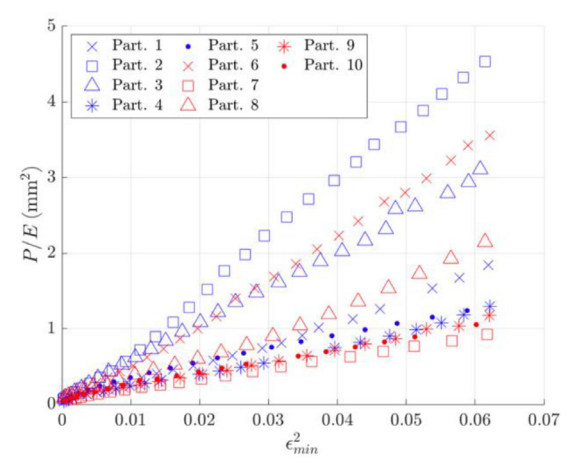


Figure 3: Finite Element (FE) simulation results of elastic layer response for all ten participants. Axes selected for interpretation with elastic foundation model. If a constant equivalent radius, a linear relationship exists between load divided by modulus of elastic layer (P/E) and maximum compressive strain squared (ε^2_{\min}).

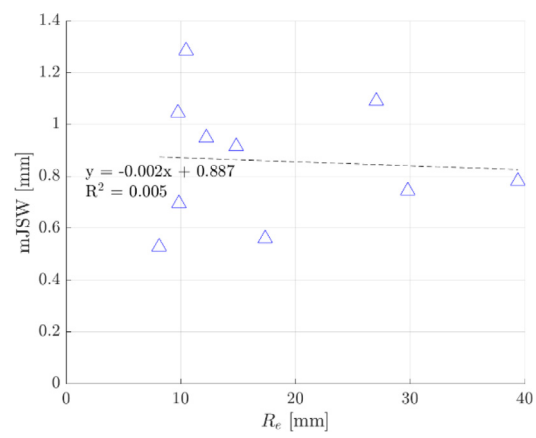


Figure 4: Relationship between minimal joint space width (mJSW) and equivalent radius (R_e) .

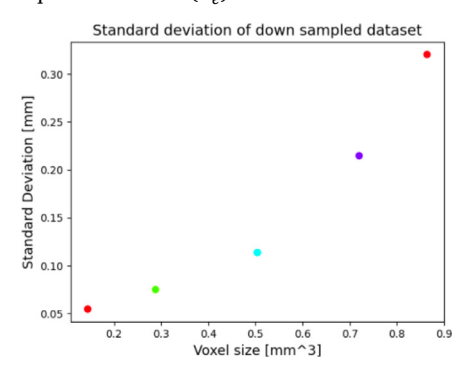


Figure 5: SD of surface difference of segmented bones when downsampling μ CT scan of hand.

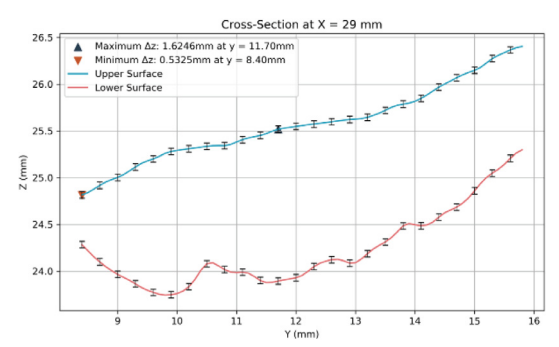


Figure 6: Cartilage and subchondral bone 2D profile from the proximal surface of a first metacarpal from a μ CT scan of a hand.

WHAT IS THE DISTRIBUTION OF MRI-ASSESSED CARTILAGE DAMAGE AND OSTEOPHYTES WITHIN RADIOGRAPHIC KL GRADE?

J.E. Collins 1 , A. Guermazi 2,3 , C.K. Kwoh 4 , S. Demehri 5 , D.J. Hunter 6 , F.W. Roemer 2,7

- ¹ Brigham and Women's Hospital, Harvard Medical School, Boston, MA, USA
- ² Chobanian & Avedisian School of Medicine, Boston University, Boston, MA, USA
- ³ VA Boston Healthcare System, West Roxbury, MA, USA
- ⁴ University of Arizona, Tucson, AZ, USA
- ⁵ Johns Hopkins University, Baltimore, MD, USA
- ⁶ University of Sydney, Sydney, Australia
- ⁷ Universitätsklinikum Erlangen & Friedrich-Alexander-Universität Erlangen-Nürnberg (FAU), Erlangen, Germany

INTRODUCTION: Previous studies have shown that mild-to-moderate radiographic disease severity of knee osteoarthritis (OA), i.e. grades 2 and 3 on the Kellgren-Lawrence (KL) scale, reflects a wide spectrum of cartilage morphology including knees with KL2 having no cartilage damage at all, and KL 3 knees having far-advanced wide-spread full-thickness cartilage loss, raising questions on the validity of the KL grading system to classify knees. Radiographic KL grade 2 or 3 is often an inclusion criterion in disease- modifying drug (DMOAD) trials, with the assumption that these knees represent mild-to-moderate OA, i.e. definite OA but not end-stage. No data is available on whether KL0 and 1 knees, considered pre-radiographic OA -, exhibit osteophytes (OPs) or cartilage damage to a relevant extent or whether more advanced disease, i.e. KL3 and 4, may also reflect knees without or only little relevant cartilage damage or OP presence.

OBJECTIVE: The current study aimed at investigating the distribution of MRI-based measures of OP and cartilage damage scores by radiographic KL grade.

METHODS: Centrally MOAKS MRI and radiographic KL readings were included from the following Osteoarthritis Initiative (OAI) substudies: FNIH Biomarker consortium, POMA and BEAK. In order to match the anteroposterior (a.p.) radiograph, four locations for OPs assessed in the coronal plane (central medial femur, central medial tibia, central lateral femur, central lateral tibia) were considered. Eight tibiofemoral subregions matching the a.p. radiograph were considered for cartilage damage: anterior medial tibia, central medial tibia, posterior medial tibia, central medial femur, anterior lateral tibia, central lateral tibia, posterior lateral tibia and central lateral femur (Figure 1). Cartilage was classified as focal damage only (MOAKS 0, 1.0, 1.1), damage with no advanced full thickness wide-spread damage (MOAKS 2.0, 2.1, 3.0, 3.1), and full thickness wide-spread damage (MOAKS 2.2, 3.2, 3.3). Meniscal damage was assessed with MOAKS, which considered both meniscal morphology and extrusion scores. Descriptive statistics were used to show the frequencies of maximum MOAKS osteophyte and cartilage grades by radiographic KL grade.

RESULTS: In total, the dataset includes 4924 visits from 1981 participants contributing 2276 knees for up to four timepoints. The radiographic KL distribution for the sample is KL0 n=1463 (29.7%), KL1 n=1457 (29.6%), KL2 n=1282 (26.0%), KL3 n=703 (14.3%) and KL4 n=19 (0.4%). There was a definite trend of increasing cartilage damage and osteophyte score with an increasing KL grade (p<0.001 for both). However, there was marked heterogeneity in both measures within KL grade. More than 20% of KL 0 knees showed wide-spread superficial cartilage damage and a minority wide-spread full-thickness damage (**Figure 2, Panel A**). Almost 20% had a definite MRI-defined osteophyte

(Figure 2, Panel B). For KL1, considered no structural OA, almost 50% showed wide-spread superficial or full-thickness cartilage damage. Among KL2 knees, i.e. definite OA as defined by a definite osteophyte on the a.p. X-ray, more than 20% did not have osteophytes on MRI, while 35% did not have more than focal cartilage damage. 462 (23%) of 2004 knees with radiographic OA (KL grade ≥2) did not have more than focal cartilage damage in any of the 8 tibiofemoral subregions. Of these, 42% had no meniscal tear and a meniscal extrusion score of 0 (<2mm), 19% had no meniscal tear and meniscal extrusion >2mm, and 39% had a meniscal tear with or without extrusion >2mm.

CONCLUSION: Different radiographic KL grades represent a wide range of cartilage damage and OP presence and severity. Knees without OA have OPs to a large extent and knees with advanced OA may not exhibit full thickness cartilage damage. Meniscal damage may explain lack of cartilage damage for some, - but not all -, knees with radiographic OA and no cartilage damage on MOAKS. This study focused on only four TFJ locations for OP presence and eight subregions for cartilage damage and ignored the patellofemoral joint and the posterior femur. We conclude that the radiographic KL grade is not an ideal instrument to classify knees according to OP presence and cartilage damage in the matching TFJ locations and subregions as assessed on MRI.

SPONSOR: The Beak study is supported by an NIAMS/NIOH grant to Dr. Kwoh: R01AR066601. Scientific and financial support for the FNIH OA Biomarkers Consortium are made possible through grants and direct contributions provided by: AbbVie; Amgen Inc.; Arthritis Foundation; Bioiberica S.A.; DePuy Mitek, Inc.; Flexion Therapeutics, Inc.; Glaxo-SmithKline; Merck Serono; Rottapharm | Madaus; Sanofi; and Stryker. The OAI is a public-private partnership comprised of five contracts (N01-AR-2-2258; N01-AR-2-2259; N01-AR-2-2260; N01-AR-2-2261; N01-AR-2-2262) funded by the National Institutes of Health. Funding partners include Merck Research Laboratories; Novartis Pharmaceuticals Corporation, GlaxoSmithKline; and Pfizer, Inc. Private sector funding for the Consortium and OAI is managed by the Foundation for the National Institutes of Health. POMA: The image analysis for the POMA study was partly funded by Novartis Pharma AG (Basel, Switzerland), in part by a contract with the University of Pittsburgh (Pivotal OAI MRI Analyses [POMA]: NIH/NHLBI Contract No. HHSN2682010000 21C), and in part by a vendor contract from the OAI coordinating center at University of California, San Francisco (N01-AR-2-2258).

DICLOSURE STATEMENT: JEC has received consulting fees from Boston Imaging Core Lab.; AG has provided consulting services to Pfizer, TissueGene, Coval, Medipost, TrialSpark, Novartis, ICM. He is a shareholder of Boston Imaging Core Lab (BICL), LLC. He is president of the International Society of Osteoarthritis Imaging (unpaid). CKK has received grant funding from GSK, BMS, Cumberland. Lilly, Artiva. He serves as a consultant for AposHealth, Formation Bio, Xalud, Express Scripts, TLC Biosciences, and Kolon TissueGene. SD reported that he received funding from Toshiba Medical Systems (for consultation) and grants from GERRAF and Carestream Health (for a clinical trial study). DJH is the editor of the osteoarthritis section for UpToDate and Co-Editor in Chief of Osteoarthritis and Cartilage. He provides consulting advice on scientific advisory boards for TLCBio, Novartis, TissueGene, Biobone, Sanofi, Enlivex. FWR is shareholder and Chief Medical Officer of Boston Imaging Core Lab (BICL), LLC, a company providing image assessment services to academia and the pharmaceutical industry. He is consultant to Grünenthal, GmbH. He is Editor in Chief of Osteoarthritis Imaging.

CORRESPONDENCE ADDRESS: jcollins13@bwh.harvard.edu







Figure 1. Locations (osteophytes) and subregions (cartilage damage) considered for the MRI definition mirroring the radiographic assessment. A. Coronal intermediate-weighted MRI shows the four locations considered in the coronal plane for osteophyte evaluation (arrows). B. Subregions considered in the lateral compartment for cartilage assessment (central femur, anterior, central and posterior tibia). The identical subregions were also considered for the medial compartment (not shown). C. The central medial femur and tibia (M) and central lateral femur and tibia (L) are shown in the coronal plane. S designates the subspinous region, which was not considered.

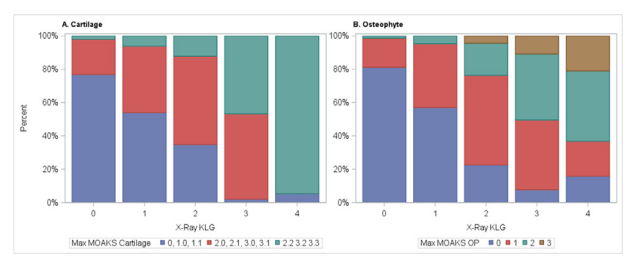


Figure 2. Distribution of MOAKS cartilage damage (A.) and osteophytes (B.) within each radiographic KL grade

NEURAL SHAPE MODEL QUANTIFIES EARLY AND PROGRESSIVE BONE SHAPE CHANGES AFTER ACLR

S.A. Pai, M. Black, K. Young, S. Sherman, C. Chu, A. Williams, G. Gold, F. Kogan, B. Hargreaves, A. Chaudhari, A. Gatti

Stanford University, Stanford, CA, USA

INTRODUCTION: Femoral bone shape scores (B-Score) derived from shape models quantify 3D structural features associated with OA^{1,2}. A higher B-Score is indicative of more OA-like bone shape. B-Scores have high sensitivity to quantify OA progression and stratify patients for interventions¹. Neural Shape Models (NSM) capture non-linear bone shape features and outperform traditional Statistical Shape Models (SSMs) in encoding OA-related shapes³. Prior work that used a SSM-based B-Score showed that anterior cruciate ligament reconstructed (ACLR) knees exhibit higher B-Scores than their contralateral knees 2 years post-surgery, reflecting OA-like bone shape features⁴. However, little is known about how femoral bone shape changes immediately following ACLR and how it progresses during the early post-surgical period—a critical window when post-traumatic osteoarthritis (PTOA) may still be most responsive to intervention.

OBJECTIVE: To use a Neural Shape Model-based B-Score to quantify femoral shape differences between ACLR and contralateral knees immediately post-surgery (3-weeks) and to detect early PTOA bone shape changes over 30 months.

METHODS: ACLR and contralateral knees of 17 subjects (11M/6F, age=38±10 yrs, BMI=24±2 kg/m²) were scanned at 3 weeks (baseline), 3, 9, 18, and 30 months post-ACLR in a 3T MRI scanner (GE Healthcare, USA) using a qDESS sequence (TE/TR=6/22 ms. flip angle=25°, $FOV=160 \times 160$ mm, bandwidth=31.25 kHz, pixel spacing=0.42 \times 0.50 mm, slice thickness=1.5 mm). The femur was automatically segmented, and the B-Score was computed for each subject at all visits using a NSM that was trained on 9,376 femoral segmentations from the baseline DESS images in the OAI dataset1. To assess bone shape differences immediately after surgery, we compared B-Scores between the ACLR and contralateral knees at the baseline visit using a linear mixed effects model. To capture longitudinal bone shape changes after surgery, we calculated change in B-Score at each follow-up visit with respect to the baseline visit. We used a linear mixed effects model to assess the effect of kneetype and time post-surgery on B-Scores. Effect sizes $[\eta_p^2]$ is small (0.01), medium (0.06), or large (0.14)] were computed for significant effects

RESULTS AND DISCUSSION: At baseline, the ACLR knee B-Score was significantly lower than the contralateral knee (η_p^2 =0.40, p=0.005; Fig. 1A). Longitudinally, ACLR knees showed a significantly greater increase in B-Score than contralateral knees (η_p^2 =0.19, p<0.001; Fig 2A). The lower B-Scores in ACLR knees at baseline indicate that the surgical knee had a healthier, less OA-like bone shape than the contralateral knee. Visualization revealed that ACLR knees had a wider intercondylar notch compared to their contralateral knee resulting from notchplasty that were confirmed on surgical notes (Fig. 1B). Since idiopathic OA-like features typically include notch narrowing², the surgically altered geometry, particularly the widened intercondylar notch yields a shape less characteristic of OA, resulting in a lower B-Score. Longitudinally, however, we observe early osteophyte lipping, particularly in the trochlea, intercondylar notch, and medial-posterior condyle-bone shape changes that align with idiopathic OA and likely explain the steep increase in B-Score for ACLR knees over time (Fig. 2B and C).

CONCLUSION: Neural shape modeling characterizes femoral shape changes due to ACLR surgery. Accounting for surgically induced shape changes enables detection of OA-like features as early as 3 months post-ACLR and enhances sensitivity to track these changes longitudinally, potentially serving as a sensitive biomarker for early detection and monitoring of PTOA.

SPONSOR: NIH, CIHR, Stanford Graduate Fellowship, Wu Tsai Human Performance Alliance.

DICLOSURE STATEMENT: A.C. has provided consulting services to Patient Square Capital, Chondrometrics GmbH, and Elucid Bioimaging; is co-founder of Cognita; has equity interest in Cognita, Subtle Medical, LVIS Corp, Brain Key. A.G is a shareholder of NeuralSeg, GeminiOV, and NodeAI.

CORRESPONDENCE ADDRESS: anoopai@stanford.edu

REFERENCES:

- [1] Bowes, M.A. et al. Ann Rheum Dis 80, 502-508 (2021).
- [2] Gatti, A.A. et al. IEEE Transac on Medical Imaging 1-1 (2024).
- [3] Gatti, A.A., et al. Osteoarthritis Imaging 3, 100101 (2023).
- [4] Williams, A.A. et al. Am J Sports Med 51, 3677-3686 (2023).

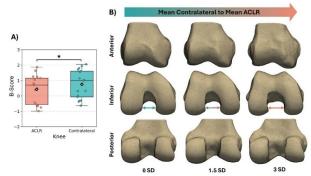


Figure 1: Neural Shape Model based analysis of the femur bone of ACLR and contralateral knees 3-weeks following surgery. A) The B-Score in ACLR knees was significantly lower compared to the contralateral knees $(\eta_p^2=0.40,\ p=0.005)$. B) Neural shape model visualizations illustrate the transition from the mean contralateral femur (0 SD) to the mean ACLR femur shape (3 SD). The most prominent shape difference is a widening of the intercondylar notch (indicated by double-sided allow) in the ACLR knees—consistent with surgical alterations such as notchplasty. Since idiopathic OA-like bone shape features typically include notch narrowing, the surgically altered geometry leads to an initially healthier looking bone shape and thus lower B-Score. ACLR=Anterior cruciate ligament reconstruction. OA=Osteoarthritis. SD=Standard deviation. * indicate statistically significant difference (p<0.05).

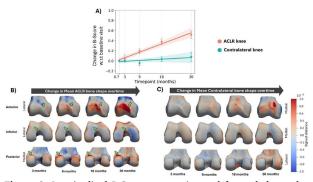


Figure 2: Longitudinal B-Score progression and femoral shape changes in ACLR and contralateral knees with respect to baseline (3-weeks post-ACLR). A) ACLR knees exhibit a significant (η_p^2 =0.19, p<0.001) increase in B-Score compared to contralateral knees from 3 to 30 months after surgery. B and C) Neural shape model-based visualizations of the mean bone shape at each follow-up timepoint. The colormap is the signed distance of the bone surface at a given visit relative to baseline. Red indicates outward protrusion from baseline (i.e., osteophyte growth), blue indicates surface contraction. B) The visualization reveals that bone shape changes in ACLR knees begin as early as 3 months post-surgery and show continual OA-like progression, particularly in the trochlear region, intercondylar notch, and medial posterior condyle (green arrows) over 30 months. C) The contralateral knees show minimal, random, and spatially diffused shape changes over the same period, that are not consistent and progressive as in the ACLR knees.

STUDY POPULATION SELECTION USING MACHINE LEARNING FROM THE FNIH BIOMARKERS CONSORTIUM PROGRESS OA COHORT

E.B. Dam^1 , J. Collins 2 , F. Eckstein 3,4 , F.W. Roemer 5 , A. Guermazi 6 , D.J. Hunter 7

INTRODUCTION: Stringent participant selection criteria for DMOAD trials are crucial, but there is no consensus on the criteria currently accepted by the regulatory authorities, particularly not criteria adapted to different treatment targets. Ensuring a population with a higher probability of treatment-specific OA progression may facilitate cost-effective trials with less risk of failure.

OBJECTIVE: To investigate whether simple Machine Learning (ML) methods provide more effective and/or transparent selection criteria than conventional statistical methods.

METHODS: We investigated the FNIH Biomarkers Consortium cohorts. Phase 1 included 600 subjects from the OAI, as a case/control cohort wrt. OA progression defined by JSW and/or pain progression (JSN decrease ³ 0.7 mm, WOMAC total pain increase ³ 9). Phase 2 included control groups from DMOAD trials (SEKOIA, VIDEO, ILLUSTRATE-K, ROCCELLA), in total 1233 subjects, using the same JSW/Pain endpoints. Consortium members provided biomarker scores for potentially prognostic biomarkers. We focused on the baseline imaging biomarkers submitted for both phases, including semi-quantitative MOAKS readings

and quantitative cartilage morphology from MRI. We analyzed the subcohorts with complete imaging and clinical biomarkers, i.e. 600 and 366 subjects, respectively. We used a k-nearest neighbor classifier to predict progression as defined by the endpoints selecting a biomarker subset using sequential forward feature selection (SFFS). Model training and validation were performed using 10-fold cross-validation (CV). We measured model performance by the median AUC score across the CV test sets. The performance was compared to a classical logistic regression model with elastic-net regularization, which was trained and scored using the same SFFS and CV.

RESULTS: The AUC scores and selected imaging biomarkers for each progression endpoints are shown in Table 1 below. In general, compared to the Logistic Regression models, the kNN models performed on par or slightly better (Phase 1: 0.80 vs 0.79 for JSN and 0.66 vs 0.68 for Pain; Phase 2: 0.76 vs 0.77 for JSN and 0.82 vs 0.73 for Pain).

CONCLUSION: The ML model possibly performed slightly better than classical logistic regression. However, it should be analyzed whether the two models include the same biomarkers and what the implications are for the required study sample size. Further, the feature selection step is very relevant for clinical trial design, to ensure a limited yet predictive set of features.

SPONSOR: ED was supported by grant NNF24OC0090977 from the Novo Nordisk Foundation and grant CF24-1028 from the Carlsberg Foundation.

DISCLOSURE STATEMENT: AG and FWR are shareholders of BICL. FE is shareholder of Chondrometrics GmbH. Multiple authors are consultants to pharmaceutical companies.

ACKNOWLEDGMENT: The OA Initiative and the FNIH OA Biomarkers Consortium.

CORRESPONDENCE ADDRESS: erikdam@di.ku.dk

¹ University of Copenhagen, Denmark

² Harvard Medical School & Brigham and Women's Hospital, Boston, MA, USA

³ Chondrometrics GmbH, Freilassing, Germany

⁴ Paracelsus Medical University, LBIAR & Center for Anatomy & Cell Biology, Austria

⁵ Universitätsklinikum Erlangen & Friedrich-Alexander-Universität Erlangen-Nürnberg, Germany

⁶ Chobanian & Avedisian School of Medicine, Boston University, Boston, MA, USA

⁷ University of Sydney, Australia

Table 1. For Phase 1 and Phase 2, the model performance using the baseline biomarkers for prediction of progression in a 10-fold cross-validation given as AUC. Progression was defined as either JSN (decrease > 0.7 mm) or Pain (WOMAC total pain increase > 9). For references to biomarkers: Hunter et al, Arthritis Care & Research, 2022 (vol 74, no 7).

Ph	Out	Group	N	Log AUC	Biomarkers included in Logistic Regression	kNN AUC	Biomarkers included in kNN
1	JSN	Demo	600	0.59	AGE + SEX	0.50	SEX
		SQ-MRI	600	0.79	MCMFLA + MCMFMC + MBMSSS + MBMPTMA + MBMSTMC + MBMSPL + MMSLA + MMXMA + MOSFMA + MOSTL + MANSBUR + MSYIC	0.80	2 x MBMPTMC + MCMFMC + MBMPFMA + MBMNFMA + MBMPFMC + MBMNFLC + MBMNTMC + MMXMA
		Q-MRI	600	0.70	WMTACV + EMTPD + PMTPD + EBMFPD + ILTPD + ALTPD + BLFMAV	0.68	2 x BMFPD + 2 x EBMFPD + 2 x IBMFPD + WMTVCL + WMTACV + IMTMTH + ALTMTH
	Pain	Demo	600	0.53	AGE	0.52	BMI + SEX
		SQ-MRI	600	0.68	MBMNFLA + MBMPSS + MBMNTLC + MMXLL + MOSPS + MOSFLP + MOSFMC + MACLBML + MPCLBML + MPTSIG + MGCTIB	0.66	2 x MOSFLP + MMTMA + MMSLB + MMSMP + MACLBML + MACLRP + MPCLBML + MPTSIG + MGCACL + MGCTIB + MANSBUR + MIPBUR
		Q-MRI	600	0.60	CMTMAT + AMTPD + CBMFMAT + EBMFMTH + BLTFMAT	0.64	3 x BMTFMAT + CBMFMAT
2	JSN	Demo	334	0.60	AGE + BMI	0.61	SEX + WOMAC_PAIN
		SQ-MRI	334	0.77	BML_PERCAMF + BML_SIZESST + CARTALT + CARTCMF + MEN_EXTRL + OSTSP	0.76	BML_NaLF + BML_NcMT + BML_NpLF + BML_PERCssT + CARTaLT + CARTpLF + MEN_EXTRL + OSTIP
		Q-MRI	334	0.71	cLF.ThCtAB.aMav + cLF.ThCtAB.aSD + iLT.dABp	0.74	2 x iLT.dABp + LFTC.ThCtAB.aMav + MFTC.ThCtAB.aMe
	Pain	Demo	356	0.58	SEX	0.54	SEX
		SQ-MRI	353	0.73	BML_PERCcLT + BML_PERCpLT + CARTcMF	0.82	3 x BML_NaLF + 2 x BML_NpLT + BML_PERCMP + BML_PERCaMF + BML_PERCpMT + BML_SIZEcLT + OSTcMF + OSTpLF
		Q-MRI	356	0.76	2 x cLF.dABp + MFTC.ThCtAB.aMav + aMT.ThCtAB.aMe + cLF.AC + cMF.cAB + cMT.ThCtAB.aMiv + ccLF.dABp + iLT.dABp + icMF.dABp	0.81	LT.dABp + MT.ThCtAB.aCV + MT.VCtAB + ccMF.dABp + eLT.dABp + ecMF.dABp + pMT.ThCtAB.aMe + pMT.dABp

PHOTON-COUNTING CT-BASED TRABECULAR BONE ANALYSIS IN THE KNEE: A COMPARATIVE STUDY OF ADVANCED OSTEOARTHRITIS AND HEALTHY CONTROLS

M. Jarraya ¹, W. Issa ¹, C. Chane ¹, A. Zheng ¹, D. Guermazi ², K. Sariahmed ³, M. Mohammadian ¹, M. Kim ¹, K.A. Flynn ¹, T.L. Redel ¹, F. Liu ¹, M. Loggia ¹

INTRODUCTION: The advent of photon counting CT is a major advance in the development of CT technology. Its enhanced spatial resolution, compared to conventional CT, and its much-reduced radiation dose make it a promising tool for in vivo assessment of bone microarchitecture in clinical settings. For example, prior studies relying on HR-pQCT and Micro CT have shown greater volumetric bone mineral density (vBMD) and trabecular (Tb) thickness (Th) were significantly higher in the medial compartment and associated with increased disease severity. There is no data on trabecular bone structure using photon counting CT in patients with osteoarthritis (OA).

OBJECTIVE: To compare High-Resolution PCCT-defined trabecular bone microstructure between patients with advanced OA versus healthy controls.

METHODS: We used data from the ongoing DIAMOND knee study which investigates the role of neuroinflammation in chronic postoperative pain after TKR. To date, 9 healthy controls and 36 patients with advanced knee OA scheduled for total knee replacements have been recruited, including 7 patients who underwent unilateral PCCT. All other patients and healthy controls had bilateral knee scans. We used a Naeotom 144 Alpha PCCT scanner manufactured by Siemens Healthineers (Erlangen, Germany). Scans were performed with a tube voltage of (120 keV) and, to provide maximum scan performance and minimum noise deterioration, slice increments of 0.2 were used. We also utilized a slice thickness of 0.2 mm, rotation time 0.5 seconds, and pitch 0.85 Images were reconstructed with sharp bone kernel Br89 and matrix 1024 × 1024.. The field of view varied depending on the patient's size, thus resulting in a variable voxel in plane dimension (0.2-0.4 mm). Regions of interests were defined for the proximal tibia and distal femur in a stack height defined by slices equivalent to $1/6^{\text{th}}$ to $1/4^{\text{th}}$ of the measured joint width, prescribed distally or proximally from the joint line, respectively. Images were analyzed using a previously reported iterative threshold-seeking algorithm with 3D connectivity check to separate trabecular bone from marrow. Apparent structural parameters were derived from bone volume (BV), bone surface (BS), and total volume (TV) according to equations by Parfitt's model of parallel plates (Tb.Th, Tb.Separation, BV/TV). These trabecular bone measures were compared between OA and healthy knees using independent sample t-test or nonparametric Wilcoxon tests, depending on normality assumptions. All of the analyses were performed compartment-wise in all four ROIs. These images analyses steps were derived from methods previously published by Wong et al. (DOI: https://doi.org/10.1016/j.jocd.2018.04.001).

RESULTS: We analyzed data from 12 knees of 12 patients with advanced knee OA (mean age 66.0 ± 9.4 years, 67% female) and 17 knees from 9 healthy controls (mean age 60.8 ± 10.7 years, 56% female). Total

Tb volume was consistently greater in OA knees compared to controls in both the medial (OA: $M = 267.15 \text{ mm}^3$, SD = 31.53; HC: $M = 245.26 \text{ mm}^3$, SD = 26.51) and lateral (OA: $M = 278.45 \text{ mm}^3$, SD = 43.83; HC: $M = 252.99 \text{ mm}^3$, SD = 30.54) tibial compartments. Although differences in other bone parameters were not consistent across the four compartments, OA knees tended to show slightly higher trabecular thickness and lower BV/TV. Variability between compartments was observed, particularly in the femur, where group differences were less apparent, though none of these measures reached statistical significance.

CONCLUSION: In this preliminary study using high-resolution PCCT, knees with advanced OA consistently exhibited larger trabecular regions in the tibia compared to healthy controls. Subtle differences in bone structure were also observed, which may reflect early subchondral bone remodeling in response to altered joint loading and mechanical stress. However, interpretation of these microstructural changes is limited by the small sample size and variability in voxel size across scans, both of which could affect the precision of morphometric estimates.

SPONSOR: The study was funded by the David Borsook Project (Cathedral Fund), and the International Skeletal Society (ISS) Seed Grant. **DICLOSURE STATEMENT**: None.

CORRESPONDANCE: mjarraya@mgh.harvard.edu

Table 1. Patients' characteristics patients with osteoarthritis and healthy control group.

Variable	OA group (n = 12)	Healthy controls (n = 9)	P-value
Age, mean ± SD	66.00 ± 9.44	60.78 ± 10.71	0.26
Female sex, n (%)	8 (66.7)	5 (55.6)	0.67*
Height cm, mean ± SD	170 ± 6.3	166 ± 5.2	0.18
Weight kg, mean ± SD	85.43 ± 18.41	74.15 ± 16.02	0.21

^{*} These P-values were measured by non-parametric tests.

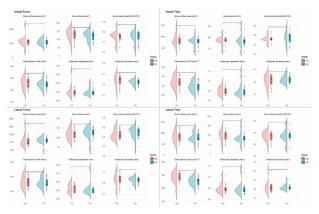


Figure 1. Raincloud plots showing trabecular bone measures across four knee compartments comparing OA (red) and healthy controls (blue). Each plot includes a half-violin (distribution), boxplot (central tendency and spread), and individual data points. Asterisks indicate group differences: $p < 0.2^*$, $p < 0.1^{**}$, $p < 0.05^{***}$.

¹ Mass General Brigham, Harvard Medical School, Boston, MA, USA

² The Warren Alpert Medical School of Brown University, Providence, RI, USA

 $^{^3}$ Boston Medical Center, Chobanian and Avedisian School of Medicine, Boston University, Boston, MA, USA

REVEALING THE HIDDEN CULPRIT: CONTRALATERAL KNEE'S ROLE IN OSTEOARTHRITIS DISEASE ACTIVITY: DATA FROM THE OSTEOARTHRITIS INITIATIVE

J.B. Driban 1 , J. Baek 1 , J.C. Patarini 1 , E. Kirillov 2 , N. Vo 2 , M.J. Richard 2 , M. Zhang 3 , M.S. Harkey 4 , G.H. Lo 5,6 , S.-H. Liu 1 , C.B. Eaton 7,8 , J. MacKay 9,10 , M.F. Barbe 11 , T.E. McAlindon 1

- ¹ UMass Chan Medical School, Worcester, MA, USA
- ² Tufts Medical Center, Boston, MA, USA
- ³ Boston University, Boston, MA, USA
- ⁴ Michigan State University, East Lansing, MI, USA
- ⁵ Baylor College of Medicine, Houston, TX, USA
- ⁶ Michael E. DeBakey Medical Center, Houston, TX, USA
- ⁷ Kent Hospital, Pawtucket, RI, USA
- ⁸ Brown University School of Public Health, Providence, RI, USA
- ⁹ University of Cambridge, Cambridge, UK
- 10 Norwich Medical School, University of East Anglia, Norwich, UK
- 11 Lewis Katz School of Medicine, Temple University, Philadelphia, PA USA

INTRODUCTION: An impediment to our current treatment strategies and clinical trials for people with knee OA is focusing only on one knee, often ignoring the contralateral knee. Failing to address the contralateral knee may explain why many localized therapeutic approaches fail to achieve optimal results.

OBJECTIVE: We explored whether an MRI-based composite score of BM lesion and effusion-synovitis volumes related to contralateral knee OA disease severity.

METHODS: Using data from the OAI, we conducted cross-sectional knee-based analyses among participants with bilateral knee MRIs and at least one knee with KLG ≥1 and a WOMAC pain score ≥10/100 (n=693). We included 1,386 knees from participants with an average age of 62 (SD=9) years. Most participants were overweight and had mild-to-moderate radiographic OA. MR images were collected at each OAI site using Siemens 3.0 Tesla Trio MR systems and knee coils. Acquisitions included a sagittal IM fat-suppressed sequence (field of view=160mm, slice thickness=3mm, skip=0mm, flip angle=180 degrees, echo time=30ms, recovery time=3200ms, 313×448 matrix, x-resolution=0.357mm, y-resolution=0.357mm), which was used to measure BML and effusion-synovitis volumes. BM lesion and effusion-synovitis volumes on MRIs were used to calculate a composite score

("disease activity"). A disease activity score of 0 approximated the average score for a reference sample (n=2,787, 50% had radiographic knee OA, average [SD] WOMAC pain score = 2.8 [3.3]); lower scores (negative scores) indicate milder disease, while greater values indicate worse disease. We divided the disease activity score into tertiles. We used four separate multinomial logistic models to explore the association between disease activity in knees with and without radiographic OA (outcome) and the contralateral disease severity (KLG or disease activity; exposure).

RESULTS: Disease activity among knees without radiographic OA had statistically significant relationships with contralateral disease activity (range of odds ratios: 4.86-23.22) but not contralateral KLG (range of odds ratios: 0.86-1.01; Table). Disease activity among knees with radiographic OA had statistically significant relationships with contralateral disease activity and KLG; however, the association was stronger for contralateral disease activity than KLG (range of odds ratios: 3.67-21.29 versus 1.96-2.20; Table).

CONCLUSION: Contralateral knee OA severity is related to disease activity. Disease activity in the contralateral knee is a more informative measure of disease severity than relying on radiographs. Future studies need to explore how the contralateral knee could impact clinical trial screening, monitoring, and intervention strategies, especially when testing localized therapies.

SPONSOR: National Institute of Health, National Institute of Arthritis and Musculoskeletal and Skin Diseases Award No R01-AR076411. VA's Health Services Research and Development Service Center for Innovations in Quality, Effectiveness, and Safety #CIN 13-413.

DICLOSURE STATEMENT: Timothy McAlindon reports a relationship with Sanofi, Kolon TissueGene, Medidata, & Organogenesis that includes: consulting or advisory. Timothy McAlindon reports a relationship with Ambulomics and Arthrometrics that includes: equity or stocks. Matthew Harkey reports a relationship with Osteoarthritis Research Society International that includes: board membership. Jeffrey Driban, Timothy McAlindon, Ming Zhang have patent #Objective Assessment of Joint Damage (US-20220202356) pending to Tufts Medical Center, Inc.

CORRESPONDENCE ADDRESS: timothy.mcalindon@umassmed.edu

 Table 1. Disease Activity is Associated with Contralateral Osteoarthritis Severity

Strata: Radiographic Severity of Study Knee (Outcome)	Contralateral Knee Status (Exposure)	Tertiles of Disease Activity in the Study Knee			Odds Ratios (95% CI) Adjusted for gender and ag		
		Low (range: -3.3 to -2.0)	Moderate (range: -2.0 to -0.2)	High (range: -0.2 to 34.9)	Moderate vs. Low	High vs. Low	
Knees without Radiographic OA							
Contralateral KL = 0 or 1		124 (51%)	70 (51%)	40 (52%)	Reference	Reference	
Contralateral KL = 2		79 (32%)	44 (32%)	22 (29%)	0.99 (0.61, 1.58)	0.86 (0.47, 1.56)	
Contralateral KL = 3 or 4		41 (17%)	24 (17%)	15 (19%)	1.01 (0.56, 1.81)	1.00 (0.49, 2.01)	
Contralateral Disease Activity	- Low (-3.3 to -2.0)	154 (63%)	34 (25%)	9 (12%)	Reference	Reference	
Contralateral Disease Activity	- Moderate (-2.0 to -0.2)	54 (22%)	66 (48%)	18 (23%)	5.63 (3.34, 9.51)	5.54 (2.33, 13.19)	
Contralateral Disease Activity	- High (-0.2 to 34.9)	36 (15%)	38 (28%)	50 (65%)	4.86 (2.69, 8.81)	23.22 (10.38, 51.93)	
Knees with Radiographic OA							
Contralateral KL = 0 or 1		73 (33%)	68 (21%)	84 (22%)	Reference	Reference	
Contralateral KL = 2		91 (42%)	162 (50%)	172 (45%)	2.20 (1.43, 3.38)	1.93 (1.27, 2.93)	
Contralateral KL = 3 or 4		54 (25%)	95 (29%)	128 (33%)	1.96 (1.21, 3.15)	2.09 (1.32, 3.30)	
Contralateral Disease Activity	- Low (-3.3 to -2.0)	128 (59%)	84 (26%)	53 (14%)	Reference	Reference	
Contralateral Disease Activity	- Moderate (-2.0 to -0.2)	64 (29%)	164 (50%)	97 (25%)	4.01 (2.68, 6.00)	3.67 (2.33, 5.79)	
Contralateral Disease Activity	- High (-0.2 to 34.9)	26 (12%)	77 (24%)	234 (61%)	4.46 (2.63, 7.56)	21.29 (12.64, 35.86)	

NEW JSW MEASUREMENTS INCREASE RESPONSIVENSS TO CHANGE

J. Duryea

Department of Radiology, Massachusetts General Brigham, Boston, MA, USA

INTRODUCTION: Knee radiography is a low cost, convenient, and widely available modality for assessing KOA change longitudinally. Although seen on MRI, soft tissues such as cartilage and the meniscus are invisible radiographically and their change is measured indirectly as loss of radiographic JSW. This indirect association has the potential to reduce the responsiveness to change for JSW. JSW loss is likely due to a combination of cartilage and meniscus change but the level of contribution from each structure is not currently discernable from a radiograph.

OBJECTIVE: To develop and validate new measurements of JSW with improved responsiveness to change compared to the current method. We also hope this will begin to shed light on the individual contributions of cartilage and meniscus to JSW loss by systematically evaluating different JSW locations across the knee joint.

METHODS: We randomly placed all 4,796 OAI participants into either a training or testing group and selected all knees where fixed-location JSW (fJSW) was available at the x=0.15 to 0.3 (medial compartment) and x=0.7 (inner-most lateral compartment) locations at each of 6 follow-up time points (12, 24, 36, 48, 72, and 96 months). We defined a new JSW metric (JSW $_{New}$) that was a linear combination of three individual fJSW measures:

 $JSW_{New} = fJSW(x=0.25) + w_1 \times fJSW(x=0.7) + w_2 \times fJSW(x=x_1)$, where x_i was one of 6 values in the medial compartment: 0.15, 0.175, 0.2, 0.225, 0.275 or 0.3; lower x_i values corresponded to more peripheral locations. Using the training group, we varied w_1 , w_2 and x_i to achieve the maximum responsiveness, defined as the magnitude of the standardized response mean (SRM) for baseline to the follow-up time point. Once optimized, the performance was evaluated using the independent testing set and compared in the test group to the SRM found for fJSW(x=0.25), which is generally considered the most responsive fixed location JSW. We performed separate optimization and testing for the 5 different baseline KL values and 6 distinct follow-up time points.

RESULTS: Table 1 summarizes the results. There is substantial improvement in the responsiveness (magnitude of the SRM values) for all followup time points and KL values. We did not observe a consistent pattern for the \mathbf{x}_i values other than the absence of \mathbf{x} =0.15 (most peripheral) as an optimal value. \mathbf{w}_1 was generally negative for KL4 knees suggesting that JSW $_{\mathrm{New}}$ may be capturing pseudo-widening (seesaw effect) or possibly medial compartment meniscus extrusion for these knees. \mathbf{w}_2 , the weight factor for the other medial compartment locations, was consistently positive although no discernable dependence on KL or follow-up time point was observed. Positive \mathbf{w}_2 is consistent the understanding that KOA is generally a medial compartment disease.

CONCLUSION: We report more responsive JSW metrics that have the potential to improve the utility of radiographs for clinical trials and other studies of KOA. The results suggest that this measurement may capture additional information related to the underlying cartilage and meniscal changes. However, further work incorporating MRI data will be necessary to better understand the patterns of locations and weights and the full implications of these results.

SPONSOR: NIH R01AR078187 DICLOSURE STATEMENT: None ACKNOWLEDGMENT: None

CORRESPONDENCE ADDRESS: jduryea@bwh.harvard.edu

Table 1: SRM values for JSW $_{New}$ evaluated with the test group compared to SRM for fJSW(x=0.25) stratified by follow-up time point and baseline KL grade. The x_i , w_1 , and w_2 values are also reported along with the number (N) in each group.

FU Vis	KL grade	N	$\mathbf{x}_{\mathbf{i}}$	W_1	W_2	SRM [fJSW(x=0.25]	SRM [fJSW _{New}]
12 months	0	587	0.3	-0.6	0.6	-0.097	-0.12
12 months	1	411	0.225	-0.2	0.6	0.024	-0.072
12 months	2	1034	0.225	0.2	1.4	-0.122	-0.185
12 months	3	508	0.225	2	0.6	-0.231	-0.301
12 months	4	107	0.175	-0.8	0.2	-0.234	-0.271
24 months	0	558	0.2	2	1.8	-0.246	-0.383
24 months	1	406	0.175	1.6	2	-0.28	-0.416
24 months	2	972	0.2	0.6	1.4	-0.358	-0.442
24 months	3	476	0.2	0.8	0.8	-0.537	-0.728
24 months	4	92	0.175	-0.8	0.4	-0.107	-0.42
36 months	0	577	0.3	0.4	1.2	-0.477	-0.593
36 months	1	400	0.2	0.2	0.8	-0.469	-0.595
36 months	2	929	0.2	0.2	1	-0.505	-0.665
36 months	3	447	0.225	1.6	1.2	-0.714	-0.931
36 months	4	83	0.175	-0.8	0.6	-0.538	-0.989
48 months	0	555	0.2	1.4	1.6	-0.554	-0.682
48 months	1	392	0.2	0.6	1.8	-0.5	-0.722
48 months	2	897	0.3	1.4	2	-0.61	-0.799
48 months	3	404	0.225	0.6	0.8	-0.807	-0.989
48 months	4	76	0.175	-0.8	0.6	-0.652	-0.854
72 months	0	452	0.2	0.6	1	-0.529	-0.65
72 months	1	309	0.25	0.8	2	-0.606	-0.809
72 months	2	661	0.3	1	1.6	-0.674	-0.85
72 months	3	208	0.175	1.2	1	-0.924	-1.183
*72 months	4	11	0.25	-1	0.4	-0.011	-0.619
96 months	0	481	0.3	1.4	2	-0.633	-0.832
96 months	1	301	0.3	0.4	2	-0.697	-0.898
96 months	2	698	0.3	1	2	-0.732	-0.9
96 months	3	203	0.175	1.2	1.6	-1.11	-1.347
*96 months	4	10	0.25	0.4	2	-0.267	-0.363

 $^{^{\}ast}~$ Since N is very small for KL=4 at the 72- and 96-month time points, the results may be unreliable.

POTENTIAL IMPACT OF DIABETES MELLITUS ON CARTILAGE THICKNESS AND COMPOSITION IN SUBJECTS WITH AND WITHOUT OSTEOARTHRITIS – A MATCHED CASE-CONTROL STUDY

F. Eckstein 1,2, W. Wirth 1,2, A. Eitner 3

- ¹Ludwig Boltzmann Institute for Arthritis & Rehabilitation (LBIAR) & Center for Anatomy and Cell Biology, Paracelsus Medical University, Salzburg, Austria
- ² Chondrometrics GmbH, Freilassing, Germany
- ³ Department of Trauma, Hand and Reconstructive Surgery, Jena University Hospital, Jena. Germany

INTRODUCTION: Diabetes mellitus (DM) and osteoarthritis (OA) are interconnected through metabolic and inflammatory pathways that independently contribute to joint pain and structural degeneration [1]. Elevated blood glucose can induce systemic inflammation and oxidative stress, promoting joint symptoms and cartilage damage. Also, DM is frequently associated with obesity, potentially increasing mechanical loading and cartilage wear, particularly in weight-bearing joints.

OBJECTIVE: To assess the association of DM with femorotibial cartilage morphology and composition (T2 relaxation time), compared with matched controls without DM. Matching included age, sex, obesity status, knee pain, and radiographic OA (ROA) status. Analyses were stratified by the presence or absence of ROA.

METHODS: Participants were selected from the Osteoarthritis Initiative (OAI) [2]. A total of 362 individuals with DM were identified based on the Charlson Comorbidity Index. Of those, 260 were successfully matched to DM-negative controls based on the same/similar sex, age $(\pm 5 \text{ years})$, BMI $(\pm 5 \text{ kg/m}^2)$, WOMAC pain score $(\pm 5 \text{ on a 0-100 scale})$, pain frequency (±1 on a 0-2 scale), body height (±10 cm), and Kellgren-Lawrence (KL) grade [2]. Femorotibial cartilage thickness was derived from sagittal DESSwe MRIs at 3T using fully automated segmentation methodology. This involved a deep-learning-based pipeline combining 2D U-Net segmentation of subchondral bone and cartilage with atlasbased post-processing for subchondral bone area reconstruction [3]. Laminar cartilage T2 (deep 50%, superficial 50%) were calculated from MESE MRI (7 echoes), also using automated segmentation [3]. Statistical comparisons between DM and non-DM subjects were performed using paired t-tests, without correction for multiple comparisons across joint regions. For cartilage thickness, analyses were stratified by ROA status (KLG 2-4 vs. KLG 0-1). T2 analysis was restricted to KLG 0-2, as laminar T2 becomes less interpretable once cartilage loss is present.

RESULTS: DM participants were 63.4 ± 8.9y old, 53% female, BMI 31.5±4.5 kg/m². A total of 244 matched pairs were available with cartilage data at baseline (234 with thickness, 222 with T2; 78x KLG0, 46×1 , 62×2, 52×3, 6x KLG4). In non-arthritic participants, the medial cartilage thickness was 3.45 mm (95% CI: 3.35-3.55) in DM subjects and 3.43 mm (3.33-3.54) in controls. Lateral thickness was 3.90 mm (3.80-4.00) in DM vs. 3.87 mm (3.76-3.97) in controls. Among ROA cases, medial thickness was 3.16 mm (3.03-3.29) in DM vs. 3.30 mm (3.17-3.42) in controls; lateral thickness was 3.68 mm (3.53-3.83) vs. 3.76 mm (3.64-3.88), respectively. None of the DM vs. non-DM differences reached statistical significance. In the 170 matched pairs that were KLG 0-2, no significant differences in cartilage T2 were identified: In the medial superficial layer, T2 was 48.2 ms (47.7-48.7) in DM vs. 48.7 ms (48.2-49.3) in controls, and in the deep layer, 37.4 ms (37.0-37.7) vs. 37.7 ms (37.4–38.1). Laterally, superficial T2 was 47.0 ms (46.6–47.5) in DM vs. 47.5 ms (47.0-47.9) in controls, and in the deep layer, 36.3 ms (36.0-36.6) vs. 36.4 ms (36.1-36.7).

CONCLUSION: This study utilized state-of-the-art 3T MRI data from the OAI and fully automated, deep-learning-based methods for evaluating cartilage morphology and composition [3]. The findings suggest that DM status, when tightly matched for demographic and clinical factors (especially BMI and pain), is not substantially associated with reduced cartilage thickness or increased T2 relaxation times. Future analyses will have assessed the impact of less stringent matching—particularly for BMI and pain—and will explore longitudinal changes in these participants.

REFERENCES:

- [1] Eitner A et al. Arthritis Care Res 2021;73:540-548.
- [2] Eckstein F et al. Ann Rheum Dis. 2014;73:1289-300.
- [3] Wirth W, et al.; Skeletal Radiol. 2024 Sep 4.

SPONSOR: Ludwig-Boltzmann Institute of Arthritis and Rehabilitation (LBIAR)

DICLOSURE STATEMENT: FE &WW: Chondrometrics GmbH (ownership and employment) and consultancies/ sponsorships to/from various pharmaceutical companies.

CORRESPONDENCE ADDRESS: felix.eckstein@pmu.ac.at

EXPLORING THE RELATIONSHIP BETWEEN LIGAMENT MICROSTRUCTURE AND MECHANICS IN OA-AFFECTED HUMAN KNEES

A. Gheisari ¹, A. Kositsky ^{1,2}, V.-P. Karjalainen ¹, S. Das Gupta ¹, V. Virtanen ¹, E. Nippolainen ², H. Kröger ², J. Töyräs ^{2,3,4}, S. Saarakkala ¹, I.O. Afara ², R.K. Korhonen ², M.A.J. Finnilä ¹

INTRODUCTION: Knee ligaments play a critical role in providing joint stability and limiting excessive motion. Altered joint loading due to OA can affect various knee tissues, including the ligaments. Previous studies using post-traumatic OA animal models have reported changes in affected knee's ligament viscoelasticity. This study investigates the microstructural characteristics of OA-affected human knee ligaments and examines whether these features are related to their viscoelastic properties.

OBJECTIVE: This study examines whether clustered bundle thickness and the proportion of non-collagenous volume to total ligament volume differs among ligaments in OA-affected knees. It also examines if the mechanical properties of the ligaments are dependent on the bundle thickness and proportion of non-collagenous volume.

METHODS: Anterior (ACL; n = 6) and posterior (PCL; n = 7) cruciate ligaments, and medial (MCL; n = 8) and lateral (LCL; n = 7) collateral ligaments were collected from eight fresh-frozen cadaveric knees (five female; age: 65 ± 8 years). All knees had histology-confirmed osteoarthritis (average OARSI grade of tibial cartilage samples: >2). Following preconditioning, samples underwent a mechanical testing protocol that included a two-step stress relaxation (to 4% and 8% strain, 30 min each) and cyclic loading up to 5.0 Hz with ±0.5% strain amplitude and 20 cycles per frequency. Equilibrium modulus was derived from the stress-relaxation data, while dynamic modulus and phase difference were calculated from cyclic loading. After mechanical testing, samples were stored in formalin and underwent gradual dehydration in ethanol and critical point drying. Subsequently, they were imaged by an Xradia 610 Versa X-ray microscopy (XRM, with 4x objective, 40kV voltage, 2s exposure, 10µm voxel size, and binning of 4). The reconstructed XRM images of ligaments were visualized in CTVox, and collagen bundle thickness and non-collagenous volume (by open and close porosity analyses) were calculated in CTAn software. Pearson correlation analysis between collagen bundle thickness and non-collagenous volume and mechanical properties was performed in R 4.2.2.

RESULTS: Among the four ligaments, the LCL exhibited the highest bundle thickness, while the PCL showed the highest non-collagenous volume ratio; however, these differences were not statistically significant. Equilibrium modulus was negatively correlated with bundle thickness across all ligaments, and with non-collagenous volume in all but the MCL. The phase difference at 5 Hz in the PCL showed a strong positive correlation with bundle thickness (r = 0.82). The ACL displayed a strong negative correlation between dynamic modulus at 5 Hz and non-collagenous volume (r = -0.82).

CONCLUSION: Although collagen is the primary load-bearing component of ligaments, increased bundle thickness did not correlate with either equilibrium modulus or dynamic modulus at 5 Hz. In contrast, greater bundle thickness was associated with a higher phase difference,

indicating increased viscosity, possibly due to increased number of fibers and interaction surface. Additionally, higher non-collagenous volume in the ACL was associated with reduced stiffness.

SPONSOR: Finnish Cultural Foundation, Research Council of Finland (307932, 315820, 320135, 353755), Finnish State Research Funding (VTR: 5063579, 5203118), EU Horizon 2020 H2020-ICT-2017-1 (780598), Novo Nordisk Foundation (NNF21OC0065373), Biocenter Kuopio.

CORRESPONDENCE ADDRESS: anahita.gheisari@oulu.fi

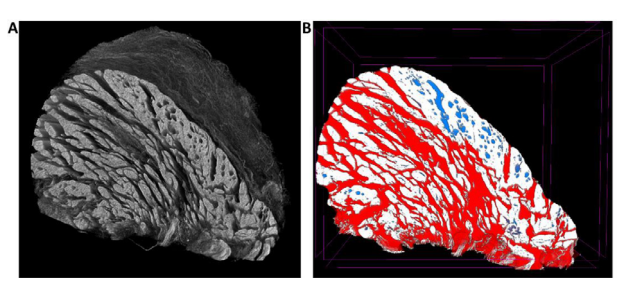


Figure 1. Reconstructed XRM image of a ligament cross-section (A). Segmentation of collagen bundles (white), non-collagenous regions between (red) and within (blue), used for calculating bundle thickness and non-collagenous volume (B).

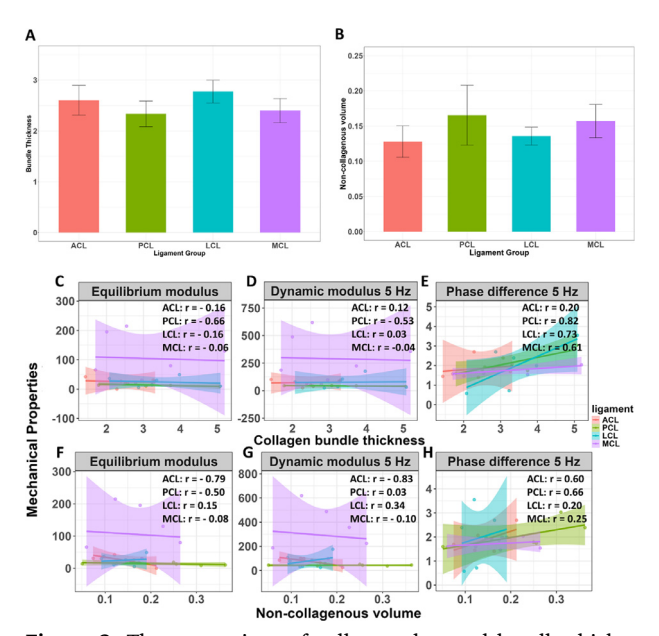


Figure 2. The comparison of collagen clustered bundle thickness (A) and non-collagenous volume (B) of knee ligaments: anterior cruciate ligament (ACL), posterior cruciate ligament (PCL), lateral collateral ligament (LCL) and medial collateral ligament (MCL). The second row illustrates the correlations between collagen bundle thickness and equilibrium modulus (C), dynamic modulus at 5 Hz (D), and phase difference at 5 Hz (E). The bottom row shows the correlations of non-collagenous volume with equilibrium modulus (F), dynamic modulus at 5 Hz (G), and phase difference at 5 Hz (H).

¹ University of Oulu, Oulu, Finland

² University of Eastern Finland, Kuopio, Finland

³ Kuopio University Hospital, Kuopio, Finland

⁴ The University of Queensland, Brisbane, QLD, Australia

AUTOMATING IMAGING BIOMARKER ANALYSIS FOR KNEE OSTEOARTHRITIS USING AN OPEN-SOURCE MRI-BASED DEEP LEARNING PIPELINE

A. Goyal ¹, F. Belibi ¹, V. Sahani ¹, R. Pedersen ², Y. Vainberg ¹, A. Williams ¹, C. Chu ¹, B. Haddock ², G. Gold ¹, A.S. Chaudhari ¹, F. Kogan ¹, A.A. Gatti ¹

INTRODUCTION: Quantitative MRI and [¹⁸F]NaF PET enable assessment of cartilage composition, bone shape, and subchondral bone metabolism in knee OA. Current workflows rely on manual segmentation that is time-consuming and subject to inter- and intra-reader variability. Furthermore, computing quantitative metrics requires considerable time and expertise. An open-source, automated, deep learning (DL) pipeline with standardized biomarker extraction has the potential to enhance reproducibility and make large-scale analysis accessible to clinical research communities, including non-technical users.

OBJECTIVE: Develop and validate an automated DL-based pipeline for comprehensive MRI-based segmentation and quantitative analysis of multiple knee tissues from multi-modal MR and PET images.

METHODS: We developed and open-sourced a comprehensive segmentation and analysis pipeline. A 2D U-Net was trained to segment 9 tissues using a dataset of 347 DESS and qDESS images: 3 bones (femur, tibia, patella), 4 cartilage regions (femoral, medial and lateral tibial, patellar), and 2 menisci (medial and lateral). Subchondral bone masks and femoral cartilage subregions were fitted automatically. Quantitative imaging biomarkers were computed as follows: cartilage T2 was computed analytically from qDESS scans; cartilage thickness was computed as the 3D Euclidean thickness of cartilage overlying the bone surface; meniscal volume was calculated as the product of voxel count and voxel volume; OA bone shape (BScore) was derived using a neural shape model; PET-derived subchondral bone metabolism was computed as regional SUVmean/max, and kinetic modeling via Hawkin's method was used to extract KiNLR (bone mineralization rate) and K1 (perfusion to subchondral bone). To evaluate the pipeline, 20 unilateral qDESS and [18F]NaF PET knee scans (10 symptomatic OA, 10 controls) were analyzed by the automated pipeline, and two manual annotators. Manual and automated segmentations were compared using the Dice Similarity Coefficient (DSC) and average symmetric surface distance (ASSD). Biomarkers were compared using ICC and normalized mean RMSE (NRMSE).

RESULTS: All automated segmentations had good to excellent overlap measured using DSC (bone: 0.95-0.98; cartilage: 0.84-0.91; menisci: 0.85-0.89) and small surface errors (bone: 0.13-0.32 mm; cartilage: 0.11-0.21 mm; menisci: 0.17-0.30 mm). Notably, automated segmentations had better DSC and ASSD than the inter-rater comparison (Fig. 2). With the exception of cartilage thickness and patellar cartilage whole T2 values, all quantitative metrics showed excellent agreement with ICC >0.96 and NRMSE <0.1, comparable to inter-rater comparison. Bone metrics (BScore, SUV, PET kinetics) had ICC >0.96. Cartilage metrics had more variability, with the best reproducibility for whole cartilage T2 (ICC 0.89-0.98, NRMSE 0.01-0.04), then superficial T2 (ICC 0.93-0.99, NRMSE 0.01-0.05), and finally deep T2 (ICC 0.7-0.97, NRMSE 0.01-

0.06). Cartilage thickness showed the worst reproducibility but still was comparable to inter-rater measures. Meniscus volume also shows high concordance (ICC 0.93-0.97; NRMSE 0.05-0.10). Overall, we found that most of the metrics derived from automated segmentations are comparable to those derived from manual segmentations.

CONCLUSION: Our open-source, AI-driven pipeline delivers rapid, accurate segmentation and quantitative analysis of multimodal knee MRI and PET data. Next steps include support for other MR sequences, multisite validation, and 3D Slicer integration to facilitate translation. This resource provides a foundation for reproducible and scalable imaging biomarker analysis in OA research and clinical trials.

SPONSOR: Wu Tsai Human Performance Alliance, Stanford DARE Fellowship, NIH R01AR079431.

DICLOSURE STATEMENT: AAG is a shareholder of NeuralSeg, NodeAI, and GeminiOV

ACKNOWLEDGMENT: Dawn Holley and Drew Dreisbach for their assistance with PET.

CORRESPONDENCE ADDRESS: agoyal5@stanford.edu

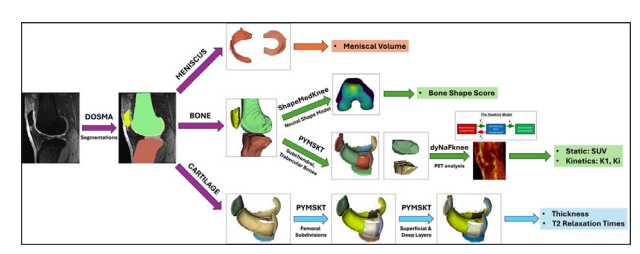


Figure 1. Overview of the Knee Pipeline which uses a qDESS volume as input and automatically segments knee tissues. It allows for calculation of cartilage T2 and thickness, meniscus volumes, bone shape scores, and subchondral bone [18F]NaF PET SUV and kinetic measures.

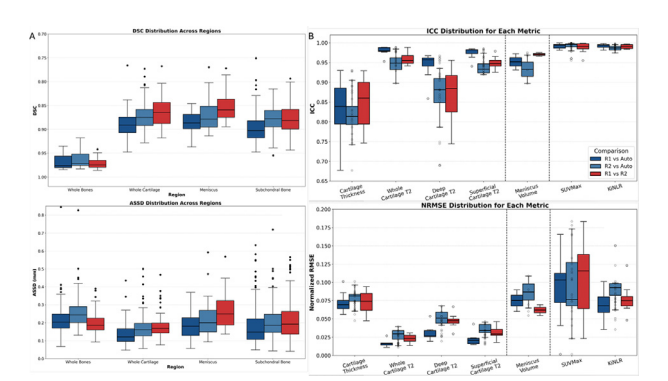


Figure 2. Results showing A) DSC and ASSD across subjects and readers for different groups of segmentations; and B) Average ICC and NRMSE values across subregions for quantitative metrics of cartilage, bone, and menisci. Blue boxplots are manual versus automated, and red are interreader comparisons.

¹ Stanford University, Stanford, CA, USA

² Rigshospitalet, Copenhagen University Hospital, Copenhagen, DK

PAIN PHENOTYPE AS AN EFFECT MODIFIER: EXPLORING THE ROLE OF PAIN-DETECT IN THE ASSOCIATION BETWEEN WOMAC SCORES AND MRIDETECTED STRUCTURAL DAMAGE

H. Harandi ¹, F.W. Roemer ², S. Mastbergen ³, J. Collins ⁴, A. Guermazi ⁵, C.K. Kwoh ⁶, T. Neogi ⁷, M. Loggia ⁴, R. Edwards ⁴, E. Duscova ⁸, M. Kloppenburg ⁹, F.J. Blanco ¹⁰, I.K. Haugen ¹¹, F. Berenbaum ¹², M.P. Jansen ³, M. Jarraya ⁴

- ¹ Tehran University of Medical Sciences, Tehran, Iran
- 2 Friedrich-Alexander-Universität Erlangen-Nürnberg, Erlangen, Germany & Boston University School of Medicine, Boston, MA, USA
- ³ University Medical Center Utrecht, Utrecht University, Utrecht, Netherlands
- ⁴ Mass General Brigham, Harvard Medical School, Boston, MA, USA
- $^5\,V\!A$ Boston Healthcare System & Boston University School of Medicine, Boston, MA, USA
- ⁶ University of Arizona College of Medicine Tucson, Tucson, AZ, USA
- ⁷ Boston University School of Medicine, Boston, MA, USA
- 8 Thomas Jefferson University, Philadelphia, PA, USA
- ⁹Leiden University Medical Center, Leiden, Netherlands
- 10 Complexo Hospitalario Universitario de A Coruña (CHUAC), Sergas, A Coruna, Spain
- ¹¹ Diakonhjemmet Hospital, Oslo, Norway
- ¹² Sorbonne Université, INSERM, AP-HP Hôpital Saint-Antoine, Paris, France

INTRODUCTION: A fundamental challenge in treating patients with OA is the discordance between pain and structural abnormalities, reflecting the fact that numerous factors outside of joint pathology can contribute to the pain experience. Thus, pain in OA represents different phenotypes, including nociceptive and neuropathic-like pain. The Pain-DETECT (PD-Q) can be used to help distinguish between the two, with lower PD-Q scores suggesting nociceptive pain. While associations between different MRI-based MOAKS measures and traditional pain outcomes (such as WOMAC) have been reported, whether those associations are modified by pain phenotype (as assessed by PD-Q) is not known.

OBJECTIVE: To test whether the association between WOMAC scores and MRI-detected OA structural pathology is modified by PD-Q score.

METHODS: We performed a pooled cross-sectional analysis with repeated measures using data from all 4 visits of the IMI-APPROACH cohort (baseline, 6-, 12-, and 24-months), where participants were administered the total WOMAC and PD-Q. For each participant, an index knee with OA was selected based on ACR clinical criteria. MRI of the index knee was obtained for all participants and visits, and scored using MOAKS, including bone marrow lesions (BML); Hoffa's synovitis and effusion-synovitis. WOMAC scores ranged from 0-96. Participants with no symptoms or functional limitation (WOMAC = 0) were excluded to avoid floor effect. We conducted the analysis in 3 steps: Step 1: We fit linear mixed-effects models with random intercepts for each participant to account for multiple observations per participant and included a MOAKS × PD-Q interaction term to test for effect modification. The MOAKS features we tested included: presence of full-thickness cartilage loss, presence of osteophytes \geq grade 2, total number of BML, sum of total scores of BML, presence of BML ≥ grade 2, presence of effusion ≥grade 2 and grade 3 separately, presence of synovitis ≥ grade 2 and grade 3 separately, presence of any meniscus tear. Step 2: for each MOAKS measure identified as significant in step 1 (using a liberal threshold of p<0.2) we conducted a Johnson-Neyman (J-N) analysis to locate PD-Q regions where the conditional association between MOAKS and square root of WOMAC (sqrtWOMAC) changed from being statistically significant (using the 95% CI) to non-significant. Step 3: for each MOAKS measure identified in step 1, we stratified the cohort into two PD-Q subgroups (at the J-N cutoff identified in step 2) and refitted stratified linear mixed-effects models to estimate the MOAKS-sqrtWOMAC association within each subgroup.

RESULTS: We included 287 participants (mean age 66.5 (SD=7.2), 77.7% female, mean/median PD-Q score 9.36 / 9), who contributed 949 observations. Significant effect modification was observed for sum

of BML size, presence of grade ≥ 2 osteophytes, and grade 3 effusion synovitis (PD-Q cutoff using J-N were 17.2, 4.7, and 11.6, respectively) (Figure 1). In participants with lower PD-Q scores (based on threshold identified in Step 2), large effusion synovitis was positively associated with WOMAC ($\beta = 1.073$; 95% CI: 0.520–1.627). Higher sum of BML sizes was also associated with higher sqrtWOMAC ($\beta = 0.076$; 95% CI: 0.039–0.112) (Figure 2). These associations were not statistically significant among participants with higher PD-Q scores (higher likelihood of neuropathic-like pain).

CONCLUSION: The PD-Q score potentially modifies the relationship between WOMAC and MRI-detected sum of BML, and grade 3 effusion. Those with lower PD-Q scores (suggestive of nociceptive pain) show stronger associations between these structural features and WOMAC score

SPONSOR: MJ is funded by a K23 award (K23-AR084603) from the National Institute of Arthritis and Musculoskeletal and Skin Diseases (NI-AMS) of the NIH, The David Borsook Project, supported by The Cathedral Fund, and The International Skeletal Society Seed Grant

DICLOSURE STATEMENT: AG has received consultancies fees from Novartis, ICM, Levicept, Scarcell, Peptinov, Pacira, Coval, 4Moving, Formation Bio, Paradigm, Medipost and TissueGene and is shareholder of Boston Imaging Core Lab (BICL), LLC a company providing image assessment services. JC and MJ have received consultancy fees from BICL, LLC. CKK received institutional grants from GSK, BMS, Cumberland, Lilly, Artiva, and has advisory Board/Consulting role with: AposHealth, Formation Bio, Xalud, Express Scripts, TLC Biosciences

CORRESPONDENCE: mjarraya@mgh.harvard.edu

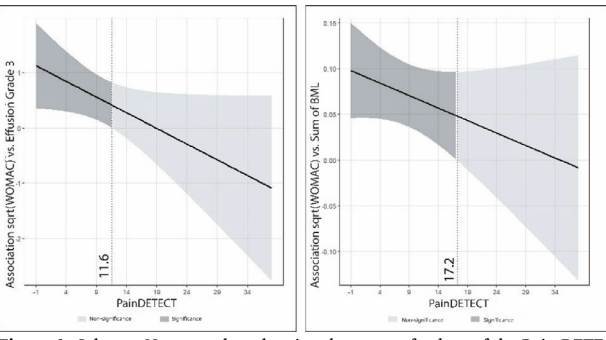


Figure 1: Johnson-Neyman plots showing the range of values of the Pain-DETECT score (PD-Q) for which there is significant association between square root (sqrt) of WOMAC and MOAKS grade 3 effusion (A), and sqrt(WOMAC) and MOAKS sum of BML scores (B). For each graph, areas of significance are to the left of the PD-Q cutoff, which is 11.6 for panel A and 17.2 for panel B.

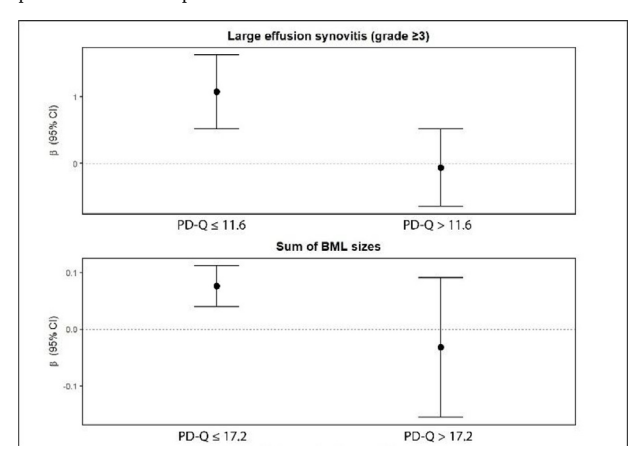


Figure 2: Associations of square root (sqrt) WOMAC scores to MOAKS grade 3 effusion (A), sqrt(WOMAC) to Sum of BML size (B), stratified by PD-Q group using the J-N defined cutoffs, as defined in **figure 1**. Associations are positive and statically significant for the lower PD-Q group for each presented MOAKS variable.

FROM MENISCAL DEGENERATION TO OSTEOARTHRITIS: TRACKING EARLY DISEASE PROGRESSION WITH MRI-BASED COMPOSITE SCORES: DATA FROM THE OSTEOARTHRITIS INITIATIVE

J.T. Harvey 1 , T.E. McAlindon 1 , J. Baek 1 , J. MacKay 2,3 , M. Zhang 4 , G.H. Lo 5,6 , S.-H. Liu 1 , C.B. Eaton 7,8 , M.S. Harkey 9 , J.C. Patarini 1 , J.B. Driban 1

- ¹ University of Massachusetts Chan Medical School, Worcester, MA, USA
- ² University of Cambridge, Cambridge, UK
- ³ Norwich Medical School, University of East Anglia, Norwich, UK
- ⁴ Boston University, Boston, MA, USA
- ⁵ Baylor College of Medicine, Houston, TX, USA
- ⁶ Michael E. DeBakey Medical Center, Houston, TX, USA
- ⁷ Kent Hospital, RI, USA
- ⁸ Brown University School of Public Health, Providence, RI, USA
- ⁹ Michigan State University, East Lansing, MI, USA

INTRODUCTION: Meniscal degeneration predisposes knees without radiographic OA to develop a future meniscal tear and an accelerated onset and progression of OA. Understanding the relationship between meniscal degeneration and OA-related biomarkers in knees without radiographic OA is essential for improving early detection, monitoring disease progression, and developing intervention strategies to prevent or slow the progression of this debilitating condition.

OBJECTIVE: To explore the relationship between meniscal degeneration (intrameniscal signal alteration without a tear) and future OA pathology measured by composite scores based on MRI: disease activity (BM lesion and effusion-synovitis volumes) and cumulative damage (articular cartilage damage).

METHODS: Our sample included 225 participants from the OAI with intact menisci (defined as normal or meniscal degeneration without tear) on MRI and no radiographic knee OA at baseline. There were 110 participants with normal menisci (77% Female, 55 [SD 7] average years of age) and 115 with meniscal degeneration (60% Female, 61 [SD 9] average years of age). We used longitudinal MRIs from an existing study to calculate disease activity and cumulative damage. Negative values represent milder disease activity or cumulative damage than the average of a reference sample, among whom 93% had moderatesevere radiographic knee osteoarthritis (KLG = 3 or 4), and the average WOMAC knee pain score was 5.0 (SD=3.6). MR images were collected at each OAI site using Siemens 3.0 Tesla Trio MR systems and knee coils. Acquisitions included a sagittal IM fat-suppressed sequence (field of view=160mm, slice thickness=3mm, skip=0mm, flip angle=180 degrees, echo time=30ms, recovery time=3200ms, 313×448 matrix, x-resolution=0.357mm, y-resolution=0.357mm), which was used to measure BML and effusion-synovitis volumes. Cartilage damage was quantified using a 3D DESS sequence: field of view=140mm, slice thickness=0.7mm, skip=0mm, flip angle=25 degrees, echo time=4.7ms, recovery time=16.3ms, 307 × 384 matrix, x-resolution=0.365mm, yresolution=0.365mm. We used robust regression models with M estimation and Huber weights to assess the association between baseline meniscal degeneration (exposure) and disease activity or cumulative damage at baseline and four annual follow-up visits (outcomes), adjusting for gender, race, age, static alignment, and body mass index.

RESULTS: Knees with meniscal degeneration were more likely to have, on average, 0.21 greater disease activity at 12 months than knees with normal menisci (parameter estimate=0.21, 95% confidence interval [CI]=0.09, 0.33); this association persisted over time. The association

between meniscal degeneration and cumulative damage only became statistically significant at the 48-month visit (parameter estimate=0.74, 95% CI=0.18, 1.31).

CONCLUSION: This study illuminates the pivotal role of meniscal degeneration in the early stages of OA, demonstrating its association with increased disease activity and subsequent cartilage damage. The use of MRI-based composite scores provides a powerful tool for tracking disease progression, offering valuable insights for early intervention strategies. By identifying meniscal degeneration as a precursor to osteoarthritis, we can better target preventive measures and therapeutic approaches, ultimately aiming to mitigate the impact of this debilitating condition on patients' lives.

SPONSOR: National Institute of Health, National Institute of Arthritis and Musculoskeletal and Skin Diseases Award No R01-AR076411 and R01-AR065977. VA's Health Services Research and Development Service Center for Innovations in Quality, Effectiveness, and Safety #CIN 13-413.

DICLOSURE STATEMENT: Timothy E. McAlindon declares he is a consultant for Sanofi, Kolon TissueGene, Medidata, Organogenesis, and is the owner of Ambulomics and Arthometrics. Timothy E. McAlindon, Jeffrey B Driban, and Ming Zhang hold a patent for Objective Assessment of Joint Damage, US-20220202356, 2020.

CORRESPONDENCE ADDRESS: timothy.mcalindon@umassmed.edu

Table 1. Baseline Meniscal Signal Alterations Relate to Disease Activity and Cumulative Damage Cross-Sectionally and Future Visits.

	Disease Ac	tivity ¹		Cumulativ	ve Damage ¹	
	Normal Menisci (n = 110)	Meniscal Degener- ation (n = 115)	Parameter Estimate ² (95% CI)	Normal Menisci (n = 110)	Meniscal Degener- ation (n = 115)	Parameter Estimate ² (95% CI)
Visit	Mean ² (95% CI)	Mean ² (95% CI)		Mean ² (95% CI)	Mean ² (95% CI)	
Baseline	-2.30	-2.22	0.08	-0.18	0.23	0.41
(n = 225)	(-2.38,	(-2.29,	(-0.02,	(-0.58,	(-0.11,	(-0.11,
	-2.23)	-2.16)	0.18)	0.22)	0.57)	0.93)
12 month	-2.26	-2.04	0.21	0.5	0.46	0.41
(n = 221)	(-2.35,	(-2.12,	(0.09,	(-0.37,	(0.11,	(-0.13,
	-2.16)	-1.97)	0.33)	0.46)	0.80)	0.95)
24 month	-2.10	-1.82	0.28	0.20	0.67	0.47
(n = 221)	(-2.22,	(-192,	(0.13,	(-0.21,	(0.32,	(-0.06,
	-1.99)	-1.73)	0.43)	0.60)	1.01)	1.01)
36 month	-2.03	-1.62	0.41	0.35	0.86	0.51
(n = 205)	(-2.17,	(-1.75,	(0.22,	(-0.07,	(0.49,	(-0.06,
	-1.89)	-1.50)	0.60)	0.78)	1.23)	1.07)
48 month	-2.02	-1.71	0.31	0.37	1.11	0.74
(n = 220)	(-2.16,	(-1.83,	(0.13,	(-0.61,	(0.74,	(0.18,
	-1.89)	-1.59)	0.49)	0.80)	1.48)	1.31)
Change 0 to	0.22	0.49	0.27	0.46	0.66	0.20
48 months	(0.11,	(0.39,	(0.11,	(0.31,	(0.53,	(0.00,
	0.34)	0.59)	0.42)	0.61)	0.78)	0.40)

¹ Higher values indicate worse damage. Negative values represent milder disease activity or cumulative damage than the average of a reference sample, among whom 93% had moderate-severe radiographic knee osteoarthritis (Kellgren-Lawrence Grade = 3 or 4), and the average WOMAC knee pain score was 5.0 (SD=3.6; Supplemental Table 1).

 $^{^2~}$ Adjusted for gender (2 levels), race (3 levels), baseline age, baseline static alignment (adjusted FTA), and baseline body mass index. 95% CI = 95% Confidence interval

A FIRST-IN-HUMAN PHASE 1/2A CLINICAL STUDY OF ICM-203 AAV GENE THERAPY: PROMISING SIGNALS AS A DMOAD CANDIDATE

A. Heald 1,2 , L. Bogdan Solomon 3,4 , R. Page 5,6 , Y.N. Yum 1 , M. Park 1,7 , J. Myung 1 , J.E. Collins 8 , A. Guermazi 9 , D.W. Kim 1,7

INTRODUCTION: ICM-203, a recombinant AAV vector designed to express a truncated form of human Nkx3.2, a transcription factor which plays an important role in both chondrocyte and synoviocyte activity, is in clinical development as a potential DMOAD.

OBJECTIVE: An unblinded interim analysis of the low dose cohort of the first-in-human phase 1/2a study of ICM-203 was conducted to assess the safety, immunogenicity, and biological activity of ICM-203.

METHODS: In the low dose cohort of this phase 1/2a, double-blind, placebo-controlled, dose escalation study (NCT04875754), 8 subjects with Kellgren-Lawrence grade 3 osteoarthritis (OA) of the knee were randomized to receive a single intra-articular injection of ICM-203 or placebo in a 3:1 ratio. The primary safety endpoint was safety and tolerability of ICM-203 through assessment of treatment-emergent adverse events (TEAEs). Immunogenicity endpoints included measuring serum neutralizing antibody (NAb) titers and T-cell responses to ICM-203's AAV capsid. As efficacy endpoints, changes in knee pain and function were assessed by the Knee Injury and Osteoarthritis Outcome Score (KOOS) pain subscale and KOOS activities of daily living (ADL) subscale, respectively; these KOOS scores were converted to calculate Western Ontario and McMaster Universities Osteoarthritis Index (WOMAC)

scores. Imaging endpoints included Magnetic Resonance Imaging (MRI) Osteoarthritis Knee Scores (MOAKS) focusing on bone marrow lesions (BML), synovitis, articular cartilage damage, and osteophytes.

RESULTS: Of 11 screened subjects, 8 qualified and received a single intra-articular injection of ICM-203 (N=6) or placebo (N=2); all subjects completed 52 weeks of follow-up. Subject age ranged from 56 to 73 years; body mass index (BMI) ranged from 24.6 to 38.6 kg/m2. No significant concerns about safety or tolerability arose. The most common treatment-related TEAE was mild to moderate arthralgia, which occurred in 3 of 6 ICM-203 subjects and 1 of 2 placebo subjects. At baseline, 3 ICM-203 subjects had positive NAb responses to AAV capsid; no subjects had significant T-cell responses. All 6 ICM-203 subjects developed both a humoral and cellular response against AAV capsid, whereas neither placebo subject did. ICM-203 subjects with negative NAb at baseline (N=3) demonstrated greater improvement over placebo subjects (N=2) in KOOS pain, KOOS ADL, WOMAC, as well as in imaging endpoints, including MOAKS BML and synovitis. For articular cartilage and osteophytes, no significant changes were observed in any subject between baseline and week 52.

CONCLUSION: Intra-articular injections of ICM-203 were safe and well tolerated. ICM-203 appeared to show greater therapeutic activity over placebo in subjects with negative NAb at baseline. Current findings indicate ICM-203 may demonstrate potential as a disease-modifying osteoarthritis drug (DMOAD), between reducing osteoarthritis symptoms, ameliorating structural joint damage, and alleviating synovial inflammation. Investigation of higher doses of ICM-203 is in progress.

SPONSOR: ICM Company Limited

DICLOSURE STATEMENT: Dae-Won Kim is CEO and Stockholder of ICM. Ali Guermazi and Jamie E. Collins provide consulting services for ICM.

CORRESPONDENCE ADDRESS: dae-won.kim@icm-bio.com

¹ ICM Co., Ltd., Seoul, Korea

² University of Washington School of Medicine, Seattle, WA, USA

 $^{^3\,}Royal$ Adelaide Hospital, Adelaide, SA, Australia

⁴ University of Adelaide, Adelaide, SA, Australia

⁵ Barwon Health, University Hospital Geelong, Geelong, VIC, Australia

⁶ Deakin University, Geelong, VIC, Australia

⁷ Yonsei University, Seoul, Korea

⁸ Brigham and Woman's Hospital, Boston, MA, USA

⁹ Boston University School of Medicine, Boston, MA, USA

PREVALENCE OF ACETABULAR DYSPLASIA IN 6-YEAR-OLDS IN A GENERAL POPULATION

N. Hendriks 1 , F. Boel 1 , C. Lindner 2 , F. Rivadeneira 1 , C.J. Tiderius 3 , S.M.A. Bierma-Zeinstra 1 , R. Agricola 1 , J. Runhaar 1

INTRODUCTION: Acetabular dysplasia (AD) is an important risk factor for early hip OA in adults. In Europe, infants are screened for developmental hip dysplasia. However, AD can also develop during skeletal maturation and these cases often remain unrecognized. Potentially, AD could be influenced prior to the closure of the hip growth plates. Understanding AD development during growth is crucial to prevent future joint degeneration. Different definitions are used to measure AD, depending on the stage of skeletal maturation. More knowledge of the prevalence of AD in the general population is required to understand its development during growth.

OBJECTIVE: 1) To estimate the prevalence of AD in 6-year-olds from the general population, and 2) to compare different AD definitions in this age group.

METHODS: Data from The Generation R Study, a population-based study examining growth and health from fetal life to adulthood, was used. All participants aged 6 years, with high-resolution dual-energy x-ray absorptiometry (DXA) anteroposterior image of the right hip available were included. The hip shape was outlined with 70 landmarks using BoneFinder®. Using these landmarks, the acetabular index (AI), a measurement of acetabular roof inclination, was calculated to assess AD (AI>20°). While AI is commonly used in children, the lateral center-edge angle (LCEA), as indicator for acetabular roof coverage of the femoral head, was also calculated. Mean LCEA and prevalence of AD (LCEA<15°) were compared to measures using AI.

RESULTS: In total, 3,270 participants were included with a mean age of 6.2 (SD 0.6) years, and 51% was female. The mean AI was 11.3° (SD 5.0°) and the mean LCEA was 19.5° (SD 5.9°). The distribution for both AD definitions is shown in Figure 1. An AI>20° was found in 124 participants, indicating a AD prevalence of 3.8% (95%CI, 3.1% - 4.5%). Based on the LCEA, the AD prevalence was 21.3% (95%CI, 19.9% - 22.7%).

CONCLUSION: The prevalence of AD in 6-year-olds is 3.8%, based on the AI. The LCEA classifies more hips as dysplastic in 6-year-olds. The validity of the LCEA in this age group and clinical relevance of these newly classified dysplastic hips need to be determined. A better understanding of the development of AD is important, as recovery during growth may be feasible and could contribute to the prevention of OA.

SPONSER: ERC Consolidator **DISCLOSURE STATEMENT:** none

ACKNOWLEDGEMENT: project team HIPSTAR

CORRESPONDENCE ADDRESS: n.hendriks@erasmusmc.nl

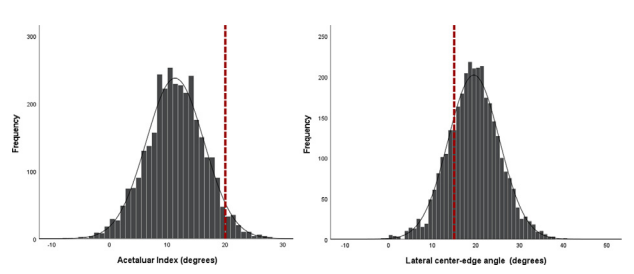


Figure 1. The distribution of the acetabular index and the lateral centeredge angle within the study population. The dashed red lines indicate the cut-off values (AI $> 20^{\circ}$, and LCEA $< 15^{\circ}$).

¹ Erasmus MC University Medical Center Rotterdam, Rotterdam, The Netherlands

² The University of Manchester, Manchester, UK

³ Lund University, Skåne University Hospital, Sweden

GENETIC SULFATE WASTING, A MONOGENIC CAUSE OF SEVERE INTERVERTEBRAL DISC HEIGHT LOSS

J.M. Hou 1 , D.D.G. Chappell 2 , E. Gkrania-Klotsas 3 , S.M. Park 4 , P. Freeman 5 , M. Duer 6 , K.E.S. Poole 1

INTRODUCTION: Loss of function SLC13A1 variants cause failure to reabsorb sulfate in proximal tubule, reduced serum sulfate, and intervertebral disc disease via glycosaminoglycan abnormalities. A rheumatology patient was found to be homozygous for SCL13A1, explaining an extraordinary spinal disc loss phenotype.

OBJECTIVE: To define intervertebral disc heights and measure sulfate levels and excretion.

METHODS: The homozygote is a 45-year-old female who was only 14 when her already severe degenerative disc disease necessitated her first lumbar laminectomy, with a second performed 4 years later. Her lumbar and thoracic range of motion is greatly reduced. She suffers from severe back pain. Whole genome sequencing identified a stop-gain variant on chromosome 7 at ex.2 c.34C>T p. (Arg12Ter). We measured her radiographic intervertebral disc heights to compare with matched reference values from other studies and older controls from previous Cambridge studies, with 3D reconstructions given the extraordinary disc loss phenotype. The homozygote has a decreased plasma sulfate compared to reference values (149 vs225-494 μ mol/l). Her urine sulfate is high at 2086umol/l for plasma level. Sulfate excretion rate is excessive 1605mmol/mol creatinine (ref. 444-5431mmol/mol)

RESULTS: Radiographic measurements showed widespread loss of disc height. The proband's brother is also under our care for multiple musculoskeletal (MSK) problems; he is heterozygous for SLC13A1 but has normal disc heights.

CONCLUSIONS: How renal sulphate wasting results in intervertebral disc degeneration in SLC13A1 homozygotes is unclear. Studying such patients might provide an avenue for therapeutic intervention to target widespread disc disease.

SPONSOR: Cambridge NIHR Biomedical Research Centre

DICLOSURE STATEMENT: No disclosures

ACKNOWLEDGEMENT: N/A

CORRESPONDENCE ADDRESS: kesp2@cam.ac.uk

Table 1. Intervertebral disc heights of homozygous patient and controls

	Female	middle interver	tebral disc heig	hts (mm)
	Patient	Machino et al.	Bach et al.	Previous Cambridge studies
Disc level	N=1	N=50	N=18	N=20
	Age 38 years	Ages 30-39 years	Ages 30-39 years	Ages 55-71 years
T10-11	4.7	6.2±1.2	-	2.7 ±1.2
T11-12	4.3	7.0±1.1	-	3.7 ±1.6
T12-L1	6.1	7.3±1.0	5.9 ± 0.8	4.5 ±1.7
L1-L2	4.4	8.3±1.3	7.0 ±0.9	5.9 ±1.8
L2-L3	3.5	9.7±1.8	8.7 ±1.3	6.4 ±1.9
L4-L5	4.4	10.5±1.9	9.5 ±1.4	6.9±2.0
L5-S1	5.9	8.9±2.0	9.0±2.4	6.8±1.9



Figure 1. Sagittal CT and 3D reconstruction appearance of severe disc height loss at all levels

 $^{^{\}rm 1}$ Department of Medicine and NIHR Cambridge Biomedical Research Centre, University of Cambridge, Cambridge, UK

 $^{^2\,\}mathrm{Department}$ of Medicine, Cambridge University Hospitals NHS Foundation Trust, Cambridge, UK

³ Department of Infectious Diseases, Cambridge University Hospital NHS Foundation Trust, Cambridge, UK

⁴Department of Clinical Genetics, Cambridge University Hospitals NHS Foundation Trust, Cambridge, UK

⁵ Department of Veterinary Medicine, University of Cambridge, Cambridge, UK

⁶ Department of Chemistry, University of Cambridge, Cambridge, UK

REGIONAL DEPTH-SPECIFIC SUBCHONDRAL BONE DENSITY IN OA AND NORMAL DISTAL FEMORA: PRECISION AND PRELIMINARY COMPARISONS

J.D. Johnston ¹, A.E. Sacher ¹, C.E. McLennan ², J.A. Lynch ³, T. Neogi ⁴, D.J. Hunter ⁵, D.R. Wilson ⁶, S.A. Kontulainen ⁷

INTRODUCTION: The exact role of altered subchondral bone in OA pathogenesis and pain is unclear. Clinical quantitative CT (QCT) combined with depth-specific image processing has been previously used to study subchondral bone mineral density (BMD) at the proximal tibia and patella. Limited depth-specific QCT research has been completed at the OA distal femur.

OBJECTIVES: To 1) assess the short-term precision of automated, regional, depth-specific subchondral BMD measures at the distal femur in individuals with and without OA; and 2) determine whether regional and focal BMD metrics were able to discriminate differences in subchondral bone density patterns between normal and OA distal femora.

METHODS: Fourteen participants (3M:11F; mean age: 49.9 (SD: 11.9) years) were recruited and classified as normal (n=7) or OA (n=7). Each participant was scanned three times over two days using clinical QCT. Two BMD assessments were evaluated at the distal femur: mean regional density and peak focal density. BMD measures were assessed across three depths (0-2.5, 2.5-5, 5-7.5 mm) and six sub-regions of the distal femur (medial/lateral, anterior/central/posterior), as per the MOAKS approach (Fig.1). We assessed precision using root mean square coefficients of variation (CV%_{RMS}). To explore potential differences between OA and normal distal femora, we performed parametric t-tests and non-parametric Mann-Whitney statistical analyses and also determined Cohen's d effect sizes, with an absolute d > 0.8 considered clinically significant.

RESULTS: CV%_{RMS} ranged from 1.6% to 3.6% (average: 2.2%) for measures of regional BMD while CV%_{RMS} ranged from 1.6% to 6.9% (average: 2.7%) for measures of focal BMD. Statistical comparisons indicated lower BMD in OA distal femoral in the medial-anterior region at depths of 2.5-5 mm (regional: -17%; focal: -19%) and 5-7.5 mm (regional: -21%; focal: -25%) (Fig. 2). All other BMD measures were similar between normal and OA distal femora (p > 0.05). Cohen's d effect sizes ranged from -1.7 to 0.76.

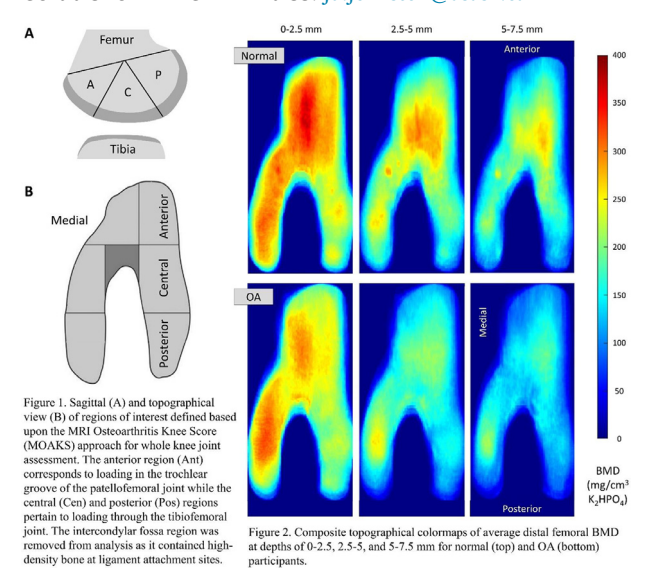
CONCLUSION: This automated technique offers precise measures of subchondral BMD at the distal femur. This approach has potential to quantify and distinguish OA-related alterations in subchondral BMD at the distal femur.

SPONSORS: Canadian Arthritis Network and Natural Sciences and Engineering Research Council (NSERC) (JDJ: RGPIN-2015-06420; SAK: RGPIN-2016-05301).

DICLOSURE STATEMENT: none

ACKNOWLEDGMENT: Altruistic volunteers who participated in this study.

CORRESPONDENCE ADDRESS: jd.johnston@usask.ca



doi: 10.1016/i.ostima.2025.100294

¹ Department of Mechanical Engineering, University of Saskatchewan, Saskatoon, SK, Canada

² Division of Research, New England Baptist Hospital, Boston, MA, USA

³ Department of Epidemiology and Biostatistics, University of California, San Francisco, CA. USA

⁴ Department of Medicine, Boston University School of Medicine, Boston, MA, USA

 $^{^{5}}$ Institute of Bone and Joint Research, Kolling Institute, University of Sydney, Sydney, Australia

⁶ Department of Orthopaedics and Centre for Hip Health and Mobility, University of British Columbia and Vancouver Coastal Health Research Institute, Vancouver, BC, Canada

⁷ College of Kinesiology, University of Saskatchewan, Saskatoon, SK, Canada

EXPLORING SEX-BASED HIP MORPHOLOGY DIFFERENCES IN YOUNG ADULTS USING AN AUTOMATED 3D METHOD

M.A. Kamphuis ¹, E.H.G. Oei ¹, J. Runhaar ², D.F. Hanff ¹, J.J. Tolk ³, R. Agricola ⁴, S.M.A. Bierma-Zeinstra ², S. Klein ¹, J. Hirvasniemi ^{1,5}

INTRODUCTION: Although many factors contribute to the development of hip OA, structural abnormalities such as acetabular dysplasia are recognized as contributing to early degenerative changes. To identify these abnormalities, conventional two-dimensional radiographic methods are still widely used to assess hip morphology. However, they inherently oversimplify the joint's complex three-dimensional anatomy and are subject to limitations such as patient positioning.

OBJECTIVE: This study aimed to develop and validate an automated method for 3D hip morphology analysis, incorporating segmentation and image feature extraction, as well as to assess morphological differences between sexes.

METHODS: We analyzed data from 2454 participants from Generation R Cohort (mean \pm standard deviation age and BMI: 18.4 \pm 0.6 years and 22.7 \pm 3.8 kg/m²) comprising 1199 males and 1255 females. Hip structures (femoral bone, acetabular bone, femoral cartilage, and acetabular cartilage) were automatically segmented from MRI. An nnU-Net ensemble model was trained on 40 manually segmented hips and its performance evaluated using the Dice score. From the segmentations, five categories of morphological features were computed: basic geometric metrics (centers and radii), cartilage volumes, angular measurements (tilt, version, neck shaft angle and coverage angles, alpha angles), coverage metrics, and joint space width measurements. Independent samples t-tests were used to evaluate sex -based differences.

RESULTS: The automatic deep learning segmentation model achieved mean \pm standard deviation Dice scores of 0.97 \pm 0.004, 0.90 \pm 0.01, 0.76 \pm 0.02, and 0.77 \pm 0.02 for femoral bone, acetabular bone, femoral cartilage, and acetabular cartilage, respectively, on a hold-out test set of 10 hips. All biomarkers showed statistically significant differences (p<0.05), we highlight those with the largest differences between male and female group means. Compared to males, females had smaller

femoral and acetabular radii, as well as reduced cartilage volumes in both the femoral and acetabular regions (Table 1). Alpha angles were lower in females, particularly in the coronal plane, but also in the axial plane, while the acetabular version angle for females was greater (Table 1).

CONCLUSION: This study demonstrates the feasibility of automated 3D analysis for comprehensive hip morphology assessment. Overall, the analysis reveals consistent and measurable differences in hip morphology between sexes. These morphological insights may help clarify structural risk factors for early hip OA.

SPONSOR: European Research Council DISCLOSURE STATEMENT: None

ACKNOWLEDGMENT: The authors would like to thank all the partici-

pants and staff of Generation R.

CORRESPONDENCE ADDRESS: j.hirvasniemi@erasmusmc.nl

 $\begin{tabular}{ll} \textbf{Table 1:} Mean \pm Standard Deviation of Hip Morphology Measurements \\ Between Males and Females. \\ \end{tabular}$

Variable	Male	Female	p-value
Femoral Radius (mm)	23.93 ± 1.32	21.19 ± 1.17	p < 0.001
Acetabular Radius (mm)	27.08 ± 1.44	24.41 ± 1.28	p < 0.001
Distance (mm)	0.887 ± 0.422	0.862 ± 0.404	0.031
Femoral Cartilage Volume	10070 ± 1350	7930 ± 1030	p < 0.001
(mm ³)			
Normalized Femoral Cartilage	17.52 ± 1.17	17.59 ± 1.06	0.047
Volume (mm ³)			
Acetabular Cartilage Volume	4330 ± 710	3400 ± 530	p < 0.001
(mm ³)			
Normalized Acetabular	5.88 ± 0.62	5.69 ± 0.58	p < 0.001
Cartilage Volume (mm³)			
Neck-Shaft Angle (°)	128.75 ± 4.61	129.31 ± 4.50	p < 0.001
Whole Coverage (%)	38.85 ± 3.09	38.36 ± 3.03	p < 0.001
Upper Coverage (%)	58.73 ± 3.93	58.27 ± 3.99	p < 0.001
Coverage Region 1 (%)	23.4 ± 6.5	21.5 ± 6.2	p < 0.001
Coverage Region 2 (%)	49.71 ± 1.50	49.38 ± 1.55	p < 0.001
Coverage Region 3 (%)	9.80 ± 2.76	9.53 ± 2.92	p < 0.001
Coverage Region 4 (%)	34.7 ± 5.4	36.1 ± 5.2	p < 0.001
12 O'clock Angle (°)	120.76 ± 5.15	119.23 ± 4.88	p < 0.001
Alpha Angle Coronal (°)	51.25 ± 8.72	41.38 ± 4.97	p < 0.001
Alpha Angle Axial (°)	38.49 ± 6.73	33.83 ± 4.53	p < 0.001
Tilt (°)	46.89 ± 2.85	46.42 ± 3.21	p < 0.001
Version (°)	14.8 ± 5.3	16.8 ± 6.2	p < 0.001
Mean Joint Space Width (mm)	3.804 ± 0.286	3.829 ± 0.256	p < 0.001
Minimal Joint Space Width	2.48 ± 0.315	2.51 ± 0.29	p < 0.001
(mm)			
Acetabular Version Angle (°)	18.40 ± 0.64	18.34 ± 0.66	p < 0.001

¹ Department of Radiology and Nuclear Medicine, Erasmus MC University Medical Center Rotterdam, The Netherlands

 $^{^{2}\,\}mathrm{Department}$ of General Practice, Erasmus MC University Medical Center Rotterdam, The Netherlands

³ Department of Orthopaedics and Sports Medicine, Erasmus MC University Medical Center Rotterdam, Sophia Children's Hospital, The Netherlands

⁴Department of Orthopaedics and Sports Medicine, Erasmus MC University Medical Center Rotterdam, The Netherlands

⁵ Department of Biomechanical Engineering, Delft University of Technology, The Netherlands

EX VIVO IMAGING OF DIFFERENT CALCIFICATION TYPES IN POSTERIOR HORN OF HUMAN MENISCUS USING MICRO-COMPUTED TOMOGRAPHY

V.P. Karjalainen ¹, I. Hellberg ¹, A. Turkiewicz ², B. Shakya ¹, N. Khoshimova ¹, E. Nevanranta ¹, K. Elkhouly ¹, S. Das Gupta ¹, A. Sjögren ², M.A.J. Finnilä ¹, P. Önnerfjord ², V. Hughes ², J. Tjörnstrand ³, M. Englund ², S. Saarakkala ¹

INTRODUCTION: Meniscal calcifications are known to be associated with OA. Specifically, two types of calcifications have been commonly identified in osteoarthritic knees: basic calcium phosphate (BCP) and calcium pyrophosphate (CPP). However, their pathological significance remains largely unclear. Characterizing differences between the calcification types and their deposition patterns inside the meniscus could help in their identification with *in vivo* imaging modalities and provide a better understanding of the role of meniscal calcifications in the OA disease process.

OBJECTIVE: 1) Identify the two different types of calcifications in human meniscus *ex vivo* in 3D using μ CT; 2) Describe the different deposition patterns observed in BCP and CPP calcifications.

METHODS: From the MENIX biobank in Lund, Sweden, we collected 82 posterior horns of medial and lateral menisci from 20 total knee replacement (TKR) patients and 21 deceased donors (50/50% female/male, average age 71 years) for the study. A 5-mm-thick subsection was dissected from the posterior horn, fixed in formalin, dehydrated, and treated with hexamethyldisilazane (HMDS) before air-drying at room temperature overnight. Subsequently, the HMDS-treaded section was imaged with a desktop μ CT imaging (SkyScan 1272, Bruker, micro-CT) with the following settings: 60 kV, 166 μ A, 2.0 μ m voxel size, 3500 ms exposure time, random movement 25 voxels, and without an additional filter. Two different image reconstruction settings were used to maximize the image quality of meniscal soft tissue and calcifications. Pieces of meniscus adjacent to the μ CT underwent histological processing and Alizarin Red staining. Calcification types from the histological sections were identified using Raman micro-spectroscopy.

RESULTS: We successfully imaged both meniscal calcification types together with soft tissue in 3D using high-resolution μ CT (Figure 1). Based on Raman spectral analysis, out of the 82 menisci, 39 had at least one calcification: 28 had BCP calcifications, 8 had CPP calcifications, and 3 had both. In μ CT, BCP calcifications were quantitatively denser, morphologically sharper, more punctuated, smaller in size as well as number, and more spherical than CPPs. Unlike CPPs, BCPs were mainly deposited in the periphery of meniscal tissue, inside complex 3D tears or fibrillations. In contrast, the CPP calcifications formed long rod-like structures, mainly inside the meniscal tissue.

CONCLUSION: Based on the 3D μ CT images, BCP calcifications were not found inside the meniscal tissue but in the peripheral area. This could suggest that larger clusters of BCP calcifications found in the meniscus come from the synovial fluid and possibly originate from articular cartilage or bone. Meanwhile, the likely place for CPPs to accumulate and expand within the meniscal tissue is in the fluid channels that follow the circumferential collagen fiber bundles, where they fill the cavity of the channel to form rod-like morphology and have a continuous supply of calcium and other constituents. Additionally, vascular walls were

observed to accumulate calcifications, supported by hollow rod-shaped structures that do not follow the circumferential fibers. Potentially, after tearing and degeneration of the meniscus, CPPs may start to accumulate on the surfaces and tears of the meniscus in an amorphous pattern. This qualitative 3D comparison of meniscal calcification patterns may help distinguish them with imaging modalities more easily in the future, as well as provide a better understanding of their role in OA.

DISCLOSURE STATEMENT: Simo Saarakkala, Associate Editor of Osteoarthritis and Cartilage Open. AT is the statistical associate editor of Osteoarthritis and Cartilage.

ACKNOWLEDGMENT: We want to thank Laboratory Technician Piia Mäkelä, MENIX clinical staff at Trelleborg Hospital, and the Department of Forensic Medicine in Lund for sample collection.

CORRESPONDENCE ADDRESS: ville-pauli.karjalainen@oulu.fi

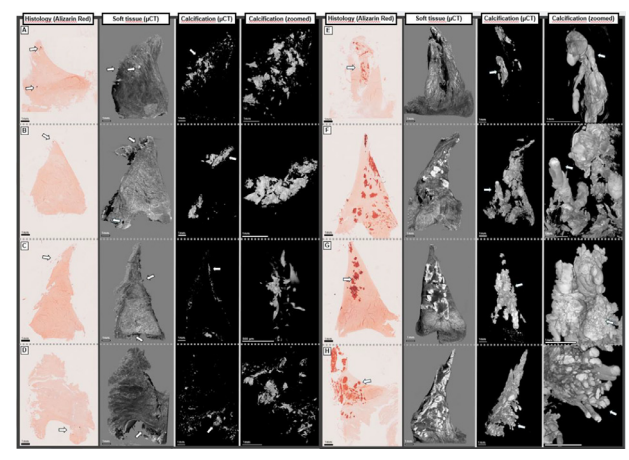


Figure 1. A, B, C, D) Examples of four different meniscus samples with basic calcium phosphate (BCP) calcifications. White arrows show areas with positive Alizarin Red staining marking meniscal calcifications in histological sections. While some BCP calcifications are seen inside the soft tissue in histology, 3D µCT images confirm that they are located in the periphery of the meniscus, stuck inside complex 3D tears or fibrillations. Zoomed calcification images show sharp morphology of the BCP calcifications, which is a likely contributor to further tearing and degradation targeted to the meniscus under biomechanical stress. In addition, this sharp morphology can promote calcifications to bury in the surface fibrillations or even advance the state of fibrillation with shearing and pro-inflammatory effects on their surroundings. E, F, G, H) Examples of four different meniscus samples with calcium pyrophosphate (CPP) calcifications. Long, rod-shaped formations cover the inner volume of the meniscus, while less dense, amorphous calcified structures are located on the surface and between the more solid calcifications. E) The inner volume of the meniscus is covered in rod-like, smooth calcifications (white arrow). F) Smooth, rod-shaped calcifications along the circumferential collagen fiber bundles are seen inside the meniscus (white arrow), while more amorphous calcification structures are seen on the tibial surface. G) Bundled together with rod-shaped collagens, a denser cluster of calcifications is seen inside the meniscus (white arrow). H) Multiple rod-shaped calcifications cover almost the whole volume of the meniscus (arrow).

¹ Research Unit of Health Sciences and Technology, University of Oulu, Oulu, Finland
² Lund University, Faculty of Medicine, Department of Clinical Sciences Lund, Orthopaedics, Clinical, Epidemiology Unit, Lund, Sweden

³ Lund University, Faculty of Medicine, Department of Clinical Sciences Lund, Rheumatology and Molecular Skeletal Biology, Lund, Sweden

STRUCTURAL EFFICACY OF INTRA-ARTICULAR SPRIFERMIN TREATMENT ON KNEE OSTEO-ARTHRITIS AS A FUNCTION OF SYMPTOMATIC AND RADIOGRAPHIC DISEASE SEVERITY - A POST-HOC ANALYSIS FROM THE FORWARD PHASE 2 RANDOMIZED CONTROLLED TRIAL

C. Knight 1 , F. Eckstein 2,3 , W. Wirth 2,3 , C. Clemmensen 4 , W. Ma 1 , A. Collins 1 , S. Basnet 1

INTRODUCTION: A putative disease-modifying osteoarthritis drug, "Sprifermin" was studied by a phase 2B RCT (FORWARD - NCT01919164). Given at a 100µg dose, sprifermin increased cartilage thickness, both in absolute terms and compared with placebo [1]. In the full cohort with MRI results (mITT), this effect did, however, not lead to a pain relief greater than placebo [1]. FORWARD contained patients with a variety of radiographic disease stages (KLG 2 or 3, with a medial minimum joint space width (JSW) > 2.5mm). Although all patients had to display > 40mm pain levels at screening, not all of them exceeded that threshold at the actual baseline measurement [2].

OBJECTIVE: To elucidate post-hoc whether structural treatment effects on cartilage (thickness) by sprifermin differ between severity strata of symptoms (WOMAC) and radiographic disease status. These observations may inform future clinical trials at which stage (sprifermin-) treatment is structurally and symptomatically most effective.

METHODS: Total femorotibial joint (TFTJ) cartilage thickness change at year (Y) 2 by MRI represented the primary endpoint; WOMAC pain was secondary [1]. Patients aged 40–85 with primary symptomatic TFTJ OA (KLG 2 or 3; medial mJSW \geq 2.5 mm) were studied. Cartilage thickness was determined quantitatively from 1.5-3T MRI by expert readers, using proprietary software (Chondrometrics). The analysis focused on the 2Y MRI TFTJ cartilage thickness change for the two highest sprifermin dose groups (100 μ g given every 6 or 12 months combined) vs. placebo. The Hedges G (sample-size-independent effect size measure) was determined, with 95% CIs obtained by bootstrapping. We studied the modified intent to treat cohort with 24-month data (mITT), and the so-called "subcohort at risk" (SAR)[2] a subgroup with baseline WOMAC pain >40 and more severe radiographic involvement by mJSW criteria.

RESULTS: Of 549 FORWARD patients randomized, 474 completed 2Y follow-up. 69% of the mITT with 24M data were female; the median age was 67 and the medial BMI 29.6. The treatment effect on cartilage thickness was 45.6µm for the mITT (Hedges G=0.63). Participants with baseline WOMAC pain ≥ the median displayed a somewhat smaller ef-

fect (17 \pm 70 μ m change over 2 years in treated vs. -15 \pm 55 μ m in placebo participants; Hedges G =0.49 [0.11, 0.86] than those with pain < median (37 \pm 69 μ m in treated vs. -27 \pm 84 μ m in placebo participants; Hedges G =0.86 [0.47, 1.25].

KLG2 subjects displayed a marginally greater treatment effect (30±75µm in treated vs. -16±46µm in placebo participants; Hedges G =0.68 [0.36, 1.00]) than KLG3 participants (13±68µm in treated vs. -33±110µm in placebo participants; Hedges G =0.55 [0.07, 1.03]). Those with JSN grade 0 (no JSN) showed a stronger treatment effect (50±59µm in those treated vs. -11±45µm in placebo participants; Hedges G =1.09 [0.63, 1.54] than those with JSN >0 (7±79µm in sprifermin treated participants vs. -26±84 µm in placebo subjects; Hedges G =0.41 [0.07, 0.75]

Structural results in the SAR were similar, with slight differences observed for JSN strata. The effect size on WOMAC pain in the SAR was relatively strong in KLG3 subjects (-34.4 \pm 20 vs. -10.6 \pm 29 in placebo; Hedges G -1.03 [-1.71, -0.35]), whereas in KLG2 participants it was weaker (-33.5 \pm 17 for sprifermin-treated vs. -36.9 \pm 18 in placebotreated participants; Hedges G 0.20 [-0.45, 0.85]). Similar observations were made for the JSN (data not shown).

CONCLUSION: These post-hoc results from the FORWARD RCT suggest that study participants with greater baseline pain and radiographic involvement tend to display a somewhat weaker anabolic structural response by sprifermin treatment (smaller increase in cartilage thickness) vs. placebo than those with less baseline pain or with less severe radiographic osteoarthritis. However, in a subcohort with advanced symptomatic and radiographic disease (SAR), the improvement in symptoms was stronger in knees with more advanced radiographic OA. This observation may be compared to a "full" tire gaining little in performance when inflating more air, whereas a "flat" tire improving considerably even with a small injection of it. In summary, whereas structural benefits may be numerically greater in knees with less disease, the translation to symptomatic benefit appears to be stronger in knees with more severe disease.

SPONSOR: Merck KGaA, Darmstadt, Germany and Formation Bio, New York, NY; USA

DICLOSURE STATEMENT: FE, WW: Chondrometrics GmbH;

REFERENCES

[1] Hochberg MC et al. JAMA. 2019, 8;322:1360-1370;

[2] Guehring H, et al. Semin Arthritis Rheum. 2021;51:450-456.

CORRESPONDENCE ADDRESS: eckstein@chondrometrics.de

¹ Formation Bio, New York, NY, USA

² Chondrometrics GmbH, Freilassing, Germany

³ Paracelsus Medical University, Center for Anatomy and Cell Biology & LBIAR, Salzburg, Austria

⁴NBCD, Copenhagen, Denmark

FEASIBILITY OF NON-CONTRAST MRI TO DETECT CHANGES IN SYNOVITIS AFTER ACL RECONSTRUCTION SURGERY

F. Kogan¹, K. Stevens¹, A. Williams², C. Chu²

INTRODUCTION: Synovitis is a recognized risk factor for post-traumatic osteoarthritis post-ACL reconstruction (ACLR). The reference standard for imaging synovitis is contrast enhanced MRI, but this adds time and cost and may be contraindicated in some patients, which may limit evaluation of this important finding. Recently, several non-contrast MRI methods have shown strong agreement with CE-MRI for semiquantitative assessment of synovitis.

OBJECTIVE: To evaluate the feasibility of quantitative double-echo in steady-state (qDESS) as a non-contrast MR technique to detect changes in synovitis in patients pre- and post-ACLR.

METHODS: 14 males and 4 females (age:27 \pm 6 years, BMI:24 \pm 3 kg/m²) with ACL tears underwent ACLR surgery (mean time from injury to surgery 10 \pm 5 weeks) and were scanned on a 3T MR scanner at three timepoints: (1) baseline post ACL tear but before reconstruction, (2) 6-weeks and (3) 6-months after ACLR. At each time point, a 3D qDESS acquisition was performed with parameters: TR/TE1/TE2 = 20.5/6.4/34.6 ms; acquisition resolution = 0.4 × 0.4 × 1.5 mm³; 80 slices; Flip Angle = 20. qDESS synovitis hybrid images were created by a weighted subtraction of the 2nd echo signal from the 1st echo to null signal from joint fluid in order to provide contrast to the synovium. Synovitis was scored in the knee overall and in 4 regional locations by a blinded radiologist on a scale of 0-3 (0 = none to 3 = severe).

RESULTS: Figure 1 shows a representative case of qDESS synovitis-weighted hybrid images at the three timepoints and their corresponding scores. Figure 2a shows a table of the % of patients (out of 18) that were scored to have improved or worsened synovitis between baseline and 6-weeks post-ACLR and between 6-weeks and 6-months post-ACLR. Overall, there was a clear trend towards synovitis worsening 6-weeks after ACLR and then improving between 6-weeks and 6-months post-surgery. Furthermore, when the 6-week and 6-month timepoints for each patient were compared directly but blinded to order, an improvement in assessed synovitis was observed in a further 82% of overall impressions that were previously scored as no change in blinded and randomized assessments (Figure 2b). Repeated synovitis scoring assessments showed very strong agreement (Gwets AC2>0.80) in overall and sub-region assessments.

DISCUSSION: While ground-truth synovitis measures were not available, the qDESS hybrid method was able to detect both worsening synovitis that is expected after ACLR surgery and improvement in synovitis that is expected during the following 5 months of recovery. The lack of differentiation of synovitis changes between timepoints may partly be attributed to the coarseness of the 4-point semi-quantitative Likert-scale which is based on synovial hypertrophy and nodularity In overall and regional assessments when no change was detected in randomized and blinded datasets on the conventional 4-point scale, subsequent direct comparison of the 6-week and 6-month timepoints for each participant, the radiologist was able to detect improvement in synovitis in the majority of cases despite being blinded to timepoint. The noted exception was in the intercondular notch where the evaluation of synovitis was confounded by surgical alteration along Hoffa's fat pad, possibly leading to over-estimation of the degree of synovitis in this region. Lastly, reproducibility agreement metrics for overall impression and regional assessments showed strong agreement, further supporting the potential utility of this approach.

CONCLUSION: Non-Contrast MRI of synovitis using the qDESS approach was able to detect changes in synovitis post-ACLR and during recovery, particularly when directly comparing intrasubject timepoints.

This approach shows new diagnostic potential to identify patients at risk for PTOA due to chronic inflammation and could potentially be used to monitor treatment effects.

SPONSOR: GE Healthcare and NIH Grants R01AR083018

DICLOSURE STATEMENT: We received Research Support from GE Healthcare

CORRESPONDENCE ADDRESS: fkogan@stanford.edu

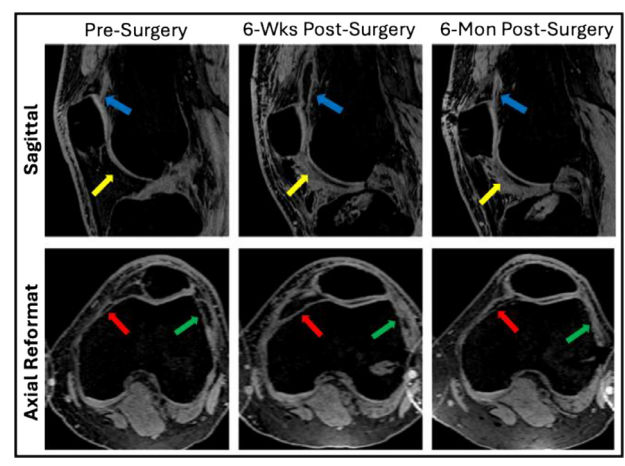


Figure 1: qDESS hybrid images in a ?? year-old, male ACLR patient at presurgery baseline, 6-weeks, and 6-months post-ACLR. Overall synovitis impression was judged to worsen between baseline and 6-weeks post-ACLR (from mild [1] to moderate [2]) and improve from 6-weeks to 6-months post-ACLR (from moderate [2] to mild [1]). Subregional scores followed a similar trend in the suprapatellar pouch (blue-arrow). The lateral patellar recess (green-arrow) was scored as moderate [2] at baseline/6-weeks and mild [1] at 6-months. The intercondylar notch (yellow-arrow) and medial patellar recess (red-arrow) were scored as mild[1] at baseline and moderate [2] at 6-weeks/6-months post-ACLR. However, direct comparison allowed more accurate assessment of synovitis improvement in the MPR at 6-months.

	6Wks Post A	CLR - Baseline	(Pre-Surgery)	6 Months Pe	ost ACLR - 6 Wk	s Post ACLR
	% Positive Change	No Change	%Negative Change	% Positive Change	No Change	%Negative Change
Overall	50%	50%	0%	11%	61%	28%
SPP	67%	33%	0%	11%	44%	44%
MPR	33%	61%	6%	0%	56%	44%
LPR	6%	94%	0%	0%	72%	28%
ICN	67%	22%	11%	39%	50%	11%

*******				*				
	Direct C	Comparisson	emparisson of No Change					
	Number	Improved Synovitis	No Change	Worsened Synovitis				
Overall	11	82%	0%	18%				
SPP	8	63%	13%	25%				
MPR	10	70%	20%	10%				
LPR	13	62%	15%	23%				
ICN	9	22%	78%	0%				

Figure 2: % of patients (out-of-18) showing positive (worse synovitis), negative (improved synovitis) and no change in synovitis scores between baseline and 6-weeks post-ACLR (green table) and between 6-weeks and 6-months post-ACLR (blue table). There was a clear trend towards synovitis worsening 6-weeks after ACLR and then improving between 6-weeks and 6-months post-surgery. Further, when the 6-week and 6-month timepoints for each patient that showed "no change" (purple box) in synovitis scores were compared directly but blinded to order, an improvement in assessed synovitis was observed in a further 82% of overall impressions, and >60% of SPP/MPR/LPR subregions (purple table).

¹ Stanford University Department of Radiology, Palo Alto, CA, USA

² Stanford University Department of Orthopedic Surgery, Palo Alto, CA, USA

REGIONAL VARIATION IN TRAPEZIOMETACARPAL BONE MICROARCHITECTURE IN FEMALES WITH OSTEOARTHRITIS USING HR-PQCT

M.T. Kuczynski $^{1,2},$ C. Hasselaar $^{1,3},$ G. Dhaliwal 3, C. Hiscox 3, N.J. White $^{1,3},$ S.L. Manske 1,4

INTRODUCTION: The trapeziometacarpal (TMC) joint, comprised of the trapezium (TRP) and first metacarpal (MC1) bones, is a mechanically complex, saddle-shaped joint. Studies have estimated that the peak forces acting on the TMC joint are up to five times higher than the corresponding external forces [1]. Moreover, cadaveric studies have shown non-uniform cartilage loss in TMC joint with OA [2]. While several cadaveric studies have investigated TMC joint cartilage and bone changes, evaluation of subchondral bone changes in the TMC joint *in vivo* is lacking.

OBJECTIVE: The objective of this study was to investigate differences in bone microarchitecture in anatomical quadrants of the TMC joint in women with TMC OA compared to age- and sex-matched controls. We hypothesized that women with TMC OA will exhibit quadrant-specific differences in bone microarchitecture compared to controls. Specifically, we hypothesized that the volar region of the TMC joint will demonstrate an increase in trabecular thickness, bone volume, and volumetric bone mineral density due to localized bone adaptations as a response to increased loading in the volar region.

METHODS: 14 females diagnosed with symptomatic TMC OA (mean age: 60 ± 6.5 years) and 12 similarly aged female controls (mean age: 59 ± 5.7 years) were scanned using HR-pQCT (XtremeCT2, Scanco Medical). A standard HR-pQCT scanning protocol was used ($61 \mu m^3$ voxels). Images were preprocessed using a Laplace-Hamming filter and segmented with a fixed threshold (15% of the maximum intensity). A bone coordinate system was automatically defined for the MC1 and TRP [3], and used to separate each bone into four anatomical quadrants: 1) radial-dorsal (RD), 2) radial-volar (RV), 3) ulnar-dorsal (UD), and 4) ulnar-volar (UV). For each whole bone and quadrant, we computed volumetric bone mineral density (vBMD, mg HA/cm³), bone volume fraction (BV/TV, %), and bone thickness (B.Th, mm). A mixed ANOVA was used to compare bone measures in each bone and quadrant between groups.

RESULTS: We did not observe a significant difference in total bone parameters between groups for the MC1 or TRP. However, we found a statistically significant interaction effect between the volar and dorsal quadrants of the TRP and group for B.Th (p=0.02, Figure 1, Table 1). Compared to controls, the mean B.Th in the TRP of the OA group was 1.9% lower in the RD quadrant, 7.5% lower in the UD quadrant, 4.8% greater in the RV quadrant, and 6.2% greater in the UV quadrant.

CONCLUSION: Our results suggest that whole bone TMC microarchitecture may not differ between OA and controls; however, we found significant differences in quadrant bone microarchitecture. This suggests that the MC1 and TRP undergo localized bone microarchitectural changes to adapt to the loading of the TMC joint. Further, our results suggest that bone thickness in the volar region of the trapezium may increase with

TMC OA. The TMC joint ligaments aid in distributing forces in the joint, which can be affected in TMC OA. Koff *et al.* found thinner cartilage in the volar region of the TMC joint in OA, which may be attributed to increased loads [2]. In this study, bones were not further subdivided into trabecular and cortical regions as the trapezium does not have a clear separation between these regions. Combined with the small sample size, this may explain the lack of significance in vBMD and BV/TV between groups. Subchondral sclerotic bone was 50% thicker in cadaveric trapezia with OA [4]. Thus, developing an algorithm to reliably separate these regions in the trapezium may provide further insights into regional effects of TMC OA on cortical and trabecular bone.

REFERENCES

- [1] W.P. Cooney & E.Y. Chao. J Bone Jt Surg. 1977.
- [2] M.F. Koff, et al. J Hand Surg. 2003.
- [3] E. Halilaj, et al. J Biomech. 2013.
- [4] P. Nufer, et al. J Ortho Res. 2007.

SPONSOR: Arthritis Society Canada (STAR-18-0189) CORRESPONDENCE ADDRESS: smanske@ucalgary.ca

Table 1: Mean bone parameters for the OA and control group, for each bone and each anatomical quadrant. Results are presented as mean value across group \pm standard deviation.

	Anatomical Quadrant	MC1			TRP		
		vBMD (mg HA/cm ³)	Mean B.Th (mm)	BV/TV	vBMD (mg HA/cm ³)	Mean B.Th (mm)	BV/TV
OA	RD	289.3 ±	0.57 ±	0.51 ±	316.4 ±	0.57 ±	0.55 ±
		81.2	0.11	0.09	65.1	0.10	0.08
	RV	$355.9 \pm$	$0.62 \pm$	$0.60 \pm$	$311.1 \pm$	$0.57 \pm$	$0.54 \pm$
		74.7	0.12	0.07	52.5	0.08	0.06
	UD	$247.7 \pm$	$0.51 \pm$	$0.45 \pm$	$330.1 \pm$	0.59	$0.58 \pm$
		73.6	0.11	0.09	53.4	± 0.12	0.06
	UV	$299.2 \pm$	$0.54 \pm$	$0.54 \pm$	$340.5 \pm$	$0.52 \pm$	$0.61 \pm$
		63.0	0.10	0.09	48.2	0.06	0.07
Control	RD	$264.9 \pm$	$0.53 \pm$	$0.46 \pm$	$324.4 \pm$	$0.59 \pm$	$0.56 \pm$
		102.8	0.15	0.13	82.8	0.14	0.10
	RV	$341.4 \pm$	$0.57 \pm$	$0.58 \pm$	$315.4 \pm$	$0.54 \pm$	$0.56 \pm$
		76.5	0.11	0.12	62.7	0.12	0.08
	UD	$227.6 \pm$	$0.47 \pm$	$0.41 \pm$	$357.1 \pm$	$0.64 \pm$	$0.61 \pm$
		99.7	0.15	0.11	62.7	0.12	0.08
	UV	$284.0 \pm$	$0.51 \pm$	$0.51 \pm$	$339.7 \pm$	$0.49 \pm$	$0.62 \pm$
		76.4	0.12	0.10	50.8	0.09	0.06

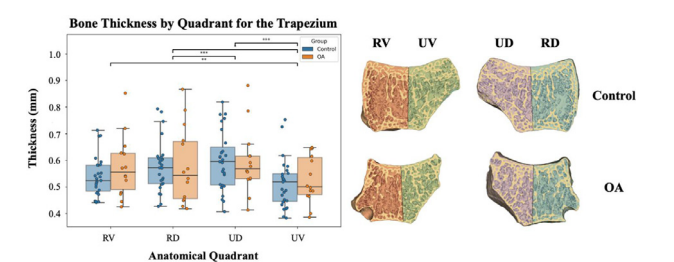


Figure 1: Bone thickness for each anatomical quadrant of the trapezium between OA and control groups. RV: radial-volar, RD: radial-dorsal, UD: ulnar-dorsal, UV: ulnar-volar. Significance: * represents p<0.05, ** represents p<0.01, and *** represents p<0.001.

 $^{^{1}\,\}mathrm{McCaig}$ Institute for Bone and Joint Health, University of Calgary, Canada

² Department of Cell Biology and Anatomy, University of Calgary, Canada

³ Department of Surgery, Cumming School of Medicine, University of Calgary, Canada

⁴Department of Radiology, Cumming School of Medicine, University of Calgary, Canada

IN VIVO MICRO COMPUTED TOMOGRAPHY IMAGING ALLOWS LONGITUDINAL ASSESSMENT OF MULTI-SCALE CHANGES TO WHOLE JOINT WITH PROGRESSION OF OA

H. Liu, J.L. Gregory, M.O. Silva, C.E. Davey, K.S. Stok

Department of Biomedical Engineering, The University of Melbourne, Parkville, VIC, Australia

INTRODUCTION: Longitudinal assessment of knee joint structure holds promise for providing invaluable spatial-temporal information on the progression of degenerative musculoskeletal (MSK) diseases involving the knee joint.

OBJECTIVE: This proof-of-concept study aims to establish a time-lapse *in vivo* imaging protocol with high temporal resolution to longitudinally track multi-scale structural changes, including mechanical alteration to whole joint structure, sensitive microstructural changes to subchondral bone, and abnormal bone remodeling activity, in a mouse collagenase-induced osteoarthritis (OA) model.

METHODS: Eight male C57BL/10 mice aged nine weeks were recruited and assigned to two longitudinal groups, control (CT) and OA. Of these, four ten-week-old mice assigned to the OA group received intraarticular injection of collagenase on the right knee to destabilize the right tibiofemoral joint. Longitudinal in vivo micro-computed tomography (microCT) scans were performed one day before collagenase injection and then weekly for eight weeks in total, resulting in nine scans for each animal. In vivo microCT (Scanco Medical) was performed with a source voltage of 70 kVp, an integration time of 350 ms, a current of 114 μ A, and an isotropic nominal resolution of 10.4 μ m with 1000 projections, with each scanning taking around 30 minutes. Quantitative morphometric analysis (QMA) was performed to measure longitudinal changes to structure of whole joint and subchondral bone, including joint space width (mm), and trabecular thickness (mm). Visualization of dynamic bone remodeling was performed by registering serial microCT scans. Bone resorption rate, BRR (%/day), and bone formation rate, BFR (%/day) were measured to quantify bone remodeling activity. To test the differences between CT and OA group at each time point from week 1 to week 8, a one-way analysis of covariance was used.

RESULTS: Three weeks post OA-induction, a significantly smaller joint space width was observed in medial osteoarthritic joint (202 μ m), when compared to CT joint (228 μ m) (p < 0.01). Regarding trabecular thickness, significant differences were observed at multiple time points between CT and OA groups, specifically in the first three weeks at the early stage of OA progression at lateral side (p < 0.01). Representative 3D visualization of bone formation and bone resorption is shown in **Figure 1 A-B**. Abnormal bone remodeling activities were observed in osteoarthritic femur. When compared to control femur, significantly larger bone resorption rate was observed in the first week post collagenase injection in both the lateral (p < 0.01) and medial femur (p < 0.01), as shown in **Figure 1 C-D**.

CONCLUSION: This proof-of-concept study, for the first time, demonstrated the application of longitudinal *in vivo* microCT imaging protocol for tracking whole joint mechanical malalignment, monitoring subchondral bone microstructure changes, visualizing and quantifying abnormal bone remodeling activity in a collagenase-induced OA mice model. Combined with future gait analysis and mechanical loading tests, we hope to use this approach to provide deeper insights into the mechanism and pathogenesis of MSK disorders, thus facilitating early diagnosis, intervention, and treatment development and assessment.

SPONSOR: Discovery Project scheme of the Australian Research Council (DP180101838), and Han Liu is a recipient of a China Scholarship Council stipend.

DICLOSURE STATEMENT: The authors declare no conflict of interest, financial or otherwise.

CORRESPONDENCE ADDRESS: kstok@unimelb.edu.au

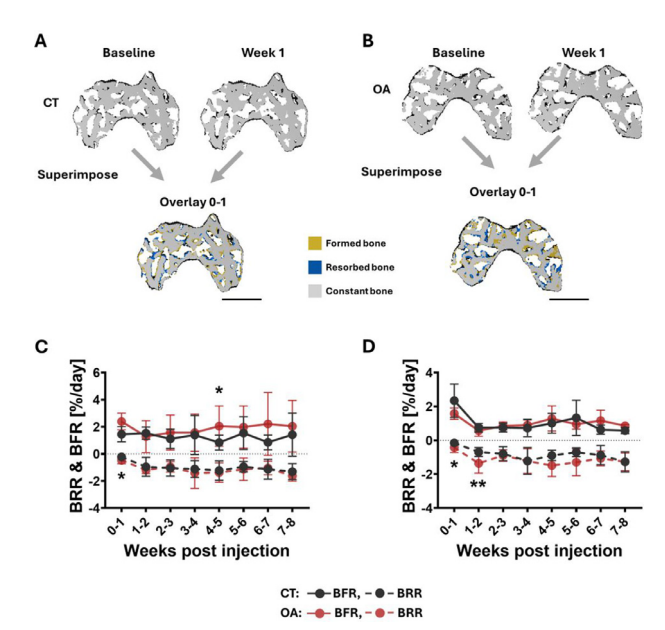


Figure 1. Representative 3D visualization of segmented trabeculae in femur after collagenase injection from (A) CT and (B) OA groups. Within each treatment group, the top row shows the registered segmented trabecular bone at two consecutive time points, i.e., baseline (week 0), and week 1 after collagenase injection. The image at the bottom - within each treatment group - shows the formed and resorbed bone between baseline (week 0) and week 1. Yellow: formed bone; blue: resorbed bone; grey: constant bone. Bar = 1.0 mm. Bone resorption rate (BRR), and bone formation rate (BFR) from CT and OA group at (C) lateral side, and (D) medial side. *, p < 0.05; **, p < 0.01.

REVEALING EARLY SUBCHONDRAL BONE STRUCTURAL CHANGES IN OSTEOARTHRITIS PROGRESSION IN A COLLAGENASE-INDUCED MOUSE MODEL USING MICRO COMPUTED TOMOGRAPHY

H. Liu, Z. Li, C.E. Davey, K.S. Stok

Department of Biomedical Engineering, The University of Melbourne, Parkville, VIC, Australia

INTRODUCTION: The deployment of micro-computed tomography (microCT) enables quantitative morphometric analysis (QMA) to quantify morphological and structural changes caused by OA in mouse knee joint with excellent spatial resolution. Previous studies quantifying microstructural changes to subchondral tibiae in fortnightly intervals, report bone loss and trabecular thinning as early as two weeks post disease induction in mouse models. However, evidence suggests that the subchondral bone turnover may occur earlier than two weeks post disease induction in a mouse OA model.

OBJECTIVE: To reveal early bone microstructural changes associated with OA progression in a mouse model with a high temporal resolution using microCT and QMA.

METHODS: Seventy-five male C57BL/10 mice aged nine weeks were recruited and randomly assigned to three cross-sectional cohorts, i.e., baseline (n=4), control (n=24) and OA (n=47) cohorts. Forty-seven ten-week-old mice assigned to OA cohort received intra-articular injection of 10 unit of filtered collagenase dissolved in 6 μ l physiological saline to the right joints (OA group) through the patellar ligament. A similar volume of saline was intraarticularly injected to the left contralateral joints (CTLR group). Prior to scanning, mice were euthanized at 0-, 1-, 2-, 3-, 4-, 5-, 6-, 7-, and 8-weeks post ten-week-old. Scans were performed using microCT (vivaCT80, SCANCO Medical AG, Brüttisellen, Switzerland) with a source voltage of 70 kVp, an integration time of 350 ms, a current of 114 µA, a nominal resolution of 10.4 µm, and 500 projections with each scan taking around 20 minutes. QMA was performed to quantify changes to subchondral bone microstructure associated with OA progression. To detect differences between treatments at each time point, a linear mixed-effect model was used. Individual mice were considered as random effects, time points (1- to 8- weeks post collagenase injection) and treatment (CT, CTLR, and OA) were considered as fixed effects.

RESULTS: Representative segmented microCT images from CT and OA group can be found in **Figure 1 A**. Typical osteoarthritic characteristics were observed in OA group at multiple time points, with changes detectable as early as one week post disease induction, shown in **Figure 1 B**. Specifically, comparing joints from CT and CTLR groups, smaller trabecular thickness, Tb.Th, were observed at both lateral and medial sides in OA femora, in accordance with the increasing trabecular spacing, Tb.Sp, and decreasing trabecular number, Tb.N.

CONCLUSION: This study, for the first time, demonstrated that prominent bone changes could be detected as early as one week after disease induction. These findings underscore the necessity of early quantification to capture rapidly changing bone microstructure alterations in early

stage OA, potentially enabling earlier diagnosis, intervention, and treatment

SPONSOR: Discovery Project scheme of the Australian Research Council (DP180101838), Early Career Researcher Grant from the University of Melbourne, and Han Liu is a recipient of a China Scholarship Council stipend.

DICLOSURE STATEMENT: The authors declare no conflict of interest, financial or otherwise.

CORRESPONDENCE ADDRESS: kstok@unimelb.edu.au

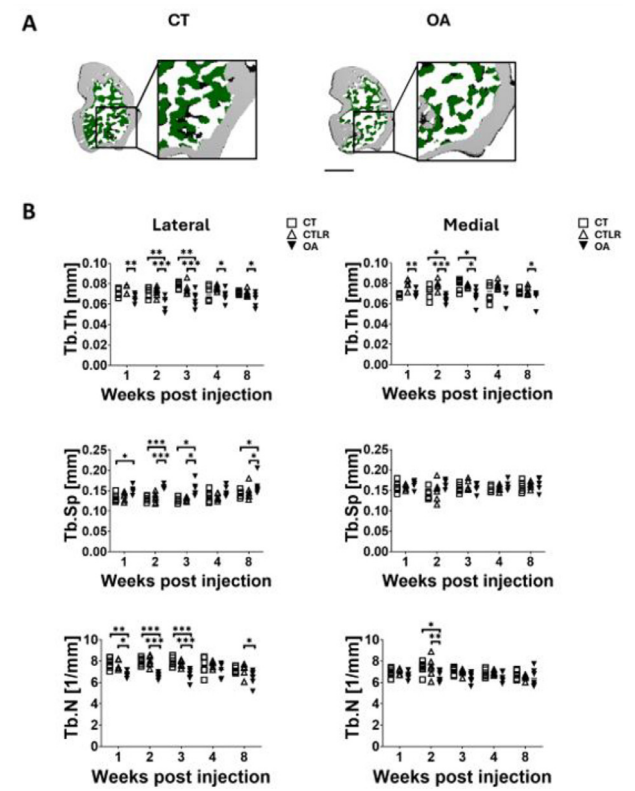


Figure 1. (A) Exemplar axial cross-sectional visualization of microCT images of tibia from CT and OA groups at week 1. When compared to CT group, an obvious loss in bone volume and bone volume fraction can be observed in OA group. Inset: segmented lateral trabeculae and cortical bone enlarged. Green: segmented epiphyseal trabecular bone; grey: cortical bone. Bar = 1.0 mm. (B) Subchondral epiphyseal trabecular bone morphometric analysis results of tibia from CT, CTLR, and OA cohorts, at one-, two-, three-, four-, and eight-week post injection. Thinner trabeculae, larger trabecular spacing, and lower trabecular number were observed mainly in lateral OA tibiae, when compared to CT and CTLR groups. * p < 0.05; ** p < 0.01; *** p < 0.001.

STATIN USE AND LONGITUDINAL CHANGES IN KNEE MRI–DERIVED THREE-DIMENSIONAL BONE SHAPE: DATA FROM THE OSTEOARTHRITIS INITIATIVE

M. Mahalleh 1 , K. Moradi 1 , A. Guermazi 2 , A. Brett 3 , F.W. Roemer 2,4 , S. Demehri 1

INTRODUCTION: Alterations in three-dimensional (3D) bone shape is strongly associated with progression of knee OA. Statins, widely used for lipid-lowering, have shown mixed effects on OA outcomes.

OBJECTIVES: To assess the impact of statin use on longitudinal changes in 3D bone shape in the Osteoarthritis Initiative (OAI) participants with Heberden's nodes (HN⁺), a hallmark of generalized OA, at baseline clinical examination.

METHODS: We conducted a longitudinal propensity score–matched (PSM) analysis of participants from the OAI. Participants without Heberden's node (HN⁻) or with traumatic knee injury, or missing data were excluded. PSM (1:1) was used to balance statin users and non-users on relevant demographic and clinical covariates. After matching, 412 knees were included (206 statin users and 206 non-users). 3D bone shape was quantified using the B-score, derived from knee MRI at baseline and Year 4, with higher scores indicating more OA-like shape. Longitudinal changes were evaluated using a linear mixed-effects model. The Reliable Change Index (RCI) was used to identify individuals with meaningful B-score changes.

RESULTS: Both groups showed significant within-group increases in B-scores from baseline to Year 4 (p < 0.001), indicating progression of OA-like shape over time. However, no significant between-group differences were observed at baseline (median [IQR]: 0.14 [–0.45, 0.90] vs. 0.15 [–0.60, 0.97]; p = 0.719) or Year 4 (0.37 [–0.44, 1.13] vs. 0.29 [–0.44, 1.11]; p = 0.666). Median 4-year B-score changes were also similar (0.12 [–0.02, 0.28] vs. 0.14 [0.02, 0.29]; p = 0.324). The proportion of individuals with meaningful B-score change did not differ significantly between groups (OR: 0.544; 95% CI: 0.179 to 1.653; p = 0.283). The difference in annual B-score change rate between groups was minimal and non-significant (0.003; 95% CI: –0.014 to 0.020; p = 0.747). No significant interactions were found with age, sex, BMI, or KL grade (all interaction p > 0.05).

CONCLUSION: Our study found no significant association between statin use and changes in 3D bone shape over four years in HN⁺ OAI participants. While statins may have protective effects against certain aspects of OA pathology, their lack of impact on bone shape progression highlights the complexity of OA pathophysiology.

SPONSOR: Supported by the NIH/National Institute on Aging (P01AG066603) and NIH/NIAMS (R01AR079620-01).

DISCLOSURE STATEMENT: AG is a BICL shareholder and consultant to Pfizer, TissueGene, Novartis, Coval, ICM, TrialSpark, and Medipost.

FWR is a shareholder of BICL and LLC and a consultant to Grünenthal GmbH. SD received consultation funding from Toshiba Medical Systems and grants from GERRAF and Carestream Health. The views expressed are those of the authors, not of the NHS, NIHR, or Department of Health. No other authors report conflicts of interest.

ACKNOWLEDGMENT: The Osteoarthritis Initiative (OAI) is a public-private partnership supported by NIH (contracts N01-AR-2-2258 through N01-AR-2-2262) and private partners including Merck, Novartis, GSK, and Pfizer. This study used publicly available OAI data. The findings do not necessarily reflect the views of the OAI investigators, NIH, or private sponsors.

CORRESPONDENCE ADDRESS: sdemehr1@jhmi.edu

Table 1. Baseline Characteristics of the Study Population After Propensity Score Matching

Characteristic	Statin Users (n=206)	Non-users (n=206)	SMD
Baseline B-score	0.15 [-0.60, 0.97]	0.14 [-0.45, 0.90]	0.047
Age	66.49 (6.87)	66.32 (7.66)	0.023
BMI	27.80 (4.05)	27.88 (4.39)	0.021
Female sex	149 (72.3)	152 (73.8)	0.033
White race a	190 (92.2)	192 (93.2)	0.037
Diabetes (Yes)	17 (8.3)	13 (6.3)	0.075
Abdominal obesity b (Yes)	192 (93.2)	193 (93.7)	0.020
Alcohol use (Yes)	89 (43.2)	90 (43.7)	0.010
Smoking (Yes)	33 (16.0)	33 (16.0)	0.000
KL grade 0	104 (50.5)	104 (50.5)	0.000
KL grade 1	60 (29.1)	62 (30.1)	0.021
KL grade 2	33 (16.0)	32 (15.5)	0.013
KL grade 3	9 (4.4)	8 (3.9)	0.024

Data are presented as mean (SD) for continuous variables and number (%) for categorical variables. SMD: standardized mean difference; KL grade: Kellgren-Lawrence grade; BMI: body mass index. A significant difference for SMD was defined as >0.1.

^bAbdominal obesity was defined as a waist circumference of ≥94 cm in men and ≥80 cm in women on physical examination according to International Diabetes Foundation criteria.

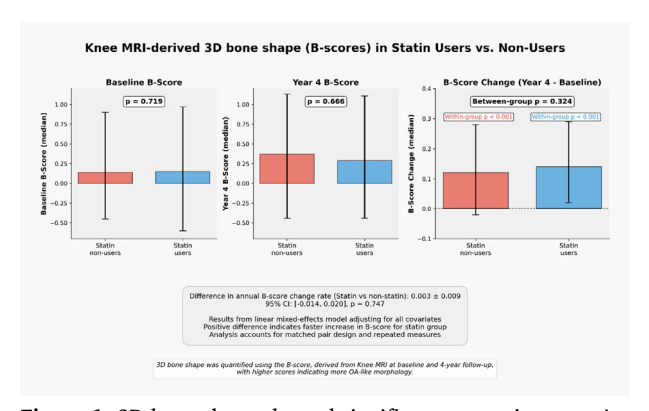


Figure 1. 3D bone shape showed significant worsening over 4 years in both statin users and non-users (p<0.001 within groups), but with no significant differences between groups at baseline, year 4, or in change rates (p>0.05 for all comparisons).

¹ The Russell H. Morgan Department of Radiology and Radiological Science, Johns Hopkins University School of Medicine, 601 N Caroline St, JHOC 3142, Baltimore, MD, USA

²Department of Radiology, Boston University Chobanian & Avedisian School of Medicine, Boston, MA, USA

³ Imorphics Ltd, Worthington House, Towers Business Park, Wilmslow Road, Manchester. UK

⁴Department of Radiology, Universitätsklinikum Erlangen & Friedrich-Alexander-Universität Erlangen-Nürnberg, Erlangen, Germany

^aRace of participants was categorized as White and non-White, considering the small number of participants in each non-White race group

CHARACTERIZING MENISCAL CALCIFICATIONS WITH PHOTON COUNTING-BASED DUAL-ENERGY COMPUTED TOMOGRAPHY

E. Nevanranta ¹, V.-P. Karjalainen ¹, M. Brix ^{1,2}, I. Hellberg ¹, A. Turkiewicz ³, B. Shakya ¹, P. Önnerfjord ³, S. Ylisiurua ^{1,2}, A. Sjögren ³, K. Elkhouly ¹, V. Hughes ³, J. Tjörnstrand ⁴, S. Saarakkala ^{1,2}, M. Englund ³, M.A.J. Finnilä ¹

INTRODUCTION: Meniscal calcifications, including basic calcium phosphate (BCP) and calcium pyrophosphate (CPP), are commonly associated with OA and may disrupt meniscal function, contributing to joint degeneration. However, the role of specific calcification types in OA is not fully understood due to the lack of non-invasive imaging techniques that can differentiate them *in vivo*. While Raman spectroscopy accurately distinguishes BCP from CPP, it is limited to 2D and requires destructive histological processing. In contrast, dual-energy computed tomography (DECT) has shown potential for differentiating calcifications in both *in vivo* and *ex vivo*, but its performance varies across previous studies. The integration of photon-counting detectors (PCD) in CT imaging improves spatial resolution and enables multi-energy acquisition, enhancing *in vivo* calcification characterization.

OBJECTIVE: We evaluated the capability of dual-energy computed tomography with a photon counting detector (PCD-DECT) to differentiate BCP and CPP calcification deposits in the posterior horns of human menisci *ex vivo*, using Raman spectroscopy as the reference.

METHODS: This study included 82 medial and lateral meniscus samples from 21 deceased donors without known knee OA and 20 TKR patients with medial compartment OA. Samples were imaged using an experimental cone-beam CT setup with PCD, operating at 120 kVp and 0.2 mA. Low energy (LE) data were collected in the 20-50 keV range, and high energy (HE) data in the 50-120 keV range, with a final voxel size of 37 μm . Only calcified samples identified using Raman spectroscopy (n = 36), 8 CPP and 28 BCP samples, were included to the analysis. Calcifications were segmented and divided between BCP and CPP groups. Subsequently, LE, HE, and Dual Energy Index (DEI) values were measured for each calcification. We used linear mixed models to estimate associations between LE and HE variables and the calcification type, and to compare the DEI values between the calcification types. Estimates are presented with 95% confidence intervals.

RESULTS: Figure 1A-C shows a 3D visualization of menisci with and without different calcifications. The results showed that CPP calcifications had consistently lower LE values than BCP for corresponding HE values. The difference increased with higher HE values, peaking at 500 HU with a difference of 166.1 HU (95% CI: 73.4, 258.8), while the smallest difference occurs at -100 HU, where the difference is 33.81 HU (95% CI: -40.38, 107.99) HU. The differences between LE and HE values are shown in Figure 1D-E. Additionally, estimated mean DEI values were higher in BCP calcifications compared to CPP, with an estimated difference of 0.035 (95%CI: 0.011, 0.059). Detailed results are shown in Table 1.

CONCLUSION: Our findings show that BCP and CPP meniscal calcifications differ in LE and HE as well as DEI values measured with PCD-DECT. The method reveals average differences between calcification

types, while precise identification of individual calcifications could be improved in the future with more advanced PCD detectors. To conclude, PCD-DECT successfully enabled *ex vivo* assessment of meniscal calcification types, highlighting its potential in future *in vivo* applications to better understand calcification mechanisms and evaluate responses to calcification-targeting therapies.

DICLOSURE STATEMENT: Simo Saarakkala, Associate Editor of Osteoarthritis and Cartilage Open

ACKNOWLEDGMENT: We want to thank Laboratory Technician Piia Mäkelä, MENIX clinical staff at Trelleborg Hospital, and the Department of Forensic Medicine in Lund for enabling sample collection.

CORRESPONDENCE ADDRESS: mikko.finnila@oulu.fi

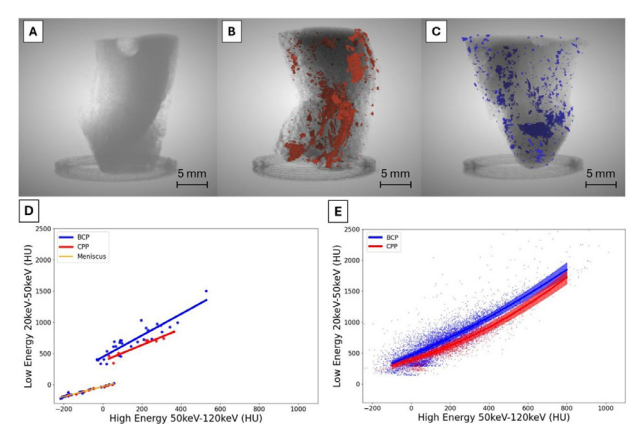


Figure 2. PCD-DECT imaging results illustrating calcification types and energy responses in meniscus samples. A) 3D reconstruction of an intact meniscus sample without any detectable calcifications. B) A meniscus sample containing calcium pyrophosphate (CPP) calcifications shown in red. C) A meniscus sample containing basic calcium phosphate (BCP) calcifications shown in blue. D) Mean LE versus HE values plotted for each sample, with fitted lines for BCP (blue) and CPP (red) groups. In addition, soft tissue HU values across all 36 samples are shown in yellow. E) All individual calcifications from all samples, showing the distribution of LE versus HE values with regression lines and 95% confidence intervals for both groups.

Table 1. The number of samples and individually identified calcifications are presented. Also, the mean dual-energy index (DEI) within all identified BCP and CPP calcifications, and the estimated differences between the BCP and CPP groups. Additionally, the soft tissue DEI for comparison is shown.

Group	No. of samples	No. of identified calcifications	Dual Energy Index (DEI) (95% CI)	Estimated difference between BCP and CPP (95% CI)
ВСР	28	7152	0.189 (0.177, 0.200)	0.035 (0.011, 0.059)
CPP	8	2746	0.154 (0.133, 0.175)	
Soft tissue	36		0.037 (0.023, 0.050)	

 $^{^1}$ Research Unit of Health Sciences and Technology, University of Oulu, Oulu, Finland 2 Department of Diagnostic Radiology, Oulu University Hospital, Oulu, Finland

³ Lund University, Faculty of Medicine, Department of Clinical Sciences Lund, Lund, Sweden

⁴Lund University, Skane University Hospital, Department of Clinical Sciences Lund, Sweden

AGREEMENT BETWEEN IN VIVO AND EX VIVO PHOTON-COUNTING CT MEASURES OF SUBCHONDRAL BONE FEATURES IN PATIENTS WITH KNEE OSTEOARTHRITIS

C.T. Nielsen 1,2,3,4 , M. Boesen 1,4 , M. Henriksen 2,4 , J.U. Nybing 1 , S.W. Bardenfleth 5 , C.K. Rasmussen 5 , M.W. Brejnebøl 1 , A.S. Poulsen 2,4 , S.M. Aljuboori 2,4,6 , K.I. Bunyoz 2,4,7 , S. Overgaard 4,6 , A. Troelsen 4,7 , H. Bliddal 2,4 , H. Gudbergsen 2,8 , F. Müller 3

INTRODUCTION: Bone changes are integral to the onset and progression of OA. Many aspects remain poorly understood due to the inability to assess bone architecture in vivo. Research has relied on ex vivo imaging, hindering evaluation of early-stage disease and longitudinal analysis. Conventional CT lacks the resolution to visualise subchondral bone microstructure. While ex vivo Photon Counting CT (PCCT) has demonstrated imaging comparable to μ CT, its ability to capture bone microstructure in vivo in knee OA patients under clinical conditions remains unproven.

OBJECTIVE: The aim of this study was to compare in vivo and ex vivo PCCT of subchondral bone features in patients with knee OA.

METHODS: Pre-surgery in vivo and post-surgery ex vivo PCCT (Siemens Naeotom Alpha, Siemens Healthineers, Germany) of the tibial plateau from participants with severe knee OA referred to arthroplasty surgery from January 2022 through September 2023 were compared. Acquisition/reconstruction details: a tube current of 120 kV, a matrix size of 1024×1024, a slice thickness of 0.2 mm, and a FOV of 150×150 mm. 18 in vivo/ex vivo PCCT pairs were included. The ex vivo scans was registered to the in vivo scans. Linear regression and Bland-Altman plots were used to assess correlation and agreement between in vivo and ex vivo measures of bone volume fraction (BV/TV), trabecular thickness (Tb.Th.), and attenuation in healthy and sclerotic trabecular bone. Delineated areas of bone sclerosis were compared using the Dice coefficient and Hausdorff distance, Fig. 1.

RESULTS: Comparing in vivo and ex vivo scans strong correlations were found for BV/TV, R^2 =0.82 and attenuation in both healthy, R^2 =0.89, and sclerotic, R^2 =0.79, bone, while a moderate correlation was found for Tb.Th., R^2 =0.55. Bias for BV/TV and Tb.Th. was -4.1% and -0.598mm, respectively, and -41.4 HU and -81.1 HU for healthy and sclerotic bone, respectively. A proportional bias was observed for BV/TV and Tb.Th., Fig. 2. There was excellent agreement between the segmentations of sclerotic areas, Dice coefficient = 0.91 and Hausdorff distance = 0.11mm.

CONCLUSION: In patients with severe knee OA, BV/TV and attenuation can be obtained with high correlation and small bias between in vivo and ex vivo scans. Tb.Th. showed moderate correlation and larger bias. Subchondral bone sclerosis, a key OA feature, is well translated from ex vivo to in vivo PCCT. Longitudinal studies using in vivo PCCT are feasible, but caution may be advised when measuring Tb.Th.

SPONSOR: none

DISCLOSURE STATEMENT: Prof. Overgaard is Editor in Chief, Acta Orthopaedica. Prof. Henriksen is affiliated with Contura International A/S, and Thuasne.

ACKNOWLEDGEMENT: The underlying trial was supported by an investigator-initiated trial grant from the Novo Nordisk Foundation (NNF20OC0064039). The Parker Institute is supported by a core grant from the Oak Foundation (OFIL-24-074). The study has received funding from the Danish Rheumatism Association and the Dept. of Radiology at Bispebjerg and Frederiksberg Hospital.

CORRESPONDENCE ADDRESS: camilla.toft.nielsen@regionh.dk

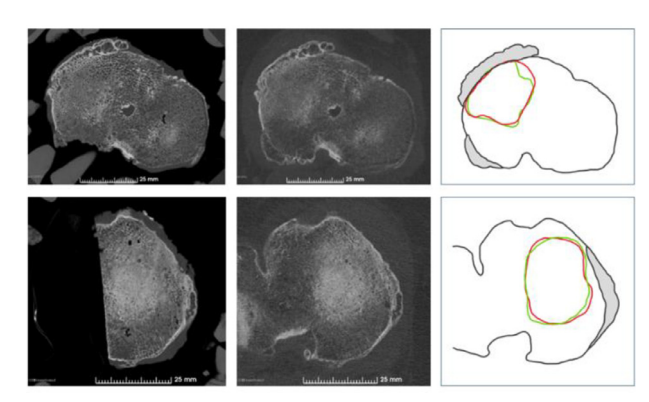


Fig. 1: Left column: PCCT *ex vivo* tibial plateau specimen in dry ice. Middle column: PCCT *in vivo* tibial plateau corresponding to *ex vivo* placement. Right column: Schematic drawing of the *ex vivo* (green) and *in vivo* (red) segmentations used to calculate Dice coefficient and Hausdorff distance.

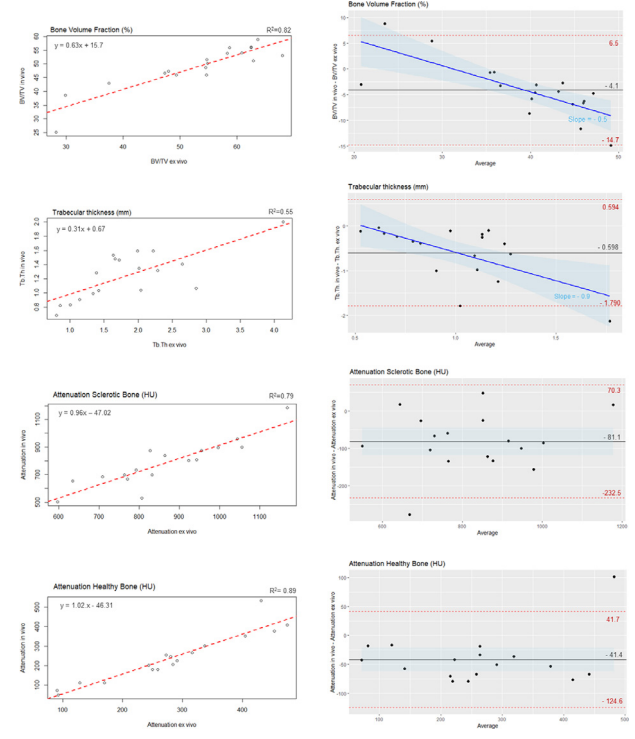


Fig. 2: Linear regression (left) and Bland-Altman (right) plots for BV/TV, Tb.Th., Sclerotic and Healthy bone. Bland-Altman plots with mean difference (black line), 95% limit of agreement (dashed red lines) and 95% confidence interval (shaded blue area) and regression fit (blue line).

¹Dept. of Radiology, Bispebjerg and Frederiksberg – Copenhagen University Hospital, Denmark

 $^{^{2}\,\}mathrm{The}$ Parker Institute, Bispebjerg and Frederiksberg – Copenhagen University Hospital, Denmark

³ Dept. of Radiology, Herlev and Gentofte – Copenhagen University Hospital, Denmark ⁴ University of Copenhagen, Department of Clinical Medicine, Faculty of Health and Medical Sciences

⁵ Visual Computing, DTU Compute, Technical University of Denmark, Kongens Lyngby, Denmark

⁶ Dept. of Orthopaedic Surgery, Bispebjerg and Frederiksberg – Copenhagen University Hospital, Denmark

 $^{^{7}}$ Dept. of Orthopaedic Surgery, Amager and Hvidovre — Copenhagen University Hospital, Denmark

⁸ Dept. of Public Health, Centre for General Practice, University of Copenhagen, Denmark

PROJECTED CARTILAGE AREA RATIO, EVALUATED USING THREE-DIMENSIONAL MRI ANALYSIS SOFTWARE, IS A USEFUL INDEX FOR ASSESSING CARTILAGE IN THE MEDIAL COMPARTMENT OF THE KNEE JOINT, COMPARABLE TO CARTILAGE THICKNESS MEASUREMENTS

N. Ozeki¹, J. Masumoto², I. Sekiya¹

INTRODUCTION: The projected cartilage area ratio, evaluated using three-dimensional MRI, is defined as the proportion of the region of interest (ROI) occupied by sufficiently thick cartilage and serves as a quantitative index for cartilage assessment (1). However, the relationships between the projected cartilage area ratio and factors such as cartilage thickness, lower limb alignment, patient characteristics, and the medial meniscus coverage ratio have not been fully clarified.

OBJECTIVE: The aim of this retrospective study was to investigate the correlations between the projected cartilage area ratio and cartilage thickness, lower limb alignment, patient characteristics, and the medial meniscus coverage ratio.

METHODS: A total of 53 patients who underwent medial meniscus repair or high tibial osteotomy for the treatment of medial knee OA were included. MRI was performed using a 3.0-T system (Achieva 3.0TX, Philips, Netherlands). Sagittal images of the knee joint were obtained using both fat-suppressed spoiled gradient echo and proton-weighted sequences. DICOM data were processed using SYNAPSE VINCENT 3D software (FUJIFILM Corp., Tokyo, Japan). Tibial cartilage was projected vertically onto a plane aligned with the bone's long axis, while femoral cartilage was projected radially around the intercondylar axis, defined as the line connecting the centers of the medial and lateral femoral condyles. These centers were identified by approximating each condyle to an ellipse on lateral views. The software automatically delineated the ROI using bone contours and divided the medial femoral condyle (MFC) into nine subregions based on anatomical morphology. The projected cartilage area ratio was calculated as the ratio of the projected cartilage area exceeding a defined thickness threshold to the total ROI area in each region and subregion. Average cartilage thickness and the medial meniscus coverage ratio were also automatically computed. The medial meniscus coverage ratio was defined as the ratio of the area covered by the meniscus within the medial tibial cartilage area to the total medial tibial cartilage area. Correlations between the projected cartilage area ratio or average cartilage thickness and patient demographics, lower limb alignment, Kellgren-Lawrence (KL) grade, and the medial meniscus coverage ratio were assessed using Spearman's rank correlation coefficient.

RESULTS: A strong positive correlation was observed between the projected cartilage area ratio and average cartilage thickness in both the MFC (r = 0.96, p < 0.001) and the medial tibial plateau (MTP) (r = 0.96, p < 0.001) (Figure 1). Body weight was not correlated with the projected cartilage area ratio or cartilage thickness; however, BMI showed significant negative correlations with the projected cartilage area ratio (MFC: r = -0.45, p < 0.001; MTP: r = -0.33, p = 0.02) and cartilage thickness (MFC: r = -0.41, p = 0.002; MTP: r = -0.35, p = 0.01) (Figure 2). Height correlated positively with the projected cartilage area ratio in the MTP (r = 0.34, p = 0.01) and with cartilage thickness in both the MFC (r = 0.29, p = 0.03) and MTP (r = 0.41, p = 0.003), but not with the projected cartilage area ratio in the MFC (Figure 1). KL grade showed significant negative correlations with both PCAR (MFC: r=-0.54, p < 0.001; MTP: r = -0.57, p < 0.001) and cartilage thickness (MFC: r = -0.53, p < 0.001; MTP: r = -0.52, p < 0.001). Regarding lower limb alignment, both the projected cartilage area ratio and cartilage thickness demonstrated moderate positive correlations with the weight-bearing line ratio and moderate negative correlations with the joint line convergence angle. Significant positive correlations were also observed between the projected cartilage area ratio and the medial meniscus coverage ratio in both the MFC (r = 0.50, p < 0.001) and MTP (r = 0.44, p < 0.001).

CONCLUSION: The projected cartilage area ratio appears to be less influenced by body physique compared with cartilage thickness and may serve as a reliable index for assessing cartilage status in the medial compartment of the knee joint.

SPONSOR: Ichiro Sekiya (Japan Agency for Medical Research and De-

velopment (AMED))

CORRESPONDENCE ADDRESS: ozeki.arm@tmd.ac.jp

ACKNOWLEDGMENT: None
DISCLOSURE STATEMENT: None

REFERENCE. (1) Hyodo A. JBJS OA 2019.

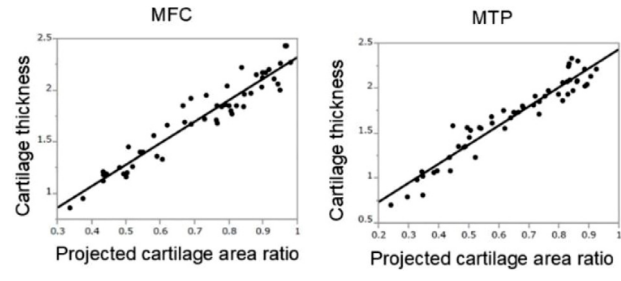


Figure 1. Correlation between PCAR and average cartilage thickness.

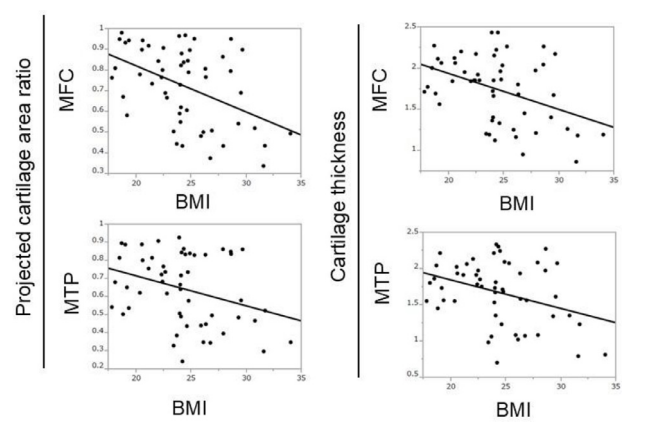


Figure 2. Correlation between BMI and PCAR or average cartilage thickness.

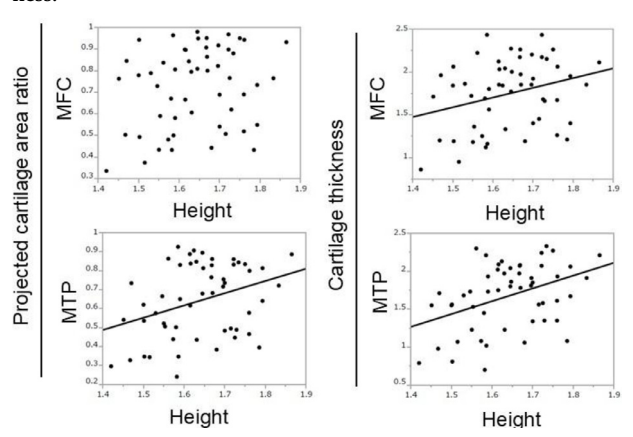


Figure 3. Correlation between height and PCAR or average cartilage thickness.

 $^{^1}$ Center for Stem Cell and Regenerative Medicine, Institute of Science Tokyo, Tokyo, Javan

² Fujifilm Corporation, Tokyo, Japan

EARLY DETECTION OF KNEE OA – THE ROLE OF A COMPOSITE DISEASE ACTIVITY SCORE: DATA FROM THE OSTEOARTHRITIS INITIATIVE

J.C. Patarini 1 , T.E. McAlindon 1 , J. Baek 1 , E. Kirillov 2 , N. Vo 2 , M.J. Richard 2 , M. Zhang 3 , M.S. Harkey 4 , G.H. Lo 5,6 , S.-H. Liu 1 , K. Lapane 1 , C.B. Eaton 7,8 , J. MacKay 9,10 , J.B. Driban 1

- ¹ University of Massachusetts Chan Medical School, Worcester, MA, USA
- ² Tufts Medical Center, Boston, MA, USA
- ³ Boston University, Boston, MA, USA
- ⁴ Michigan State University, East Lansing, MI, USA
- ⁵ Baylor College of Medicine, Houston, TX, USA
- ⁶ Michael E. DeBakey Medical Center, Houston, TX, USA
- ⁷ Kent Hospital, Pawtucket, RI, USA
- ⁸ Brown University School of Public Health, Providence, RI, USA
- ⁹ University of Cambridge, Cambridge, UK
- ¹⁰ Norwich Medical School, University of East Anglia, Norwich, UK

INTRODUCTION: BM lesions and effusion-synovitis are frequent and dynamic disease processes detected from early- to late-stage knee OA. These processes are associated with knee symptoms, representing the primary clinical manifestations of OA. Through a systematic and iterative process, we previously developed and validated a composite biomarker – the disease activity score – that combines BM lesions and effusion-synovitis volumes throughout a knee into an efficient continuous single score.

OBJECTIVE: To evaluate whether dynamic disease processes (effusion-synovitis volume and BM lesions), summarized by a validated efficient continuous composite score, are present in early OA and prognostic of incident symptomatic knee OA over the subsequent three years.

METHODS: We analyzed a convenience sample within the OAI of participants without symptomatic knee OA. Pain assessments and radiographs were collected annually. Among 913 knees (n=572 participants), most were female, white, and had a mean age of 61 (SD=9) and body mass index of 29.4 (SD=4.5) kg/m². MR images were collected at each OAI site using Siemens 3.0 Tesla Trio MR systems. We measured BM lesion and effusion-synovitis volumes on a sagittal IM fat-suppressed sequence (field of view=160mm, slice thickness=3mm, skip=0mm, flip angle=180 degrees, echo time=30ms, recovery time=3200ms, 313×448 matrix, x-resolution=0.357mm, y-resolution=0.357mm). Using MR images from the initial visit, we combined effusion-synovitis and BM lesion volumes to calculate a composite score, referred to as the dis-

ease activity score. A disease activity score of 0 approximated the average score for a reference sample (n=2,787, 50% had radiographic knee OA, average [SD] WOMAC pain score = 2.8 [3.3]); lower scores (negative scores) indicate milder disease, while greater values indicate worse disease. The outcome was incident symptomatic knee OA (the combined state of frequent knee pain and radiographic OA [KLG≥2]) within three years after the disease activity measurement. We used logistic regression with repeated measures to assess the association between disease activity (continuous measure) and incident symptomatic knee OA, adjusting for gender, age, and body mass index.

RESULTS: Disease activity ranged from -3.3 to 31.1 (lower values = less effusion-synovitis and BM lesions). Knees that developed incident symptomatic knee OA had greater disease activity (-0.3 [2.7] vs. -1.1 [2.8]): the adjusted relative risk=1.06 (per 1 unit of disease activity; 95% confidence interval: 1.02-1.10). Our stratified analyses revealed those with only radiographic OA (adjusted relative risk=1.37 [1.06-1.78]) or only symptoms (adjusted relative risk=1.15 [1.03-1.28]) at baseline drove the associations between disease activity and incident symptomatic knee OA.

CONCLUSION: Our findings underscore the critical role of the composite disease activity score in the early detection of knee OA. By integrating BM lesions and effusion-synovitis volumes, this score provides a powerful prognostic tool, enabling timely intervention to potentially alter the disease trajectory. These insights pave the way for targeted therapies that address inflammation and bone turnover, offering hope for improved patient outcomes.

SPONSOR: National Institute of Health, National Institute of Arthritis and Musculoskeletal and Skin Diseases Award No R01-AR076411 & K01-AR081389. VA's Health Services Research and Development Service Center for Innovations in Quality, Effectiveness, and Safety #CIN 13-413

DICLOSURE STATEMENT: Jeffrey B. Driban declares being on the Journal of Rheumatology Editorial Board. Timothy E. McAlindon declares he is a consultant for Sanofi, Kolon TissueGene, Medidata, Organogenesis, and is the owner of Ambulomics and Arthometrics. Jeffrey B. Driban and Timothy E. McAlindon hold a patent for Objective Assessment of Joint Damage, US-20220202356, 2020. Matthew S. Harkey declares being a member of OARSI Board.

 $CORRESPONDENCE\ ADDRESS:\ timothy.mcalindon@umassmed.edu$

Table 1. Worse Disease Activity is Associated with a Greater Chance of Incident Symptomatic or Radiographic OA

Overall Study Sample	Incident Symptoma	ntic OA	Unadjusted Relative Risk (RR)	Adjusted RR ^a
	Absent n= 630	Present n = 283	(95% CI)	(95% CI)
Disease Activity (mean (SD))	-1.10 (2.81)	-0.25 (2.67)	1.05 (1.01 - 1.09) ^b	1.06 (1.02 - 1.10) ^b
Disease Activity - Tertiles Low (-3.33 to -2.26)	244 (39%)	57 (20%)	REFERENCE	
Moderate (-2.25 to -0.88)	205 (33%)	100 (35%)	1.74 (1.30 - 2.31)	1.71 (1.29 - 2.28)
High (-0.88 to 31.14)	181 (29%)	126 (45%)	2.20 (1.66 - 2.90)	2.21 (1.67 - 2.91)
No Symptoms, No Radiographic OA	Incident Symptoma	ntic OA		
(n = 277)	Absent	Present	Unadjusted RR*	
	n= 259	n = 18	(95% CI)	
Disease Activity (continuous)	-1.58 (2.12)	-1.51 (1.98)	1.04 (0.88 - 1.22)	
Disease Activity – Tertiles Low (-3.33 to -2.26)	123 (47%)	8 (44%)	REFERENCE	
Moderate (-2.25 to -0.88)	80 (31%)	7 (39%)	1.14 (0.46 - 2.78)	
High (-0.88 to 31.14)	56 (22%)	3 (17%)	0.94 (0.30 - 2.98)	
Radiographic OA Only (No Symptoms)	Incident Symptoma	atic OA		
(n = 459)	Absent	Present	Unadjusted RR*	
	n= 211	n = 248	(95% CI)	
Disease Activity (continuous)	-0.48 (3.67)	-0.20 (2.61)	1.01 (0.98 - 1.04)	
Disease Activity - Tertiles Low (-3.33 to -2.26)	57 (27%)	45 (18%)	REFERENCE	
Moderate (-2.25 to -0.88)	72 (34%)	89 (36%)	1.30 (1.00 - 1.68)	
High (-0.88 to 31.14)	82 (39%)	114 (46%)	1.37 (1.06 - 1.78)	
Symptoms Only (No Radiographic OA)	Incident Symptoma	ntic OA		
(n = 175)	Absent	Present	Unadjusted RR*	
	n= 158	n = 17	(95% CI)	
Disease Activity (continuous)	-1.13 (2.29)	0.40 (3.78)	1.15 (1.03 - 1.28)	
Disease Activity – Tertiles Low (-3.33 to -2.26)	64 (41%)	4 (24%)	REFERENCE	
Moderate (-2.25 to -0.88)	51 (32%)	4 (24%)	1.30 (0.41 - 4.08)	
High (-0.88 to 31.14)	43 (27%)	9 (53%)	3.45 (1.16 - 10.27)	

Notes. (a). Relative risks adjusted for age, gender, and body mass index. (b). Relative risks for disease activity as a continuous measurement is per 1 unit. Bold = statistically significant associations. * Only unadjusted relative risks are reported because of the limited sample size within each strata.

HIGH-RESOLUTION 3D IMAGING OF BOVINE TAIL INTERVERTEBRAL DISC DEGENERATION USING IODINE-ENHANCED X-RAY MICROSCOPY

V. Peitso, S. Das Gupta, S. Kauppinen, M. Risteli, M. Finnilä, A. Mobasheri

Research Unit of Health Sciences and Technology, Faculty of Medicine, University of Oulu, Oulu, Finland

INTRODUCTION: The vertebral endplates of the intervertebral disc (IVD) consist of two structurally distinct layers: the cartilaginous endplate (CEP) and the bony endplate (BEP). While most research on IVD degeneration has focused on the biochemical or biomechanical failures of the annulus fibrosus (AF) and nucleus pulposus (NP), the physiology and microstructure of the CEP have often been overlooked. To address this gap, we employed iodine-enhanced X-ray microscopy (XRM) in a bovine tail IVD degeneration model. This approach enabled the simultaneous visualization of soft and hard tissues, with a specific focus on the CEP.

OBJECTIVE: 1) To simultaneously visualize soft and hard tissues in IVDs, with a specific focus on detecting changes in the CEP using iodine-enhanced XRM. 2) To validate the observed structural changes through histological analysis.

METHODS: 34 IVDs with intact vertebral endplates were harvested from six fresh bovine tails. Samples were cultured in Dulbecco's Modified Eagle Medium (DMEM) for 11 days under unloaded conditions. On day one, approximately 70-100 µL of chondroitinase ABC (chABC, 0.5 U/mL), a pro-inflammatory cytokine cocktail containing interleukin- 1β (IL-1 β) and tumor necrosis factor alpha (TNF- α) (each at 100 ng/mL), or a sham control solution of phosphate-buffered saline (PBS) with 0.1% bovine serum albumin (BSA) was injected into the NP using a 21G needle. Additional control samples received no injection. On day 11, IVDs were fixed in 4% formaldehyde and dehydrated. Samples were immersed in 1% (w/v) iodine (I2) in 100% ethanol and stained for a minimum of two weeks. Following staining, samples were washed, embedded in 1% agarose, and imaged with an XRM (Zeiss Xradia Versa 610; source voltage: 60kV; exposure: 4-6 sec; voxel size: 9.9-15.6 μm). Post-imaging, iodine was removed, and samples were decalcified and paraffin-embedded. Thin sections (7-10 µm) were prepared and stained with hematoxylin and eosin (H&E) and safranin-O and fast green. Reconstituted XRM image stacks were processed using built-in noise filtering software (Zeiss). Dragonfly 3D world (Comet) software was used for visualization and segmentation. XRM images were qualitatively compared with histological sections to assess changes in soft and hard tissues (Figures 1 and 2).

RESULTS: The interface between mineralized and non-mineralized cartilage (tidemark) was visualized using XRM, enabling the identification of calcified cartilage and CEP (Figure 1). Iodine-based contrast provided sufficient resolution to detect structural malalignments among the BEP, CEP, and NP (Figure 2). Notably, even sham injections with PBS induced degenerative changes in the disc.

CONCLUSION: Non-destructive iodine-enhanced XRM enables clear visualization of the CEP, providing sufficient contrast to simultaneously assess structural changes in both soft and hard tissues. This approach offers a powerful tool for evaluating IVD degeneration on *ex vivo* models.

SPONSOR: The Research was funded by the Research Council of Finland [351568 and Profi6 336449] and Orion Research Foundation sr. DICLOSURE STATEMENT: We have nothing to disclose. CORRESPONDENCE ADDRESS: valtteri.peitso@oulu.fi

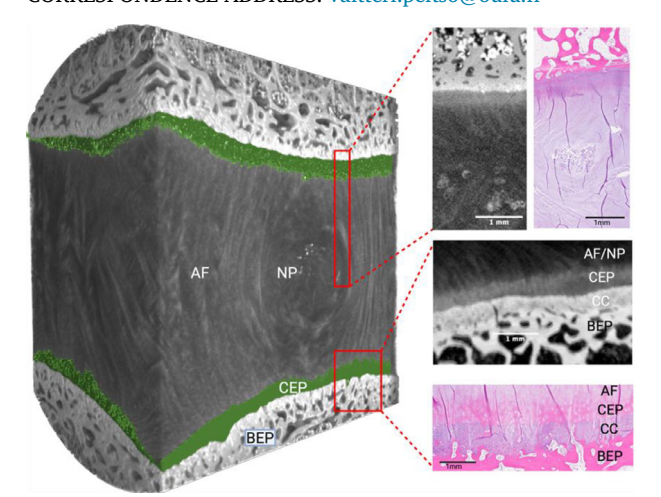


Figure 1. Representative 3D reconstructed X-ray microscopy (XRM) image of a bovine tail intervertebral disc (IVD), along with selected regions of interest comparing 2D XRM reconstructions and hematoxylin and eosin (H&E) stained histological sections. Red boxes highlight distinct anatomical features: the upper region shows cell clusters within the nucleus pulposus (NP), while the lower region illustrates the interface between mineralized and non-mineralized cartilage. Scale bar: 1 mm. Abbreviations: Annulus fibrosus (AF), bony endplate (BEP), calcified cartilage (CC), cartilaginous endplate (CEP), nucleus pulposus (NP).

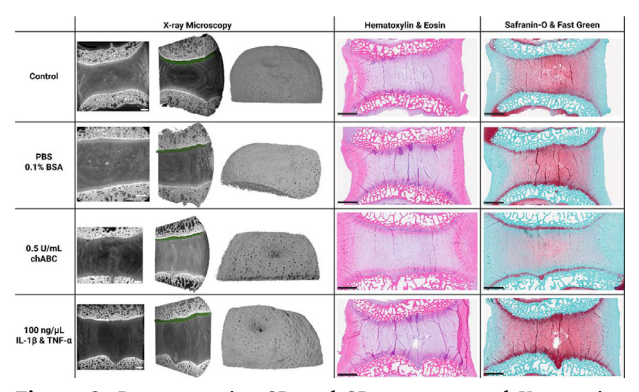


Figure 2. Representative 2D and 3D reconstructed X-ray microscopy (XRM) images (left), hematoxylin & eosin (H&E) stained sections (middle), and safranin-O & fast green stained sections (right), illustrating control and the effects of the three treatments on bovine tail intervertebral discs (IVDs) and bony endplates (BEPs; shown in the final 3D reconstructed XRM image). In the 3D XRM images, the cartilaginous endplate (CEP) is segmented with green on the upper side to highlight degeneration on the opposite side. Scale bars: 1 mm (XRM images), 2.5 mm (histological sections).

A NEW LENS ON SYNOVITIS: LABEL-FREE IMAGING OF WHOLE-MOUNT HUMAN PATHOLOGICAL SYNOVIAL MEMBRANE WITH MULTIPHOTON MICROSCOPY

M. Pradeep ¹, S. Das Gupta ¹, T. Zhang ¹, T. Liimatainen ¹, V.M. Pohjanen ^{2,3}, P. Lehenkari ^{2,3}, S. Palosaari ^{2,3}, M. Finnilä ¹

INTRODUCTION: One of the typical hallmarks of osteoarthritis progression is the inflammation of the synovial membrane, also known as synovitis. Pathological synovitis assessment is usually performed with traditional 2D histopathology, which provides limited orientation-dependent information, requires chemical labeling, and is destructive in nature. Tissue clearing of the whole synovial biopsy and non-destructive optical sectioning using multiphoton microscopy (MPM) can overcome the limitations of 2D histological approaches. MPM offers high spatial resolution and utilizes the second harmonic signal (SHG) to provide specific information about collagen fibers. This study aims to establish a tissue-clearing approach to analyze pathological human synovial tissue using label-free MPM.

OBJECTIVE: The objectives of the study are: 1) to optimize a clearingenabled label-free MPM protocol for synovial biopsies by comparing the clearing performance of a hydrophilic reagent (CUBIC protocol) and hydrophobic reagents Ethyl Cinnamate (ECi). 2) To quantitatively evaluate autofluorescence (AF) and SHG signals from synovium to understand synovial tissue morphology, cellularity, and fibrosis.

METHODS: For tissue-clearing protocol optimization, one synovial biopsy was cut into two sections. After formalin fixation, one section underwent CUBIC clearing protocol, and the other was dehydrated and immersed in ECi. For the MPM study, 12 synovial biopsies (6 OA, 6 rheumatoid arthritis [RA]) were formalin-fixed, dehydrated, and cleared with ECi solution. All samples were collected from total knee replacement surgeries at Oulu University Hospital, Finland. MPM was conducted using a 900 nm laser, capturing the SHG signal at 450 nm and the AF signal between 470-600 nm. A 16X/0.6 NA water-immersion objective was used for imaging, with a pixel size of 0.7 µm. At first, mosaics of the whole sample were acquired at depths of 600, 1000, and 1300 µm from the sample surface. Subsequently, Z-stack images (depth: 1mm; step size: 200 microns) of the AF channel that includes the lining layer were collected and used for 3D cell segmentation. Maximum intensity projections of the Z-stack were processed through intensity thresholding, binary masking, and watershed segmentation. Only particles with an area less than 500 µm² were considered individual cells. Moreover, adipocytes and vascularity within the sub-lining layer from the 2D mosaic images were manually identified. Further, the heat maps for SHG intensity and area fraction were calculated. Finally, the tissue clearing was reserved, and the standard histopathological assessment of synovitis (Krenn scoring system) was performed.

RESULTS: ECi clearing achieved complete transparency of a synovial biopsy in 3 days (cleared around 1.2 mm), while the CUBIC protocol was still partially opaque tissue even after 3 weeks (cleared around 500 μ m), as shown in Figure 1. In the optically sectioned mosaic images, OA samples had larger adipocytes but less vascularization within the sub-

lining layers than RA tissues (Figure 2). The number of segmented cells mostly followed Krenn scores, particularly in RA samples. SHG analysis revealed fibrotic regions in the tissue-cleared samples through intensity analysis and area fraction calculation, which were confirmed by histological images (Figure 2).

CONCLUSION: Here, we present a workflow that allows optical clearing and label-free assessment of whole synovial biopsy. MPM provides a detailed and quantifiable examination of tissue autofluorescence and collagen-specific SHG signal analysis. This can assess synovial inflammation and remodeling (fibrosis), making this protocol a complementary tool for standard synovial histopathology.

SPONSOR: Research Council of Finland (Flagship of Advanced Mathematics for Sensing, Imaging and Modelling Grant 359186 and 347445), and Jane and Aatos Erkko Foundation.

CORRESPONDENCE ADDRESS: Manu.Pradeep@oulu.fi

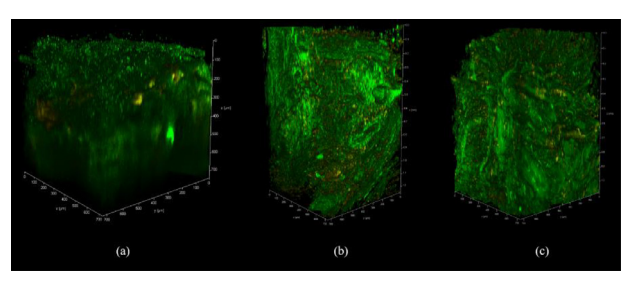


Figure 1: (a) CUBIC-cleared synovial tissue showing partially opaque clearing; (b, c) ECi-cleared synovial tissue that shows complete clearing from two sides (top and bottom of the sample, respectively).

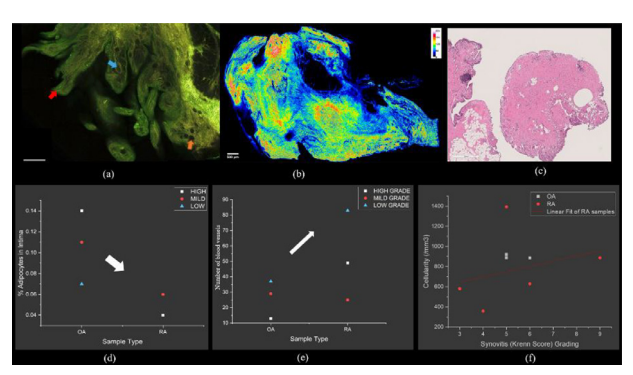


Figure 2: (a) Pathological synovial membrane in MPM (green= AF, yellow=SHG), the red arrow represents the proliferated intima, the blue arrow indicates a blood vessel, and the orange arrow indicates an adipocyte; (b) a heatmap showing the SHG signal intensity that represents the occurrence of fibrosis; (c) H&E stained section of the same sample; (d) the scatter plot shows that adipocytes are more abundant in OA synovial tissues than in RA; (e) the plot indicates that the number of blood vessels is higher in low-grade synovitic RA synovial tissues than OA; (f) the plot shows the number of segmented cells with Krenn score (all scale bars = $500 \mu m$).

¹ Research Unit of Health Sciences and Technology, University of Oulu, Finland

² Research Unit of Translational Medicine, University of Oulu, Oulu, Finland

³ Medical Research Center, Oulu University Hospital, Oulu, Finland

THE EFFECT OF RECONSTRUCTION KERNEL AND MONOCHROMATIC ENERGY PAIRS USED IN DUAL ENERGY CT IMAGING OF THE PROXIMAL HUMERUS

S. Quayyum¹, C.R. Dickerson¹, M.R. Maly¹, G.S. Athwal², N.K. Knowles¹

INTRODUCTION: Dual-energy computed tomography (DECT) allows for more accurate volumetric vBMD by accounting for marrow alterations with aging, disease and acute injuries. Tissue alterations, including vBMD, have been identified as potential biomarkers for early shoulder OA. Reconstruction kernel and energy pair images used in DECT alter vBMD and resulting estimated bone stiffness in image-based finite element models (FEMs). Prior to clinical investigation, the effect of imaging parameters must be understood.

OBJECTIVE: This study investigated how varying reconstruction kernel, and DECT monochromatic energy pair combinations influenced 1) vBMD, and 2) FEM estimated stiffness in the proximal humerus of cadaveric models.

METHODS: Cadaveric specimens (n = 7; 14 shoulders) were scanned bilaterally using DECT (GE Revolution HD GSI) with a $\rm K_2HPO_4$ calibration phantom. DECT images were reconstructed using bone sharpening (BONE) and standard (STD) kernels. Simulated monochromatic images were created at 40, 90, and 140 keV using the manufacturers GSI software and combined into energy pairs (40/90, 90/140, 40/140 keV). Images were processed with custom Python scripts and 3D Slicer software to segment and extract vBMD values in proximal humeral head and diaphysis locations. Image-based FEMs were used to compare estimated bone stiffness across models generated from each image. Results were compared using a two-way RM-ANOVA.

RESULTS: The highest vBMD values occurred in the humeral shaft diaphysis across all kernel and energy pair combinations (Table 1). There were significant differences in vBMD across energy pairs and kernels within the diaphysis region, with the greatest vBMD occurring with the 90/140 keV energy pair. No significant differences in mean vBMD values across energy pair combinations occurred for the anatomic neck. Increased vBMD input to FEMs resulted in similar trends, with the highest FEM stiffness in the diaphysis region, and those generated from 90/140 keV DECT images (Table 2). Significant differences remained in the diaphysis with no difference in the anatomic neck FEMs.

CONCLUSION: Higher vBMD values in the diaphysis reflect its cortical bone density, with significant differences by kernel and energy pair. Lower vBMD values in the anatomic neck, a trabecular-rich region, occur partially due to the heterogeneous composition, with minimal cor-

tical bone. The BONE kernel at higher energy pairs (e.g., 90/140 keV) improved contrast but resulted in the greatest vBMD, a trend that was not observed with the other two energy pairs. Trends in vBMD persisted in FEMs indicating choice of energy pair combination has a large effect on vBMD and FEM stiffness in regions of high cortical bone, with the 90/140 keV energy pair, but little effect on trabecular regions within the proximal humerus of the cadavers evaluated in this study. The results of this study indicate that when generating DECT images from simulated monochromatic energy images for vBMD and image-based FEM estimated stiffness, 40/90 and 40/140 keV energy pairs have minimal influence across trabecular and cortical regions of the proximal humerus, while those generated with 90/140 keV have larger values, which may be partially explained by increased noise. Future studies will explore the validation of FEM models and precision measurements of vBMD in cross-sectional and longitudinal cohorts.

SPONSOR: Arthritis Society Canada Ignite Innovation Grant (#22-0000000109)

DICLOSURE STATEMENT: none

ACKNOWLEDGMENT: The authors would like to thank Evelyn Francis for assistance with CT scanning and the families of the donors to the Body Bequeathal Program at the University of Waterloo CORRESPONDENCE ADDRESS: nknowles@uwaterloo.ca

Table 1: vBMD [mgK_2HPO_4/cc] in two proximal humerus locations using three monochromatic energy pairs [keV] with BONE/STD kernels as DECT image input. Significantly different values share a common letter (two-way RM-ANOVA).

Location	40/90	90/140	40/140
Diaphysis: BONE Diaphysis: STD Anatomic Neck: BONE Anatomic Neck: STD	$332 \pm 103^{a,b}$ $340 \pm 114^{d,f}$ 107 ± 38 105 ± 39	$407 \pm 130^{\text{ a,c,f,g,h}}$ $352 \pm 121^{\text{d,e,g}}$ 107 ± 38 105 ± 39	341 ± 106 ^{b,c} 341 ± 115 ^{e,h} 107 ± 38 105 ± 39

Table 2: Stiffness [kN/mm] in two proximal humerus locations using three monochromatic energy pairs [keV] with BONE/STD kernels as DECT image input. Significantly different values share a common letter (two-way RM-ANOVA).

Location	40/90	90/140	40/140
Diaphysis: BONE Diaphysis: STD Anatomic Neck: BONE Anatomic Neck: STD	$180 \pm 47^{a,b}$ $179 \pm 58^{d,g}$ 121 ± 33 108 ± 38	$223 \pm 64^{a,c,d,e,f}$ $185 \pm 63^{e,g}$ 121 ± 33 108 ± 38	$185 \pm 49^{b,c}$ 179 ± 57^{f} 120 ± 34 107 ± 38

¹Department of Kinesiology and Health Sciences, University of Waterloo, Waterloo, ON. Canada

 $^{^2\,\}mathrm{The}\,\mathrm{Roth}|\mathrm{McFarlane}\,\mathrm{Hand}$ and Upper Limb Centre, St. Joseph's Health Care, London, ON, Canada

PREDICTING KNEE OSTEOARTHRITIS PROGRESSION USING STRUCTURAL BIOMARKERS FROM MULTIPLE JOINTS: DATA FROM THE OSTEOARTHRITIS INITIATIVE

M. Raza ¹, T. Laffaye ², R. Stein ², H. Ragati-Haghi ², R. Amesbury ², A. Mathiessen ³, C.K. Kwoh ⁴, J.E. Collins ^{1,2,*}, J. Duryea ^{1,2,*}

INTRODUCTION: Clinical risk prediction models have been developed to predict knee OA progression with the goal of targeted treatment and clinical trial enrichment. It remains unclear whether, or how, OA in other joints affects knee OA progression.

OBJECTIVE: To evaluate whether imaging biomarkers from non-index joints add predictive value for knee OA progression beyond those from the index knee alone.

METHODS: We included 648 participants from the Osteoarthritis Initiative (OAI), randomly selected with baseline KL grade of 1, 2, or 3. OAI obtained bilateral knee and hip XR and index knee MRI. Baseline imaging biomarkers included quantitative measures of index and nonindex knee and hip fixed location joint space width and femorotibial angle (FTA) from XR and quantitative measures of cartilage thickness from index knee MRI. Clinical covariates were age, sex, BMI, injury history, surgery history, family history of knee replacement, and clinical hand OA (based on presence of Heberden's nodes at the baseline clinical examination). Outcomes were knee OA progression over 48 months defined as (1) decrease in medial minimum joint space width (JSW) of ≥ 0.7mm and (2) any increase in KL grade.

We used random forests to determine the combination of predictors that maximize AUC. Random forests can model complex non-linear associations, interactions among predictors, and work well in the setting of correlated data. We examined each set of biomarkers alone and in combination: clinical covariates, index knee XR, contralateral knee XR, index hip XR, contralateral hip XR, index knee MRI. Models were tuned with 5-fold cross-validation and AUCs were computed over 1000 bootstrap samples. We used permutation-based variable importance to rank the most important variables for prediction.

RESULTS: The 648 OAI participants were 23% KLG 1, 48% KLG 2, and 28% KLG 3. Average age was 61 (SD 9) and average BMI 29 (SD 5). 152 (23%) had a decrease in JSW \geq 0.7mm and 119 (18%) had an increase in KL grade.

In considering sets of covariates on their own, models with index knee MRI had the highest AUC for both outcomes (model 8), followed by models with index knee XR (model 3, Table). Adding contralateral hip XR to models with index knee XR improved AUC. For example, in predicting JSW \geq 0.7mm, the AUC increased from 0.627 (model 9) to 0.648 (model 10). Adding hip XR biomarkers did not seem to improve model discrimination (model 10 to model 11). AUCs from models from hip XR biomarkers alone were modest, though higher than for models with only clinical covariates.

Variable importance for the 10 most important biomarkers for the model with all XR biomarkers (model 12) is shown in the Figure for JSW ≥0.7mm (panel A) and KLG increase (panel B). Baseline medial minimum JSW was the most important predictor for both models. Various measures of fixed location JSW in the contralateral knee were among the top 10 most important predictors for both outcomes.

CONCLUSION: Multi-joint structural biomarkers improve predictive performance for knee OA progression, beyond index-knee imaging alone. These findings support broader imaging strategies to enhance RCT enrichment and guide targeted interventions in knee OA.

SPONSOR: NIH NIAMS K01AR075879, R01AR078187

DISCLOSURE STATEMENT: JEC: consulting fees from Boston Imaging Core Labs, LLC.

ACKNOWLEDGMENT: We would like to acknowledge OAI investigators and participants.

CORRESPONDENCE ADDRESS: jcollins13@bwh.harvard.edu

¹ Harvard Medical School, Boston, MA, USA

² Brigham and Women's Hospital, Boston, MA, USA

³ Diakonhjemmet Hospital, Oslo, Norway

⁴ University of Arizona Arthritis Center, Tucson, AZ, USA

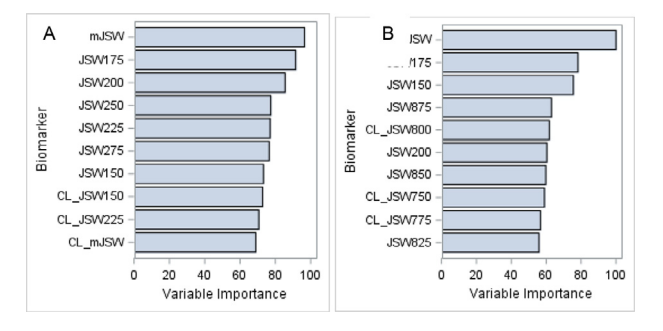
^{*}Shared senior authorship

Table 1. Discriminative performance of models predicting JSW ≥0.7mm.

Model	Clinical	i-KLG	i-k XR	c-k XR	c-KLG	i-h XR	c-h XR	i-k MRI	AUC (95% C	I)
									JSW ≥0.7mm	KLG Increase
1	X								0.500	0.541
									(0.433,	(0.469,
									0.565)	0.610)
2	X	X							0.576	0.572
									(0.511,	(0.503,
									0.638)	0.639)
3			X						0.611	0.669
									(0.545,	(0.595,
									0.676)	0.743)
4				X					0.569	0.594
									(0.498,	(0.524,
									0.638)	0.660)
5				X	X				0.568	0.594
									(0.497,	(0.524,
									0.638)	0.664)
6						X			0.525	0.533
									(0.455,	(0.457,
									0.591)	0.607)
7							X		0.515	0.493
									(0.443,	(0.421,
									0.585)	0.570)
8								X	0.636	0.689
									(0.568,	(0.609,
									0.701)	0.762)
9	X	X	X						0.627	0.685
									(0.561,	(0.608,
									0.691)	0.761)
10	X	X	X	X	X				0.648	0.707
									(0.581,	(0.630,
									0.715)	0.776)
11	X	X	X	X	X	X			0.641	0.709
									(0.573,	(0.631,
									0.708)	0.780)
12	X	X	X	X	X	X	X		0.639	0.705
									(0.571,	(0.632,
									0.706)	0.774)
13	X	X	X	X	X	X	X	X	0.656	0.729
									(0.588,	(0.656,
									0.721)	0.800)
14	X	X	X					X	0.658	0.718
									(0.591,	(0.649,
									0.721)	0.787)
15	X	X	X			X			0.620	0.685
-									(0.554,	(0.610,
									0.683)	0.755)

i-k=index knee; i-h=index hip; c-k=contralateral knee; c-h=contralaeral hip; XR-xray; KLG=Kellgren-Lawrence Grade; AUC=Area under the curve; CI=confidence interval

Figure 1. Variable importance for Model 12 (all XR biomarkers): top 10 important variables for JSW \geq 0.7mm (A) and KLG increase (B).



DO RATES OF FEMOROTIBIAL CARTILAGE LOSS IN KELLGREN-LAWRENCE 2 AND 3 KNEES DIFFER BETWEEN THOSE WITH MILD-MODERATE VS. SEVERE PATELLOFEMORAL STRUCTURAL DAMAGE?

F.W. Roemer ^{1,2}, M.P. Jansen ³, S. Maschek ⁴, S. Mastbergen ³, A. Wisser ^{4,5,6}, H.H. Weinans ³, F.J. Blanco ⁷, F. Berenbaum ^{8,9}, M. Kloppenburg ^{10,11}, I.K. Haugen ¹², D.J. Hunter ¹³, A. Guermazi ^{1,14}, W. Wirth ^{4,5,6}

- ¹ Department of Radiology, Boston University School of Medicine, Boston, MA, USA
- ² Department of Radiology, Universitätsklinikum Erlangen and Friedrich-Alexander-Universität Erlangen-Nürnberg (FAU), Erlangen, Germany
- ³ Department of Rheumatology & Clinical Immunology, University Medical Center Utrecht, Utrecht, The Netherlands
- ⁴ Chondrometrics GmbH, Freilassing, Germany
- ⁵ Research Program for Musculoskeletal Imaging, Center for Anatomy and Cell Biology, Paracelsus Medical University, Salzburg, Austria
- ⁶ Ludwig Boltzmann Inst. for Arthritis and Rehabilitation (LBIAR), Paracelsus Medical University, Salzburg, Austria
- ⁷ Grupo de Investigacion de Reumatologia, Servicio de Reumatologia, INIBIC- CICA, Universidade de A Coruña, A Coruña, Spain
- ⁸ Department of Rheumatology, AP-HP Saint- Antoine Hospital, Paris, France
- ⁹ Sorbonne University, INSERM, Paris, France
- 10 Department of Rheumatology, Leiden University Medical Center, Leiden, The Netherlands
- 11 Clinical Epidemiology, Leiden University Medical Center, Leiden, The Netherlands
- 12 Center for Treatment of Rheumatic and Musculoskeletal Diseases (REMEDY), Diakonhjemmet Hospital, Oslo, Norway
- ¹³ Department of Rheumatology, Royal North Shore Hospital and Sydney Musculoskeletal Health, Kolling Institute, University of Sydney, St. Leonards, NSW, Australia
- ¹⁴ Department of Radiology, VA Boston Healthcare System, West Roxbury, MA, USA

INTRODUCTION: Knees with radiographic disease severity of Kellgren-Lawrence (KL) 2 and 3 are commonly included in disease-modifying (DMOAD) clinical trials of knee osteoarthritis (OA). In an eligibility context, semi-quantitative (sq) MRI assessment has been used to define structural disease severity, rule out diagnoses of exclusion, and possibly define a structural phenotype. The KL system focuses on the femorotibial joint (FTJ) only, with MRI stratification being commonly limited to the FTJ. It is unclear whether sq MRI of the patellofemoral joint (PFJ) should be included for eligibility assessment.

OBJECTIVE: The aim was to assess whether rates of quantitative femorotibial (FT) cartilage loss are increased for knees with semiquantitatively (sq)-defined severe patellofemoral (PF) cartilage damage and/or large bone marrow lesions (BMLs) vs. those without over a period of 24 months.

METHODS: 626 knees with Kellgren-Lawrence 2 and 3 from the FNIH and IMI-APPROACH studies were included. MRI assessment was performed using the MRI Osteoarthritis Knee Score (MOAKS) instrument. Medial FT quantitative cartilage thickness loss was derived from baseline and 24-month manual segmentations and was compared between knees with severe vs. mild-moderate PF cartilage damage and between knees with vs. without large PF BMLs. Between-group comparisons were performed using analysis of variance (ANOVA) and were stratified by baseline medial FT cartilage damage severity (defined as mild, moderate, or severe).

RESULTS: 410 (65%) knees were categorized as mild, 92 (15%) as moderate, and 124 (20%) as severe medial FT cartilage damage. For almost all categories of FT cartilage damage, the difference in quantitative medial FT cartilage loss was not statistically significant (**Table 1**). Only for the category of knees with moderate medial FT cartilage damage, statistically higher rates of quantitative medial FT cartilage loss were observed for those with large PF BMLs compared to those without (-0.245 \pm 0.304 mm vs. -0.134 \pm 0.218 mm) (**Table 2**).

CONCLUSION: For the large majority of sq-defined FT cartilage damage categories, no statistically significant differences in FT rates of quantitative cartilage loss were detected. Screening for PF cartilage damage and BMLs does not appear to be required in a disease-modifying OA drug trial.

SPONSOR: Scientific and financial support for the FNIH OA Biomarkers Consortium are made possible through grants, direct and in-kind contributions provided by: AbbVie; Amgen Inc.; Arthritis Foundation; Bioiberica S.A.; DePuy Mitek, Inc.; Flexion Therapeutics, Inc.; GlaxoSmithKline; Merck Serono; Rottapharm | Madaus; Sanofi; Stryker; The Pivotal OAI MRI Analyses (POMA) Study, NIH HHSN2682010000. We thank the Osteoarthritis Research Society International (OARSI) for their leadership and expertise on the FNIH OA Biomarker Consortium project. The OAI is a public-private partnership comprised of five contracts (N01-AR-2-2258; N01-AR-2-2259; N01-AR-2-2260; N01-AR-2-2261; N01-AR-2-2262) funded by the National Institutes of Health. Funding partners include Merck Research Laboratories; Novartis Pharmaceuticals Corporation, GlaxoSmithKline; and Pfizer, Inc. Private sector funding for the Consortium and OAI is managed by the FNIH.

The IMI-APPROACH study consortium received support from the Innovative Medicines Initiative Joint Undertaking under Grant Agreement no 115770, resources of which are composed of financial contribution from the European Union's Seventh Framework Programme (FP7/2007–2013) and EFPIA companies' in kind contribution. See www.imi.europa.eu and www.approachproject.eu.

DISCLOSURE STATEMENT: FWR is shareholder and Chief Medical Officer of Boston Imaging Core Lab (BICL), LLC, a company providing image assessment services to academia and the pharmaceutical industry. He is consultant to Grünenthal, GmbH. He is Editor in Chief of Osteoarthritis Imaging. MPJ has not declared any conflict of interest. SM is an employee and co-owner of Chondrometrics GmbH. SCM has received research grants from the Dutch Rheumatology Society and ZonMW. AW is an employee of Chondrometrics GmbH. HHW has received grant support from EU-IMI (Approach project) to employer (UMC Utrecht) and additional grants from intereg grant Properos 2 (EU-Dutch government), Kansen voor West grant (EFRO), OA-inject NWO (Dutch government), 3DHip project (Eurostars), DartbacNWA (Dutch government, NWO) and Porospin (LSH, Dutch Governement). He holds patent with the following numbers: WO/2020/002301, WO2017209605A1, US20080262618 A1 and WO 2007053022 A3. He is minority shareholder of Replasia BV and Presurgeo BV. FJB reports payment to the institution from Gedeon Richter Plc., Bristol-Myers Squibb International corporation (BMSIC), Sun Pharma Global FZE, Celgene Corporation, Janssen Cilag International N.V, Janssen Research & Development, Viela Bio, Inc., Astrazeneca AB, UCB BIOSCIENCES GMBH, UCB BIOPHARMA SPRL, AbbVie Deutschland GmbH & Co.KG, Merck KGaA, Amgen, Inc., Novartis Farmacéutica, S.A., Boehringer Ingelheim España, S.A, CSL Behring, LLC, Glaxosmithkline Research & Development Limited, Pfizer Inc, Lilly S.A., Corbus Pharmaceuticals Inc., Biohope Scientific Solutions for Human Health S.L., Centrexion Therapeutics Corp., Sanofi, MEIJI FARMA S.A., Kiniksa Pharmaceuticals, Ltd, Fundación para la Investigación Biomédica Del Hospital Clínico San Carlos, outside the current manuscript. FB reports consultancy to Grünenthal, GSK, EliLIlly, Novartis, Pfizer and Servier. He has received payment or honoraria for lectures, presentations, speakers bureaus, manuscript writing or educational events from Viatris and Pfizer. He has received support for attending meetings and/or travel from Nordic Pharma. He is member of a Data Safety Monitoring Board or Advisory Board for AstraZeneca, Sun Pharma, Nordic Bioscience. He is shareholder of 4P Pharma and 4Moving Biotech. MK has received grant support from IMI-APPRAOCH (paid

to institution). In addition she holds grants from the Dutch Arthritis Society (among which LPP-24 2018-2023; 21-1-203). Payment or honoraria for lectures, presentations, speakers bureaus, manuscript writing or educational events from Galapagos and Jansen (to institution). She was Member of the OARSI board (2017-2022), Member EULAR council (member Advocacy Committee EULAR, since June 2023 chair elect, is President of the Dutch Society for Rheumatology. IKH reports consultancy to Novartis, GSK and Grünenthal. She has received payment or honoraria for lectures, presentations, speakers bureaus, manuscript writing or educational events from Abbvie. DJH is the editor of the osteoarthritis section for UpToDate and co-Editor in Chief of Osteoarthritis and Cartilage. He provides consulting advice on scientific advisory boards for TLCBio, Novartis, Tissuegene, Biobone, Sanofi, Enlivex. AG has provided consulting services to Pfizer, TissueGene, Coval, Medipost, TrialSpark, Novartis, ICM. He is shareholder of Boston Imaging Core Lab (BICL), LLC. He is president of the International Society of Osteoarthritis Imaging (unpaid). WW is an employee and co-owner of Chondrometrics GmbH.

CORRESPONDENCE ADDRESS: frank.roemer@uk-erlangen.de

Table 1. Change in medial and lateral cartilage thickness over 24 months stratified by PFJ cartilage damage severity.

PFJ C	PFJ Cartilage: Mild-moderate ¹			P	PFJ Cartilage: Severe ²			Severe vs. Mild-moderate			
Mean	SD	959	6 CI	Mean	SD	959	6 CI	Mean Diff	959	6 CI	P
-0.051	0.131	+0.068	+0.034	+0.062	0.179	-0.089	-0.036	-0.012	•0.042	0.019	0.451
-0.171	0.240	-0.240	-0.102	-0.187	0.284	-0.274	-0.099	-0.015	-0.124	0.093	0.779
-0.225	0.223	-0.277	-0.173	-0.202	0.209	-0.260	-0.143	0.023	-0.056	0.101	0.565
PFJ C	artilage:)	fild-mod	erate 1	P	FJ Cartila	ige: Sever	e 2	Seve	re vs. Mi	ld-moder	ate
Mean	SD	959	6 CI	Mean	SD	959	6 CI	Mean Diff	959	6 CI	P
-0.021	0.109	-0.034	-0.008	-0.023	0.122	-0.039	-0.007	-0.002	-0.023	0.018	0.819
-0.042	0.136	-0.085	0.001	-0.024	0.108	-0.065	0.018	0.019	-0.042	0.079	0.544
-0.128	0.193	-0.191	-0.064	-0.076	0.131	-0.125	-0.027	0.052	-0.030	0.134	0.209
	Mean -0.051 -0.171 -0.225 PFJ C Mean -0.021 -0.042	Mean SD -0.051 0.131 -0.171 0.240 -0.225 0.223 PEJ Cartilage: N Mean SD -0.021 0.109 -0.042 0.136	Mean SD 95% -0.051 0.131 -0.068 -0.171 0.240 -0.240 -0.225 0.223 -0.277 PFJ Cartilage: Mild-mod Mean SD 95% -0.021 0.109 -0.034 -0.042 0.136 -0.085 -0.08	Meas SD 98% CI	Mean SD 95% CI Mean	Mean SD 95% C Mean SD	Mean SD 95% CI Mean SD 95%	Mean SD 95% CI Mean SD 95% CI	Mean SD 95% CI Mean SD 95% CI Mean Diff	Mean SD 95% CI Mean SD 95% CI Mean DIF 95%	Mean SD 95% CI Mean Mean

 1 Maximum MOAKS cartilage grade in all 4 PFJ subregions: 0.0.1.0, 1.1, 2.0,2.1, 3.0, 3.1; 2 Maximum MOAKS cartilage grade of 2.2, 3.2 or 3.3 in at least 1 of 4 PFJ subregions; PFJ -patello-femoral joint, MFTJ - medial femoro-tibial joint, LFTJ- lateral femoro-tibial joint, SD- standard deviation, 95% CI - 95% confidence interval, Mean Diff - mean difference

Table 2. Change in medial and lateral cartilage thickness over 24 months stratified by PFJ BML damage severity

Medial FTJ Change [mm]	PFJ	PFJ BML: Mild		J BML: Mild-moderate 1 PFJ BML: Severe 2					Severe vs. Mild-moderate			
	Mean	SD	959	· CI	Mean	SD	959	6 CI	Mean Diff	959	6 CI	P
MFTJ group mild: 0.0 / 1.0 / 2.0 / 3.0	-0.048	0.136	-0.065	-0.031	-0.070	0.180	-0.099	-0.041	-0.022	-0.053	0.009	0.166
MFTJ group moderate: 1.1 / 2.1 / 3.1	-0.134	0.218	-0.193	-0.075	-0.245	0.304	-0.346	-0.144	-0.111	-0.219	-0.003	*0.044
MFTJ group severe: 2.2 / 3.2 / 3.3	-0.222	0.212	-0.267	-0.178	-0.196	0.230	-0.276	-0.116	0.026	-0.060	0.113	0.549
Lateral FTJ Change [mm]	PFJ	BML: M	ild-moder	ate 1		PFJ BMI	: Severe		Seve	re vs. Mi	ld-moder	ate
	Mean	SD	95%	CI	Mean	SD	959	6 CI	Mean Diff	95%	6 CI	P
LFTJ group mild: 0.0 / 1.0 / 2.0 / 3.0	-0.017	0.106	-0.029	-0.005	-0.030	0.128	-0.049	-0.011	-0.013	-0.035	0.008	0.210
LFTJ group moderate: 1.1 / 2.1 / 3.1	-0.038	0.129	-0.075	-0.002	-0.025	0.115	-0.079	0.029	0.013	-0.053	0.080	0.688
LFTJ group severe: 2.2 / 3.2 / 3.3	-0.113	0.179	-0.165	-0.061	-0.085	0.145	-0.153	-0.017	0.027	-0.063	0.118	0.548

 $^1\mathrm{Maximum}$ MOAKS BML grade in all 4 PFJ subregions: 0, 1, 2; $^2\mathrm{Maximum}$ MOAKS BML grade of 3 in at least 1 of 4 PFJ subregions; * statistically significant at p<0.05; PFJ -patello-femoral joint, MFTJ - medial femoro-tibial joint, LFTJ- lateral femoro-tibial joint, SD- standard deviation, 95% CI - 95% confidence interval, mean Diff - mean difference, BML - bone marrow lesion

TRANSLATION OF X-RAY TO MRI: DIAGNOSTIC PERFORMANCE OF MRIDEFINED SIMULATED KELLGREN-LAWRENCE GRADING

F.W. Roemer 1,2 , A. Guermazi 2,3 , C.K. Kwoh 4 , S. Demehri 5 , D.J. Hunter 6 , J.E. Collins 7

- 1 Universitätsklinikum Erlangen & Friedrich-Alexander-Universität Erlangen-Nürnberg (FAU), Erlangen, Germany
- ² Chobanian & Avedisian School of Medicine, Boston University, Boston, MA, USA
- 3 VA Boston Healthcare System, West Roxbury, MA, USA
- ⁴ University of Arizona, Tucson, AZ, USA
- ⁵ Johns Hopkins University, Baltimore, MD, USA
- ⁶ University of Sydney, Sydney, Australia
- ⁷ Brigham and Women's Hospital, Harvard Medical School, Boston, MA, USA

INTRODUCTION: While it has been acknowledged that mild-to-moderate radiographic disease severity of knee osteoarthritis (OA), i.e. knees with grades 2 and 3 on the Kellgren-Lawrence (KL) scale – reflect a wide spectrum of tissue damage, it is unknown whether a knee MRI can easily be translated into a specific radiographic (r) KL grade (KLG). In order to potentially use MRI as a single screening tool for eligibility in clinical trials, it is necessary to define which knees correspond to the current inclusion criteria of rKLG 2 and 3.

OBJECTIVE: The aim of this study was to assess the diagnostic performance of a priori-determined definitions of MRI-assessed KLG based on osteophytes (OPs) and cartilage damage in the tibiofemoral joint (TFJ).

METHODS: We included MRI readings from the following Osteoarthritis Initiative substudies: FNIH Biomarker consortium, POMA and BEAK. Included are visits with centrally read rKLG and available MOAKS readings. In order to match the anteroposterior (a.p.) radiograph, four locations for OPs assessed in the coronal plane (central medial femur, central medial tibia, central lateral femur, central lateral tibia) were considered. Eight subregions were considered for cartilage damage to mirror the weight bearing tibiofemoral joints on X-ray: anterior medial tibia, central medial tibia, posterior medial tibia, central medial femur, anterior lateral tibia, central lateral tibia, posterior lateral tibia and central lateral femur. Cartilage damage was classified as minor: focal damage only (MOAKS 0, 1.0, 1.1); moderate: damage with no advanced full thickness wide-spread damage (MOAKS 2.0, 2.1, 3.0, 3.1); and severe: full thickness wide-spread damage (MOAKS 2.2, 3.2, 3.3).

The definitions were derived based on expert consensus opinion as follows:

MRI KL0: no OP (=grade 0 in all 4 locations), minor cartilage damage only

MRI KL1: grade 1 OP in at least 1 of 4 TFJ locations, maximum OP grade 1, minor cartilage damage only

MRI KL2: grade 1, 2 or 3 OP in at least 1 of 4 TFJ locations, moderate cartilage damage

MRI KL2a ("atrophic"): no OP (=grades 0 in all 4 TFJ locations), moderate cartilage damage

MRI KL 3: grade 1, 2 or 3 OP in at least 1 of 4 TFJ locations, severe cartilage damage in at least 1 of 8 subregions.

MRI KL3a ("atrophic"): no OP (=grades 0 in all 4 TFJ locations), severe cartilage damage in at least 1 of 8 subregions

MRI KL 4: grade 1, 2 or 3 OP in at least 1 of 4 TFJ locations, severe cartilage damage in at least 2 of 4 corresponding subregions medially or laterally or both.

Sensitivity, specificity, negative and positive predictive values were determined using radiographic KLG as the reference.

RESULTS: In total, the dataset includes 4924 visits from 1981 participants contributing 2276 knees for up to 4 timepoints. The rKL distribution for the sample is KL 0 n=1463 (29.7%), KL1 n=1457 (29.6%), KL2 n= 1282 (26.0%), KL3 n= 703 (14.3%) and KL4 n=19 (0.4%). Sensitivities of the different MRI KLG to diagnose the corresponding rOA KLG ranged between 14.3% (MRI KL1) to 66.5% (MRI KL0), specificities ranged from 79.3% (MRI KL0) to 96.7% (MRI KL4), NPV ranged from 71.2% (MRI KL1) to 99.8% (MRI KL4) and PPV from 6.4% (MRI KL4) 57.6% (MRI KL0). Details are shown in Table 1. Numbers were comparable when excluding knees with an "atrophic" manifestation of KL2 or 3. Figure 1 illustrates the percentages of each MRI KLG within the different rKLGs

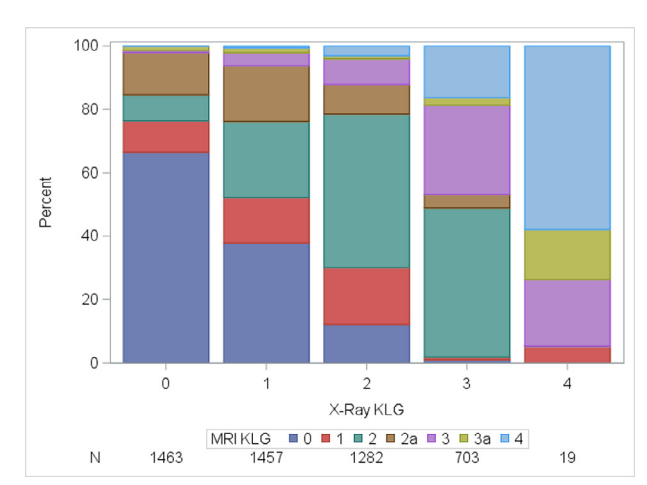
CONCLUSION: MRI-defined KLG shows moderate performance when used as a diagnostic instrument to simulate radiographic KLG. Reasons are multifold but mainly include the wide range of cartilage damage and OP severity within each rKLG. This was particularly relevant for simulating rKL1. Given MRI is the more sensitive tool to diagnose OPs and cartilage damage cannot be evaluated by X-ray directly, likely X-ray scoring based on KL grading does not adequately reflect OP or cartilage status and should be omitted from eligibility screening in clinical trials of knee OA.

SPONSOR: The Beak study is supported by a NIAMS/NIOH grant to Dr. Kwoh: R01AR066601. Scientific and financial support for the FNIH OA Biomarkers Consortium is made possible through grants and direct contributions provided by: AbbVie; Amgen Inc.; Arthritis Foundation; Bioiberica S.A.; DePuy Mitek, Inc.; Flexion Therapeutics, Inc.; Glaxo-SmithKline; Merck Serono; Rottapharm | Madaus; Sanofi; and Stryker. The OAI is a public-private partnership comprised of five contracts (N01-AR-2-2258; N01-AR-2-2259; N01-AR-2-2260; N01-AR-2-2261; N01-AR-2-2262) funded by the National Institutes of Health. Funding partners include Merck Research Laboratories; Novartis Pharmaceuticals Corporation, GlaxoSmithKline; and Pfizer, Inc. Private sector funding for the Consortium and OAI is managed by the Foundation for the National Institutes of Health. POMA: The image analysis for the POMA study was partly funded by Novartis Pharma AG (Basel, Switzerland), in part by a contract with the University of Pittsburgh (Pivotal OAI MRI Analyses [POMA]: NIH/NHLBI Contract No. HHSN2682010000 21C), and in part by a vendor contract from the OAI coordinating center at University of California, San Francisco (N01-AR-2-2258).

DICLOSURE STATEMENT: FWR is a shareholder and Chief Medical Officer of Boston Imaging Core Lab (BICL), LLC, a company providing image assessment services to academia and the pharmaceutical industry. He is consultant to Grünenthal, GmbH. He is Editor in Chief of Osteoarthritis Imaging. AG has provided consulting services to Pfizer, TissueGene, Coval, Medipost, TrialSpark, Novartis, and ICM. He is a shareholder of Boston Imaging Core Lab (BICL), LLC. He is president of the International Society of Osteoarthritis Imaging (unpaid). CKK has received grant funding from GSK, BMS, Cumberland. Lilly, Artiva. He serves as a consultant for AposHealth, Formation Bio, Xalud, Express Scripts, TLC Biosciences, Kolon TissueGene. SD reported that he received funding from Toshiba Medical Systems (for consultation) and grants from GER-RAF and Carestream Health (for a clinical trial study). DJH is the editor of the osteoarthritis section for UpToDate and Co-Editor in Chief of Osteoarthritis and Cartilage. He provides consulting advice on scientific advisory boards for TLCBio, Novartis, TissueGene, Biobone, Sanofi, Enlivex. JEC has received consulting fees from Boston Imaging Core Lab. CORRESPONDENCE ADDRESS: frank.roemer@uk-erlangen.de

Table 1. Diagnostic performance of MRI considering radiographic KL assessment as the reference standard

		Radiogra	Radiographic OA		Diagnostic Performance					
Definition	MRI KL	No	Yes	Specificity (%)	Sensitivity (%)	NPV (%)	PPV (%)			
	No	2746	490							
KLG0	Yes	715	973							
				79.3	66.5	84.9	57.6			
	No	3085	1248							
KLG1	Yes	382	209							
				89.0	14.3	71.2	35.4			
	No	2842	661							
KLG2	Yes	800	621							
				78.0	48.4	81.1	43.7			
	No	3986	391							
KLG3	Yes	235	312							
				94.4	44.4	91.1	57.0			
	No	4743	8							
KLG4	Yes	162	11							
				96.7	57.9	99.8	6.4			



 $\label{eq:Figure 1. Distribution of MRI-defined KL grades within the different X-ray defined rKL categories.$

SPONTANEOUS CARTILAGE THICKENING IN OSTEOARTHRITIS KNEES: DATA FROM IMI-APPROACH AND THE OAI

C. Salzlechner 1 , W. Wirth 2 , S.C. Mastbergen 3 , M. Kloppenburg 4 , F.J. Blanco 5 , I.K. Haugen 6 , F. Berenbaum 7 , M.P. Jansen 3

INTRODUCTION: Articular cartilage was thought to have minimal repair capacity, but treatments like knee joint distraction show that regeneration is possible. Preliminary analyses have also suggested the possibility of spontaneous thickening of cartilage: thickening without external regenerative intervention.

OBJECTIVE: This study aims to evaluate spontaneous thickening in osteoarthritic knees.

METHODS: Patients from IMI-APPROACH and OAI cohorts were included. MRI-based mean medial and lateral cartilage thickness (ThCtAB; Chondrometrics) and knee radiographs were obtained at baseline, 1-year, and 2-year follow-up. Minimum medial and lateral joint space width (mJSW) and Kellgren-Lawrence grade (KLG) were automatically assessed from radiographs using KOALA (ImageBiopsy Lab). For each knee, mean whole-joint mJSW and ThCtAB changes over 2 years were calculated using linear regression. Knees were categorized as 'thickening' if both the mJSW and ThCtAB change were positive and as 'thinning' if both were negative; knees with inconsistent results were excluded. This approach was chosen because an increase in mJSW may reflect joint wedging or positional changes and increased ThCtAB may indicate swelling; especially in these expectedly relatively small changes, only an increase in both likely reflects true structural thickening.

Patient characteristics and two-year changes were compared using Mann-Whitney U and chi-square tests.

RESULTS: Out of 1,457 knees analyzed, 203 (14%) demonstrated thickening and 658 (45%) thinning. Patients with thickening were younger, predominantly female, had less pain and a lower KLG compared to those with thinning (all p<0.05). Over 2 years, knees with thickening received significantly fewer injections (p=0.043) and showed greater improvements in both mJSW and ThCtAB (both p<0.001). Complete results are presented in Table 1.

CONCLUSION: Spontaneous cartilage thickening can occur in osteoarthritic knees and is more prevalent in younger females with less severe joint damage. Future research is needed to determine whether

this thickening (repair) potential can be predicted and may guide regenerative treatment options.

SPONSOR: NWO/ZonMW VENI grant to M.P. Jansen.

DICLOSURE STATEMENT: NA. **ACKNOWLEDGMENT:** NA.

CORRESPONDENCE ADDRESS: m.p.jansen-36@umcutrecht.nl

Table 1: Characteristics at baseline and over 2-year follow-up for cartilage thickening and thinning patients.

Parameter	Thickening (n=203)	Thinning (n=658)	P-value
Baseline			
Age, years	59.0 (14.0)	64.0 (14.0)	< 0.001
Female sex, n (%)	140 (69)	389 (59)	0.012*
BMI, kg/m ²	29.8 (6.3)	29.5 (6.4)	0.661
Weight, kg	81.9 (21.3)	83.6 (21.8)	0.178
Kellgren-Lawrence grade, n (%)	1		< 0.001*
- 0	21 (10)	52 (9)	
- 1	44 (22)	87 (13)	
- 2	93 (46)	228 (35)	
- 3	34 (17)	229 (35)	
- 4	11 (5)	62 (9)	
mJSW mean joint (mm)	4.6 (1.4)	4.6 (1.3)	0.958
ThCtAB mean joint (mm)	3.4 (0.8)	3.4 (0.8)	0.964
WOMAC pain (100 best)	90.0 (25.0)	85.0 (25.0)	0.020
WOMAC stiffness (100 best)	75.0 (37.5)	75.0 (37.5)	0.121
WOMAC function (100 best)	89.4 (25.0)	85.3 (26.8)	0.070
WOMAC total (100 best)	88.5 (24.1)	84.4 (27.0)	0.038
Previous surgeries, n (%)			
- Any	47 (23)	122 (19)	0.148*
- Arthroscopy	37 (18)	107 (16)	0.512*
- Meniscectomy	32 (16)	85 (13)	0.301*
Changes over two years			
BMI (Δ/yr)	0.1 (0.9)	0.0 (1.0)	0.444
Weight (∆/yr)	0.2 (2.5)	0.0 (2.6)	0.569
mJSW mean joint (Δ/yr)	0.11 (0.14)	-0.15 (0.23)	< 0.001
ThCtAB mean joint (Δ/yr)	0.03 (0.04)	-0.05 (0.07)	< 0.001
WOMAC pain (Δ/yr)	0.0 (8.0)	0.0 (10.0)	0.752
WOMAC stiffness (Δ /yr)	0.0 (12.5)	0.0 (15.0)	0.393
WOMAC function (Δ/yr)	0.0 (8.4)	0.0 (8.7)	0.151
WOMAC total (Δ/yr)	0.1 (7.4)	-0.2 (7.9)	0.235
Injections during follow-up, n (` '	
- Any	10 (5)	62 (9)	0.043*
- Steroids	8 (4)	41 (6)	0.218*
- Hyaluronic acid	3 (2)	30 (5)	0.046*
Surgeries during follow-up, n (9			
- Any	3 (2)	28 (4)	0.063*
- Arthroscopy	3 (2)	28 (4)	0.063*
- Meniscectomy	3 (3)	21 (3)	0.195*

Median and interquartile ranges or, where indicated, n (%) are provided. P-values were calculated with Mann-Whitney U tests or, where indicated with *, with Chi-square tests. Statistically significant p-values (<0.05) are bold.

¹ ImageBiopsyLab, Vienna, Austria

² Paracelsus Medical University, Salzburg, Austria & Chondrometrics GmbH, Freilassing, Germany

³ University Medical Center Utrecht, Utrecht, The Netherlands

⁴Leiden University Medical Center, Leiden, The Netherlands

⁵ University of A Coruna, A Coruna, Spain

⁶ Diakonhjemmet Hospital, Oslo, Norway

⁷ Sorbonne University & AP-HP Saint-Antoine Hospital, Paris, France

COORDINATED VARIATIONS IN HIP SHAPE WITH SEX, AGE AND OA IN UK BIOBANK

F.R. Saunders ¹, B.G. Faber ², R. Ebsim ³, J.S. Gregory ¹, N.C. Harvey ⁴, T. Cootes ³, C. Lindner ³, J.H. Tobias ², R.M. Aspden ¹

- ¹ University of Aberdeen, Aberdeen, UK
- ² University of Bristol, Bristol, UK
- ³ University of Manchester, Manchester, UK

INTRODUCTION: A shortage of methods for early identification of OA, stratification of patients, and a robust biomarker to identify structural endpoints is partly responsible for hindering the development of treatments that inhibit structural damage or target the underlying pathophysiology. We have previously shown that statistical shape modelling (SSM) from Dual Energy X-ray Absorptiometry (DXA) imaging has the potential to address these issues but requires a standardized approach to be developed taking account of sex and shape changes with ageing.

OBJECTIVE: To establish variations in hip shape with sex, age and OA in UK Biobank (UKB) DXA images.

METHODS: Hip iDXA scans (GE-Lunar, Madison, WI) were recorded from the UKB imaging enhancement study along with participants' age and sex. The outline of the left hip, excluding osteophytes, was identified using 85 points placed by a machine-learning trained software (BoneFinder®, University of Manchester). Points were manually reviewed and corrected where necessary. Hip shape size and rotation were standardized by Procrustes analysis. Principal components analysis was used to build an SSM producing a set of orthogonal hip shape modes of variation (HSM) normalized to zero mean and unit SD. Radiographic hip OA (rHOA) was graded using a semi-quantitative DXA-based atlas using a combination of grades of osteophytosis and joint space narrowing.

RESULTS: Left hip DXA images were available from 41,160 UKB participants. HSM score data were generated for 40,339 individuals comprising 21,045 (52.2%) females and 19,294 (47.8%) males (aged 45 to 84 years). The first 10 HSMs were analyzed explaining 86.3% of variance. Differences between males and females were expressed as an effect size (Cohen's d). The largest differences were found in HSMs 3 (d=0.62), 1 (d=0.59) and 9 (d=0.59), all moderate effect sizes, indicative of a smaller femoral head with less acetabular coverage and a narrower femoral neck in women compared with men. Participants were grouped into quintiles of age and the mean HSM score for each quintile calculated. Linear regression identified strong linear relationships between the mean quintile HSM scores and age for females for HSMs 1,2,4,6 and 7, and HSMs 1,4,9 and 10 in males, all $R^2 > 0.8$ (Fig. 1). Closer examination suggested that HSMs 4,9 and 10 in males may level-off at about 65-70 years old, and a quadratic fit produced R² values around 0.95. HSMs 6 and 9 varied monotonically with severity of rhOA (Fig. 2).

CONCLUSION: This large cross-sectional study establishes differences in HSMs between females and males and variations with ageing. There are measurable changes with increasing severity of rhOA. These deepen our understanding of how bone shape changes with age and provide essential context for longitudinal studies.

SPONSOR: The Wellcome Trust (Grant No. 209233)

DISCLOSURE STATEMENT: No competing financial interests exist **ACKNOWLEDGMENT:** We thank the participants and staff of UK Biobank (application 17925)

CORRESPONDENCE ADDRESS: r.aspden@abdn.ac.uk

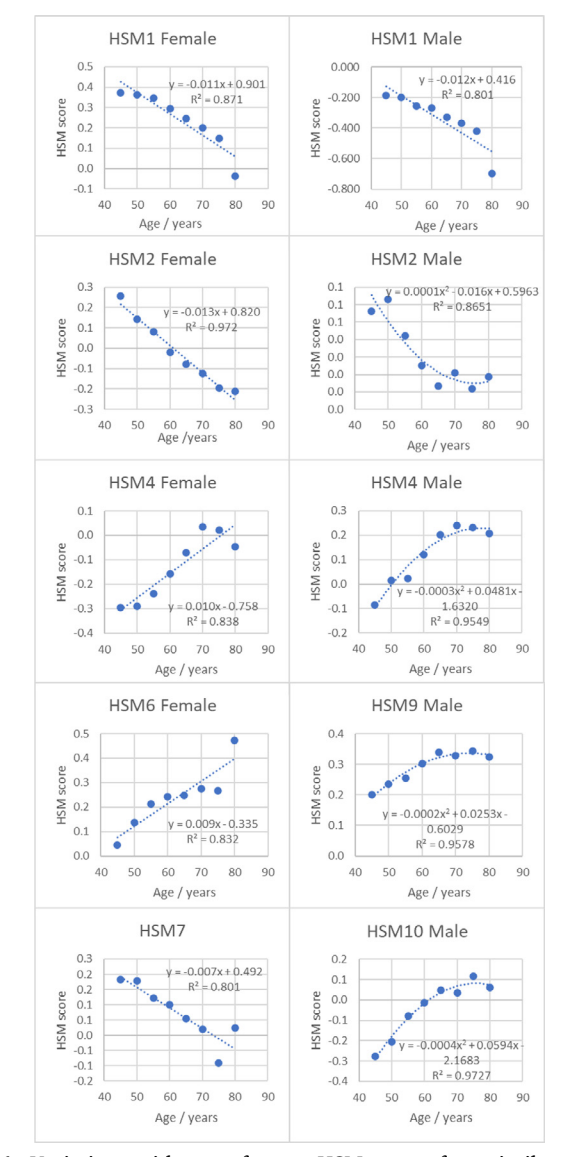


Fig. 1. Variations with age of mean HSM scores for quintiles of age with linear $\rm R^2>0.8.$ Several of the male HSMs suggest a non-linear relationship.

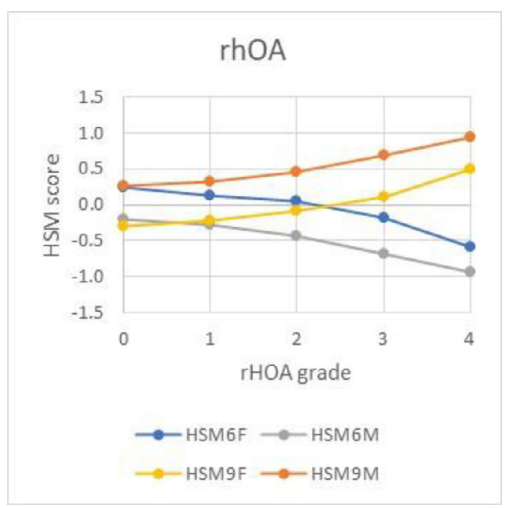


Fig 2. Variation in scores of HSMs 6 and 9 with severity of rhOA.

 $^{^4}$ University of Southampton & University Hospital Southampton NHS Foundation Trust, Southampton, UK

OSTEOARTHRITIS AND CHRONIC BACK PAIN ARE ASSOCIATED WITH LATERAL SPINE SHAPE: A STUDY USING THE UK BIOBANK

F.R. Saunders 1, J. Parkinson 2, R.M. Aspden 1, T. Cootes 2, J.S. Gregory 1

INTRODUCTION: Chronic back pain is very common and affects over 600 million adults worldwide and has been partly attributed to OA. We have previously shown that the lateral spine has an intrinsic shape and that specific shapes have been shown to be associated with back pain in early old age. However, there is little evidence in the literature that directly links lateral spine shape with OA.

OBJECTIVE: To explore the relationships between OA, chronic back pain and lateral spine shape in a sub-cohort of the UK Biobank.

METHODS: Lateral spine iDXA scans (n=4784) from the UK Biobank imaging enhancement study were used. The cohort was 52.1% female, and the mean age was 62.2±7.5 years (Table 1). Images were annotated semi-automatically using a 143-point template encompassing the vertebral bodies from T7 to the superior margin of L5 using custom software (The University of Manchester). The points were subjected to Procrustes transform and then Principal Component Analysis to build a statistical shape model (SSM). Self-reported OA and chronic back pain (greater than 3 months duration) were taken from the questionnaire data provided at the imaging centre visit. Binary logistic regression was used to explore the associations between self-reported OA, chronic back pain, and the first 10 modes of variation. The model was adjusted for age, sex, height, weight and total spine BMD. We report odds ratios (OR) with 95% confidence intervals (CI) for each standard deviation change in mode.

RESULTS: 537 participants reported OA (not site specific) and 630 reported chronic back pain. The first 10 SSM modes accounted for 88.9% of the total model variation. We found that three modes were associated with self-reported OA (modes 3,9 & 10) and a single mode was associated with chronic back pain (mode 3). It was observed that mode 3 (6.5% total model variation; Fig 1.), describing vertebral height and decreased vertebral column height was negatively associated with both self-reported OA [OR 0.88 95% CI 0.8-0.97, p=0.007] and chronic back pain [OR 0.81 95% CI 0.70-0.94, p=0.005]. Mode 3 also described a loss of spinal curvature (Fig. 1). Mode 9 (0.7% of total model variation), describing narrowing of the lumbar vertebrae) and mode 10 (0.5% of total model variation), describing a disconnect between lumbar and thoracic sections of the vertebral column were associated with an increased risk of OA [mode 9 OR 1.11 95% CI 1.01-1.022, p=0.031; mode 10 OR 1.12 95% CI 1.02-1.23, p=0.011].

CONCLUSION: We found that loss of spinal curvature and decreased vertebral body height were negatively associated with OA. Our data indicated that there was an increased risk of OA with rotation of the spine.

SPONSOR: Wellcome Trust Collaborative Award ref. 209233.

ACKNOWLEDGMENT: Thank to the participants and staff of UK Biobank (application 17295)

CORRESPONDENCE ADDRESS: f.r.saunders@abdn.ac.uk

Table 1. UK Biobank spine shape model cohort demographics.

Variable	Women (mean ± SD) (n=2494)	Men (mean \pm SD) (n=2490)	Total (mean ± SD) (n=4874)
Age	61.5 ± 7.4	62.8 ± 7.6	62.2 ± 7.5
Height (cm)	162.1 ± 6.4	176.7 ± 6.4	169.6 ± 9.3
Weight (kg)	68.5 ± 12.5	82.8 ± 12.5	75.4 ± 14.4
Self-reported OA (not site specific)	324	231	537
Back pain (>3 months duration)	339	291	630

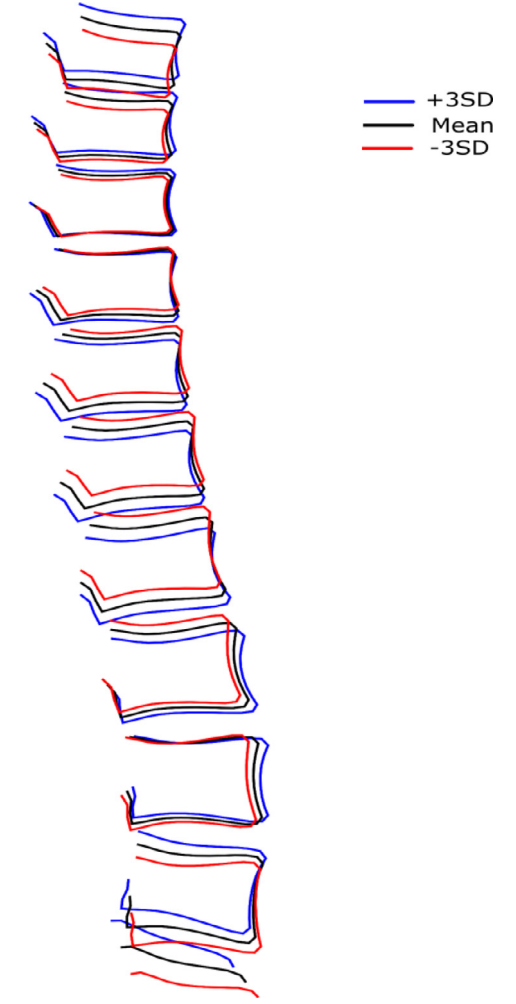


Figure 1. Spine shape mode 3 showing mean (black) $\pm 3SD$.

¹ University of Aberdeen, Aberdeen, UK

² University of Manchester, Manchester, UK

UNCOVERING STRUCTURAL DISEASE PATTERNS OF EARLY POST-TRAUMATIC OSTEOARTHRITIS IN A DMM MOUSE MODEL USING CONTRAST-ENHANCED MICRO-COMPUTED TOMOGRAPHY

J.E. Schadow ¹, E.C. Boersma ¹, A.M. Cagnoni ¹, H. Liu ¹, R.A. Davey ², K.S. Stok ¹

INTRODUCTION: Contrast-enhanced micro-computed tomography (CECT) is a non-destructive method to assess cartilage degeneration seen in diseases such as OA whilst also allowing for analysis of bone changes [1, 2]. Application has been limited to *ex vivo* and *in situ* studies but using CECT *in vivo* holds the potential to quantify and track structural cartilage and bone changes and illuminate new understanding of disease onset and progression.

OBJECTIVE: The aim of this study was to uncover structural disease patterns of early post-traumatic osteoarthritis in a destabilized medial meniscus (DMM) mouse model using time-lapse CECT.

METHODS: DMM (n=22) or sham surgery (n=22) was performed on ten-week-old C57Bl/6 mice. A further three mice did not undergo surgery but were euthanized at 10 weeks of age and processed for histology. Of the mice that had surgery, three mice per group were euthanised and processed for histology at seven-, 14-, 21- and 28-days post-surgery. The remaining ten mice per group received an intra-articular injection of Dotarem (Guerbet) and were scanned at 10.4 μ m, 70 kVp, 114 μ A using microCT (vivaCT80, Scanco Medical AG) at one-day pre-surgery and seven-, 14-, 21-, 28-, and 56-days post-surgery. After scanning at the final timepoint, three mice per group were euthanised after scanning at 56-days post-surgery and processed for histology. Safranin-O histology was used to score joints following the OARSI guidelines [3]. Mean attenuation of cartilage, joint alignment, joint space morphometry, subchondral bone morphometry, and osteophyte presence were analysed from microCT images. Mixed-effects analysis was used to investigate effects of osteoarthritis, time, and joint side (medial/lateral) on mean attenuation, joint space, subchondral bone, and osteophytes as well as the effects of osteoarthritis and time on joint alignment.

RESULTS: OARSI score of medial tibia in DMM OA group increased compared to the lateral side in DMM OA group and medial side of sham controls (Figure 1A). Mean attenuation of medial tibial cartilage in DMM OA mice did not change over time whereas that of sham controls increased over time. The number of voxels in the thinnest joint space layer increased on the medial side of DMM OA group post-surgery but did not change on medial side of sham controls or lateral side of either group (Figure 1B). There was increased variability in dorsal axis and midsagittal axis angles α and γ of DMM OA mice at 14-, 21-, and 28-days post-surgery. There was no difference in shape κ and scale θ of osteophyte thickness distribution of DMM OA tibia compared to sham control, despite osteophyte development on the lateral and medial side of DMM OA tibiae and frontal side of both groups. Cortical porosity and trabecular

thickness of medial tibia in DMM OA mice increased over time before decreasing at 56-days post-surgery, whereas all other groups steadily decreased.

CONCLUSION: Mean attenuation was not sensitive to cartilage degeneration as intra-articular distribution and diffusion of contrast agent were impacted by joint space narrowing and increased synovial turnover. Bone structure changed as a reaction to altered mechanical loading. Change patterns were non-linear, likely because the mechanical environment changed over the course of disease development.

REFERENCES

1-Schadow J.E., et al., Cartilage, 2025: 19476035251323373. 2-Bansal, P. et al., Osteoarthritis and cartilage, 2010. 18: 184-191. 3-Glasson, S. et al., Osteoarthritis and cartilage, 2010. 18: S17-S23.

SPONSOR: FWO and F.R.S.-FNRS under the Excellence of Science (EOS) programme (EOS No. 40007553) Australian Research Council Discovery programme (DP180101838), KU Leuven – University of Melbourne International Research Training grant, University of Toronto – University of Melbourne International Research Training grant and ANZBMS Bone Health Foundation Grant.

DICLOSURE STATEMENT: None

ACKNOWLEDGMENT: We would like to thank Cynthia Louis, PhD from Walter + Eliza Hall Institute of Medical Research, Prof Christopher Little from Kolling Institute, University of Sydney, Dr Pholpat Durongbahn, Melbourne Bioresources Platform, Melbourne Histology Platform and Statistics Consulting Centre from University of Melbourne for their technical assistance with this work.

CORRESPONDENCE ADDRESS: kstok@unimelb.edu.au

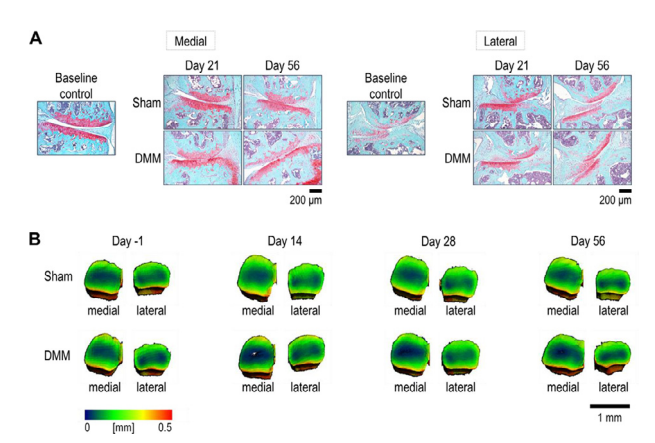


Figure 1. Representative images of A) medial and lateral histology sections of DMM OA model compared to baseline and sham controls and B) medial and lateral joint space thickness map of DMM OA model compared to sham control.

 $^{^{\}rm 1}$ Department of Biomedical Engineering, The University of Melbourne, Melbourne, Australia

² Department of Medicine, Austin Health, University of Melbourne, Melbourne, Australia

ASSESSING TEST-RETEST RELIABILITY OF JSW MEASUREMENTS FOR THE MOST4 KNEE RADIOGRAPH POSITIONING PROTOCOL

N.A. Segal ^{1,2}, N.H. Degala ¹, T.D. Turmezei ^{3,4}, J.A. Lynch ⁵

- ¹ University of Kansas Medical Center, Kansas City, KS, USA
- ² The University of Iowa, Iowa City, IA, USA
- ³ Norfolk and Norwich University Hospital, Norwich, UK
- ⁴ University of East Anglia, Norwich Research Park, Norwich, UK
- ⁵ University of California-San Francisco, San Francisco, CA, USA

INTRODUCTION: Despite challenges, joint space width (JSW) on weight-bearing radiographs has remained the most common structural outcome for Phase III trials approved by either the FDA or the EMA. The JSW is the distance between the projected femur and tibia margins on radiographic images. Superimposition of the posterior and anterior edges of the tibial plateau is required to accurately measure radiographic JSW. Knees must be positioned correctly at both baseline and follow-up to maximize reliability of measures of JSW and reliability metrics are useful to calculate sample sizes for studies that depend on JSW measurements.

OBJECTIVE: To establish the test-retest reliability of knee joint 2D imaging protocols used by the Multicenter Osteoarthritis Study (MOST4) at the 20-year visit.

METHODS: This cross-sectional, observational study compared joint space width (JSW) measurements between baseline and 2-week followup on PA radiographs acquired using an XFI scanner (Planmed Oy, Helsinki, Finland), using the same protocol used for the MOST4-V1 (20year) visit. Participants were age ≥ 50 years, Kellgren-Lawrence grade 0-4, met MOST4 inclusion criteria, and could safely undergo WBCT (i.e. body mass< 230kg, able to stand for 5 minutes with support). Participants were positioned using a customized Perspex frame which could be tilted in the sagittal plane (5°, 10° or 15°) to make the tibial plateaus coplanar with the x-ray beam for a PA radiograph of both knees. Shrout-Fleiss intraclass correlation coefficients (ICC 2.1) and limits of agreement (mm) were calculated for joint space width (JSW) measurements on radiographs acquired at baseline and 2-week follow-up. For the medial compartment, JSW was measured at 50%, 60%, 70%, 80%, and 90% of the distance from the medial tibial spine (0%) to the outer margin of the medial tibial plateau (MTP; 100%). For the lateral compartment, JSW was measured at 50%, 60%, 70%, 80%, and 90% of the distance from the lateral tibial spine (0%) to the outer margin of the lateral tibial plateau (100%). JSW could not be measured in one knee due to poor alignment of the MTP and some knees could not be measured at JSW 90% due to the relative position of the femur on the tibia.

RESULTS: A total of 28 knees for 14 participants (demographics in Table 1) were imaged. ICC for JSW at each position in the medial and lateral

compartments at JSW 50% to 90% are presented in Table 2 and limits of agreement are presented in Table 3. ICC for JSW measurements in the medial compartment were all \geq 0.92 and ICC for JSW measurements in the lateral compartment were all \geq 0.76.

CONCLUSION: These data support that the MOST4 knee radiograph acquisition protocol using the XFI has acceptable test-retest reliability for measurement of JSW at locations within the medial and lateral compartments.

SPONSOR: None.

DISCLOSURE STATEMENT: NS is a consultant for Trice Medical, Arthrex, and Pacira Biosciences. TT is director of KNEE3D Ltd.

ACKNOWLEDGEMENT: None.

CORRESPONDENCE ADDRESS: nsegal@kumc.edu

Table 1. Demographics of Study Participants.

Age (years) BMI (kg/m²)	63.5 ± 7.7 32.1 ± 5.5
KL Grade (N)	
0	5
1	7
2	6
3	6
4	4

Table 2. Test-Retest Reliability of JSW Measurements Using the MOST4 Knee Radiograph Acquisition Protocol.

JSW	Medial Compartment ICC (95% CI)	Lateral Compartment ICC (95% CI)
50%	0.94 (0.88, 0.97)	0.76 (0.55, 0.88)
60%	0.93 (0.84, 0.96)	0.79 (0.59, 0.89)
70%	0.96 (0.91, 0.98)	0.87 (0.73, 0.94)
80%	0.96 (0.91, 0.98)	0.80 (0.61, 0.90)
90%	0.92 (0.83, 0.96)	0.81 (0.45, 0.93)

Table 3. Limits of Agreement for JSW Measurements Using the MOST4 Knee Radiograph Acquisition Protocol.

JSW	Medial Compartment (mm)	Lateral Compartment (mm)
50%	-1.09, 1.08	-1.82, 2.20
60%	-1.19, 1.00	-1.88, 2.12
70%	-0.83, 0.76	-1.41, 1.70
80%	-0.81, 0.62	-1.47, 2.51
90%	-1.34, 1.24	-0.14, 2.26

CAN COMBINED NEUROPHYSIOLOGICAL AND MRI EVALUATION HELP GAIN NEW INSIGHTS IN ARTHROGENIC MUSCLE INHIBITION AMONG PATIENTS WITH KNEE PAIN? PROOF OF CONCEPT

D. Sherman 1 , J. Stefanik 1 , A. Guermazi 2 , W. Issa 3 , X. He 3 , A.W. Jang 3 , F. Liu 3 , M. Jarrava 3

INTRODUCTION: Arthrogenic muscle inhibition (AMI) is a neuromuscular impairment that is commonly described in patients after knee joint injuries and surgeries. AMI is characterized by profound quadriceps muscle atrophy and persistent muscle weakness secondary to neural inhibition of motor pathways due to altered afferent feedback. While AMI is well-recognized in rehabilitation research, there is a critical lack of standard clinical diagnostic criteria limiting rehabilitation practitioners' ability to prescribe treatments. In this context, MRI can be a helpful adjunct tool to neurophysiological testing by identifying joint pathology causing AMI and quadriceps muscle inhibition resulting from it.

OBJECTIVE: Describe MRI and neurophysiological findings of the knee joint and thighs among patients with AMI secondary to knee injury or surgery.

MEHTODS: Four patients with marked quadriceps weakness (presumed AMI) following knee joint injury or surgery are presented. All patients had MR imaging data, including two with unilateral thigh MRI (Patients A-B), 1 with unilateral knee and thigh MRI (Patient C), and 1 with bilateral knee and thigh MRIs, as well as neurophysiological testing (Patient D). Neurophysiological testing included muscle activation failure, Hoffman stretch reflex testing, and cortical inhibition using peripheral nerve and transcranial magnetic stimulation techniques. All imaging data was acquired 12-16 weeks post knee injury or surgery.

RESULTS: Patients A-C (each 12-14 weeks status-post ACL reconstruction, uni-compartment arthroplasty, and arthroscopic drilling, respectively) present with marked quadriceps volume loss and diffuse increased T2 signal, resembling denervation edema (Figure 1). Patient C, who underwent arthroscopic drilling, had osteochondral fracture prior to surgery which worsened on the postoperative imaging. Patient D (12-16 weeks post soccer injury) presented with osteochondral fracture of the lateral trochlea with marked atrophy of the quadriceps muscle (Figure 2A-B). Neurophysiological testing revealed volitional quadricep activation failure (51%, Figure 2C), as well as intracortical inhibition (37%, Figure 2D), afferent inhibition (81%, Figure 2E), and Hoffmann reflex facilitation on the involved limb (cf. 29%, Figure 2F vs. 15%, Figure 2G). These findings suggest a cortically mediated muscle activation failure and paradoxical reflex facilitation to preserve strength (spinal cord involvement). The absence of denervation edema could be plausibly explained by the central nervous involvement rather than a peripheral nerve or neuromuscular problem.

CONCLUSION: These cases highlight the value of combined MR imaging and neurophysiological assessment in AMI. The presence of denervation-like edema on MRI, alongside quantifiable neural inhibition patterns, offers potential diagnostic markers for AMI subtypes. Further research incorporating both modalities is needed to develop targeted rehabilitation strategies that address specific inhibitory mechanisms, potentially improving outcomes for patients with persistent post-injury weakness.

SPONSOR: MJ is funded by a K23 award (K23-AR084603) from the National Institute of Arthritis and Musculoskeletal and Skin Diseases (NIAMS) of the NIH.

DICLOSURE STATEMENT: AG has received consultancies fees from Novartis, ICM, Levicept, Scarcell, Peptinov, Pacira, Coval, 4Moving, Formation Bio, Paradigm, Medipost and TissueGene and is shareholder of Boston Imaging Core Lab (BICL), LLC a company providing image assessment services. M.J. is consultant to BICL. Other authors have nothing to declare.

ACKNOWLEDGMENT: We thank the four patients who agreed to have their data presented for this abstract.

CORRESPONDENCE ADDRESS: mjarraya@mgh.harvard.edu

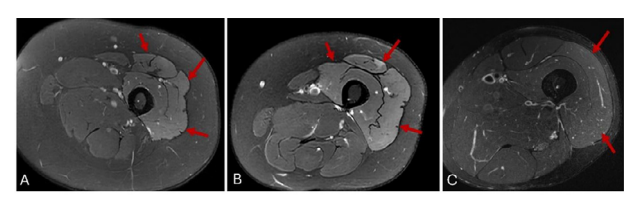


Figure 1: Axial T2-weighted MR images with fat suppression in three patients with arthrogenic muscle inhibition (AMI) showing quadriceps atrophy and increased T2 signal resembling denervation edema. Patient $\bf A$ is a 46-year-old female with marked weakness of the quadriceps persistent for 12 weeks after ACL reconstruction. Patient $\bf B$ is a 45-year-old woman with weakness persistent more than 10 weeks after uni-compartment arthroplasty of the same knee. Patient $\bf C$ is 42-year-old man with pain and atrophy of the quadriceps for more 11 weeks after arthroscopic drilling of the lateral trochlea. In this case the increased T2 signal of the quadriceps is less prominent in comparison with the other cases.

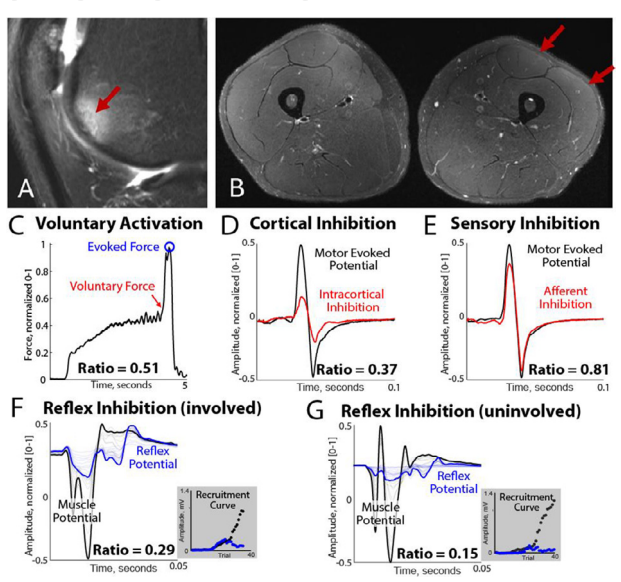


Figure 2: MRI and neurophysiological evaluation of patient with arthrogenic muscle inhibition (AMI) of the left quadriceps. A. Sagittal MR T2-weighted image with fat suppression (T2FS) shows an osteochondral fracture of the lateral trochlea with marked subchondral edema (arrow). B. Axial T2FS images of both thighs show atrophy of the left quadriceps muscle (arrows). C. Peripheral nerve stimulation during active muscle contraction shows low volitional activation at 51% indicating significant muscle activation failure (inability to recruit the full motor unit pool despite maximal effort (voluntary/evoked force). Panel (C) reveals muscle inhibition as a "symptom", but not its mechanism or etiology. The waveforms in D-G are quadriceps electromyographic activity in response to transcranial magnetic stimulation, TMS (D-E) and peripheral nerve stimulation (F-G). D. shows elevated intracortical inhibition, at 37% (decreased excitability at the motor cortex level), potentially learned to reduce limb use and prevent further injury, which suggests that brain-muscle pathway is impaired. E. In contrast, afferent inhibition is largely preserved (81%), which suggests inhibition does not arise from pain or from the joint. F-G. Facilitated Hoffmann reflex in the involved limb (29% vs. 15% is uninvolved) indicates a shift in spinal in spinal excitability despite cortical inhibition. This is equivalent to a relative "hyperreflexia" and suggesting a central nervous system impair $ment,\ whereas\ hyporeflexia\ would\ have\ suggested\ a\ peripheral\ nerve\ /\ neuromuscular$ junction problem.

¹ Physical Therapy, Movement, and Rehabilitation Science, Northeastern University, Boston. MA. USA

² Department of Radiology, VA Boston Health Care, West Roxbury & Chobanian & Avedisian School of Medicine, Boston University, Boston, MA, USA

³ Division of Musculoskeletal Imaging and Intervention & The Athinoula A. Martinos Center for Biomedical Imaging, Department of Radiology, Massachusetts General Hospital, Harvard Medical School, Boston, MA, USA

OPTIMIZED DEEP LEARNING METHOD FOR AUTOMATED SEGMENTATION OF BONE MARROW LESIONS

Q. Shihua¹, W. Qiong¹, S. Juan², B.D. Jeffrey³, M. Timothy³, Z. Ming¹

INTRODUCTION: Bone Marrow Lesions (BMLs), characterized by highsignal intensity on fat-suppressed MRIs, are associated with the progression of knee osteoarthritis (OA). In early OA or when joint damage is not visible on radiographs, BMLs are predictive markers for progression. However, their irregular distribution, potentially large size, and low-contrast boundaries challenge BML segmentation.

OBJECTIVE: This study introduces a novel training strategy for enhancing automated BML segmentation accuracy

METHODS: We aimed to optimize a deep learning method for automatic BML detection and segmentation in MRI, using the Osteoarthritis Initiative (OAI) dataset split into 70% training (210 participants), 15% validation (45 participants), and 15% testing (45 participants), totaling 1025, 190, and 201 MRIs, respectively. Images were employed using data augmentation like brightness, contrast, and geometric transformations. We applied a closing operation, a morphological technique combining dilation and erosion, to smooth edges, addressing the coarse manual labels that impair training. Several models (U-net, SwinUnetR, AttentionUnet, and U-net++) were trained with single-label (BML) and dual-label (BML+femur bone) outputs. Model performance was measured with the Dice Similarity Coefficient (DSC) for overlap and HD95 for boundary error. Cross-entropy and Dice loss functions improved sensitivity during training, particularly in dual-label channels where the femur bone location helped constrain BML positions. We also applied Pixel-Wise Voting (PWV) to improve segmentation stability and accuracy by averaging results from image variations, reducing false positives, and enhancing final segmentation outcomes.

RESULTS: UNet++ model with dual-label (BML+ femur bone) yielded the best accuracy, outperforming U-net, SwinUnetR, and AttentionUnet. Figure 1 shows its predicted region (yellow) overlapping well with the manually labeled BML and aligning with boundaries. Specifically, the dual-label Unet model with PWV improved DSC from 62.21% to 64.88% for BML and to 96.52% for bone, while HD95 dropped to 26.82% for BML and 15.52% for bone. SwinUnetR with dual-label and PWV also showed improved DSC (65.06% to 66.70% for BML; 96.34% for bone) and reduced HD95 to 28.31% for BML and 11.54% for bone. AttentionUnet exhibited notable PWV improvements in bone segmentation. Overall, Unet++ achieved the highest performance with dual-label and PWV, increasing DSC from 66.16% to 68.48% for BML and 96.66% for bone, with the lowest HD95 values.

CONCLUSION: This study employed augmentation strategies, a closing operation, and both single- and dual-label analyses to train four models—Unet, SwinUnetR, AttentionUnet, and Unet++. Cross-entropy loss and Pixel-Wise Voting (PWV) enhanced model performance, with dual-

label consistently outperforming single-label, especially with PWV. Our findings highlight the potential of automated segmentation as a powerful tool for researchers.

SPONSOR: N/A

DISCLOSURE STATEMENT: N/A ACKNOWLEDGMENT: N/A

CORRESPONDENCE ADDRESS: mzhang2@bu.edu

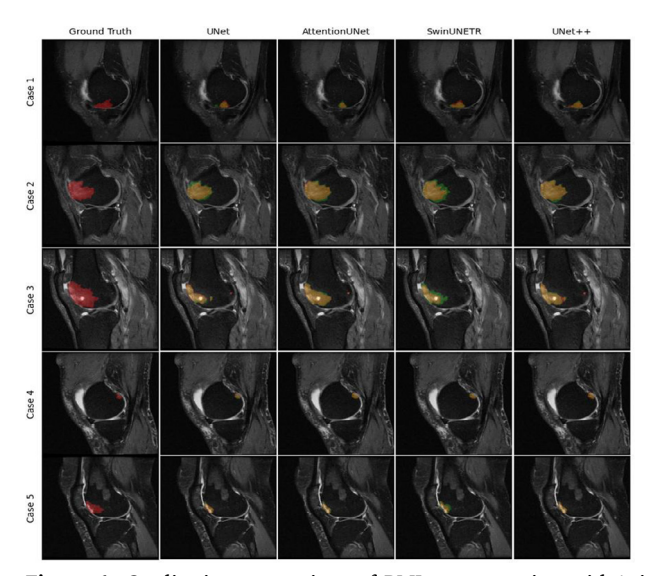


Figure 1: Qualitative comparison of BML segmentation with/without bone guidance. The first column shows manually labeled BML (red); other columns are red (no guidance), green (with guidance), and yellow (overlap).

Table 2: Model Performance on BML and Bone Segmentation

Architecture	Label Type	PWV	BML (DSC↑ / HD95↓)	Bone (DSC↑ / HD95↓)
Unet	Single	No	62.21% / 42.25	-
	Single	Yes	64.55% / 30.07	-
	Dual	No	63.87% / 29.24	96.15% / 23.27
	Dual	Yes	64.88% / 26.82	96.52% / 15.52
SwinUnetR	Single	No	65.06% / 45.71	-
	Single	Yes	66.51% / 32.17	-
	Dual	No	65.76% / 33.75	95.96% / 15.64
	Dual	Yes	66.70% / 28.31	96.34% / 11.54
AttentionUnet	Single	No	63.25% / 62.45	-
	Single	Yes	63.76% / 50.46	-
	Dual	No	66.16% / 33.90	95.96% / 36.78
	Dual	Yes	66.94% / 29.20	96.10% / 30.64
Unet++	Single	No	66.16% / 35.99	-
	Single	Yes	67.33% / 33.00	-
	Dual	No	68.09% / 34.20	96.58% / 14.01
	Dual	Yes	68.48 % / 29.46	96.66% / 13.97

 $^{^{1}}$ Department of Computer Science, Boston University, MA, USA

² Department of Computer Science, Pace University, NY, USA

³ UMass Chan Medical School, University of Massachusetts, MA, USA

THE INFLUENCE OF WEIGHT-BEARING AND FLEXION ON 3D JOINT SPACE WIDTH IN KNEE OSTEOARTHRITIS

F.F.J. Simonis 1 , W.M. Brink 1 , F.F. Schröder 2,3 , W.C. Verra 3 , T.D. Turmezei 4,5 , S.C. Mastbergen 6 , M.P. Jansen 6

- $^{\rm 1}$ Magnetic Detection and Imaging Group, TechMed Centre, University of Twente, Enschede, Netherlands
- $^2\,\mathrm{Department}$ of Orthopaedic Surgery and Traumatology, Medisch Spectrum Twente, Enschede, Netherlands
- 3 Department of Biomechanical Engineering, TechMed Centre, University of Twente, Enschede, Netherlands
- ⁴ Department of Radiology, Norfolk & Norwich University Hospital, Norwich, UK
- ⁵ Norwich Medical School, University of East Anglia, Norwich, UK
- ⁶Department of Rheumatology & Clinical Immunology, University Medical Center Utrecht, Utrecht, Netherlands

INTRODUCTION: In knee OA, radiographic JSW is used as a surrogate for MRI-measured cartilage thickness, though they often do not correlate well. Variations in positioning between radiography (weightbearing semi-flexion) and MRI (non-weight-bearing extension) may contribute to discrepancies.

OBJECTIVE: This study aimed to evaluate differences in 3D JSW and cartilage thickness distribution between these positions in knee OA patients.

METHODS: 21 symptomatic knee OA patients (KLG 2/3) were included. Exclusion criteria included prior knee surgery, MRI ineligibility, inability to stand unassisted for 15 minutes, or knee width > 15 cm (knee coil limit). A knee MRI protocol was performed using a 0.25T weightbearing MRI system (G-scan Brio, Esaote). A coronal 3D dual-echo SSFP sequence (SHARC) was acquired to obtain images with an isotropic resolution of 0.66mm in both extended and flexed knee positions under weight-bearing conditions by rotating the system to 81°. Both scans were repeated under non-weight-bearing conditions by rotating the system to a horizontal position (0°). Knee flexion angles were measured, and the femur and tibia bones were segmented in 3D Slicer. 3D models were exported to Stradview to measure the tibia-femur distance at each vertex as a measure of JSW. The models and data were registered to canonical surfaces in wxRegSurf and further analyzed in MATLAB using the Surfstat package for statistical parametric mapping to derive p-values corrected for multiple vertex-wise comparisons.

RESULTS: The average knee angles of the 21 patients were $7.4\pm3.7^{\circ}$ (extended) and $19.1\pm5.5^{\circ}$ (flexed). The average JSW ranged from 3.1 mm to 14.7 mm across patients (Figure 1). A significantly smaller JSW for weight-bearing vs non-weight-bearing conditions, particularly in the outer medial and posterior lateral tibia for extended positions, and in the posterior medial tibia for flexed positions, was seen (Figure 2). Flexion increased the JSW in the anterior tibia and decreased it in the posterior tibia, particularly laterally in weight-bearing positions.

CONCLUSION: JSW distribution in knee OA patients varies significantly depending on both weight-bearing and knee flexion angle, and radiographic JSW measurements may not accurately reflect the joint space in non-weight-bearing positions, such as those used in MRI, especially in the lateral compartment. Currently ongoing cartilage analyses will indicate to which extent these JSW variations are attributable to changes in cartilage thickness or meniscal positioning.

SPONSOR: NA

DICLOSURE STATEMENT: NA ACKNOWLEDGMENT: NA

CORRESPONDENCE ADDRESS: m.p.jansen-36@umcutrecht.nl

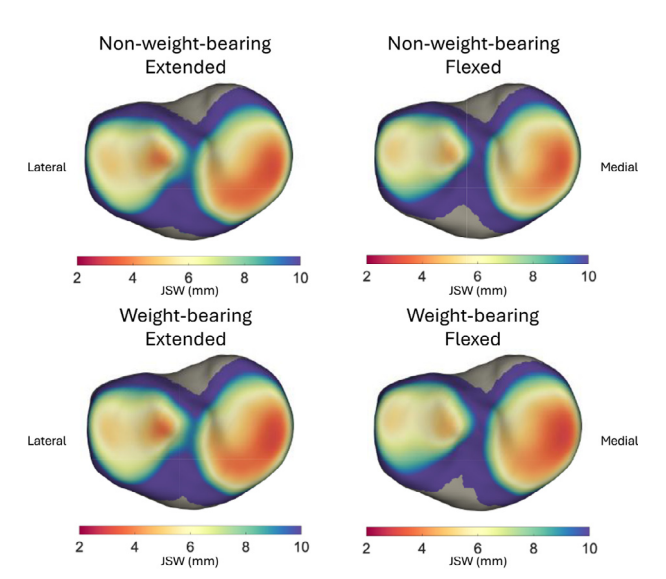


Figure 1: Joint space width distribution throughout the tibia for the four scan positions A superior view of the right tibia is shown, indicating the mesh-to-mesh tibia-femur distance in millimeters at each vertex. Values represent the average of 21 optients.

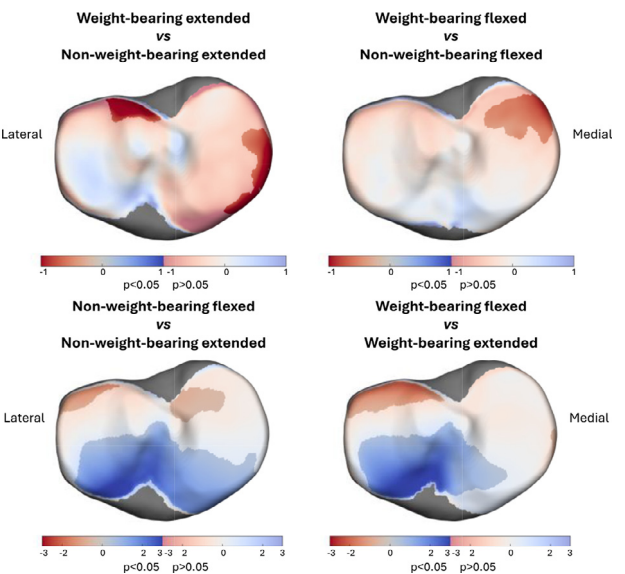


Figure 2. Difference in joint space width between scan positions. The top row figures indicate the difference in weight-bearing compared to non-weight-bearing in extended position (left) and flexed position (right); red colors indicate smaller distances during weight-bearing while blue colors indicate larger distances during weight-bearing. The bottom row figures indicate the difference in flexion compared to extension, both in non-weight-bearing position (left) and weight-bearing position (right); red colors indicate smaller distances during flexion while blue colors indicate larger distances during flexion. For all figures, saturated areas indicate statistically significant differences (p<0.05) and washed-out areas indicate changes taht are not statistically significant.

VALIDATING INTERNAL DENSITY CALIBRATION IN THE PROXIMAL HUMERUS TO ESTIMATE BONE STIFFNESS FOR STEMLESS SHOULDER ARTHROPLASTY

C.K.A. Stiles 1 , B.E. Matheson 2 , S.K. Boyd 2 , G.S. Arthwal 3 , J.P. Callaghan 1 , C.R. Dickerson 1 , N.K. Knowles 1

INTRODUCTION: Stemless humeral head components have emerged as a popular choice for patients undergoing shoulder arthroplasty for end-stage OA since they preserve non-diseased bone for future surgical revisions. Current pre-operative clinical measures are limited in assessing volumetric bone mineral density (vBMD) and mechanical properties in the region of bone directly supporting the component. Gold-standard phantom calibration, used to determine vBMD in CT images, is seldom utilized in clinical practice requiring alternative density measures for accurate vBMD. Internal density calibration using internal tissues as references has yet to be validated in the proximal humerus, and vBMD values have yet to be linked to finite element model (FEM) estimated stiffness in the context of stemless shoulder arthroplasty.

OBJECTIVE: 1) To determine the correlation between vBMD and finite element model (FEM) estimated stiffness 2) To determine the bias in internal density-based vBMD using three different referent tissue combinations compared to phantom-based vBMD, in the proximal humerus.

METHODS: Non-pathologic cadaveric single-energy CT images (n = 25), containing a $\rm K_2HPO_4$ phantom, were used to analyze a 10 mm region directly below the anatomic neck. Phantom-based vBMD was calculated for each region and used as input to image-based FEMs (ROD). Internal calibration used air (A), adipose (A), skeletal muscle (M), and cortical bone (C) to generate calibrated images from three different referent tissue combinations (AACM, ACM, AAC). Images were used to generate FEMs for each tissue combination. Results were compared between vBMD (mg $\rm K_2HPO_4/cc)$) and apparent modulus ($\rm E_{app}$) for each internal calibration tissue combination to the phantom calibration using linear regression. Bland-Altman analysis was used to determine the agreement between tissue combination and phantom calibration for estimated stiffness values ($\rm E_{app}$).

RESULTS: Linear regression (Figure 1) showed strong correlations between estimated stiffness and vBMD values for each calibration method (AACM $R^2 = 0.7524$; ACM $R^2 = 0.7723$; AAC $R^2 = 0.7384$; ROD $R^2 = 0.7854$) and slopes not significantly different from 1 (p < 0.001). Bland-Altman analysis (Figure 2) revealed the ACM tissue combination had the lowest error bounds in apparent modulus, compared to phantom-vBMD derived FEMs, with a mean bias of 80.15 MPa and 95% limits of agreement ranging from -164.55 to 324.86 MPa.

CONCLUSION: The results of this study support the use of internal density calibration as a valid method for using internal density calibrated images as input to FEMs for estimating stiffness in the proximal humerus. The ACM tissue combination provided the highest agreement

with the gold standard phantom calibration. This internal density calibration method may provide a solution for determining vBMD in patients undergoing shoulder arthroplasty for end-stage OA where phantoms are not present in the CT image. By linking bone density measures with estimated stiffness values, the mechanical properties of bone in the region supporting the humeral component are considered, which has the potential to improve preoperative planning for stemless shoulder arthroplasty. Next steps are to apply the ACM internal calibration method and estimated stiffness values in retrospective CT images from patients who have undergone shoulder arthroplasty for end-stage OA (n = 88) to link surgical outcomes to stiffness measures.

SPONSOR: Arthritis Society Canada Stars Career Development Award (#23-0079)

DICLOSURE STATEMENT: None

CORRESPONDENCE ADDRESS: ckastile@uwaterloo.ca

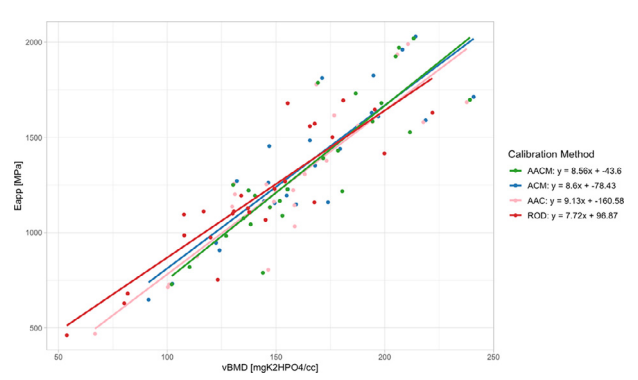


Figure 1: Linear regression showing correlation between estimated stiffness [MPa] and vBMD [mgK2HPO4/cc] for each calibration method.

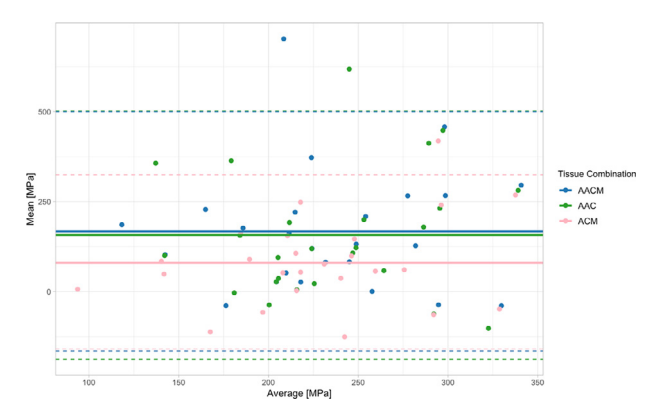


Figure 2: Bland-Altman plot for estimated stiffness [MPa] values for internal calibration according to tissue combination vs. phantom calibration. Dashed lines indicate \pm 1.96 standard deviations (SD) of the mean (solid line).

¹ Kinesiology and Health Sciences, University of Waterloo, Waterloo, ON, Canada

² McCaig Institute for Bone and Joint Health, University of Calgary, AB, Canada

³ Roth | McFarlane Hand and Upper Limb Centre, London, ON, Canada

FINITE ELEMENT MODELING OF IN VIVO HUMAN KNEE BONES USING HR-PQCT: EFFECTS OF BOUNDARY CONDITIONS AND MODEL CONFIGURATION ON PREDICTED STRAIN ENERGY DENSITY

C.E. Stirling 1,2, S.K. Boyd 1,2,3

INTRODUCTION: Bone strength assessment is essential in musculoskeletal research for understanding bone mechanics under loading. High-resolution peripheral quantitative computed tomography (HR-pQCT) and micro-finite element (μ FE) analysis provide insights into bone strength. While widely used for the distal radius and tibia, knee joint modeling is more complex due to interactions of bone, cartilage, and soft tissue, and the significantly larger size of the joint. This study aims to develop a knee bone μ FE model using HR-pQCT data, focusing on boundary conditions and material properties affecting strain energy density (SED) in the femur and tibia.

OBJECTIVE: 1) Investigate the influence of boundary conditions on stress distribution in knee joint finite element models. 2) Evaluate how the elastic modulus of load transfer material influences bone mechanics.

METHODS: HR-pQCT scans of a 35-year-old female with a recent ACL injury were performed on the knee joint in full extension. A boundary material was applied to simulate a transitional layer between the bone and surrounding tissues. The material was generated using a voxelbased approach that mapped to the bone shape by extruding filled slices along the Z-axis (Figure 1). Finite element models with uniaxial compression boundary conditions were generated with two configurations of boundary materials: bone-shaped boundary material, which adapts to the shape of the largest epiphysis of the bone, or rectangular boundary materials, which create a square-shaped material around the minimum/maximum bounds of the epiphysis bone regions. Both types of models were solved with a range of boundary material elastic moduli (2000, 2500, 3000, 3500 MPa) and lengths extending from the bone surface of 1, 3, 5, and 7 mm. The primary output was model SED in subchondral regions of interest (ROI) to test the boundary material's impact on mechanical predictions.

RESULTS: Tibial models contained 500 million degrees of freedom, and femur models included 900 million. As load transfer material length increased beyond 1 mm, the mean SED within ROIs initially decreased,

then increased beyond 3 mm—suggesting an optimal load transfer material length between 3 mm and 7 mm. SED skewness and kurtosis increased with material length, indicating more heterogeneous stress distributions. Longer segments (e.g., 5-7 mm) substantially increased computational cost, highlighting a trade-off between the extent of material used for load transfer and simulation efficiency. The bone-shaped boundary material method was more computationally efficient and produced less variability as material length increased. As the elastic modulus of the load transfer material increased, average SED values also increased, particularly with longer PMMA segments.

CONCLUSION: We found that load transfer material length and elastic modulus significantly influence tibial stress distribution, with an optimal material length between 3 mm and 5 mm balancing mechanical performance and computational efficiency.

SPONSOR: Canadian Institutes of Health Research (CIHR) Grant [PJT 162189].

DICLOSURE STATEMENT: The authors declare that they have no conflicts of interest.

ACKNOWLEDGMENT: The authors thank the technicians at the Centre for Mobility and Joint Health, University of Calgary.

CORRESPONDENCE ADDRESS: callie.stirling@ucalgary.ca

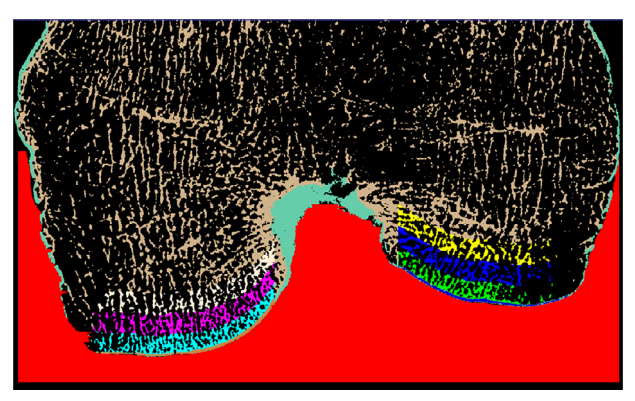


Figure 1: Segmented regions of the subchondral bone used for μ FE analysis. HR-pQCT-based segmentation masks include cortical bone, trabecular bone, and subregions of the subchondral bone. A synthetic region representing boundary material is also shown, constructed by extruding from the most distal point of the femur along the Z-axis. This region simulates the transitional contact area during mechanical loading.

¹ Department of Biomedical Engineering, Schulich School of Engineering, University of Calgary, Calgary, AB, Canada

 $^{^2\,\}text{McCaig}$ Institute for Bone and Joint Health, Cumming School of Medicine, University of Calgary, Calgary, AB, Canada

³ Department of Radiology, Cumming School of Medicine, University of Calgary, Calgary, AB, Canada

LONGITUDINAL PROGRESSION OF TRAUMATIC BONE MARROW LESIONS FOLLOWING ANTERIOR CRUCIATE LIGAMENT INJURY: ASSOCIATIONS WITH KNEE PAIN AND CONCOMITANT INJURIES

C.E. Stirling 1,2, N. Pavlovic 1,2, S.L. Manske 2, R.E.A. Walker 2,3, S.K. Boyd 1,2,3

INTRODUCTION: Traumatic BM lesions occur in about 80% of ACL injuries, typically caused by tibia-femur collisions, indicating significant joint damage and an increased risk of post-traumatic OA (PTOA). MRI is effective for detecting BM lesions, but quantitative assessment of their volume and distribution over time can help identify PTOA risk factors. While BM lesions typically resolve over time, their relationship with knee pain and functional outcomes remains unclear.

OBJECTIVE: This study aimed to investigate the longitudinal prevalence, characteristics, and progression of BM lesions following ACL injury, with a focus on their association with knee pain, ligamentous injuries, and meniscal tears.

METHODS: This prospective observational study analyzed data from 100 individuals (68 females, 32 males) with acute ACL tears in previously uninjured knees. MRI scans were obtained within 6 weeks of their injury using a 1.5-T MR scanner (GE OptimaMR430S, 1.5T, Waukesha, WI, USA). The imaging protocol included T2-weighted fat-suppressed fast spin echo images [TR/TE, 4300/56 ms; echo train length, 11; matrix, 320×256; field of view, 140 mm; slice thickness, 3.5 mm; gap, 0.3 mm;] for evaluating BM lesions. BM lesion volume quantified using a previously developed automated segmentation tool. Knee pain and symptoms were assessed using the Knee Injury and Osteoarthritis Outcome Score (KOOS). Statistical analyses included paired t-tests, Mann-Whitney U tests, Pearson's Chi-squared test, and Spearman's rank

correlation. Multiple comparisons were corrected using the Benjamini-Hochberg procedure to control for false discovery rate. A subset of 77 participants completed follow-up KOOS surveys, and 19 participants who did not undergo ACL reconstruction had follow-up MRIs at one year.

RESULTS: BM lesions were present in 95% of participants (N=100), predominantly in the lateral tibial plateau and lateral femoral condyle. Males exhibited significantly higher BM lesion volumes than females (p=0.03). Significant associations were identified between medial collateral ligament tears and both lateral collateral ligament (p=0.01) and posterior cruciate ligament tears (p < 0.01). The BM lesion volume at baseline was negatively correlated with KOOS Symptoms at baseline (r=-0.270, p=0.01). Longitudinal analyses revealed strong predictive relationships between baseline KOOS scores and future outcomes, with baseline KOOS Pain predicting follow-up Symptoms (r=0.500) and Pain (r=0.542). At the one-year follow-up, BM lesions in non-surgical participants (N=19) showed substantial resolution (mean change=-96.7%). Surgery had no significant impact on pain or functional outcomes compared to non-surgical participants.

CONCLUSION: BM lesion volume had only a weak association with knee pain after ACL injury, but longitudinal KOOS analyses revealed consistent associations between baseline symptoms and future outcomes.

SPONSOR: Canadian Institutes of Health Research (CIHR) Grant [PJT 162189].

DICLOSURE STATEMENT: The authors declare that they have no conflicts of interest.

ACKNOWLEDGMENT: The authors are grateful for efforts from the Acute Knee Injury Clinic at the University of Calgary, Banff Sports Medicine, and Innovative Sports Medicine.

CORRESPONDENCE ADDRESS: callie.stirling@ucalgary.ca

¹ Department of Biomedical Engineering, Schulich School of Engineering, University of Calgary, Calgary, AB, Canada

² McCaig Institute for Bone and Joint Health, Cumming School of Medicine, University of Calgary, Calgary, AB, Canada

³ Department of Radiology, Cumming School of Medicine, University of Calgary, Calgary, AB, Canada

STATISTICAL SHAPE MODELING OF COMPUTED TOMOGRAPHY-DERIVED CARPAL BONES REFLECTS SCAPHOLUNATE INTEROSSEOUS LIGAMENT INJURY

T.P. Trentadue 1,2, A.R. Thoreson 1, K.D. Zhao 1

INTRODUCTION: Injuries to the scapholunate interosseous ligament (SLIL) are among the most common upper extremity injuries. Early, accurate diagnosis is essential to minimize progression of scapholunate advanced collapse (SLAC)-pattern radiocarpal OA ¹. SLIL injuries widen the SL interval and contribute to the scaphoid palmar flexion and lunate extension of dorsal intercalated segment instability ². Radiographs are limited by carpal overlap and sensitivity to forearm pronosupination angle ³. Volumetric imaging-derived three-dimensional (3D) bone models can be used in statistical shape modeling (SSM) to compare joint alignment and morphology, mitigating challenges of planar imaging.

OBJECTIVE: The objective of this study is to compare 3D carpal alignment in wrists with and without SLIL injury using a multi-level (shape and alignment), multi-object (three bone) (MLMO) SSM. We hypothesize that (1) there will be differences in the 3D morphology of the radius, scaphoid, and lunate between wrists with versus without SLIL injury and (2) these differences will affect joint space width.

METHODS: Twenty-one participants (14.3% female, median [25th-75th percentile] age 42.0 [26.8-50.0] years, 57.1% dominant hand injury) with arthroscopically-confirmed, unilateral SLIL injuries were recruited to a prospective clinical trial evaluating the role of CT in detecting SLIL injuries 4. Bilateral wrist CT images were acquired (SOMATOM Force and NAEOTOM Alpha, Siemens Healthineers, Germany) using published acquisition parameters 4. The radius, scaphoid, and lunate were segmented from static CT with semi-automated algorithms (Analyze Pro, Mayo Foundation for Medical Education and Research, Rochester, MN). Segmentation maps were used to generate 3D stereolithography meshes of each bone. Left-handed images were reflected to right-handed anatomies. MLMO SSM was performed (ShapeWorks v6.3.2 5) 6. Linear discriminant analysis (LDA), a form of supervised machine learning for dimensionality reduction and class separation, was used to compare uninjured and injured morphologies 7. Discriminant scores between wrists were compared with a Wilcoxon signed rank test. SSM-derived bone surface particles of the mean uninjured and mean injured bones were used to calculate interosseous proximities, a metric approximating joint space width, at the SL interval and radioscaphoid joint using k-nearest neighbor methods within distance thresholds of 5.0 mm and 2.5 mm, respectively ^{8,9}. Interosseous proximity distributions were compared using two-sided Kolmogorov-Smirnov (KS2) tests. Significance was defined as α =0.05 with Bonferroni corrections as appropriate.

RESULTS: There was a significant difference in LDA joint shape and alignment discriminant scores between uninjured (-1.23 [-2.07-0.17]) and injured (1.45 [-1.20-3.31]) wrists (z=-3.146, p=0.002). There was a significant difference between uninjured versus injured scapholunate (KS2 =0.54, p<0.001) but not radioscaphoid (KS2 =0.08, p=0.894) proximity distributions (Figure 1).

CONCLUSION: SSM, a robust methodology to analyze 3D anatomies, revealed differences in scaphoid and lunate alignment between uninjured and injured wrists, with injured-sided wrists having descriptively more palmar-flexed scaphoid and extended lunate bones. These alignment differences were reflected in scapholunate but not radioscaphoid mean interosseous proximity distributions. CT-derived 3D osseous anatomies reflect injury, with implications for detection and intervention before SLAC OA progression.

REFERENCES

- 1. Watson HK, Ballet FL. The SLAC wrist: scapholunate advanced collapse pattern of degenerative arthritis. *J Hand Surg Am.* May 1984;9(3):358-65. doi:10.1016/s0363-5023(84)80223-3
- Linscheid RL, Dobyns JH, Beabout JW, Bryan RS. Traumatic instability of the wrist. Diagnosis, classification, and pathomechanics. *J Bone Joint Surg Am*. Dec 1972;54(8):1612-32.
- 3. Campbell M, Schurmans G, Suh N, Garvin G, Lalone E. The sensitivity of the scapholunate interval and bony landmarks to wrist rotation on posteroanterior radiographs. *Hand (N Y)*. May 30 2024:15589447241255705. doi:10.1177/15589447241255705
- 4. Trentadue TP, Thoreson AR, Lopez C, Breighner RE, An KN, Holmes DR, 3rd, Moran SL, Kakar S, Murthy NS, Leng S, Zhao KD. Detection of scapholunate interosseous ligament injury using dynamic computed tomography-derived arthrokinematics: A prospective clinical trial. *Med Eng Phys.* Jun 2024;128:104172. doi:10.1016/j.medengphy.2024.104172
- Cates J, Elhabian S, Whitaker R. ShapeWorks: particle-based shape correspondence and visualization software. In: Zheng G, Li S, Székely G, eds. Statistical Shape and Deformation Analysis: Methods, Implementation and Applications. Academic Press; 2017:257-298:chap 10.
- Trentadue TP, Thoreson A, Lopez C, Breighner RE, Leng S, Holmes DR, 3rd, Kakar S, Rizzo M, Zhao KD. Morphology of the scaphotrapeziotrapezoid joint: A multi-domain statistical shape modeling approach. *J Orthop Res.* Nov 2024;42(11):2562-2574. doi:10.1002/jor.25918
- Trentadue TP, Thoreson A, Lopez C, Breighner RE, Leng S, Kakar S, Rizzo M, Zhao KD. Sex differences in photon-counting detector computed tomography-derived scaphotrapeziotrapezoid joint morphometrics. Skeletal Radiol. Feb 5 2025;doi:10.1007/s00256-024-04863-5
- 8. Moeller TB. Normal Findings in Radiography. Thieme; 2000.
- Schimmerl-Metz SM, Metz VM, Totterman SM, Mann FA, Gilula LA. Radiologic measurement of the scapholunate joint: implications of biologic variation in scapholunate joint morphology. *J Hand Surg Am*. Nov 1999;24(6):1237-44. doi:10.1053/jhsu.1999.1237

SPONSOR: US NIH R01 AR071338, F31 AR082227, T32 AR056950, T32 GM065841, T32 GM145408. **DISCLOSURE STATEMENT:** The authors have no relevant disclosures.

ACKNOWLEDGMENT: We thank Kai-Nan An, Ph.D., Ryan Breighner, Ph.D., David Holmes III, Ph.D, Shuai Leng, Ph.D., Cesar Lopez, M.S., Naveen Murthy, M.D., Steven Moran, M.D., Sanjeev Kakar, M.D., and Nikkole Weber, R.T.(R)(CT) for their invaluable contributions to the clinical trial.

CORRESPONDENCE ADDRESS: trentadue.taylor@mayo.edu

¹ Assistive and Restorative Technology Laboratory, Mayo Clinic, Rochester, MN, USA
² Mayo Clinic Medical Scientist Training Program, Mayo Clinic, Rochester, MN, USA

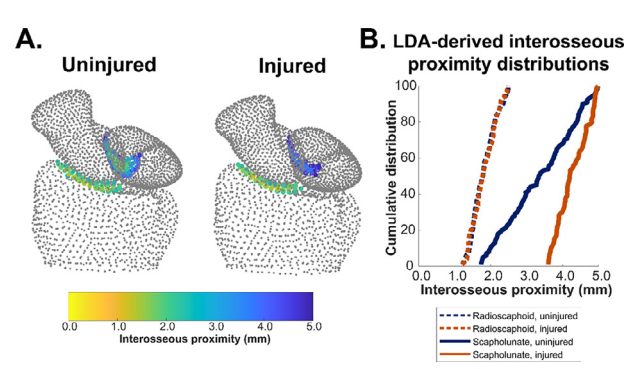


Figure 1. (A) Multi-level, multi-object (MLMO) statistical shape modeling (SSM)-derived mean scaphoid, lunate, and radius bones, viewed from a dorsal-radial perspective, by injury status. Compared to the uninjured wrist, the scaphoid is more palmar-flexed and the lunate more extended in the injured wrist. Interosseous proximities at the scapholunate interval and radioscaphoid joint within distance thresholds of 2.5 and 5.0 mm, respectively, are colorized by the k-nearest neighbors-derived distances. (B) Interosseous proximity distributions for the mean uninjured (blue) and injured (orange) scapholunate intervals (solid lines) and radioscaphoid joints (dashed lines). LDA: linear discriminant analysis.

REPEATABILITY OF CT OSTEOARTHRITIS KNEE SCORE (COAKS) MULTICOM-PONENT MEASURES

T.D. Turmezei ^{1,2}, A. Boddu ¹, N.H. Degala ³, J.A. Lynch ⁴, N.A. Segal ³

- ¹ Norfolk and Norwich University Hospital, Norwich, UK
- ² University of East Anglia, Norwich, UK
- ³ University of Kansas Medical Center, Kansas City, KS, USA
- ⁴ University of California San Francisco, San Francisco, CA, USA

INTRODUCTION: The CT Osteoarthritis Knee Score (COAKS) is a semiquantitative system for grading structural disease features in knee OA from weight bearing CT (WBCT). Previous work has demonstrated excellent inter- and intra-observer reliability of COAKS with the aid of a feature scoring atlas, but test-retest repeatability has not yet been evaluated. There is growing interest in multicomponent measures in knee OA imaging research because they may provide granularity in structural feature evaluation, in particular with respect to study baseline stratification and monitoring progression. The multi-feature and multi-compartment nature of COAKS means that it could provide novel insights into OA morphotypes and structural disease progression if found to be robust.

OBJECTIVE: To evaluate test-retest agreement of COAKS multicomponent scores based on WBCT imaging.

METHODS: 14 individuals recruited and consented at the University of Kansas Medical Center had baseline and follow-up WBCT imaging suitable for analysis. Participants were (mean \pm SD) 61.3 \pm 8.4 years old, with BMI 30.7 \pm 4.3 kg/m² and had a male:female ratio of 8:6. All scanning was performed on a single XFI WBCT scanner (Planmed Oy, Helsinki, Finland) with the mean \pm SD interval between baseline and follow-up attendances 14.9 \pm 8.1 days. A SynaflexerTM device was used to standardize knee positioning during scanning. Imaging acquisition parameters were 96 kV tube voltage, 51.4 mA tube current, 3.5 s exposure time. A standard bone algorithm was applied for reconstruction with 0.3 mm isotropic voxels and a 21 cm vertical scan range. All scans were anonymised prior to analysis both according to the individual and imaging attendance. All knees were reviewed for COAKS by an experienced musculoskeletal radiologist (T.D.T.). Scores were recorded in a cloud-based file on Google Sheets (alongside the feature atlas in Google Docs) and read by custom MATLAB scripts to generate baseline versus follow-up difference plots and intraclass correlation coefficients for absolute agreement from a single observer, Shrout-Fleiss ICC(3,1). Scores for individual COAKS features (JSW, osteophytes, subchondral cysts, subchondral sclerosis) were combined across compartments. Compartment scores (medial tibiofemoral, lateral tibiofemoral, patellofemoral, proximal tibiofibular) were combined across features. Multicomponent scores were also summated for the whole tibiofemoral compartment (medial-lateral combined) and from across the whole knee joint.

RESULTS: ICC values were excellent (>0.81) for all multicomponent scores apart from subchondral sclerosis combined across all compartments (0.69, 0.43-0.84) and all features combined at the proximal tibiofibular joint (0.65, 0.38-0.82). Best agreement was seen for osteophytes combined across all compartments (0.93, 0.85-0.96) (Figure 1), all features combined at the medial tibiofemoral compartment (0.95, 0.90-0.98) and the lateral tibiofemoral compartment (0.97, 0.94-0.99). Full ICC results are given in Table 1. ICCs for all features combined across the whole tibiofemoral compartment (0.93, 0.86-0.97) (Figure 2) and across the whole knee joint (0.90, 0.79-0.95) were also near-perfect with data values.

CONCLUSION: These data support excellent agreement for COAKS multicomponent scores by compartment, by feature, and as a whole. These results suggest that a multicomponent approach could offer sensitivity

in distinguishing morphotypes and monitoring structural progression as personalised medicine approaches become more realistic in developing treatment strategies for OA. Having established the excellent repeatability of a multicomponent COAKS approach, it will now be essential to validate.

SPONSOR: None.

DISCLOSURE STATEMENT: NS is a consultant for Trice Medical, Arthrex, and Pacira Biosciences. TT is the director of KNEE3D Ltd. TW is director of Minogame Ltd.

ACKNOWLEDGEMENT: None.

CORRESPONDENCE ADDRESS: tom@turmezei.com

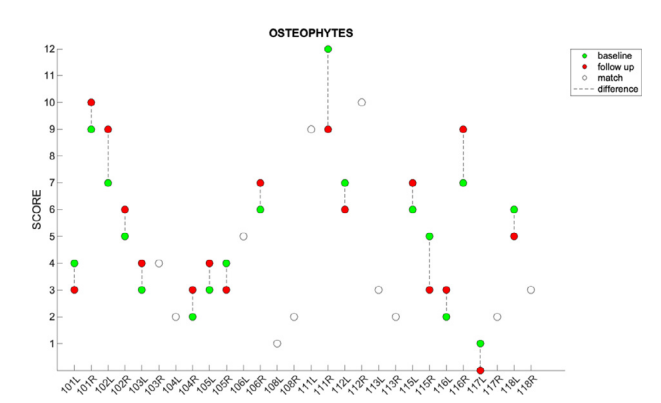


Figure 1.

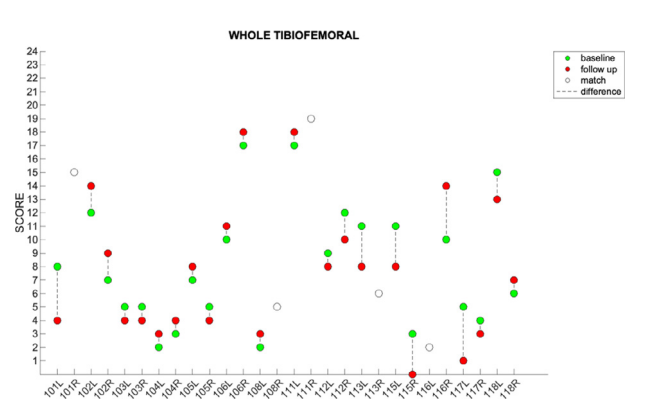


Figure 2.

Table 1.

COAKS composite	Mean ± SD at baseline	Mean \pm SD at follow-up	ICC(3,1) + 95%CI
Joint space width	3.8 ± 1.7	3.9 ± 1.7	0.82 (0.65,0.91)
Osteophytes	4.7 ± 2.9	4.8 ± 2.9	0.93 (0.85,0.96)
Cysts	2.6 ± 2.5	2.3 ± 2.1	0.86 (0.72,0.93)
Sclerosis	3.7 ± 2.1	3.6 ± 2.4	0.69 (0.43,0.84)
Medial tibiofemoral	5.3 ± 3.2	5.0 ± 3.5	0.95 (0.90,0.98)
Lateral tibiofemoral	3.1 ± 2.4	3.0 ± 2.5	0.97 (0.94,0.99)
Patellofemoral	5.2 ± 2.9	5.1 ± 2.9	0.88 (0.76,0.94)
Proximal tibiofibular	1.3 ± 1.6	1.5 ± 1.4	0.65 (0.38, 0.82)
Whole tibiofemoral	8.3 ± 5.0	8.0 ± 5.4	0.93 (0.86,0.97)
All features	14.8 ± 7.5	14.6 ± 7.6	0.90 (0.79,0.95)

OSTEOARTHRITIS IS A MULTI-JOINT DISEASE. OR IS IT?

M.A. van den Berg¹, E. Panfilov², J.H. Krijthe³, R. Agricola¹, A. Tiulpin²

- ¹ Erasmus Medical Center, Rotterdam, The Netherlands
- ² Research Unit of Health Sciences and Technology, University of Oulu, Finland
- ³ Delft University of Technology, Delft, The Netherlands

INTRODUCTION: OA frequently affects both the hip and knee joints; however, most prognostic studies evaluate these joints in isolation. Given the biomechanical and systemic connections between them, this joint-specific focus may overlook important patterns of disease progression. A better understanding of combined hip and knee OA progression could support the development of more accurate prediction models and treatment strategies.

OBJECTIVE: To determine whether combined hip and knee OA progression exhibits a distinct phenotype compared to isolated OA progression.

METHODS: This study used the OAI data, which comprises data from participants aged 45-79 years at risk of developing knee OA. The dataset features bilateral posteroanterior knee radiographs and standardized weight-bearing anteroposterior pelvic radiographs obtained at the baseline and 48-month follow-up visits. Minimal JSW (mJSW) was measured manually for knees and automatically for hips. OA progression was defined as JSN of \geq 0.5 mm in either hip or \geq 0.7 mm in either knee. Participants with no JSN in any of the four joints at the 48-month follow-up were excluded. The selected participants were classified as having isolated (either hip or knee) or combined (both hip and knee) progression. A logistic regression model incorporating clinical and structural baseline features was used to explore associations with combined progression compared to isolated progression. Baseline radiographic OA (ROA) status of each of the four joints was classified as no ROA (0), early ROA (1) and definite ROA (2) based on the KLG and modified Croft grades. Adjusted odds ratios (aOR) and their 95% confidence intervals, estimated using bootstrapping with 10,000 iterations, and the goodness-of-fit of the model were assessed.

RESULTS: Among the 1,190 included participants with any ROA progression (mean age 61.5 ± 8.8 years; BMI 29.1 ± 4.5 ; 55.1% female), 281 (23.6%) showed combined ROA progression. The co-occurrence of baseline hip and knee ROA grades was reviewed descriptively (Table 1). The observed relatively small prevalence of combined progression in this population prevented including these ROA status interaction effects within our model. The logistic model showed improved fit over an intercept-only model (likelihood ratio test, p < 0.0001), and acceptable goodness-of-fit (Hosmer-Lemeshow test, p = 0.40). Several baseline features were associated with higher odds of combined progression compared to isolated, including older age, female sex, varus knee alignment in the right knee, higher mJSW in the hip, and having definite ROA in the left hip (Figure 1). Interestingly, having ROA in the right hip or valgus knee alignment in the left knee would decrease the odds of combined progression.

CONCLUSION: Our findings suggest that combined hip and knee OA progression may represent a distinct clinical phenotype with identifiable characteristics. While the model showed statistically significant associations and demonstrated adequate fit, these results should be interpreted cautiously. Larger and more diverse datasets are needed to further validate these findings and investigate the heterogeneity of multi-joint OA progression.

SPONSOR: The Dutch Arthritis Society (grant no. 18-2-203 and 21-1-205), the Dutch Research Council (NWO Veni grant scheme no. 09150161910071) and the Erasmus MC, University Medical Center, Rotterdam (Erasmus MC Fellowship). 6GESS Profiling Research Programme (Research Council of Finland, project 336449).

DISCLOSURE STATEMENT: We have nothing to disclose.

ACKNOWLEDGMENT: We would like to thank the staff, team members, and all participants of OAI for their contribution.

CORRESPONDENCE ADDRESS: m.a.vandenberg@erasmusmc.nl

Table 1. Baseline co-occurrence of ROA severity in hip and knee joints, as well as the prevalence of combined JSN progression when definite ROA is present in both of the compared joints

	No Diff	erence	e One Grade Two Grade Difference Difference														Cramers' Combin V progres both jo definite	
	N	%	N	%	N	%	-	N	%									
Right Hip vs Left Hip	1,009	85%	146	12%	35	3%	0.48	8	1%									
Right Knee vs Left Knee	645	54%	389	33%	156	13%	0.31	151	13%									
Right Hip vs Right Knee	436	37%	497	42%	257	22%	0.06	9	1%									
Left Hip vs Left Knee	432	36%	472	40%	286	24%	0.01	14	1%									
Right Hip vs Left Knee	433	36%	468	39%	289	24%	0.04	9	1%									
Left Hip vs Right Knee	444	37%	499	42%	247	21%	0.05	18	2%									

ROA: Radiographic OA. ROA status was defined as no ROA (0), early ROA (1) and definite ROA (2)

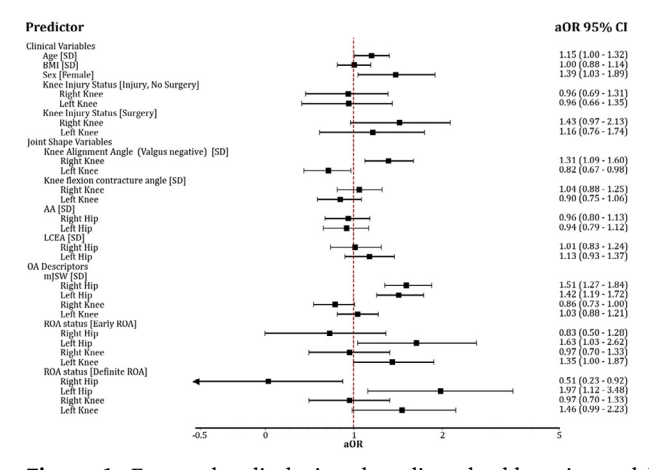


Figure 1. Forest plot displaying the adjusted odds ratios and bootstrapped 95% confidence intervals for the combined OA progression group compared to the isolated OA progression group x-axis is in logarithmic scale. AA: alpha angle, aOR: adjusted odds ratio, BMI: Body Mass Index, CI: confidence interval, LCEA: lateral center edge angle, mJSW: minimal JSW, ROA: radiographic OA

AUTOMATIC EXTRACTION OF KNEE ALIGNMENT AND MORPHOLOGY MEASURES FROM 3D MODELS IN A YOUNG-ADOLESCENT OPEN-POPULATIONS COHORT STUDY

R. van Paassen 1 , N. Tumer 2 , J. Hirvasniemi 1,2 , E.M. Macri 1 , I. Bosch 1 , E. Langius 1 , A. Roos 1 , T.M. Piscaer 1 , A.A. Zadpoor 2 , S.M.A. Bierma-Zeinstra 1 , E.H.G. Oei 1 , M. van Middelkoop 1

INTRODUCTION: Proper knee alignment is crucial for knee joint function. Little is known about knee alignment and morphology during growth; most research and current normal values were determined in adults. Imaging-based landmarks have to be identified to determine knee alignment parameters such as bisect offset or patellar translation. Currently, these landmarks are often determined manually on 2D image slices, which is time-consuming and can lead to interrater variability. Automatic extraction of these landmarks in 3D could help overcome these inconsistencies.

OBJECTIVE: To determine the concurrent validity of automatically extracted alignment parameters and morphology measures from two previously developed 3D statistical shape models (SSMs) - one for the patella and one for the distal femur- and to establish normative values and evaluate sex-based differences in these parameters among a young adolescent population.

METHODS: We included data from 1912 participants (aged 14.1 ± 0.67) who underwent knee MRI in the Generation R study, a large prospective population cohort study that follows children from fetal life until adulthood. MRI was performed using a 3.0T MRI (Discovery MR750w, GE Healthcare, Milwaukee, WI, USA), with both knees fully extended, using a water excitation Gradient Recalled Acquisition in Steady State sequence. Using a combined multi-atlas and appearance-based segmentation technique, 3638 patellae and 3355 femora were segmented from MRI scans. The 3D reconstructed bone samples derived from these segmentations were used to create two separate SSMs: one for the patella and one for the distal femur. Six patella and ten femur landmarks were annotated on the mean patella and femur shapes. Using the automatically established correspondences across bone samples during the SSMs generation, the landmarks identified on the mean bone shapes were transferred to the individual bone samples used to build the SSMs. One researcher manually annotated 30 randomly selected MRIs twice (15 boys and 15 girls) to determine the reliability of landmarks automatically extracted from the SSMs. Using these landmarks, we calculated 17 alignment parameters and morphology measurements: bisect offset; epicondylar width; femoral notch depth; femoral notch width; medial and lateral inclination angles; lateral patellar tilt; medial and lateral anterior-posterior (AP) length to epicondylar width ratio; patellar lateral translation; patellar length, thickness, and width; patellar tilt angle; sulcus angle; sulcus depth; and trochlear angle. Inter-method concurrent validity between the manually annotated parameters (mean of the two annotations) and automatically calculated parameters was determined using the intraclass correlation coefficient (ICC) for absolute agreement, calculated with a two-way mixed-effects model for single rater measurements. For alignment and morphology parameters with an ICC > 0.75, reference values (mean (SD)) and differences between these parameters in boys and girls were determined using a two-tailed t-test.

RESULTS: Six of the 17 calculated parameters, using landmarks from the SSMs, demonstrated reliable agreement, with an ICC>0.75 for bisect offset (ICC=0.86), epicondylar width (ICC=0.91), patellar width (ICC=0.75), femoral notch width (ICC=0.82), medial (ICC=0.88) and lateral condyle thickness to epicondylar width ratio (ICC=0.85). All six alignment parameters differed significantly between boys and girls (Table 1).

CONCLUSION: Only about a third of the alignment parameters and morphology measures calculated could be determined reliably. One reason might be that the position of two specific landmarks, i.e., the trochlear groove's deepest point and the patella's most posterior point, strongly influences the calculated angles. In 2D analyses, the deepest point of the trochlear groove is annotated on the same slice as the most anterior and posterior points of the femoral condyles. In 3D, these landmarks were not annotated on a 2D slice but in 3D space, resulting in different angles and distances. The low ICCs may not necessarily indicate that the 3D measurements are incorrect; they might even be more accurate; they are not directly comparable to the current clinically used 2D measurements on conventional imaging.

SPONSOR: Dutch Arthritis association (21-1-204).

DISCLOSURE STATEMENT: None

CORRESPONDENCE ADDRESS: r.vanpaassen@erasmusmc.nl

Table 1: Intraclass correlation coefficients (ICCs > 0.75) and 95% confidence intervals (CIs) for knee alignment parameters and morphology measures, along with sex-based statistical comparisons. A significance threshold of p < 0.05 was used

Parameter	ICC [95% CI]	Total study sample* mean(SD)	Boys ** mean(SD) [95% CI]	Girls *** mean(SD) [95% CI]	<i>p</i> -value
Bisect offset [%]	0.86 [0.73;0.93]	65.63 (11.26)	63.78 (10.62) [45.91; 88.21]	67.10 (11.54) [48.19; 92.88]	<0.001
Epicondylar width [mm]	0.91 [0.00;0.98]	74.78 (5.45)	78.53 (5.08) [67.73; 87.93]	71.78 (3.34) [65.17; 79.17]	<0.001
Patellar width [mm]	0.75 [- 0.07;0.93]	38.14 (3.21)	39.42 (3.43) [32.69; 46.09]	36.99 (2.49) [32.16; 41.79]	<0.001
Femoral notch width [mm]	0.82 [0.66; 0.91]	19.67 (1.88)	21.11 (1.50) [18.39; 24.13]	18.51 (1.24) [16.27; 21.08]	<0.001
Medial condyle thickness (AP) to epicondylar width ratio	0.88 [0.71;0.95]	0.76 (0.03)	0.74 (0.03) [0.69; 0.80]	0.78 (0.03) [0.72; 0.84]	<0.001
Lateral condyle thickness (AP) to epicondylar width ratio	0.85 [0.71;0.93]	0.80 (0.03)	0.78 (0.03) [0.72; 0.84]	0.82 (0.03) [0.76; 0.88]	<0.001

^{*} N=3691 knees included in the total study sample, ** N=1755 knees from boys, *** N=1936 knees from girls.

¹ Erasmus MC University Medical Center Rotterdam, Rotterdam, The Netherlands ² Delft University of Technology, Delft, The Netherlands

CHANGES IN JOINT SPACE WIDTH ONE YEAR AFTER WEIGHT LOSS SURGERY

L.T. Vuononvirta 1 , T.D. Turmezei 2 , T.J. Frondelius 1 , M.T. Nevalainen 1,3,5,7 , S.J.O. Rytky 1,3 , J.H. Määttä 1 , S.A. Meriläinen 4,6 , P.P. Lehenkari 5,6 , M.A.J. Finnilä 1,7

INTRODUCTION: Weight loss—either conservative or surgical—can slow OA progression. Traditional radiography has limited sensitivity in detecting early or subtle joint changes induced either by OA or weight loss. The limitations of conventional radiography can be alleviated by using CT. Weight-bearing cone-beam CT -imaging can be used to detect the OA induced changes in JSW. These changes can be evaluated by using joint space mapping (JSM), a novel CT-based technique, which enables quantitative 3D assessment of JSW with high spatial resolution.

OBJECTIVE: To assess longitudinal changes in left knee joint space width following Roux-en-Y gastric bypass (RYGB) surgery using weight-bearing cone-beam CT, expecting that substantial weight loss would be associated with joint space widening.

METHODS: This one-year longitudinal study included 86 morbidly obese subjects (72 F, 14 M), of whom 45 underwent RYGB surgery and 41 served as a control group following conservative weight loss. Subgroup analyses were stratified by weight loss success. Unilateral weight-bearing cone-beam CT scans of the left knee in full extension were acquired at baseline and 1-year follow-up using Planmed Verity (voxel size: $0.2 \, \mathrm{mm}^3$; $801 \times 801 \times 651$; $96 \, \mathrm{kVp}$, $12 \, \mathrm{mA}$). Images were processed in DICOM format. JSM was performed using Stradview (v7.21) for segmentation and measurement of JSW, and WxRegSurf (v23) for coregistration to a canonical surface. Subregions were manually defined based on standard tibial cartilage thickness maps. Statistical parametric mapping (SPM) was conducted using MATLAB (2022) and SurfStat. Group differences in subregional mean JSW changes were assessed using two-sample t-tests.

RESULTS: In the control group, BMI change was $0.0 \pm 5.8 \text{ kg/m}^2$. RYGB patients with successful weight loss ($\geq 20\%$ BMI reduction) showed a mean BMI change of $-11.2 \pm 8.4 \text{ kg/m}^2$, while the unsuccessful subgroup had a change of $-5.7 \pm 8.1 \text{ kg/m}^2$. Regarding JSW, both surgical subgroups exhibited a general trend toward joint space redistribution in the knee (Figure 1). However, subregional analysis revealed significant JSW widening (p < 0.05) in the successful group, particularly in the central region ($+0.13 \pm 0.05 \text{ mm}$) and the medial quarter ($+0.22 \pm 0.23 \text{ mm}$) of the medial tibiofemoral compartment (Figure 2). Nonsignificant narrowing was seen anteriorly in the lateral compartment along with posterior widening.

CONCLUSION: This study demonstrates that successful weight loss following RYGB surgery is associated with significant region-specific increases in JSW in the medial compartment of the knee at a one-year interval, specifically in the central and inner regions of the medial tibiofemoral compartment. These findings suggest that weight reduc-

tion may lead to unloading of joint structures, especially at the medial compartment, which may alleviate cartilage compression and meniscal extrusion

SPONSOR: This work was supported by the Finnish Ministry of Education and Culture's Pilot for Doctoral Programmes (Pilot project Mathematics of Sensing, Imaging and Modelling).

DICLOSURE STATEMENT: Tom Turmezei is Director of KNEE3D Ltd. CORRESPONDENCE ADDRESS: lassi.vuononvirta@oulu.fi

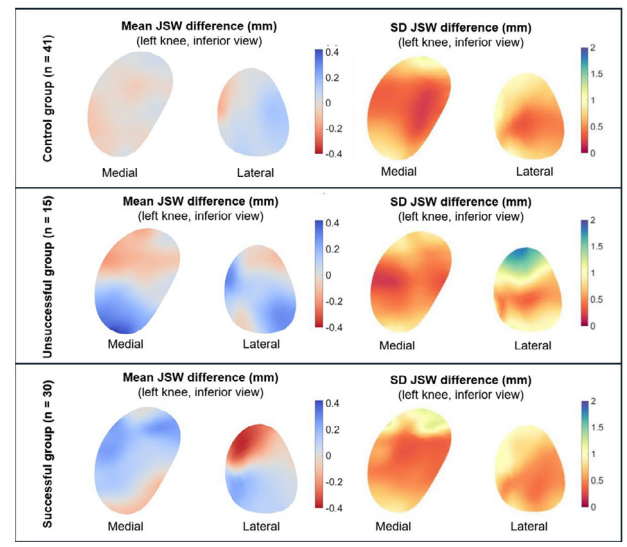


Figure 3. Mean and standard deviation (SD) maps of joint space width (JSW) changes (mm) in the left knee (inferior view) after one year, shown by group: control (n=41), unsuccessful (n=15), and successful (n=30). The successful group shows greater medial JSW widening. SD maps show spatial variability within each group.

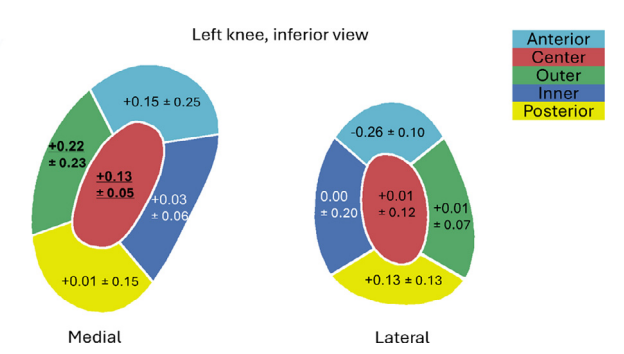


Figure 4. Mean (± SD) JSW changes (mm) in the successful group after one year, mapped on the canonical left knee surface. The joint is divided into medial and lateral compartments with five subregions. Medial areas showed consistent widening, especially centrally and at the outer aspect, while lateral compartment changes were more variable with some anterior narrowing and posterior widening.

¹ Research Unit of Health Sciences and Technology, University of Oulu, Oulu, Finland
² Department of Radiology, Norfolk and Norwich University Hospitals NHS Foundation

² Department of Radiology, Norfolk and Norwich University Hospitals NHS Foundation Trust, Norwich, UK; Norwich Medical School, University of East Anglia, Norwich, UK

³ Department of Diagnostic Radiology, Oulu University Hospital, Oulu, Finland

⁴ Department of Anesthesiology, Surgery, and Intensive Care, Oulu University Hospital, Oulu, Finland

⁵ Medical Research Center Oulu, University of Oulu, Oulu, Finland

⁶ Research Unit of Translational Medicine, University of Oulu, Oulu, Finland

⁷ Biocenter Oulu, University of Oulu, Oulu, Finland

IMPROVED DCE-MRI OF OA SYNOVITIS IN THE PRESENCE OF EFFUSION

J.C. Waterton 1,2 , J.H. Naish 1 , M. Tibiletti 1 , L. Edwards 1 , M.J. Heaton 1 , J.D. Kaggie 3 , M.J. Graves 3 , R.J. Janiczek 4 , A. McCaskie 5 , F.J. Gilbert 3 , G.J.M. Parker 1,6 , J.W. MacKay 3

- ¹ Bioxydyn, Manchester, UK
- ² Centre for Imaging Sciences, University of Manchester, UK
- ³ Department of Radiology, University of Cambridge, UK
- ⁴ Johnson & Johnson, Spring House, PA, USA
- ⁵ Department of Surgery, University of Cambridge, UK
- ⁶ Centre for Medical Image Computing, University College London, UK

INTRODUCTION: Synovitis is increasingly important in OA, both for disease understanding and as a therapeutic target. Dynamic contrastenhanced (DCE) MRI is a powerful tool providing regional pharmacodynamic biomarkers. Investigators commonly map synovitis using compartmental models, such as the Extended Tofts model (ETM) originally developed for neuroscience and oncology (1). ETM assumes the extravascular extracellular space (v_e) is a well-mixed compartment, an assumption commonly violated in the presence of effusion. Use of an unsuitable compartmental model sometimes produces physiologically implausible imaging biomarkers which lack face validity and damage confidence in the interpretation of any changes.

OBJECTIVE: 1) to develop a 3-compartment model (3CM) suitable for DCE-MRI in OA in the presence of effusion; 2) to characterize the model by simulation; 3) to compare performance of new 3CM and conventional ETM in an OA study with between- and within-subject comparison.

METHODS: The model (2) (figure 1A), includes v_e in exchange with a well-mixed vascular plasma compartment v_p , and also with a third effusion-like compartment receiving contrast from, but not returning it to, v_e . It has previously been characterized in an RA setting (2). A previously-reported (3) knee OA DCE-MRI study includes 61 datasets from 21 subjects (6 healthy, 11 KL2, 4 KL3) imaged on multiple occasions, all segmented by a musculoskeletal radiologist (JWM). Data were fit voxelwise in VoxelFlow (Bioxydyn) using 3CM, ETM, and a Patlaktype uptake-only model (UOM). Akaike Information Criterion (AIC) was used to determine which model each voxel preferred. Between-subject means \pm SD and between-scan repeatability coefficients of variation (CoV) were determined for each biomarker, and also for the AIC-imposed parcellations.

RESULTS: In simulations when the generative model was 3CM, ETM performed poorly (except at low k_1), but when the generative model was ETM, 3CM performed almost as well as the generative model across the whole parameter space. In OA subjects (Figure 1B, Table 1), extreme

unphysiologic values of v_e (red in Figure 1C) were seen with ETM but not 3CM, while repeatability CoV did not deteriorate for the new 3CM k_1 in comparison to conventional ETM (Table 1). Differences between healthy and OA subjects were preserved.

CONCLUSION: The new 3CM model provides plausible biomarker values and informative maps, avoiding unphysiologic parameter estimates. This offers drug developers greater confidence in interpreting druginduced pharmacodynamic responses.

SPONSOR: The original study was sponsored by the University of Cambridge and partially funded by GlaxoSmithKline. This further analysis of the study data is funded by Bioxydyn.

DISCLOSURE: employment and/or ownership in Bioxydyn (JCW, JHN, MT, LE, MH, GJMP).

CORRESPONDENCE ADDRESS: john.waterton@bioxydyn.com

REFERENCES:

- 1-Tofts PS. J Magn Reson Imaging. 1997 (7):91-101.
- 2-Waterton JC, et al. Proc. ISMRM 2025 1115.
- 3-MacKay JW,et al. Eur Radiol. 2021 (8):5746-5758.

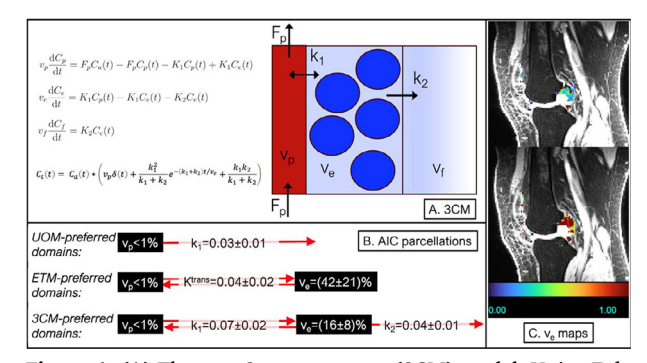


Figure 1. (A) The new 3-compartment (3CM) model. Units: F, k, min⁻¹; C, mM; f, min; v, dimensionless; δ , the Dirac delta. (B) AIC parcellation of all enhancing knee voxels in the union RoI at baseline in 15 OA subjects. Top, AIC prefers UOM, 26% of enhancing voxels. Middle, AIC prefers ETM, 30% of enhancing voxels. Bottom AIC prefers new 3CM, 43% of enhancing voxels. Note K^{trans} in ETM is equivalent to k₁ in UOM and 3CM. (C) part of v_e parameter map from one slice from a typical subject (i.e. has average values for k₁). Top: fit to 3CM. Bottom: fit to ETM. Extreme unphysiologic values of v_e (red≥1) are common with ETM but not with 3CM.

Table 1. Imaging biomarker values in seven OA subregions, and for the union of all subregions in HV and OA. Data for each biomarker represent voxelwise medians over: \dagger all enhancing voxels in the region; \ddagger only voxels in the region which prefer that model. Shown are subjectwise means \pm between-subject SD at baseline. For the union RoIs, shown in parenthesis are within-subject between-timepoint CoV for paired scans 31 \pm 9 days apart. Note (a) non-inferior CoV for 3CM k_1 compared to ETM K^{trans}; (b) high v_e with ETM compared to 3CM.

		HV union	OA union		ıpra-patellar fat pad -	OA perimeniscal		OA inter-	OA posterior femoral condyle	
				supra-patellar		medial	lateral	condylar	medial	lateral
† 3CM k ₁ /min ⁻¹	l	0.038±0.021 (27%, note a)	0.051±0.023 (30%, note a)	0.049±0.024	0.061±0.038	0.119±0.081	0.059±0.027	0.064±0.034	0.038±0.018	0.035±0.019
† ETM K ^{trans} /mi	in ⁻¹	0.029±0.016 (26%)	0.037±0.018 (31%)	0.036±0.019	0.044±0.025	0.099±0.057	0.043±0.019	0.045±0.024	0.029±0.015	0.025±0.013
† 3CM v_e		12%±8% (43%)	17%±12% (55%)	16%±12%	19%±16%	56%±40%	20%±14%	19%±14%	15%±13%	11%±8%
\dagger ETM $v_{\rm e}$ (note l	b)	38%±19% (32%)	55%±28% (46%)	48%±29%	54%±48%	123%±126%	59%±33%	74%±46%	56%±30%	42%±21%
Enhancing proportion	‡ 3CM	43%±26% (21%)	43%±29% (55%)	44%±33%	39%±32%	54%±40%	45%±30%	40%±27%	39%±27%	37%±24%
preferring: (by AIC)	‡ ETM	29%±12% (14%)	30%±12% (27%)	27%±12%	33%±18%	34%± 33%	32%±17%	29%±13%	32%±14%	32%±16%

TOWARD OPENLY AVAILABLE KNEE MRI SEGMENTATIONS FOR THE OAI: MULTI-MODEL EVALUATION AND CONSENSUS GENERATION ON 9,360 SCANS

M.S. White 1 , K.T. Gao 2 , V. Pedoia 2 , S. Majumdar 2 , G.E. Gold 1 , A.S. Chaudhari 1 , A.A. Gatti 1

INTRODUCTION: Many deep learning methods exist for segmentation of bone and cartilage in knee MRI, but their agreement and impact on quantitative metrics (e.g., cartilage thickness) remain unclear. Prior studies have not investigated whether combining segmentations from independent deep learning models can improve sensitivity to detect clinically relevant differences. Understanding these effects in large cohorts is essential to guide deep learning in OA research and clinical trials.

OBJECTIVE: To generate consensus segmentations from independent deep learning models developed at Stanford and UCSF, evaluate agreement between bone and cartilage segmentations across all models, and assess each method's sensitivity to detect cartilage thickness differences between KL2 and KL3 knees.

METHODS: Bone and cartilage segmentations of 9360 knees from the OAI baseline dataset were independently generated in prior work by Stanford and UCSF using separately validated deep learning models. A consensus segmentation was generated using the Simultaneous Truth and Performance Level Estimation (STAPLE) algorithm, with the threshold tuned to minimize cartilage volume differences between the two models. Segmentations were compared using volume differences (%), Dice Similarity Coefficient (DSC), and average symmetric surface distance (ASSD). Mean cartilage thickness was computed in sub-regions (femur: anterior, medial/lateral weight-bearing, posterior; tibia: medial and lateral, and patella) and compared using Pearson correlations and intraclass correlation coefficients (ICC). Each method's (UCSF, Stanford, and STAPLE's) sensitivity to detect between group (KL2 and KL3) differences in cartilage thickness was assed using effect sizes (Cohen's d).

RESULTS: Comparing Stanford and UCSF models, bone demonstrated better overlap (DSC=0.95-0.97) compared to cartilage (DSC=0.79-0.82). However, cartilage had smaller volume differences (-0.2-1.9% vs. 2.5-6.2%) and lower ASSD (0.24-0.33 mm vs. 0.33-0.47 mm) relative to bone. Both Stanford vs. STAPLE and UCSF vs. STAPLE yielded better segmentation agreement (higher DSC, lower ASSD) compared to Stanford vs. UCSF, despite larger volume differences (Table 1A). Compared to one another, Stanford and UCSF cartilage thickness measurements had high correlation (r=0.96-0.99) and agreement (ICC=0.96-0.99, mean differences < 0.04 mm). STAPLE produced systematically greater

thickness values (mean difference = 0.16 ± 0.08 mm), and slightly lower ICCs (ICC = 0.88-0.96), and correlations (r = 0.92-.97) when compared with Stanford or UCSF. Effect sizes for mean cartilage thickness between KL2 and KL3 knees were small (Cohen's d < 0.5), except for the medial weight-bearing femur, which had moderate effects for Stanford (-0.60) and UCSF (-0.58), and small-to-moderate for STAPLE (-0.48; Table 1B).

CONCLUSION: Cartilage thickness measurements were highly correlated across methods and regions, indicating preservation of key quantitative information, despite lower DSC between Stanford and UCSF and lower absolute agreement in thickness (ICC) between STAPLE and each method. Importantly, STAPLE slightly reduced sensitivity to detect changes in medial weight-bearing femoral cartilage. Leveraging the many other existing OAI DESS segmentation models has the potential to further improve the consensus. Future work will refine the consensus segmentations, scale analyses to the full OAI dataset, and open source the resulting consensus segmentation masks.

DICLOSURE STATEMENT: A.C. has provided consulting services to Patient Square Capital, Chondrometrics GmbH, and Elucid Bioimaging; is co-founder of Cognita; has equity interest in Cognita, Subtle Medical, LVIS Corp, Brain Key. A.A.G is a shareholder of NeuralSeg, GeminiOV, and NodeAI.

CORRESPONDENCE ADDRESS: kenziew@stanford.edu

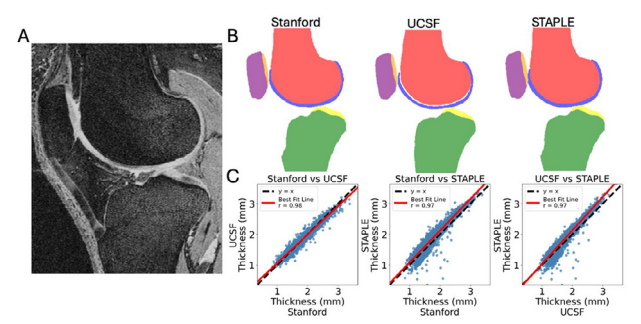


Figure 1. Representative Segmentations and Scatter Plot Comparisons. Panel A shows an example DESS MRI slice. Panel B shows example segmentations from Stanford (left), UCSF (middle), and STAPLE (right). Note the separation between bone and cartilage masks in UCSF (middle), which reflects a boundary offset relative to Stanford and likely contributed to the observed differences in volume, despite highly correlated thickness (r = 0.96-0.99). Panel C shows correlation plots between methods for the medial weight-bearing femur thickness. Perfect agreement is indicated by the dashed black line (y = x). The line of best fit (solid red) shows systematic differences between methods. Stanford and UCSF demonstrated nearly perfect agreement (left), while STAPLE systematically overestimated cartilage thickness (middle and right).

¹ Department of Radiology, Stanford University, Stanford, CA, USA

 $^{^2\,\}mathrm{Department}$ of Radiology and Biomedical Imaging, University of California, San Francisco, CA, USA

Table 1. Segmentation Agreement and Cartilage Thickness Comparisons by KL Grade. Top (A): Pairwise comparisons between Stanford, UCSF, and STAPLE segmentations showing volume difference (VD, %), Dice similarity coefficient (DSC), and average symmetric surface distance (ASSD, mm) averaged across the bone (femur, tibia, patella) and cartilage (femur, tibia, and patella) regions. ASSD values were primarily less than the in-plane resolution (\sim 0.37 mm). Bottom (B): Cartilage thickness for KL grades 2 (n=2311) and 3 (n=1202) knees across regions and methods. Values are indicated as mean \pm standard deviation and reported in millimeters. Effect sizes between KL 2 and 3 within each method are reported as Cohen's d (d).

A. Segmentati	on Evaluation								
	Stanford vs. UCSF			Stanford vs. ST	APLE		UCSF vs. STAPLE		
	VD	DSC	ASSD	VD	DSC	ASSD	VD	DSC	ASSD
Bone Cartilage	4.04±20.0 0.82±9.7	0.96±0.02 0.80±0.04	0.40±0.21 0.28±0.22	-0.6±19.8 -7.2±15.6	0.99±0.01 0.91±0.06	0.08±0.16 0.13±0.28	-4.97±3.9 -9.90±141.9	0.98±0.01 0.90±0.06	0.31±0.14 0.16±0.25
B. Cartilage T	hickness Evaluation								
Region	Stanford		UCSF			(Stanford + UCSF) STAPLE			
	KL 2	KL 3	d	KL 2	KL 3	d	KL 2	KL 3	d
TrF	2.26±0.30	2.30±0.30	0.15	2.28±0.30	2.33±0.30	0.18	2.58±0.38	2.62±0.38	0.12
cMF	1.92±0.35	1.71±0.35	-0.60	1.91±0.33	1.72 ± 0.34	-0.58	2.04±0.36	1.87±0.37	-0.48
cLF	1.94±0.31	1.94 ± 0.32	-0.02	1.98 ± 0.30	1.96 ± 0.32	-0.05	2.10 ± 0.34	2.08 ± 0.35	-0.05
pMF	2.02 ± 0.27	2.00 ± 0.26	-0.07	2.04 ± 0.24	2.02 ± 0.24	-0.06	2.27 ± 0.31	2.26 ± 0.31	-0.03
pLF	2.07 ± 0.32	2.06 ± 0.33	-0.03	2.08 ± 0.30	2.08 ± 0.31	0.02	2.29 ± 0.35	2.28±0.36	-0.01
MT	1.90 ± 0.31	1.85 ± 0.32	-0.17	1.89 ± 0.31	1.83 ± 0.31	-0.19	1.98±0.43	1.89 ± 0.44	-0.19
LT	2.23±0.39	2.13±0.45	-0.22	2.23 ± 0.38	2.14 ± 0.43	-0.21	2.29 ± 0.51	2.15±0.58	-0.25
P	2.11±0.48	2.21±0.48	0.22	2.08±0.44	2.20±0.44	0.26	2.20±0.63	2.36±0.63	0.26

CAN REGISTRATION-BASED LOCATION-INDEPENDENT MEASUREMENT INCREASE THE SENSITIVITY TO BETWEEN-GROUP DIFFERENCES IN LONGITUDINAL CHANGE OF LAMINAR CARTILAGE T2?

W. Wirth 1,2, F. Eckstein 1,2

- ¹ Chondrometrics GmbH, Freilassing, Germany
- $^2{\it Center}$ for Anatomy and Cell Biology & LBIAR, Paracelsus Medical University, Salzburg, Austria

INTRODUCTION: Location-independent measurements of cartilage thinning and thickening were shown to be more sensitive to differences in longitudinal change between groups than location-based measures [1,2]. They remove the link between the magnitude and direction of the change and its location, and hence are sensitive to local changes in the joint, independent of where they occur. Location-independent measures of T2 lengthening and shortening computed from 16 femorotibial subregions have been previously applied to a model of early OA. The model compared 3y T2 change in KLG 0 knees with contralateral (CL) joint space narrowing (JSN) vs that in KLG 0 knees with CL KLG 0 (controls) [3]. In this model, location-independent measures were found to provide similar discrimination between these two groups as location-based measures. However, location-independent measures obtained across all individual voxels in the joint (instead of subregions) have been previously suggested to provide more detailed insights into OA-related cartilage thickness changes [4], but no study previously evaluated the sensitivity of such voxel-based shortening and lengthening scores to differences in change of laminar T2.

OBJECTIVE: To compare the sensitivity of voxel-based location-independent lengthening and shortening T2 scores to between-group differences in longitudinal change vs. the previously established technique of subregion-based location-independent and location-based measures in the above early OA model.

METHODS: Multi-echo spin-echo (MESE) MRIs were acquired at year 1 and 4 in the OAI (3T Trio, Siemens). We studied 39 KLG 0 knees with CL JSN, and 39 matched controls (criteria: same sex pain frequency, similar age (±5y) and BMI (±5kg/m2)) with bilateral KLG 0 [2]. Segmentation of the 4 femorotibial cartilages (medial/lateral tibia: MT/LT and central medial/lateral femoral condyle: cMF/cLF) was performed manually by experienced readers. Laminar T2 was computed for each segmented cartilage voxel and classified as deep or superficial, based on the distance to the cartilage surfaces. Location-based and subregionbased location-independent measures were obtained as described previously [2]. Voxel-based location-independent changes in laminar T2 were derived, summarizing the negative/positive changes across all voxels, for each of the femorotibial cartilages using the voxel-based approach (Fig. 1) These were then summarized across the entire femorotibial joint (FTJ). Location-based, subregion-based location independent, and voxel-based location-independent laminar T2 change was compared between the CL JSN vs. control knees using Cohen's D as a measure of effect size with 95% confidence intervals obtained using boot-strapping.

RESULTS: In the deep layer, location-based longitudinal change in femorotibial T2 revealed a Cohen's D between both groups of 0.37 [0.04, 0.69]), the subregion-based location independent analysis of 0.33 [0.00, 0.65]), and the voxel-based location-independent analysis of 0.36 [0.04, 0.68]) (Fig. 2). In the superficial layer, only the voxel-based absolute change score was sensitive to differences in longitudinal T2 change between both groups (Cohen's D: 0.34 [0.02, 0.66]). Figure 3 shows the pattern of voxel-wise differences in superficial layer cMF and cLF T2 change between KLG 0 knees with CL JSN vs. control knees.

CONCLUSION: Effect sizes for the different location-based and location-independent T2 analyses (subregion and voxel-based) were similar for the deep cartilage. However, the new voxel-based method appeared to be also sensitive to between-group differences in T2 change in the

superficial cartilage layer, where location-based and subregion-based location-independent measures failed to provide notable discrimination. In addition, the voxel-based technique allows to visualize patterns of differences in change between groups that can inform future analyses focusing on specific regions of interest.

SPONSOR: Eurostars-2 (E! 114932, OA-BIO) & BMBF DICLOSURE STATEMENT: FE, WW: Chondrometrics GmbH

REFERENCES:

- [1] Eckstein et al. Semin Arthritis Rheum. 2017;46:404-410.
- [2] Eckstein et al. Ann Rheum Dis. 2020; 79:525-528.
- [3] Wirth et al. Osteoarthritis Cartilage. 2019;27:1663-1668.
- [4] Fuerst et al. Osteoarthritis Cartilage 2021; 29:S316-S317.

CORRESPONDENCE ADDRESS: wolfgang.wirth@pmu.ac.at

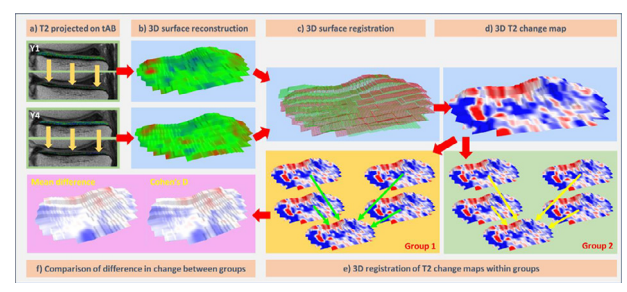


Fig. 1: Laminar thinning and thickening scores are computed by a) projecting superficial and deep layer T2 from each of the cartilage voxels to the nearest total area of subchondral (tAB) voxels for both the year-1 (Y1) and year-4 (Y4) visits, b) reconstructing the tAB surfaces using a slice-wise triangulation, c) registering the Y4 tAB to the BL tAB using the iterative closes point (ICP) algorithm, and d) by computing smoothed laminar T2 change maps for each BL tAB voxel. The laminar shortening/lengthening scores are then computed for each Y1/Y4 pair by suming the tAB voxels with negative/positive sign of the T2 change and are exported for analysis. e) The T2 change maps can additionally be registered using the ICP algorithm across all knees within each group for f) visualizing the differences in change between groups (mean difference and Cohen's D).

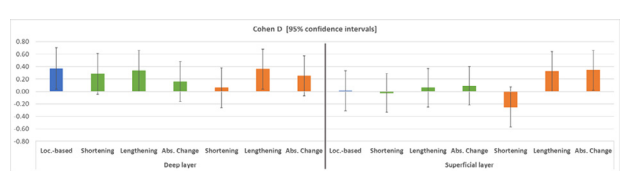


Fig. 2: Cohen's D for differences in change in the entire femorotibial joint in deep (left) and superficial layer (right) T2 between knees with KLG 0 knees with contralateral (CL) JSN and KLG 0 knees with CL KLG 0. The graph shows the Cohen's D for the location-based change (blue), location-independent measures computed from 16 femorotibial subregions (green), and location-independent measures computed across voxels using the voxel-based approach (orange).

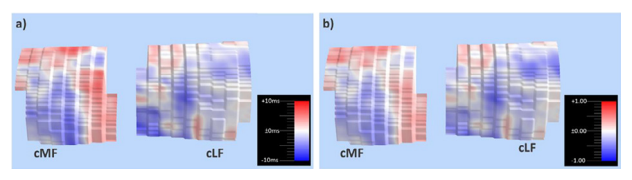


Fig. 3: Illustration of differences in change in the superficial layer of the central medial (cMF) and lateral (cLF) femoral condyle between KLG 0 knees with contralateral (CL) JSN and KLG 0 knees with CL KLG 0. a) shows the voxel-wise differences and b) shows the voxel-wise Cohen's D.

A SYSTEMATIC POST-PROCESSING APPROACH FOR \mathbf{T}_{1P} IMAGING OF KNEE ARTICULAR CARTILAGE

J. Zhong 1,* , Y. Yao 1,2,* , F. Xiao 3 , T.Y.M. Ong 4 , K.W.K. Ho 4 , S. Li 1 , C. Huang 1 , Q. Chan 5 , J.F. Griffith 1 , W. Chen 1

 $^1\,\mbox{CU}$ Lab of AI in Radiology, Department of Imaging and Interventional Radiology, CUHK, Hong Kong, China

INTRODUCTION: $T_{1\rho}$ imaging is an emerging technique in knee MRI for the evaluation of OA. This modality possesses the unique capability to image biochemical components, such as proteoglycans, facilitating early detection and post-treatment monitoring of knee OA. However, a significant challenge associated with $T_{1\rho}$ imaging lies in the complexity of its post-processing, which encompasses parameter fitting, cartilage segmentation, and subregional parcellation.

OBJECTIVE: This abstract presents a systematic methodology for automating knee $T_{1\rho}$ MRI post-processing by leveraging deep learning and advanced computational techniques.

METHODS: Our methodology automated the three primary steps of $T_{1\rho}$ knee MRI post-processing and provided the mean $T_{1\rho}$ values for 20 subregions of the femoral and tibial cartilage in the knee (Figure). In our experiments, we utilized four $T_{1\rho}$ -weighted images to generate the $T_{1\rho}$ map for 30 OA patients (age 67.63±5.80 years, BMI 26.00±4.08 kg/m²) and 10 healthy volunteers (age 24.90 ± 2.59 years, BMI 22.75 ± 4.51 kg/m²). For each subject, four $T_{1\rho}$ -weighted images were acquired using a spinlock frequency of 300 Hz and spin-lock times of 0, 10, 30, and 50 ms, with a resolution of $0.8 \times 1 \times 3$ mm³, resulting in an image matrix size of $44 \times 256 \times 256$. The spin-lock preparation was followed by an FSE readout with TE/TR = 31/2000 ms. Additionally, we computed the mean of the four $T_{1\varrho}$ -weighted images and employed this mean for automated cartilage segmentation and subregion parcellation. We employed a nnU-Net trained with all 40 subjects for cartilage segmentation, while subregion parcellation was conducted using our previously published rulebased method, CartiMorph. The performance of the approach using deep learning segmentation was assessed using the Dice Coefficient Similarity (DSC), the root-mean-squared deviation (RMSD), and the coefficient of variance of RMSD (CV_{RMSD}) against the manual segmentation. We excluded 3 OA patients with full cartilage loss above 50% of one cartilage area (FC, MTC, or LTC) in subregion analysis.

RESULTS: Our experimental results demonstrated the satisfactory performance of our proposed approach. The mean DSC values for the FC, MTC and LTC in OA patients and healthy volunteers were 0.83, 0.80, and 0.82, respectively. Table 2 provides a comprehensive breakdown of the performance metrics of the agreement in $T_{1\rho}$ quantification across 20 subregions.

CONCLUSION: We proposed a systematic approach for post-processing knee $T_{1\rho}$ MRI data. The experimental results demonstrated the efficacy of the proposed approach.

SPONSOR: Innovation and Technology Commission of HKSAR Government (MRP/001/18X)

DICLOSURE STATEMENT: none.

ACKNOWLEDGMENT: We extend our gratitude to the contributions from Ms. Cherry Cheng, Mr. Ben Choi, Mr. Adam Kwong and Mr. Zongvou Cai.

CORRESPONDENCE ADDRESS: wtchen@cuhk.edu.hk

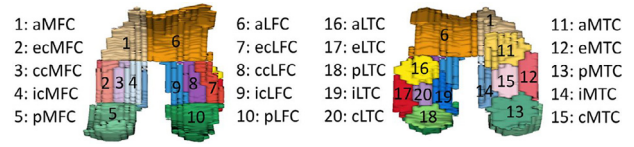


Figure 1. Parcellated cartilage subregions. Examples images of a healthy participant (V014, right knee, female, 22 y, 20.76 kg/m²) were processed. Note. a=anterior, p=posterior, e=exterior, i=interior, c=central, ic=interior-central, cc=central-central, ec=exterior-central, MFC=medial femoral cartilage, LFC=lateral femoral cartilage, MTC=medial tibial cartilage, LTC=lateral femoral cartilage.

Table 2. Regional Mean $T_{1\rho}$ Agreement in Cartilage Subregions

	Patients, $n=27$	•	Healthy volur	iteers, $n=10$	
Subregion	RMSD (ms)	CV _{RMSD} (%)	RMSD (ms)	CV _{RMSD} (%)	
aMFC	0.71	1.51	0.44	0.96	
ecMFC	0.79	2.11	0.53	1.40	
ccMFC	1.73	4.58	1.07	2.50	
icMFC	0.59	1.28	0.27	0.57	
pMFC	0.60	1.30	0.15	0.38	
aLFC	1.12	2.46	0.37	0.78	
ecLFC	0.55	1.43	0.67	1.70	
ccLFC	0.95	2.41	1.24	3.01	
icLFC	1.18	2.62	0.63	1.46	
pLFC	0.36	0.81	0.20	0.47	
aMTC	0.73	1.82	0.57	1.34	
eMTC	0.94	2.26	0.52	1.23	
pMTC	0.50	1.31	0.46	1.16	
iMTC	0.63	1.59	0.40	0.98	
cMTC	1.09	3.09	0.72	1.84	
aLTC	0.67	1.81	0.45	1.27	
eLTC	0.71	1.76	0.95	2.30	
pLTC	0.64	1.61	0.66	1.68	
iLTC	0.80	2.01	0.51	1.47	
cLTC	0.60	1.73	0.34	1.05	
Average	0.79	1.97	0.56	1.38	

Note. Three of 30 OA patients were excluded. a = anterior, p = posterior, e = exterior, i = interior, c = central, i = interior central, i = c

² The University of Edinburgh, UK

³ Department of Radiology, Shanghai Sixth People's Hospital Affiliated to Shanghai Jiao Tong University School of Medicine, Shanghai, China

⁴ Department of Orthopaedics & Traumatology, CUHK, Hong Kong, China

⁵ Philips Healthcare, Hong Kong, China

^{*}Authors share the same contribution

AUTOMATED QUANTIFICATION OF MENISCUS EXTRUSION IN MRI VIA AI FOUNDATION MODEL: PROOF OF CONCEPT USING A TRAINING-FREE FEWSHOT SEGMENTATION APPROACH

Z. Zhou ¹, X. He ^{1,2}, Y. Hu ^{1,2}, H.A. Khan ¹, F. Liu ^{1,2}, M. Jarraya ¹

INTRODUCTION: Manual assessment of meniscus extrusion (ME) in magnetic resonance (MR) images is time-consuming and prone to variability, limiting efficiency in clinical and research settings. While deep learning methods have shown promise in MR image segmentation, their reliance on task-specific training and large annotated datasets limits scalability and adaptability.

OBJECTIVE: Building upon our previously developed AI foundation model, we aim to establish a fully automated pipeline for quantifying ME in knee MRI with our model training and eliminate the need for large annotated datasets.

METHODS: By providing a support set including a minimal number of segmentation examples, the AI Foundation Model enables accurate segmentation of knee anatomy and reliable ME measurement in a trainingfree, few-shot manner. In the study, we analyzed 3T MR images acquired using either T2-weighted or proton density MR sequences from 10 patients with mild osteoarthritis. Manual segmentations of femur, tibia, medial, and lateral menisci were performed by experts. Two patients, one with T2-weighted and one with proton density images, were randomly selected to build the support set. The remaining 8 patients comprised the testing set, which was used for both automated segmentation and model evaluation. Segmentation performance was assessed using the Dice Coefficient. For ME evaluation, an experienced radiologist manually identified the slice containing the tibial spine and measured extrusion as the reference. Automated ME measurement was computed from the segmentation by detecting the femoral condyle and tibial plateau edge, then measuring the distance from the most medial point of the medial meniscus to a reference line connecting the femoral condyle and tibial plateau edge.

RESULTS: The average Dice Coefficient was $94.07 \pm 3.97\%$ for the femur, $97.09 \pm 0.93\%$ for the tibia, $82.91 \pm 6.72\%$ for the medial meniscus, and $85.49 \pm 5.24\%$ for the lateral meniscus. ME measurements predicted by the model were also compared with ground truth values. The human measured ME was 4.26 ± 1.46 mm, while the model-predicted ME was 4.18 ± 1.16 mm.

CONCLUSION: This study demonstrates that the foundation model enables reliable and fully automated quantification of meniscus extrusion from knee MR images without requiring training or large annotated datasets. With only two support examples, the model achieved accurate segmentation and ME measurement across eight testing subjects, underscoring its efficiency and strong generalization. Its consistent per-

formance across key anatomical structures highlights its potential for expert-level evaluation in both clinical and research settings with minimal manual effort. Further work will explore semi-automated expansion of the support set and extension to diverse MRI protocols and osteoarthritis severities, and validation on larger-scale datasets.

SPONSOR: This work was supported in part by the U.S. National Institute of Biomedical Imaging and Bioengineering under grant NIBIB R21EB031185, and in part by the U.S. National Institute of Arthritis and Musculoskeletal and Skin Diseases under grant NIAMS R01AR079442, R01AR081344 and R56AR081017. MJ is supported by NIAMS under grant K23-AR084603.

DISCLOSURE STATEMENT: None

ACKNOWLEDGMENT:

CORRESPONDENCE ADDRESS: mjarraya@mgh.harvard.edu

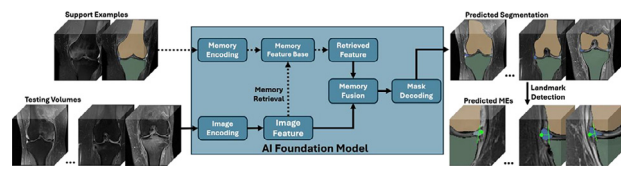


Figure 1. Overview of the framework of the AI Foundation Model for automated meniscus extrusion quantification from knee MRI. Left: Input support and query MR images with anatomical annotations including femur (orange), tibia (green), and meniscus (blue). Middle: The architecture performs image encoding and memory-guided segmentation via feature retrieval and fusion without requiring model training. Right: Predicted segmentations and extrusion measurements, showing medial meniscus displacement quantified relative to detected femoral and tibial landmarks.

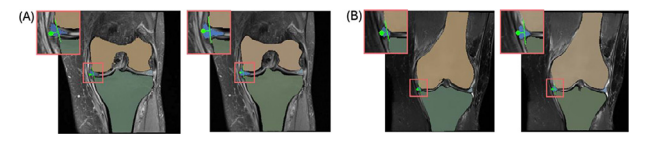


Figure 2. Representative examples of automatic segmentation and meniscus extrusion (ME) quantification. (A) The left image shows segmentation and ME quantification produced by the foundation model, while the right image displays the expert-generated ground truth. Dice coefficients for the femur, tibia, medial meniscus, and lateral meniscus were 93.09%, 98.41%, 84.34%, and 90.48%, respectively. The model-predicted ME was 3.77 mm, compared to the ground-truth ME of 3.98 mm. (B) The left image shows the model output, and the right image shows the corresponding expert annotation. Dice coefficients were 96.16% for the femur, 96.95% for the tibia, 80.41% for the medial meniscus, and 85.48% for the lateral meniscus. The model-predicted ME was 3.85 mm, while the ground-truth ME was 3.98 mm.

¹ Department of Radiology, Massachusetts General Hospital, Harvard Medical School, Boston, MA, USA

 $^{^2\,\}text{Matinos}$ Center for Biomedical Engineering, Massachusetts General Hospital, Charlestown, MA, USA